The Dissertation Committee for Tiffany Faye Kautz Certifies that this is the approved version of the following dissertation:

Characterization of a Low-Fidelity Live-Attenuated Vaccine for Venezuelan Equine Encephalitis Virus

Committee:

Naomi Forrester, Ph.D., Mentor

Scott Weaver, M.S., Ph.D., Co-mentor

David Beasley, Ph.D.

Yuriy Fofanov, Ph.D.

Greg Ebel, Ph.D.

Dean, Graduate School

Characterization of a Low-fidelity Live-Attenuated Vaccine For Venezuelan Equine Encephalitis Virus

by

Tiffany Faye Kautz, B.A., B.S., M.S.

Dissertation

Presented to the Faculty of the Graduate School of

The University of Texas Medical Branch

in Partial Fulfillment

of the Requirements

for the Degree of

Doctor of Philosophy

The University of Texas Medical Branch

May, 2018

Acknowledgements

Characterization of a Low-fidelity Live-Attenuated Vaccine For Venezuelan Equine

Encephalitis Virus

Publication No._____

Tiffany Faye Kautz, Ph.D.

The University of Texas Medical Branch, 2018

Supervisor: Naomi L. Forrester, Scott C. Weaver

During RNA virus replication, there is the potential to incorporate mutations that affect virulence or pathogenesis. For live-attenuated vaccines, this has implications for stability, as replication may result in mutations that either restore the wild-type phenotype via reversion or compensate for the attenuating mutations by increasing virulence (pseudoreversion). Recent studies have demonstrated that altering the mutation rate of an RNA virus is an effective attenuation tool. To validate the safety of low-fidelity mutations to increase vaccine attenuation, several mutations in the RNA-dependent RNA-polymerase (RdRp) were tested in the live-attenuated Venezuelan equine encephalitis virus (VEEV) vaccine strain, TC-83. Next generation sequencing after passage in the presence of mutagens revealed a mutant containing 3 mutations in the RdRp, TC-83 3x, to have decreased replication fidelity, while a second mutant, TC-83 4x displayed no change in fidelity, but shared many phenotypic characteristics with TC-83 3x. Both mutants exhibited increased, albeit inconsistent attenuation in an infant mouse model, as well as increased immunogenicity and complete protection against lethal challenge of an adult murine model compared to the parent TC-83. The TC-83 3x mutant was selected for further study due its decreased replication fidelity. While infection of live mosquitoes with TC-83 and TC-83 3x proved difficult, *in vitro* mosquito cell

infection suggested increased attenuation of the TC-83 3x mutant in this host. TC-83 3x genetic stability was high, with no reversion of the 3 RdRp mutations during passaging *in vitro* and *in vivo*. Passaging of the TC-83 3x mutant using a reporter construct showed this mutant to have increased levels of recombination, as well as lowered fidelity. During serial passaging in a highly permissive mouse model, TC-83 3x increased in virulence but remained less virulent than the parent TC-83. These results suggest that the incorporation of low-fidelity mutations into the RdRp of live-attenuated vaccines for RNA viruses can confer increased immunogenicity whilst showing some evidence of increased attenuation. However, while in theory such constructs may result in more effective vaccines, the instability of the vaccine phenotype decreases the likelihood of this being an effective vaccine attenuation strategy.

TABLE OF CONTENTS

List of Tables

List of Figures

List of Illustrations

List of Abbreviations

5FU	5' fluorouracil
Ae.	Aedes
APOBEC	apolioporotein B mRNA editing enzyme, catalytic polypepetide-like
AURA	Aura virus
BHK	baby hamster kidney
cDNA	complementary DNA
CHIKV	chikungunya virus
CMV	cytomegalovirus
CNS	central nervous system
CPE	cytopathic effect
Cu. (Mul.)	Culex (Melanoconion)
CVB3	coxsackie virus B3
DI particle	defective interfering particle
DMEM	Dulbecco's minimal essential medium
DNA	deoxyribonucleic acid
dNTP	deoxyribonucleoside triphosphate
DPI	days post-infection
dsRNA	double-stranded RNA
DTT	dithiothreitol
EDTA	ethylenediaminetetraacetic acid
EILV	Eilat virus
EEEV	eastern equine encephalitis virus
EP	electroporation
ER	endoplasmic reticulum
FAM	carboxyfluorescein
FBS	fetal bovine serum
FLU	influenza virus
FMDV	foot and mouth disease virus
GFP	green florescent protein
GTP	guanosine triphosphate
HEV71	human enterovirus 71
HIV	human immunodeficiency virus
HLA	human leukocyte antigen
HPI	hours post-infection
IC	intracranial
ID	intradermal
IFN	interferon
IM	intramuscular
IN	intranasal
IND	investigational new drug
IP	intraperitoneal
IT	intrathoracic

IRES	internal ribosome entry site
LAV	live-attenuated vaccine
LB	Luria broth
LD_{50}	Lethal dose 50
MAYV	Mayaro virus
MHV	murine hepatitis virus
miRNA	micro RNA
mL	milliliter
MOI	multiplicity of infection
NEB	New England Biolabs
NGS	next generation sequencing
NHP	non-human primate
NoV	norovirus
nt	nucleotide
NTP	nucleoside triphosphate
nsP	non-structural protein
PBS	phosphate-buffered saline
PCR	polymerase chain reaction
PFU	plaque forming unit
piRNA	Piwi-interacting RNA
PPi	pyrophosphate
PRNT	plaque reduction neutralization test
PRRSV	porcine reproductive and respiratory syndrome virus
Ps.	Psorophora
PV	poliovirus
PVR	poliovirus receptor
RdRp	RNA-dependent RNA polymerase
RNA	ribonucleic acid
RNAi	RNA interference
rNTP	ribonucleoside triphosphate
rpm	rotations per minute
RT PCR	reverse transcriptase polymerase chain reaction
RT-qPCR	reverse transcriptase quantitative polymerase chain reaction
SARS-CoV	severe acute respiratory syndrome coronavirus
SC	subcutaneous
SCID	severe combined immunodeficiency
SFV	Semliki Forest virus
SINV	Sindbis virus
siRNA	short interfering RNA
SLEV	St. Louis encephalitis virus
$SMicLD_{50}$	suckling mouse intracranial LD_{50}
SNP	single nucleotide polymorphism
SPDV	salmon pancreas disease virus
SSIII	superscript III
TAE	tris base, acetic acid, and EDTA
UTMB	University of Texas Medical Branch

UTR	untranslated region
VEE	Venezuelan equine encephalitis
VEEV	Venezuelan equine encephalitis virus
WEEV	Western equine encephalitis virus
WNV	West Nile virus
wt	wild-type
RCSB PDB	Research Collaboratory for Structural Bioinformatics Protein Data Bank

INTRODUCTION

Chapter 1. AN INTRODUCTION TO RNA VIRUS FIDELITY AND VENEZUELAN EQUINE ENCEPHALITIS VIRUS

RNA and other nucleic acids are unique in their ability to store and replicate the information necessary for life. Unlike DNA, any changes made to an RNA molecule are immediately realized as proteins, resulting in many deleterious mistakes, but also the potential for rapid evolution. This is the life of an RNA virus, where the risks of error-prone replication are balanced by the ability to immediately respond to change.

Although virus research is arguably biased towards viruses that infect mammals, and thus humans, it is estimated that there are greater than 320,000 viruses that infect mammals alone, the vast majority of which are unknown (1). This and recent metagenomic studies (2, 3) suggest that only the smallest tip of the RNA virosphere has been identified (4). With the exception of viroids (5), RNA viruses have the highest mutation rate of all known species, ranging from 10^{-4}-10^{-6} per round of genome replication (6-8). This is several orders of magnitude higher than DNA viruses (7) and thousands to tens-of-thousands of times higher than the mutation rates exhibited by bacteria and eukaryotes (9, 10). The abundance of RNA viruses demonstrates that the benefits of a high mutation rate may outweigh the risks. Therefore, it is important to understand how this successful balance of a high mutational burden came to be, beginning with the evolution and optimization of the RNA virus mutation rate.

RNA VIRUS REPLICATION

RNA-Dependent RNA Polymerase

Excluding retroviruses, the RdRp protein is required for RNA virus genome replication. Although each RNA virus family contains a unique RdRp with specialized features, there are conserved motifs and domains between different RdRps, as well as other polymerases.

The RdRp gene consists of 7 conserved motifs (A-G), each with its own specific and conserved fold (11). As a protein, the RdRp can be visualized as a right hand (Figure 1.1) with the finger and thumb subdomains connecting to form a channel for RNA replication, also known as the closed hand conformation. Forming the conserved catalytic core are the thumb, finger (motifs F and G), and palm (motifs A-E) domains. The thumb domain is responsible for RNA binding, usually in the minor groove of the double-stranded RNA following template recognition (12), as well as stabilization of the incoming NTPs (13, 14). It is also an integral member of the highly positively charged NTP tunnel, which likely acts as a pump to bring nucleotides into the RdRp (15). The finger domain assists replication by binding the major grooves of the RNA template to hold it in place, while the palm domain ensures the addition of the correct nucleotide to the RNA chain (12).

When the correct NTP enters the RdRp, Watson-Crick base pairing occurs between the NTP and the RNA template (16). This causes a conformational change that properly aligns motifs A and C, which bind and position the incoming NTP using metal ions (known as the two-metal-ion mechanism), as well as positioning of the RNA template by motif B (12). Motif D acts as the final checkpoint to confirm correct NTP addition by binding the NTP β-phosphate. This causes closure of the active site so that

the phosphoryl transfer reaction can occur, allowing the NTP to be added to the nascent RNA chain (17, 18). Of course, RdRps are notoriously unfaithful, and make errors approximately once per round of genome replication (7). Several residues in the RdRp have been found to be important to increasing and decreasing replication fidelity, which are further discussed in the RNA virus fidelity subchapter.

Other enzymatic activities, such as 5'cap synthesis, are also performed by RdRps, but these functions are distinct to different virus families. Alphavirus replication and other RdRp functions are further discussed in "alphavirus replication."

RNA Virus Quasispecies

Most virus RdRps generate an estimated 1 mutation for every 10,000 bases, which is the approximate genome size of many RNA viruses (7). Theoretically, a mutation is equally likely to occur at every possible base during a replication cycle, with some mutations occurring more than once. This cloud of virus sequence diversity is termed a quasispecies, defined as a collection of closely related virus variants. These variants all cooperate together to contribute to the overall population phenotype (19, 20). Although the mutation rate for RNA viruses is high, with most mutations acting as deleterious or neutral depending on the effects on RNA secondary structure or protein sequence, the large population sizes produced during the rapid population growth of RNA viruses results in an overall effective strategy for swift adaptation (21).

While it is valid to assume that every position in the genome will mutate during the infection of each cell to result in a somewhat balanced amount of virus diversity at each position, this is not what actually occurs. Instead, hot and cold spots of diversity are produced (22). Hot spots likely represent malleable regions where mutations are unlikely

3

to decrease fitness, while mutations in cold spots are apt to result in adverse or possibly lethal outcomes for the virus. It is not well understood how these regions are determined, but the distribution of these hot and cold spots likely has ramifications for viral fitness.

For viruses, fitness is generally defined as the ability of the virus to replicate and produce progeny, usually measured by virus growth in cell culture (23). Even when examined *in vivo*, these methods can oversimplify or misrepresent the real world effects of the analyzed mutations, so it is important to be mindful of over interpretation of results. For example, the ability of a virus to form plaques does not necessarily correlate well with pathogenesis *in vivo*. Additionally, attenuation *in vitro* does not always translate to attenuation *in vivo*. For example, a clone-derived ZIKV was attenuated in mosquito *Ae. albopictus* C6/36 cells, but not in *Ae. aegypti* mosquitoes. (24). However, careful use of multiple measures of fitness can help to better understand the role of novel mutations during scenarios such as outbreaks or host switching. Additionally, there is the potential to predict high fitness mutations before they become actualized in the real world. For example, studies using PV and CHIKV have separately demonstrated that fitness-increasing mutations can be identified in ancestral virus populations (25, 26). However, it is much easier to validate a mutation that is already known to increase virus fitness than it is to predict one that will occur in the future, especially when many fitness-increasing mutations are reliant upon epistatic interactions (27-29).

The mutational spectrum for an RNA virus can be visualized as a 3D field, with multiple peaks and valleys representative of virus fitness (Illustration 1). The virus consensus sequence forms the foundation of the fitness landscape, allowing the virus population to explore this landscape through genetic drift, with the prospect of finding

and climbing new fitness peaks (30). This landscape is prone to change, with the magnitude, location, and frequency of the peaks and valleys changing through both time and space (20, 22). Due to the high mutation rates produced during RNA virus replication, the best strategy for an RNA virus to succeed in this plane is to produce a foundation composed of low rolling hills, termed survival of the flattest (31, 32). Thus, mutations away from the consensus sequence should not have large, detrimental effects as the sequence space is explored, but there is still the potential to find fitness peaks that aid in survival during a changeable environment. However, survival is not guaranteed, and the mechanisms that allow for the ubiquity of RNA viruses can also be used against them.

It is hypothesized that RNA viruses live on the edge of an error threshold, such that any increased mutational burden will cause the extinction of the virus population (30). This error threshold is difficult to define, and likely dependent upon a fluid environment, making the exact definition even more difficult, if not impossible (22). Pushing virus populations over this error threshold has been examined empirically by exposing RNA viruses to various mutagens, most commonly with Ribavirin, a nucleoside analog that is able to pair with cytosine or uracil. As the concentration of a nucleoside analog is increased, so does the virus mutation frequency, until finally the population succumbs to the pressure and becomes extinct (33-36). Recently, CVB3 and FLU mutants were engineered to be 1 mutation away from a stop codon for each leucine or arginine codon. These mutants replicated identically compared to the unaltered viruses. However, when exposed to nucleoside analog treatment, these viruses were very sensitive, with sharp decreases in virus titer, demonstrating how close viruses are the

edge of a tolerable mutation burden (37). When the nucleoside analog concentration is high enough to cause virus extinction, this is termed error catastrophe, broadly defined as an overproduction of mutations resulting in an unstable virus population that is unable to rescue itself from extinction (22).

The multifactorial effects of nucleoside analog treatment complicate the accurate detection of error catastrophe, however. For example, in addition to acting as a nucleoside analog, Ribavirin has been shown to have other functions (38), such as decreasing intracellular GTP levels, resulting in downstream effects such as interfering with the capping of RNA and impeding RNA virus transcription and translation (39-43). There is also evidence that Ribavirin treatment alters the immune responses (44) and inhibits viral RNA polymerases (40). Additionally, the nucleoside analog 5FU not only acts as an analog for uracil, but has also been show to inhibit thymidylate synthase, required for the synthesis of DNA (45).

Work with fidelity mutants suggests that error catastrophe can still occur without pressure from a nucleoside analog. Regarding the study that mutated CVB3 to be more likely to produce stop codons, drops in titer were even more dramatic when a low-fidelity mutation was inserted into the genome, resulting in very little infectious virus (37). Additionally, other studies have found that low-fidelity mutants subjected to bottleneck passaging can quickly become extinct, providing further evidence of an error threshold (18, 46).

The ability of RNA viruses to rapidly restore their quasispecies diversity helps them survive severe bottlenecks, which occur many times within as well as between hosts (32). Bottlenecks occur when a population undergoes a reduction in the size of the

population, potentially changing the proportion of different genotypes. Importantly, bottlenecks act stochastically, which can have large effects on evolution as minority variants may come to dominate the population after a bottleneck, changing the course of evolution. It is not uncommon for viruses to undergo severe bottlenecks, with only a few virions seeding an infection or crossing barriers within the host (32, 47, 48). This could partially explain why so many viruses cause asymptomatic infections.

When viruses are passaged using bottlenecks, such as plaque-to-plaque transfers, this usually results in rapid attenuation of the virus (48-52). This attenuation is believed to be due to Muller's ratchet, which is the inability of an organism that does not reproduce using sex (e.g. viruses) to revert mutations that reduce fitness, resulting in an over-accumulation of deleterious mutations and possible, although unlikely, virus extinction (51). Interestingly, viruses attenuated by bottleneck transfers can be rescued by just a few large population passages (36), and there is evidence that quasispecies can retain memory of previous infections (i.e. minority variants previously associated with fitness gains in a different environment tend to remain in the virus population unless removed by bottlenecks), possibly aiding in this rescue (53, 54).

Another compelling piece of evidence for the existence of an RNA virus error threshold is the conserved host APOBEC protein family (55). Members of this family are cytosine deaminases, which change cytosine bases to uracil. Some of these members, such as AG3, appear to have antiviral functions, acting primarily by targeting and mutating retroviruses, such as HIV (56). This demonstrates that mutating a virus' sequence is an effective mechanism of protecting the host.

Advances in sequencing have allowed for a much better understanding of the subtle variation found within virus populations. Research using fidelity mutants as controls will be necessary to better understand quasispecies dynamics and how this correlates with important factors such as LAV safety, virulence, and host jumping.

RNA Virus Recombination

For RNA virus recombination to occur, at least two viruses must infect the same cell. Recombination can occur for any RNA virus, but positive-sense, monopartite RNA genomes that replicate using an RdRp will be the focus of this subsection.

RNA virus recombination primarily occurs when the RdRp switches from the RNA strand being replicated to a new RNA strand (i.e. copy choice recombination) or, less frequently, by ligating together cleaved RNA strands. Both homologous recombination, where the RdRp switches to a template with high sequence similarity, and nonhomologous recombination, where the RdRp switches to a template with low sequence similarity, can occur (Illustration 1.2). However, because homologous recombination is more likely to result in viable virus genomes, these are more likely to be identified (57).

It is not well understood why recombination occurs in all cases, but it is more likely to arise in regions with high amounts of RNA secondary structure and AU-rich sequences (57). Additionally, other factors, such as sequence homology between the two RNA strands and altered replication kinetics have been implicated in changing the rate of RNA recombination (57).

Depending on the RNA virus family, recombination is believed to be highly common (e.g. *Picornaviridae* (58)) or uncommon (e.g. *Flaviviridae* (59)). Even in virus

families not believed to undergo recombination frequently, DI particles (i.e. viruses with large deletions in their genomes that require a helper virus and interfere with the growth of untruncated virus) have been frequently observed (60). These DI particles are usually observed *in vitro* (60, 61), and are thought to be an artifact of passaging virus at high MOIs, but have also been found *in vivo* (62).

The importance of recombination to RNA virus evolution is hotly debated, and likely differs depending on the virus. Indeed, it may be an artifact of the RdRp, with the quasispecies produced during replication, as well as the large population sizes, as the true forces under selection for high RNA virus fitness (57). A PV mutant with a decreased ability to recombine was recently isolated (63). Interestingly, no change in fidelity was observed, suggesting that the two mechanisms for RNA virus genome evolution are not necessarily connected. This may not be true in all cases, however, as a low-fidelity SINV mutant was found to create more DI particles, indicating a link between fidelity and recombination for this virus (64).

The advent of new NGS techniques designed specifically to examine RNA virus recombination is now allowing recombination to be understood at the level of minority variants (65). This technology in combination with fidelity and recombination mutants presents an exciting new opportunity towards better understanding where recombination occurs in the virus genome, the frequency of this occurrence, and its role in RNA virus evolution.

RNA Virus Fidelity

Poliovirus

The first and most famous RNA virus fidelity variant was first discovered by passaging PV in the presence of the nucleoside analog, Ribavirin (66). During this passaging, multiple synonymous transition mutations appeared in the RdRp, as well as one nonsynonymous mutation, G64S. When this mutation was inserted into the PV genome, this mutant was found to grow as well as the parent virus *in vitro*, was resistant to multiple nucleoside analogs, and was much slower to revert a mutated sequence necessary for PV guanidine hydrochloride resistance, all suggestive of a high-fidelity phenotype. Although the mutant grew well *in vitro*, G64S PV was slightly, but consistently outcompeted by the parent virus when passaged together (66). Later, it was reported that this mutant was attenuated *in vivo* using PVR transgenic mice, as G64S PV was able to grow well in the muscle when injected IM, but severely restricted in its ability to disseminate into the brain (67). This was not caused by an inability to grow in these tissues, however, as mice infected IC were completely susceptible to infection by G64S or parent virus.

Soon after these reports, Vignuzzi et al. (68) independently recovered the G64S mutant, also by passaging PV in cells cultured with Ribavirin. The G64S mutant acted very similarly in the hands of a different lab, with no alteration of growth kinetics *in vitro*, as well as reduced lethality *in vivo* and restricted tissue tropism, with G64S virus unable to infect the CNS when introduced by the IM route. Confirmation of high-fidelity genome replication was performed by RT-PCR of passage 3 virus stock followed by high throughput TOPO cloning and sequencing of a fragment of the virus genome. This found the G64S virus population to be approximately 5.6 times less error-prone than the parent virus. Most intriguingly, artificial expansion of the G64S virus quasispecies caused this

virus to increase in lethality while still maintaining the G64S mutation. However, when virus isolated from these mice was used to infect naive PVR mice, the G64S mutant was attenuated once again. This experiment provided very strong evidence for the quasispecies theory of RNA virus evolution by demonstrating that it was the diversity in the population that caused severe virulence *in vivo,* not any single mutation.

Later, Vignuzzi et al. (69) demonstrated that other amino acids in this position were also able to increase fidelity, such as G64A and G64T, albeit to a lesser extent than G64S. These initial studies with PV provided a strong prototype for future fidelity variants to be compared against.

Common Characteristics of Fidelity Mutants

In the years since the identification of high-fidelity PV, a large number of fidelity variants have been identified from a diverse number of RNA virus families, such as *Picornaviridae* (18, 46, 67, 68, 70-79), *Togaviridae* (80-82), *Flaviviridae* (83, 84), *Caliciviridae* (85), *Arteriviridae* (86), *Orthomyxoviridae* (87, 88), and *Coronaviridae* (89, 90). The first fidelity mutants were identified similarly to the high-fidelity PV mutant by passaging virus multiple times in the presence of a nucleoside analog, usually Ribavirin. Over the course of this passaging, the virus titer would rise as it adapted to the nucleoside analog, and the full genome or RdRp would be sequenced until promising SNPs appeared. Of course, this usually revealed that many mutations had occurred, and these would be inserted individually or as a collection into the original virus using reverse genetic techniques and tested for fidelity perturbations. This is a rather laborious process with no guarantee of success, so most fidelity mutants have been identified by rationally targeting conserved residues that were previously implicated as fidelity regulators. Using

these different techniques, over 50 fidelity mutants have been identified and characterized. Although the virus families are highly diverse, fidelity mutants share many common characteristics.

One necessary test for altered fidelity is to examine resistance to different nucleoside analogs. High-fidelity viruses are resistant to multiple nucleoside analogs, likely due to decreased nucleoside misincorporation, which correlates with higher fidelity overall. Low-fidelity mutants are less straightforward. Low-fidelity mutants generated by mutating residues important for high-fidelity are more sensitive to nucleoside analog treatment, regardless of the analog. However, low-fidelity mutants identified during nucleoside analog passaging are resistant to the nucleoside analog used for the identification, but are not necessarily resistant to other analogs (74, 83, 88). In concordance with this, low-fidelity mutants have been shown to exhibit higher fidelity for the specific mutations selected against by the nucleoside analog, but lower fidelity for other mutations, balancing out to lower fidelity overall.

Fidelity mutants generally do not exhibit attenuation during 1-step growth curves, which are typically performed using HeLa or BHK cells. The only exceptions to this are the arbovirus low-fidelity mutants (82, 83), which exhibit significant attenuation in mosquito cells but not vertebrate cells, and the high-fidelity PV mutant (67), which was attenuated in primary mouse embryonic fibroblast cells but not HeLa cells. Replication kinetics assays may not be sensitive to small differences between viruses (e.g. due to slight differences in timing the beginning of the virus infection, collection times, and pipetting errors, it is difficult to determine if 2-3-fold differences in titer are accurate between different viruses), so if the RdRp is able to be isolated, a biochemical assay can

be used to determine the exact rate of nucleotide addition (further detailed in "Molecular and structural determinants underlying fidelity"). In brief, high-fidelity mutants incorporate nucleotides at a slower rate, but more accurately (38, 71, 77, 83), while low-fidelity mutants incorporate nucleotides at a faster rate, but with more mistakes (18, 46, 77, 83). These differences are sometimes severe enough to change the specific infectivity of a virus (i.e. the ratio of virus RNA to PFU) (46, 70, 82, 83, 89, 90) or relative fitness (66, 68, 76, 78-80, 88, 90).

Many different methods have been used to calculate fidelity changes. One method isolates virus RNA from EP stock or low passage virus, ranging from 1 to 5 passages. Many groups have used these stocks to measure mutation frequency as in the early PV studies, using RT-PCR followed by TOPO cloning to screen for variants. NGS analysis has improved dramatically since these first studies, so newer publications also include data showing the amount of diversity generated across the entire virus genome. Due to differences in NGS pipelines and diversity calculations, as well as differences in the number of virus passages, it is difficult to compare mutation frequencies from different papers. For example, differences in methods are likely why the HEV71 fidelity mutants (72) produce such a large difference in diversity relative to the other fidelity mutants (Figure 1.2). While using virus stocks grown in cells make it difficult to tease apart mutations promoted by selection versus inherent differences in the production of mutations, most fidelity mutants appear to produce ±1.5-2-fold change in diversity compared to the parent virus (Figure 1.2). Although these differences in diversity appear small, these alterations have been shown in multiple viruses to translate to significant attenuation *in vivo* (18, 46, 67, 69, 71, 73, 76-80, 82, 86, 87).

Fidelity mutants are generally attenuated *in vivo*, with increased survival and tissue restriction. It is not well understood why certain organs fail to become infected with fidelity variants, especially when different routes of inoculation are used, but this is likely due to increased sensitivity to host bottlenecks. IFN may be a factor, but this was only observed for a high-fidelity low-recombination PV mutant (91). Arbovirus fidelity variants are usually more attenuated in the mosquito host, with lower virus titers or even almost complete restriction (80, 82, 83). This pressure can be intense enough to select for complete reversion of the fidelity altering mutation, as observed for the low-fidelity CHIKV and SINV mutants (82).

Molecular and Structural Determinants Underlying Fidelity

To date, fidelity mutants have mostly been identified in the viral RdRp. The only exceptions are the coronavirus ExoN mutants (89, 90) and a mutation in the alphavirus helicase gene, nsP2, found to increase CHIKV fidelity (81). Coronaviruses are members of the Nidovirus family, some of which have evolved uniquely large RNA genomes (i.e. >20kb). The ability of these large RNA viruses to persist is credited to the ExoN gene, which is a proofreading exoribonuclease (92). When this proofreading function is ablated, RdRp fidelity drops by approximately 20-fold (89, 93). Interestingly, when a MHV ExoN mutant was passaged hundreds of times, fidelity slowly increased, likely due to compensatory mutations that occurred in ExoN, as well as the RdRp, but reversion of the original ExoN mutations never occurred (90).

Of the fidelity mutants that induce changes in the RdRp, structural analyses show negligible effects on RdRp structure. Instead, changes in fidelity appear to be mediated by alterations in RdRp kinetics and molecular dynamics (94).

RdRp NTP addition can be broken down into 5 steps (Illustration 1.3) (94). First, an NTP binds the RdRp, which causes a conformational change (step 2) and activates the RdRp (step 3). The NTP is then added to the RNA chain, leading to another conformational change and translocation of the RNA (step 4). Finally, the pyrophosphate leaving group is released (step 5), allowing the cycle to begin again. Steps 2 and 4 are rate-limiting, so fidelity changes are believed to only alter these two steps.

Fidelity mutants are usually found in motifs A and D of the RdRp active site (18, 46, 70, 71, 77), although other regions of the RdRp have been implicated in modulating fidelity. Mutations in the active site appear to alter fidelity by mutating residues that change conformation depending on whether the incoming nucleotide is correct or not by acting on the rate of polymerase incorporation, not the rate of NTP selection (74, 95, 96).

Unlike the RdRp mutations found in the polymerase core, high and low-fidelity G64S and H273R PV mutants are found on the periphery of the RdRp protein in the fingers domain. The current mechanistic theory for high-fidelity PV is that the G64S substitution interacts with other conserved residues in the RdRp active site, specifically motif A, to hydrogen bond to and orient the incoming nucleotide. The G64S mutation causes a misalignment of this hydrogen bond, which causes the misalignment to be even more severe when an incorrect nucleotide binds, thus increasing RdRp fidelity (97). Alternatively, low-fidelity H273R PV decreases fidelity by favoring an open state of the RdRp, which decreases the duration of this fidelity checkpoint, thus increasing the likelihood of NTP misincorporation (98).

Fidelity Mutants as Live-Attenuated Vaccines

RNA virus fidelity mutants are promising vaccine candidates due to increased *in vivo* attenuation and therefore an increased safety profile. High-fidelity vaccines for RNA viruses are of particular interest, because reducing the naturally high replication error rate should also increase the genetic stability of the vaccine. However, few of the above described fidelity mutants have ever been tested as vaccines.

Early in the fidelity variant literature, high-fidelity G64S PV was tested for its genetic stability and efficacy as a vaccine (69, 99). To examine stability, the miRNA let-7 was inserted into the PV genome, and cells expressing the miRNA were infected with parent or high-fidelity PV. The parent PV quickly mutated this miRNA sequence and began a productive infection, while G64S variant necessitated an additional 48 hours before it was also able to overcome this selection pressure. Interestingly, all G64S isolates contained the same deletion to remove the let-7 miRNA, while the parent virus isolates reverted using different nucleotide mutations and deletions. This suggests that although high-fidelity viruses are able to revert that these reversions are predictable, and can thus be anticipated and prepared for. When tested as a vaccine, the G64S mutant was shed approximately 100-fold less in feces than the parent virus. Additionally, G64S vaccinated mice produced slightly, but not significantly higher neutralizing antibody titers, and were able to fully protect against challenge.

More recently, a low-fidelity PV mutant, H273R (79), was found to provide complete protection when used as a vaccine, but only after a high dose of 10^7 PFU, which resulted in the paralysis of approximately 10% of vaccinated mice. Neutralizing antibody titers were correlated with protection, but the fidelity mutant appeared to require a 100 to 1000-fold higher dose to produce a similar neutralizing antibody titer to the parent virus.

While it is unknown whether H273R is prone to reversion, this mutant was shown to be very sensitive to bottlenecks, undergoing population extinction at a 10-fold higher PFU than the parent virus. This suggests that additional attenuating mutations would be necessary to improve the safety of this vaccine, but only if these mutations would not further reduce immunogenicity, necessitating a higher vaccine dose.

The only non-PV fidelity mutant to have been studied as a vaccine was a mouse-adapted SARS CoV (99). When the ExoN gene from SARS-CoV was mutated to remove its proofreading activity, the mutation frequency increased 11.5-fold, but there was no change in replication kinetics compared to the parent virus (99). This decrease in fidelity was stable, with a much higher accumulation of mutations during ExoN mutant SCID mice infection compared to a similar infection with the parental virus. Even after 3 murine passages, the virus remained attenuated, while the parent virus became completely lethal after 1 passage. As a vaccine, the mutant was well tolerated, even in immunocompromised hosts. The ExoN mutant was protective against challenge, and stimulated a neutralizing antibody response. However, how this compares to the parent virus or any other vaccine is unknown.

While the vaccines described above were designed to exhibit altered fidelity, these might not be the only LAV candidates with altered fidelity. Although empirically derived decades ago (100), the live-attenuated YFV vaccine 17D has been implicated as a putative high-fidelity vaccine due to multiple studies that have shown decreased 17D genetic variation compared to the YFV Asibi strain used to generate 17D (101, 102). The major success of 17D could be partially attributed to this increased fidelity, with only a small number of potential vaccine-associated YF out of the hundreds of millions of total

17

vaccinees (103, 104). This suggests that an attenuated fidelity mutant could indeed serve as a safe, effective vaccine.

ALPHAVIRUS

In the ongoing arms race between humans and arboviruses, arboviruses (arthropod-borne viruses) and their vectors are winning. The global incidence of arboviral disease is steadily increasing, and there remains a dearth of vaccines and antivirals for the overwhelming majority of these pathogens (105). Interestingly, all arboviruses, with the exclusion of African swine fever virus (106), are RNA viruses, suggesting that the diversity generated during RNA replication aids greatly during a two-host transmission cycle. Most arboviruses are from the *Bunyaviridae*, *Flaviviridae*, or *Togaviridae* virus families, all of which include pathogens of high importance to human health.

Of the two genera *Togaviridae* family, the alphavirus group is composed of 10 virus complexes, containing over 30 species (Figure 1.3), most of which are mosquito-transmitted arboviruses maintained in enzootic cycles (107). Species belonging to these different complexes are found worldwide, with members both on land and in the ocean. Due to the wide geographic distribution of alphaviruses, it is hypothesized that the original alphavirus members originated in the Pacific Ocean, where viruses repeatedly emerged on land and adapted to new hosts (108).

Alphaviruses are roughly classified as belonging to Old World or New World virus groups. However, this classification is not a hard rule, as some Old World viruses are found in the Americas, such as MAYV and AURA, and vice versa (109). Human disease caused by New World alphaviruses can result in encephalitic manifestations, while Old World alphaviruses are primarily associated with arthralgias (109). Although

human disease due to alphavirus infection is prevalent, there are no vaccines or antivirals that have been approved for human use.

Alphavirus Structure

Alphaviruses form an approximately 70nm in diameter icoahedron structure (T=4) (110), constituted by a nucleocapsid coated with an envelope (111, 112). The nucleocapsid is comprised of 240 capsid proteins, which encapsulate the viral RNA (111). Surrounding the nucleocapsid, the lipid envelope contains 80 spikes composed primarily of E2 and E1, with small amounts of 6k (113, 114) and occasionally E3 (109, 111). Spikes are formed by three heterodimer E2/E1 glycoprotein complexes, which twist together at the spike base in a counter-clockwise orientation. At the spike peak, this relaxes and the complexes separate (109).

Alphavirus Genome

The alphavirus genome is a 5' capped and 3' polyadenylated single-stranded RNA genome of approximately 11.5kb. The first two-thirds of the genome encode the nonstructural genes, while the last third of the genome encodes the structural genes under the control of a subgenomic promoter (Illustration 1.4) (109).

Alphavirus Lifecycle

ALPHAVIRUS ATTACHMENT AND ENTRY

Virus attachment occurs when the E2 glycoprotein binds a host-cell receptor, commencing cell-mediated endocytosis (Illustration 1.5) (115). Alphavirus host cell receptors are not well understood, but studies with SINV have shown that DC-SIGN and L-SIGN (116), especially when using virus isolated from mosquito cells, and laminin (117) are important for efficient SINV entry into mammalian cells. Heparin sulfate has

also been reported as a potential alphavirus receptor, but it is not well understood if this is just a cell culture adaptation or important in a natural virus lifecycle (118-120), although a recent study found heparin sulfate binding to increase EEEV neurovirulence in natural isolates (121). Occasionally, viruses are transported into the cell using the caveolar/raft pathway or other GTPase-dependent pathways, but the most common transportation pathway uses clathrin-coated pits (117).

Once internalized, these clathrin-coated vesicles fuse with an endosome (122, 123), leading to a drop in pH, which irreversibly changes the virion spike structure. E1 homotrimers then penetrate and fuse with the endosomal membrane, allowing release of the virus genome into the cytoplasm (124-126). While Old World viruses, such as SINV and SFV, fuse with early endosomes, studies with VEEV suggest that this is not universal, as VEEV also uses late endosomes (127). Additionally, most alphaviruses require cholesterol for efficient fusion, with the exception of VEEV (127), likely due to a serine residue at position 226 in E1, which when inserted into SINV and SFV reduces cholesterol dependence (128). This residue was also implicated in increasing *Ae. albopictus* mosquito CHIKV infectivity during the explosive 2005-2006 La Reunion outbreak (27, 28, 129, 130), as well as later outbreaks in Asia (131).

ALPHAVIRUS REPLICATION

After genome escape into the cytosol, the nsPs are immediately translated by host ribosomes (Illustration 1.5) (109). The nonstructural proteins, nsP1, nsP2, nsP3, and nsP4, are necessary for alphavirus genome replication (132). Also needed are the 5' and 3' UTRs, which bind the replication complex (133, 134).

Each nsP has specialized functions to contribute to replication. nsP1 aids in 5' capping of the virus genome and subgenome (135), and acts as the anchor for the replication complex (136). The nsP2 C-terminus contains a protease, and a helicase in its N-terminus (137, 138). The N-terminus of nsP3 is believed to bind host ADP-ribose 1-

phosphate phosphatase (139), while the C-terminus contains a hypervariable region that has been shown to interact with stress granules of the G3B family for Old World alphaviruses (140, 141) or fragile X syndrome protein family members for New World alphaviruses (142). These stress granules are required for virus replication complex assembly and increase its avidity to RNA (141). Finally, nsP4 is the RdRp, which has a high turnover rate due to an N-terminal tyrosine that targets the protein for degradation via ubiquitin-dependent proteolysis (143). The C-terminus of nsP4 shares similarity with other RdRps (144, 145), while the function of the N-terminus is unknown but necessary for replication (146). However, one function of the N-terminus is to add adenosines to the terminal end of the 3'UTR (132, 134, 147). Importantly, various amino acid mutations in nsP4 have been shown to alter binding to different nucleotides, suggesting that different protein residues are involved in the addition of each nucleotide (148, 149).

Pull-down experiments have shown that each nsP binds the other three nsPs (150). It is believed that as the polyprotein is cleaved, different conformations form, changing the virus genome strands that are replicated (109). Unfortunately, the structures for most alphavirus nsPs are unsolved or only partially solved, making it incredibly difficult to completely understand the steps that occur during replication. However, biochemical and genetic studies have made some characterization possible.

Due to a leaky opal stop codon between nsP3 and nsP4, there is an approximately 1:10 ratio of nsP1-nsP2-nsP3-nsP4 polypeptide to nsP1-nsP2-nsP3 polypeptide (151). Upon translation, nsP4 is immediately cleaved from the polyprotein chain (152). During early genome replication, when nsP1, nsP2, and nsP3 are still bound together, only minus-sense strand synthesis occurs (153, 154). This synthesis occurs in membrane-associated spherules, which are invaginations located on plasma membranes or virus-induced cytopathic vesicles (155, 156). nsP2 then cleaves the bond between nsP1 and nsP2 *in cis* (152). This begins the synthesis of positive-sense RNA, but minus-sense replication is still ongoing. Importantly, no subgenomic RNA is being produced. Finally,

21

the nsP1-nsP2 cleavage reveals an activator sequence in the N-terminus of nsP2, resulting in the cleavage of nsP2-nsP3 *in trans* by nsP2, and the production of positive-sense genomic and subgenomic RNA (152). This entire process takes approximately 3-4 hours (109).

ALPHAVIRUS GLYCOPROTEIN PROCESSING AND VIRUS EXIT

As the subgenomic RNA is translated, the capsid protein is automatically cleaved via autoproteolysis (Illustration 1.5) (157). The free capsid proteins bind full-length virus RNA using conserved sequences in the 5' end of the genome to form nucleocapsids (158).

The remainder of the structural polyprotein (PE2-6k-E1), travels to the ER, guided by a signal sequence in E3 (158). This complex anchors in the ER using hydrophobic sequences in E2 (159), and is cleaved between PE2 (the precursor to E2) and 6k by a signal peptidase (157, 160). In the ER, the glycoproteins are folded by host chaperones (161, 162) and become heavily glycosylated in the ER lumen, which are modified as the glycoproteins mature (163, 164). Following the ER, pE2 and E1 form heterotrimers (165), and travel to the Golgi complex, where E3 cleavage occurs by the host protease, furin (166-168). The E2-E1 heterotrimer migrates to the cell surface, where it anchors in the cell membrane. Finally, nucleocapsids interact with the C-terminal E2 glycoprotein tails (169), forming enveloped virions, which bud from the cell surface.

VENEZUELAN EQUINE ENCEPHALITIS VIRUS

VEEV is a mosquito-transmitted New World alphavirus found primarily in Mexico, Central America, and northern countries in South America (i.e. Colombia, Venezuela, etc.). It was first identified in the late 1930's from the brains of encephalitic horses (170, 171), and immediately realized to be similar to eastern and western equine encephalitis viruses (171).

VEEV can cause a spectrum of disease in humans, ranging from asymptomatic to flu-like illness to encephalitis (172, 173). While equine mortality during epidemic cycles is high, ranging from 19-83%, VEEV causes death in less than 1% of humans. However, encephalitis occurs in 4-14% of cases, most commonly in children, resulting in neurologic sequelae that can necessitate life-long medical care (174). The only therapeutic care available for VEE is supportive, and vaccines are only approved for use in equids.

VEEV is primarily found in swamps and forests, perpetuated in an enzootic cycle between rodents and enzootic mosquito hosts, the exact species of which are dependent upon the habitat (Illustration 1.6) (173). Spillover events from these enzootic cycles are common (175, 176), as has occurred in 1971 (177), 1995 (178), and 2003 (179). Occasionally, this spillover begins an epidemic, which is amplified between viremic horses and epizootic species of mosquitoes, resulting in a handful to hundreds-of-thousands of infected humans per outbreak (173).

Humans are believed to be dead-end hosts for VEEV (172). While equines usually only fall ill from epizootic strains (176), humans are equally susceptible to enzootic and epizootic strains (180). Spillover from the enzootic cycle is suspected to cause tens-of-thousands of human infections annually, but misdiagnosis with other circulating arboviruses (e.g. Zika virus, dengue virus) likely obscures the true incidence (180).

Within the VEEV serocomplex, there are six main subtypes and several more varieties within each subtype (Table 1.1). These subtypes were designated decades ago using cross-neutralization serology that does not always agree with more recent genetic analyses (181, 182). However, most spillover events from enzootic cycles have been from the ID and IE subtypes, as well as Mucambo virus (180). Occasionally, a mutation arises in the E2 glycoprotein that increases the outer charge of the virion. Such mutations can increase virulence and viremia in horses (183-185), as well as enhance infectivity in

mosquito vectors (186, 187). Sequencing and phylogenetic approaches have shown that IAB and IC outbreak strains are closely related to and interspersed between ID strains (188), demonstrating that small mutations in E2 can change virus serology and act as the source of major epizootic outbreaks.

Although VEEV causes many human infections using its natural transmission cycle, it can also be easily aerosolized, and is highly infectious via this route (189). This ease of aerosolization led to VEEV being developed as a biological weapon by the Soviet Union and United States during the Cold War (189). Due to this history, VEEV is categorized by the CDC and NIH as a class B agent, with epizootic VEEV strains further classified as select agents. Therefore, many vaccine candidates have been developed to protect against aerosol exposure.

VEEV Microevolution

VEEV, like other arboviruses, evolves more slowly over time than predicted by the error-prone nature of its RdRp (8). One hypothesis to explain this phenomenon is termed the trade-off hypothesis, which predicts that a two-host transmission cycle constrains fitness for a single host to permit the highest average fitness for both hosts, resulting in lack of frequent consensus sequence change (190, 191).

Microevolution studies designed to examine the trade-off hypothesis *in vitro* have generally found that virus adaptation occurs when arboviruses are passaged in one cell type (i.e. vertebrate or mosquito cells), but usually at the expense of replication fitness in the other host (192-198). However, when arboviruses alternate between mosquito and vertebrate cells, fitness increases commonly occur, usually on par with the fitness increases observed during single-host passage. Thus, most *in vitro* passaging research suggests the trade-off hypothesis to be false.

An interesting study examined the trade-off hypothesis *in vivo* using VEEV strains from the IC and ID subtypes (199). These two virus strains were passaged 10

times in *Ae. aegypti* mosquitoes, mice/hamsters, or alternating between the two hosts. As observed during *in vitro* passaging, no fitness gains occurred for mosquito-adapted VEEV in mice or hamsters, while fitness increased for murine-adapted virus. However, there was also no change in fitness for two-host passaged virus. In mosquitoes, VEEV IC and ID infectivity increased for mosquito-adapted virus, decreased for mouse-adapted, and exhibited no change during alternating passage. Importantly, this study evidenced the trade-off hypothesis to only be true during *in vivo* passaging, as these results were not repeatable *in vitro*. Giving further support to the trade-off hypothesis, few SNPs occurred during any of the passaging conditions, a common arbovirus host-cycling observation (192, 194, 197, 200), implying that all fitness gains were mediated by changes in the virus quasispecies. However, while this study supports the trade-off hypothesis, similar *in vivo* passaging studies with WNV and SLEV do not (200-202), suggesting the trade-off hypothesis is not universally applicable.

More recently, studies using NGS have shown that fitness gains in arboviruses are commonly associated with increases in sequence diversity (198, 200, 201, 203), including a new VEEV study that demonstrated a link between increased virus diversity and dissemination in the mosquito (204). At odds with this, low-fidelity SINV is attenuated *in vivo*, suggesting that virus mutant swarm composition is important for fitness (82). However, increasing the diversity of high-fidelity PV by Ribavirin passaging also increases its virulence (68), and low-fidelity SINV has been shown to also produce high amounts of DI particles (64), which is highly likely to also play a role in its attenuation. Thus, the interplay between fidelity and recombination complicates the understanding of these evolutionary processes.

Alphavirus family members display moderate levels of recombination. The most famous example is WEEV, which is a derivative of the nsPs, UTRs, and capsid of an EEEV-like ancestor combined with the remainder of the structural proteins from a SINV-like ancestor (205), which likely occurred 1,300-1,900 years ago (206). Under laboratory

conditions, alphaviruses readily recombine when cells are electroporated or transfected using multiple RNAs, resulting in attenuated viruses characterized by deletions and insertions/duplications (64, 207-210). While these earlier experiments were not conducted with VEEV, vaccine studies of attenuated VEEV constructs used to display antigens from other viruses (i.e. Lassa fever glycoproteins), were shown to frequently recombine with helper constructs, producing VEEV titers as high as $2x10^5$ PFU/mL (211, 212). Lastly, while not strictly recombination, DI particles (213-216) and other deletion mutants (217, 218) are frequently observed for alphaviruses, although the *in vivo* relevance of these is not well understood. However, a recent study found recombination to occur *in vivo* when Atlantic salmon were infected with an SPDV deletion mutant and helper plasmid, hinting at the ability of alphaviruses to recombine in a living system (219).

Mouse Models for VEEV

Rodents play a large role during enzootic VEEV transmission, so mice are an ideal model to use to investigate various aspects of VEEV infection. Although VEEV is not universally lethal for rodents (220, 221), the most commonly used mouse models are highly sensitive, with as little as 1 PFU resulting in lethal infection, making this model ideal for testing vaccine safety (189). The varieties that are most commonly used are the BALB/c, C3H/HeN, Swiss Webster, and CD-1 varieties, which have intact immune responses. Mice infected with VEEV quickly lose weight, exhibit tremors and paralysis, and appear hunched and lethargic. It is believed that the brain infection is the major cause of lethality in mice, but lymphoid tissue damage is also severe (189).

When infected SC or ID, VEEV first infects dermal dendritic cells (222), which travel to the closest draining lymph node in as little as 4 HPI (223). From there, VEEV replicates and disseminates into the bloodstream at approximately 12 HPI, where the virus travels throughout the entire body. Most organs become infected with VEEV, but

titers are especially high in lymphoid tissues, such as the spleen and thymus, causing diffuse necrosis (223, 224). The most commonly infected cells in these tissues are mononuclear phagocytes (225). At approximately 24 HPI, VEEV enters the brain through the olfactory bulb and/or the trigeminal nerves (224, 226). Neurons are the main target in the brain (225), with infection causing necrotizing panencephalitis and myelitis (227). The virus is cleared from the serum by 3-4 DPI, but the permanent damage caused by VEEV results in death at 6-9 DPI (189).

When mice are infected via the aerosol route, the first tissues to be infected are the olfactory bulb and trigeminal nerves (227, 228). From there the virus is able to travel to the brain and cause lethal disease as it does following infection via the SC or ID routes. Because this infection route avoids the bloodstream, vaccines that stimulate a primarily IgG antibody response are not completely protective against aerosol challenge (229). To remedy this, some vaccines have been developed with the goal of increasing the proportion of IgA antibodies (230), which are found in the mucosa where aerosol infection first begins.

NHP Models for VEEV

Although mouse models are excellent tools for initial vaccine development, they do not accurately recapitulate the subtler VEEV disease observed in humans. For this, NHPs, most commonly cynomolgus and rhesus macaques, are much better, albeit less characterized, models.

Unlike mouse models, most macaques are able to survive VEEV infection, with the exception of IC inoculation. The most thorough VEEV NHP study infected 67 rhesus macaques IP with the Trinidad Donkey strain (231). As in humans, early illness is characterized by viremia, followed by fever and leukopenia (189, 231, 232). The main targets for VEEV in NHPs are lymphoid tissues, with lymphocyte necrosis in the lymph nodes and spleen, and the brain, usually characterized by multifocal perivascular cuffs

but not neuronal damage (231). Occasionally, encephalitis occurs later in infection, usually beginning approximately 6 DPI, although the likelihood and timing of this depends on the animal species, age, virus, and route of infection (189, 231). In macaques infected IN or via aerosol, the rate of brain infection is much more rapid, with lesions beginning at 48 HPI, and an overall more severe infection (233, 234).

Vertebrate Immune Correlates of Protection for VEEV

The first line of defense encountered by an RNA virus is the IFN response, which is a non-pathogen specific response to infection. Spotts et al. found that resistance to interferon α and β *in vitro* was correlated with epizootic potential (235), although this is controversial(236), and confirmed this *in vivo* by infecting immunocompetent or IFN receptor KO mice with the TC-83 vaccine strain or its virulent parent, the VEEV IAB Trinidad Donkey strain. While the Trinidad Donkey strain caused much more severe illness in immunocompetent mice, there was no difference in illness severity in the IFN receptor KO mice. This study and others suggest that an ability to resist IFN is key for alphavirus infection (237-241).

The innate immune system is not the only barrier to virus infection. It is well established that antibodies are the most important correlate of protection against alphavirus infection (242, 243), including VEEV (244). In fact, humans that do not produce antibodies against equine encephalitis viruses are at higher risk of succumbing to infection (245). These antibodies are typically directed against the envelope glycoproteins. E1 derived antibodies are usually non-neutralizing, while antibodies against E2 are neutralizing, but less cross-reactive (246). Additionally, passive transfer of antibodies is an effective means of protecting against VEEV SC and ID infection (244), but not aerosol (247, 248), demonstrating the importance of the antibody response, as well as its limitations against rapid-onset infections.

Lastly, the T-cell response for VEEV infection is not well understood. However, Th_1 cells are found in high numbers post-vaccination with TC-83 (249), suggesting a predominately inflammatory response. Additionally, when αβ-T cell receptor KO mice were infected IN with TC-83, they became chronically infected and exhibited high virus titers in the brain, suggesting that T-cells are critical for virus clearance during VEEV aerosol infection (250).

Mosquito Models for VEEV

VEEV infection of the mosquito typically begins with infection of the posterior midgut epithelial cells (251). Dissemination into the hemocoel follows this, as well as infection of peripheral tissues, such as the salivary glands. Once the salivary glands are infected, VEEV accumulates in the apical cavities, awaiting transmission to a vertebrate host (173). A disseminated infection typically occurs over the course of 2-14 days, depending on the vector and the virus strain. Although a large number of mosquitoes have been confirmed as VEEV vectors, including *Ps. confinnis* (252), *Ae. sollicitans* (252, 253), and *Ae. taeniorhynchus* (253, 254) as epizootic vectors, and a large number of *Cu. (Mel.)* species of mosquitoes as enzootic vectors (255-259), few of these have been studied rigorously in the lab.

The most commonly studied epidemic VEEV vector in the lab is *Ae. taeniorhynchus*. This mosquito is an aggressive feeder found on the eastern coasts of the Americas, particularly nearby salt marshes (260). It has been well established that epizootic mutations in the E2 glycoprotein greatly enhance VEEV infectivity for *Ae. taeniorhynchus* (185, 187). However, a tight bottleneck occurs during midgut infection, with only 28 cells infected on average with an epidemic strain of VEEV IC, 3908 (251). Another stringent bottleneck likely occurs during vertebrate infection as well, with approximately 10 PFU transmitted by mosquitoes during *in vivo* transmission (261).

Using a natural, endemic vector of VEEV greatly increases VEEV infectivity, as demonstrated by multiple experiments using *Cu. (Mel.) taeniopus*. Infection of *Cu. (Mel.) taeniopus* requires as few as 5 PFU of enzootic VEEV (262). Unlike *Ae. taeniorhynchus* infection by epizootic virus, most midgut cells from *Cu. (Mel.) taeniopus* are able to be infected with enzootic strains of VEEV, such as 68U201 (263). However, the midgut still acts as a strong bottleneck, as evidenced by a study using marked virus clones (264).

The Mosquito Immune Response to VEEV

The mosquito immune response is composed of a variety of innate immune pathways, some of these with the ability to retain memory of previous pathogens. Information about the antiviral response against VEEV in the mosquito is lacking, so the information in this subsection is derived from studies using other arboviruses.

Undoubtedly, RNAi is the most important antiviral response in the mosquito. There are three RNAi pathways, which are best defined by the type of small RNA produced: small interfering RNA (siRNA), micro RNA (miRNA), and PIWI-interacting RNA (piRNA). The siRNA and miRNA pathways are stimulated by dsRNA. Dicer-1 (miRNA) or Dicer-2 (siRNA) cleave dsRNA into 21-24bp fragments (265-267). A single strand of these small RNAs is loaded into the RNA-induced silencing complex (RISC) and is used to identify similar or identical RNA sequences. RISC cleaves matching RNA strands, which targets them for destruction (268, 269). Alternatively, the PIWI pathway generates 26-31bp piRNAs from single stranded RNA precursors. These are loaded into a homolog of RISC and, like the siRNA and miRNA pathways, used to identify matching RNAs for destruction (270, 271).

Each small RNA pathway has been implicated in antiviral defense, but the clearly predominant small RNA antiviral pathway during acute viral infection is the siRNA pathway (265, 272). However, as the infection becomes chronic, or in the absence of an siRNA response (272-274), the number of piRNAs increase, and these appear to act to

30

control chronic arbovirus infections, likely through a virus-derived, circular DNA intermediate (275).

While miRNAs do not target many areas of the virus genome, siRNA and piRNA targets are more diverse and tend to cover the entire genome, with variation in targeting intensity and strand polarity (276). Studies examining the role of RNAi in virus diversity have found increases in sequence diversity in areas most targeted by RNAi (277-281), however this has only been closely examined using WNV. A study using SFV suggests that these hotspots may be decoys for the siRNA response to target (282), indicating the ability of arboviruses to subvert the host's antiviral response. However, more work is needed to better understand this balance.

The RNAi pathways are not the only immune responses that can aid in antiviral control. For example, knockdown studies have suggested that the JAK/STAT (283) and Toll (284) pathways help to control DENV infection. Additionally, apoptosis has been correlated with decreasing WNV infection (285) and transmission (286), but inhibition of apoptosis was found to increase SINV infection (287). Further work is needed to address the knowledge gap of how the mosquito immune response interacts with New World alphavirus infection.

Vaccines for VEEV

Primarily due to biodefense concerns, multiple vaccine candidates have been developed to protect against VEEV. The first vaccines made were using formalin-inactivated VEEV (288, 289). However, these vaccine preps were not always completely inactivated, resulting in many cases of vaccine-derived VEE in humans and animals (290, 291). There were several attempts to produce a live-attenuated VEEV vaccine, but there was no success until 1961, when the precursor to TC-83 was developed. TC-83 and its formalin-inactivated version, C-84, are the only vaccines approved to protect against VEEV infection in equines, although TC-83 and C-84 are also approved for IND use in

humans. The limitations of TC-83 have spurred investigators to generate more modern vaccines, which are also discussed below.

TC-83

TC-83 is a LAV for VEEV that was developed by passaging the virulent Trinidad Donkey IAB strain in guinea pig heart tissue (292). After 80 passages, the virus still caused clinical reactions in 85% of vaccinated humans, so a substrain was derived by plaque purifying the 78th passage in chicken embryo fibroblasts. After additional passaging in guinea pig heart tissue, a plaque-derived and mouse avirulent isolate was selected and termed TC-82 (i.e. tissue culture passage 82) (293). TC-82 served as the stock to prepare TC-83.

TC-83 attenuation and efficacy has been studied in multiple animal models, and is a commonly used control to compare against new VEEV vaccine constructs. While TC-83 is safe for adult mice and hamsters with few exceptions (294), the vaccine is lethal for suckling mice (295). TC-83 is able to protect mice and hamsters against subcutaneous exposure to VEEV, but protection against aerosol challenge is not always complete (296), likely because TC-83 predominately produces IgG, not IgA antibodies (297). When mice are exposed to TC-83 via the aerosol route, lesions occur in the brain, resulting in death in C3H/HeN mice, but not BALB/c (228), demonstrating incomplete neurological attenuation of the vaccine. Additionally, like wt VEEV, TC-83 is a teratogen in mice, resulting in an increased number of still births, as well as decreased litter sizes and infant survival post-birth (298). Interestingly, hamsters vaccinated with TC-83 exhibit early protection against VEEV, as well as some degree of heterologous protection against WEEV and EEEV, likely due to exclusion of the virus from cells as this protection vanished upon secondary challenge (299). In the macaque model, TC-83 was able to fully protect against SC challenge, but only protected approximately 40% of the monkeys post-aerosol challenge as evidenced by fever and low titer viremia (300).

TC-83 is available under IND status for at-risk military and laboratory personnel in the United States. When humans are vaccinated with TC-83, approximately 40% develop adverse effects (e.g. fever, transient leukopenia, and flu-like illness) and 20% fail to seroconvert (293, 301). Additionally, the neutralizing antibody titers generated following vaccination do not equally protect against all subtypes, especially against enzootic strains, and these titers wane slightly over time (297, 302). In humans with absent or low neutralizing antibody titers, boosting with C-84 (i.e. formalin-inactivated TC-83) was effective at stimulating a more robust immune response in most individuals (303). While C-84 is an effective booster for TC-83, vaccination with C-84 alone requires boosters to maintain seroconversion.

Although TC-83 is not available to the general public, it is still used as a vaccine for horses in some VEEV endemic countries. In horses vaccinated with TC-83, febrile illness and leukopenia can occur, but the majority seroconvert (304, 305). Some horses develop a low titer viremia post-vaccination, which may be enough to transmit the vaccine, as TC-83 has been isolated from field-caught mosquitoes (306).

The ability of TC-83 to potentially enter into a transmission cycle is concerning due to the instability of its attenuation. Mouse virulent isolates of TC-83 have been collected from vaccinated horses (295), and as few as two IC passages in infant mice can cause reversion of the attenuation (292). This instability is likely due to the reliance of TC-83 on only two attenuating point mutations, one in the E2 glycoprotein (nt position 8922, amino acid position 120) and another at nt position 3 in the 5'UTR (307, 308).

The E2 glycoprotein mutation is considered to be the primary determinant of TC-83 attenuation (307), and is believed to act by increased binding to heparin sulfate, a ubiquitous protein and common cell culture adaptation, allowing for rapid clearance of the vaccine *in vivo* (118). The 5'UTR mutation alters the ratio of genomic to subgenomic RNA synthesis (309), which enhances virus replication *in vitro*. However, this

overproduction causes attenuation *in vivo* by overstimulating the innate immune response, resulting in increased IFN sensitivity (309, 310).

In summary, TC-83 is a rather poor vaccine as evidenced by high levels of adverse events post-vaccination, subpar immunogenicity and protection, and unstable attenuation.

MODERN LIVE-ATTENUATED VACCINES

LAVs are typically cost-effective and protective after one dose, as all the below vaccines are. As the alphavirus lifecycle is better understood, this has allowed for rationally designed LAVs to become possible, of which there are several.

V3526 is a mutant of the Trinidad Donkey strain that was designed to ablate the PE2 cleavage signal, resulting in an immature glycoprotein. To prevent reversion of the PE2 mutations, it also contains a mutation in the E1 glycoprotein (311). V3526 is a safe and effective vaccine for rodents and primates, and is less likely than TC-83 to revert or enter a transmission cycle (312). However, this vaccine was abandoned during a phase I trial due to adverse effects, such as fever and flu-like illness (313).

A few LAV candidates have attenuated VEEV by mutating the subgenomic promoter sequence and inserting the IRES translation signal from encephalomyelocarditis virus into the genome to alter translation and replication, as well as to block mosquito infection (314-316). When this IRES was placed antecedent to the entire structural protein cassette of TC-83, attenuation was high, but immunogenicity was poor (314). However, when only the capsid gene was under IRES control, TC-83 (315) and VEEV IE strain 68U201 (316) IRES vaccines were fully protective against challenge. Infant mice infected SC with 68U201 IRES all succumbed to infection, while 100% of TC-83 IRES infected mice survived, suggesting that TC-83 IRES would be the safer IRES vaccine. Macaques vaccinated with 68U201 IRES tolerated the vaccine well, generated high neutralizing antibody titers, and were completely protected from aerosol-challenge,

demonstrating this to be a promising vaccine that should be further researched in humans (317).

There have also been a few modern LAVs that have not been as well characterized. For example, a SINV chimera expressing the TC-83 structural genes generated slightly lower neutralizing antibody titers than TC-83, but was much less virulent and able to protect against challenge (318). More recently, TC-83 that was further attenuated using a mutated capsid and packaging signal that did not induce CPE but grew well *in vitro* and was highly attenuated *in vivo*. This vaccine was a potent IFN stimulator in BALB/c mice, and was able to generate high levels of neutralizing antibody titers resulting in full protection (319).

INACTIVATED AND SUBUNIT VACCINES

Inactivated or subunit vaccines are very safe vaccine platforms, but are usually poorly immunogenic and require boosters.

As previously discussed, early vaccines for VEEV that inactivated the virus using formalin (288, 289) were unable to guarantee that each vaccine stock contained no live virus, resulting in multiple vaccine-produced infections (290, 291). It is believed that inactivated vaccines may have been the source of multiple epizootics during this period, as evidenced by later sequencing (320). Using inactivated LAVs has proven to be much safer. The two best characterized LAVs for VEEV, TC-83 and V3526, have both been inactivated using multiple mechanisms (303, 313, 321, 322). In BALB/c mice, there was no difference in efficacy between inactivated TC-83 and V3526 vaccines, but inactivation greatly reduced immunogenicity, so multiple boosters would be required for full protection from SC exposure. Additionally, these vaccines protect poorly against aerosol exposure (313). Formalin inactivated TC-83 (i.e. C-84) is currently approved for equines in the United States.

Subunit vaccines are used to present pathogen-specific antigens, either as a virus-like particle or protein recombinant. Recombinant baculoviruses expressing most or all of the structural proteins from the Trinidad Donkey strain of VEEV were highly immunogenic in BALB/c mice and able to protect against challenge (323). Immunogenicity dropped sharply when individual glycoproteins were used, however, suggesting that subunit vaccines would require the entire VEEV glycoprotein if this construct was to be further developed.

VECTORED AND REPLICON BASED VACCINES

Unlike subunit vaccines, vectored and replicon based vaccines are able to replicate their RNA, thus providing a more robust immune response.

The first replicon vaccine candidate developed for VEEV used the type 5 adenovirus platform, which requires complementation from cells expressing E1a, an adenovirus structural protein. This vaccine incorporated the E3-E2-6k structural genes from the VEEV Trinidad Donkey IAB strain, and was poorly protective when administered IN, especially against the VEEV IC subtype (324). When this vaccine was optimized for mammalian codons, higher levels of antigen were expressed, resulting in higher IgG levels. Upon aerosol challenge, 90% of vaccinated BALB/c mice survived, a 70% improvement upon the previous replicon vaccine.

Formalin-inactivated vaccines for the encephalitic alphaviruses (i.e. VEEV, EEEV, and WEEV) are typically administered to horses as a trivalent vaccine. However, protection is not long lasting, requiring annual boosters. To remedy this, one research group constructed separate VEEV replicons to express the glycoprotein cassette from each encephalitic virus, which were also modified to delete the furin-cleavage site (232). In BALB/c mice, the VEEV replicon vaccine was able to protect the majority against SC or aerosol challenge, although efficacy was decreased when all three vaccines were given together. Macaques vaccinated using a prime-boost strategy with the VEEV replicon

alone produced neutralizing antibody titers for viruses from all VEEV subtypes, but when given with the other vaccines, the only strong and consistent response was against a IAB strain. This interference is not uncommon for alphavirus combination vaccines (299, 325, 326). Macaques vaccinated with the VEEV replicon alone were not challenged, but monkeys vaccinated with all three replicons tolerated challenge well, with slightly lower fevers and only 1 of the 6 monkeys testing positive for viremia compared to 4 of the 6 mock-vaccinated controls.

The most recent vaccine candidate for VEEV replaced the structural genes of EILV, a mosquito-restricted alphavirus, with the structural genes of TC-83 (327). The resultant chimera, EILV-VEEV, was highly attenuated, with all infant mice surviving IC injection. Crucially, there was no evidence of lesions in the brain. CD-1 mice vaccinated using this construct generated high levels of neutralizing antibody and were fully protected post-challenge. Interestingly, EILV-VEEV was able to protect 40% of mice one day post-vaccination, whereas all TC-83 vaccinated mice perished. This may be due to the much higher doses of EILV-VEEV, which were 1,000-fold higher that the TC-83 dose, possibly generating higher levels of interference. EILV-VEEV's protective efficacy was reduced to 90% when delivered as a trivalent vaccine with other EILV chimeras. The high immunogenicity and safety of this vaccine warrant further studies in NHPs.

DNA VACCINES

The earliest DNA vaccine for VEEV encoded its structural genes under the control of a CMV promoter. This vaccine was delivered to the host via a gene gun, which uses pressurized helium to propel DNA into the host at high velocity (328). Post-vaccination, BALB/c mice were entirely protected against SC challenge, while 80% were protected against aerosol challenge. In guinea pigs, the vaccine was fully protective against SC challenge, but this dropped to approximately 83% when the vaccine was given in a cocktail with other DNA vaccines, again likely due to interference. Some guinea pigs

became viremic post-challenge. Interestingly, neutralizing antibody titers were absent or very low in both animal models, suggesting that these are not necessarily required for survival. When macaques were vaccinated 4 times with this vaccine and then challenged via the aerosol route, fever was reduced and only 1 of the 3 vaccinated monkeys became viremic, whereas all mock-vaccinated animals were viremic (329).

To improve upon this vaccine, multiple alternatives were designed. The first generated an array of CMV promoted DNA vaccines that were constructed using the envelope genes of various VEEV subtypes, as well as WEEV and EEEV (330). The only version that was able to fully protect BALB/c mice against a VEEV IAB strain challenge contained the E1 glycoprotein gene from a IAB strain and portions of the E2 glycoproteins from a VEEV IE strain and WEEV. A more recent collection of DNA vaccines included multiple HLA T-cell epitopes from the structural proteins of Ebola virus, Sudan virus, and VEEV. HLA-DR3 vaccinated mice generated low neutralizing antibody titers, and were poorly protected against VEEV or Ebola virus challenge (331). Lastly, an alternative CMV promoted vaccine used codon optimized (i.e. virus with codons optimized for protein translation in mammals) VEEV structural genes and was delivered via IM electroporation. This stimulated an earlier, more robust immune response in BALB/c mice, rabbits, and macaques, and was fully protective post-aerosol challenge (332).

Due to these promising results, the codon-optimized vaccine was granted a phase I clinical trial (333). Subjects were vaccinated once via ID (0.08mg or 0.3mg doses) or IM (0.5mg or 2mg doses) electroporation, and the vaccine was well tolerated with no severe adverse events. Neutralizing antibody titers appeared 40-70 days post-vaccination and correlated with dose, with all IM vaccinated subjects seroconverting, 83% of high dose ID vaccinated subjects, and 63% of low dose ID vaccinated subjects. These promising results suggest that further investigation of this vaccine, especially via the IM route, is warranted.

Finally, a more recent DNA vaccine used the entire TC-83 genome under the control of a CMV promoter (334). Termed an iDNA vaccine, when electroporated *in vitro* or *in vivo*, all of the TC-83 proteins are expressed, therefore beginning a self-perpetuating TC-83 vaccine. Moderate levels of neutralizing titers were generated in BALB/c mice, and all were protected against challenge.

IMPETUS FOR THIS PROJECT

During the replication of all RNA viruses, there is a high probability of incorporating mutations that affect virulence or pathogenesis due to the lack of an exonuclease proof reading function in the RdRp. For LAVs that utilize the virus' own replication machinery, this ability to incorporate mutations has implications for stability, as replication may result in mutations that either restore the wild-type phenotype via reversion or compensate for the attenuating mutations (pseudoreversion) by increasing virulence. There has been recent interest in increasing the safety of live-attenuated RNA virus vaccines by altering polymerase fidelity. Increasing virus fidelity results in a more clonal virus population that is less able to adapt to immune pressures or environmental changes. Alternatively, lowering virus fidelity results in an increased number of unfit progeny due to the higher number of mutations. Either way, altering RNA virus fidelity lowers virus population fitness, while also maintaining or increasing immunogenicity when used as a vaccine (69, 79, 99). However, this work has all been performed using virulent viruses, which are likely not attenuated enough for vaccine use.

To address this gap, the goal of this proposal is to test RdRp mutants of the VEEV LAV strain, TC-83, for changes in fidelity, virulence, immunogenicity, and genetic stability relative to parent TC-83. As TC-83 is a rather poor LAV, we believe that TC-83 is an excellent model to determine if altering fidelity can increase vaccine efficacy and safety. We hypothesize that TC-83 fidelity altering mutations will result in a safer, more

39

immunogenic LAV that is less able to enter and propagate itself using the VEEV transmission cycle. This will be examined using three aims.

Aim 1: Identify VEEV TC-83 fidelity mutant.

This aim will test the hypothesis that RdRp mutations identified during 5FU passaging of TC-83 will be fidelity-altering mutations, which will increase vaccine safety and immunogenicity in a vertebrate host.

Aim 2: Determine if low-fidelity TC-83 is restricted in the mosquito vector.

This aim will test the hypothesis that low-fidelity TC-83 is less fit than the original TC-83 in the mosquito.

Aim 3: Determine the stability of low-fidelity TC-83 mutations.

This aim will test the hypothesis that low-fidelity TC-83 is less able than the parent TC-83 to revert or pseudorevert attenuating mutations
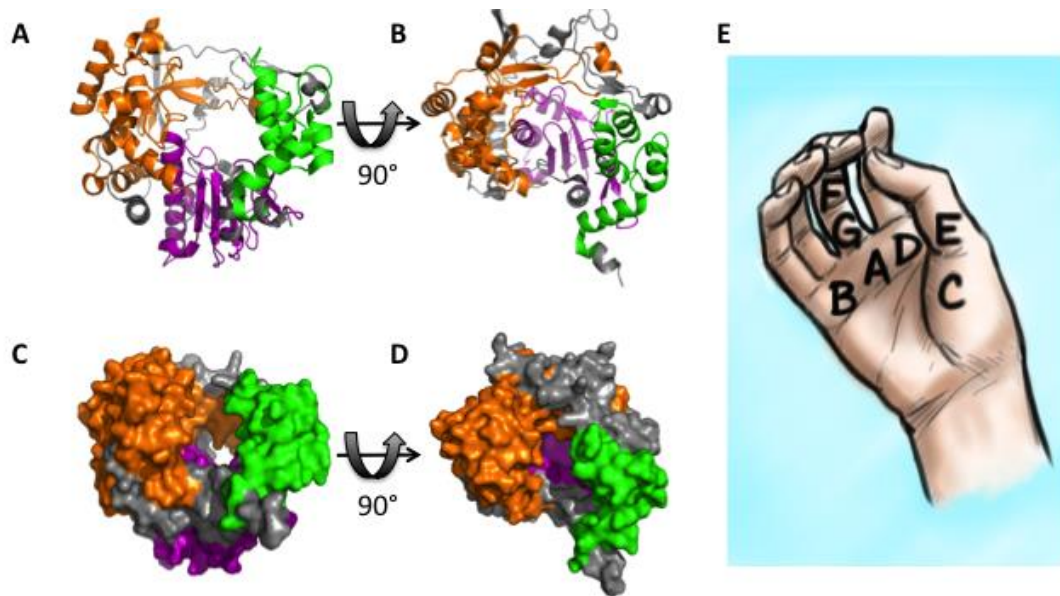
Figure 1.1: RdRp structure of the FMDV 3D polymerase protein

The FMDV RdRp structure (335) was downloaded from the RCSB PDB and visualized in PyMol v1.8.4.0 (336). Structure (A&B) and surface models (C&D) are depicted. The RdRp is color-coded with the fingers as orange, the palm as purple, and the thumb as green. Location of conserved RdRp motifs as visualized on a right hand diagram (E).
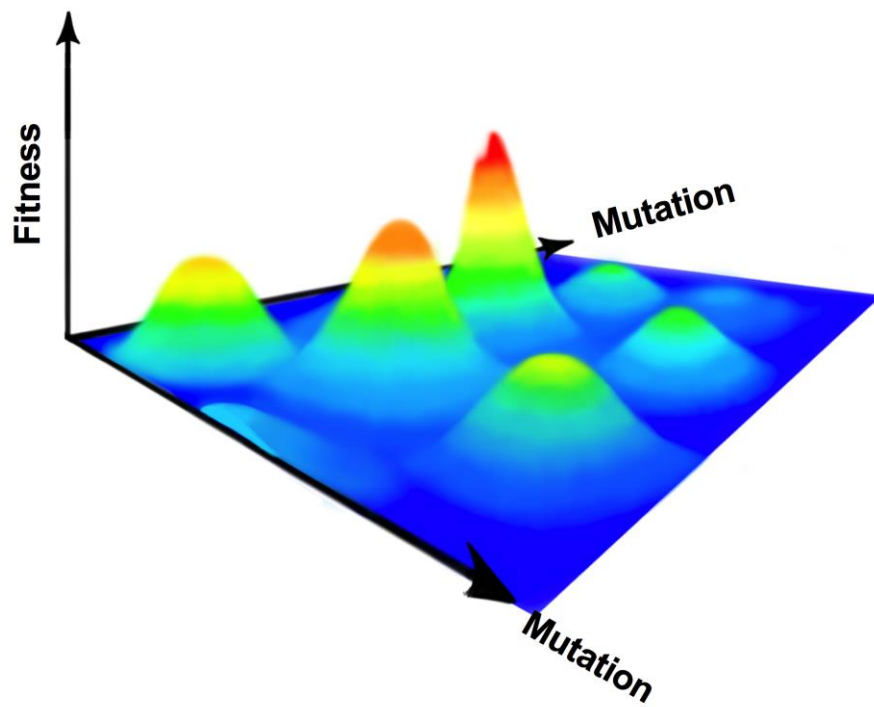
Illustration 1.1:   RNA virus mutational spectrum.

As RNA viruses mutate, the sequence space is sampled to find areas of higher fitness. This space is hypothesized to be changeable, so it is best for mutation-prone RNA viruses to exist in flatter areas of this space where decreases in fitness are slight.

Homologous recombination

| A | B | C |

| a | b | c |

↓

| a | B | C |

Non-homologous recombination

| A | B | C |

| d | e | f |

↓

| d | B | C |
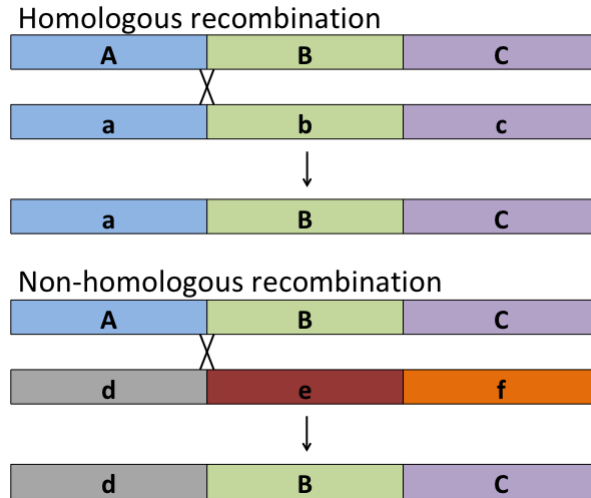
Illustration 1.2:   Recombination

Homologous recombination occurs when the RdRp switches from one RNA template to another, homologous RNA template during replication. Non-homologous recombination occurs when the RdRp switches from one RNA template to a dissimilar RNA template during recombination. The "X" indicates where RdRp movement to a new RNA template occurred.
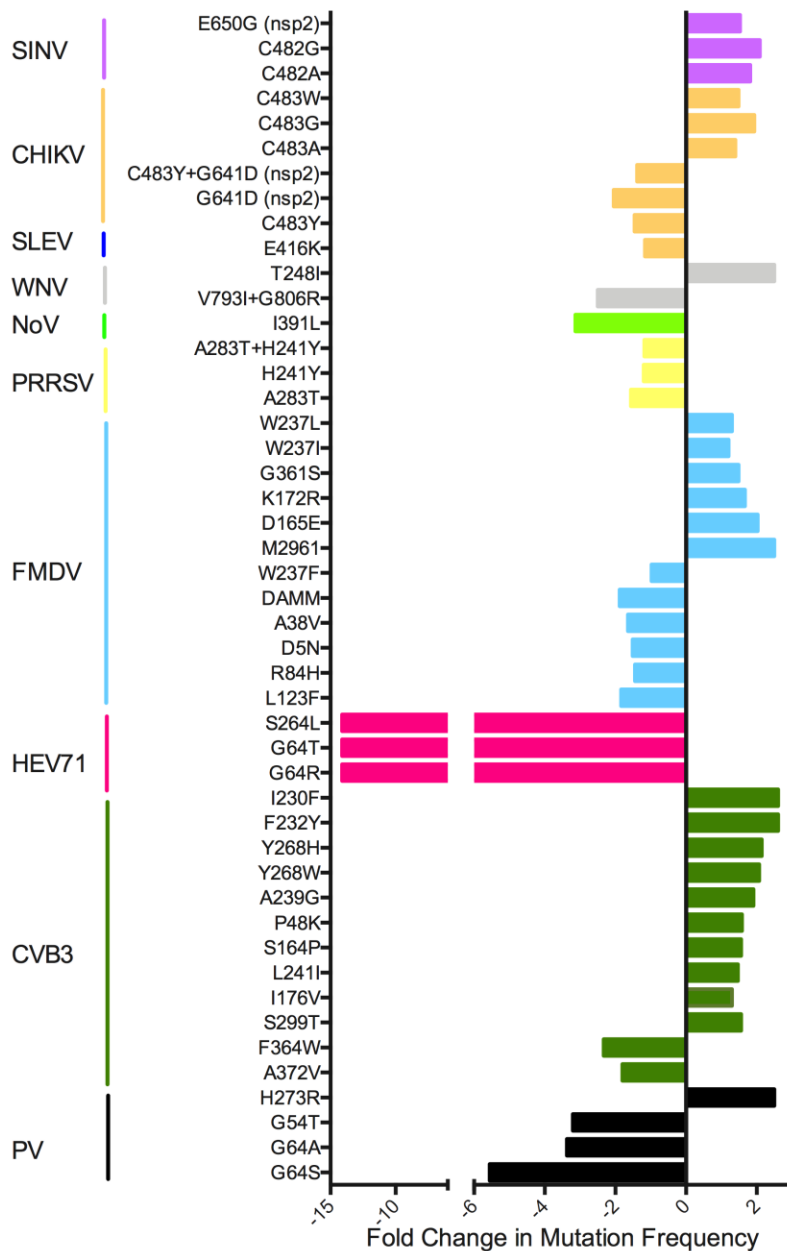
Figure 1.2:   Fold-change in fidelity mutant mutation frequency relative to the parent virus.

Most estimates are from TOPO cloning experiments, but if this information was not available fold-change NGS data was used. Mutations found outside the RdRp gene are indicated. Coronavirus data was excluded due to exceptional differences during RNA replication compared to the other RNA viruses.

$$\text{NTP} + \text{ER}_n \underset{\xrightarrow{\hspace{1cm}}}{\overset{1}{\xleftarrow{\hspace{1cm}}}} \text{ER}_n\text{NTP} \underset{\xrightarrow{\hspace{1cm}}}{\overset{2}{\xleftarrow{\hspace{1cm}}}} {}^*\text{ER}_n\text{NTP} \underset{\xrightarrow{\hspace{1cm}}}{\overset{3}{\xleftarrow{\hspace{1cm}}}} {}^*\text{Er}_{n+1}\text{PP}_i \underset{\xrightarrow{\hspace{1cm}}}{\overset{4}{\xleftarrow{\hspace{1cm}}}} \text{Er}_{n+1}\text{PP}_i \underset{\xrightarrow{\hspace{1cm}}}{\overset{5}{\xleftarrow{\hspace{1cm}}}} \text{Er}_{n+1}$$
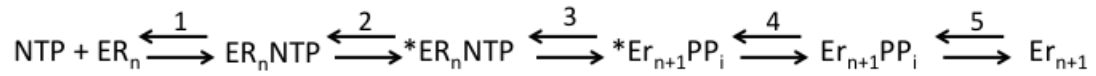
Illustration 1.3:   RdRp kinetics steps for NTP addition to an RNA chain.

First, an NTP binds the RdRp, which causes a conformational change "*" (step 2) and activates the RdRp (step 3). The NTP is then added to the RNA chain, leading to another conformational change and translocation of the RNA (step 4). Finally, the PP_i leaving group is released (step 5), allowing the cycle to begin again.
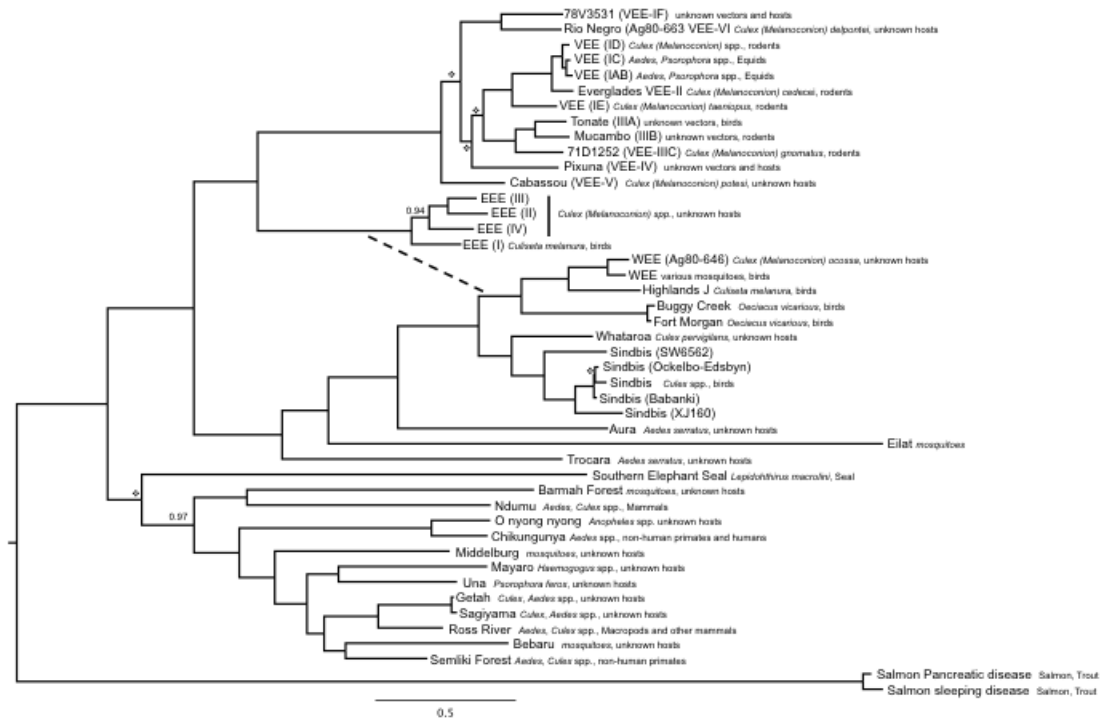
Figure 1.3:   Alphavirus phylogeny.

Bayesian alphavirus phylogenetic tree kindly provided by Naomi Forrester.
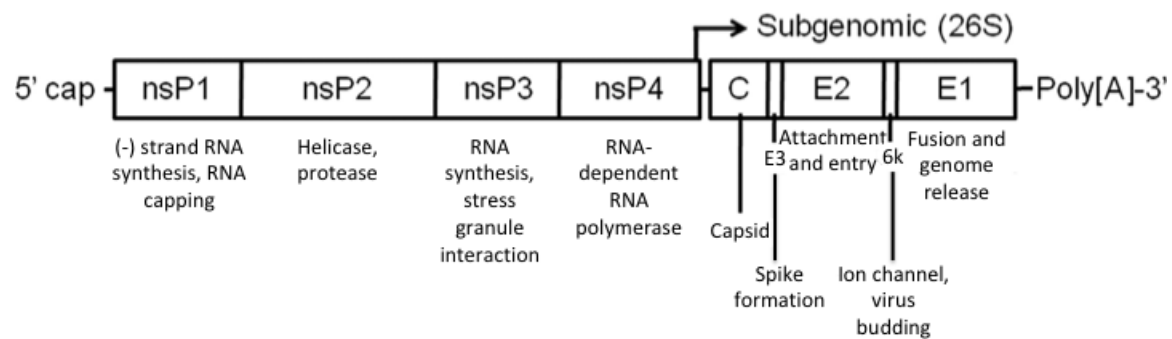
Illustration 1.4:   Alphavirus genome.
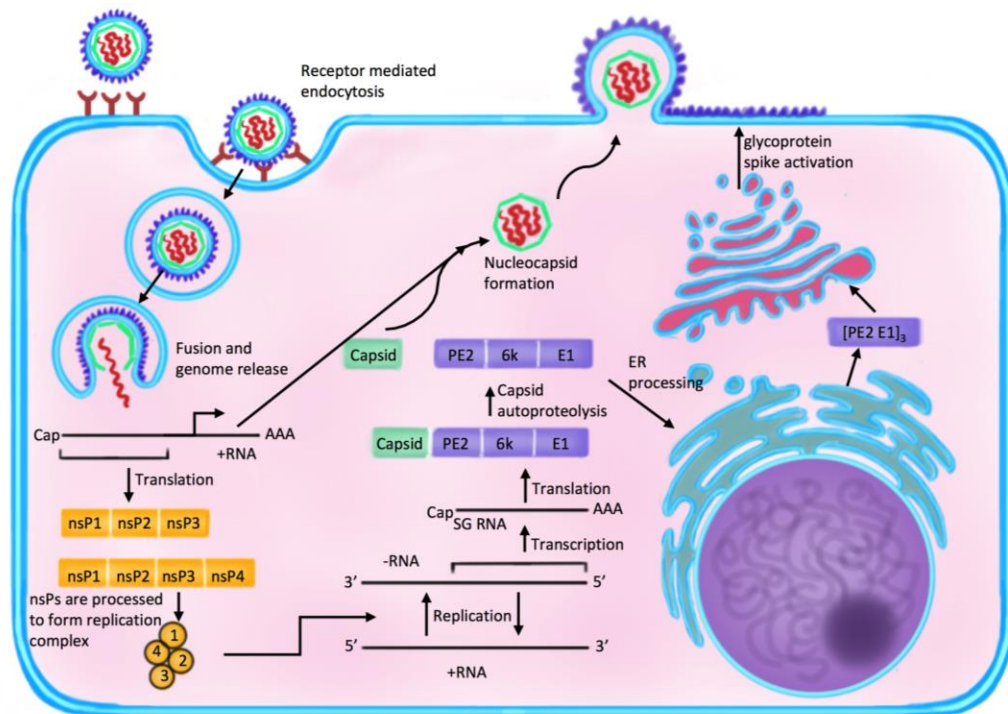
Illustration 1.5:   Alphavirus lifecycle.

Alphaviruses enter the host cell via receptor-mediated endocytosis. The pH drops in the endosome, causing virion fusion with the endosome cell membrane. This allows for release of the virus genome, which is translated by host ribosomes to generate the nonstructural polyprotein. Due to a leaky stop codon between nsP3 and nsP4, nsP4 is only present in a fraction of these polyproteins. As the nsPs are processed to from various combinations of the replication complex, the virus genome is replicated. From the –RNA genome, the subgenomic (SG) RNA is transcribed and used to produce the structural proteins. The capsid protein is immediately cleaved and complexes with viral genomic RNA to form nucleocapsids. The remainder of the polyprotein is processed in the ER and Golgi complex, where it finally travels to the plasma membrane. Nucleosomes bind the cytoplasmic tails of the glycoproteins to complete virion formation, which bud and release from the cell surface.
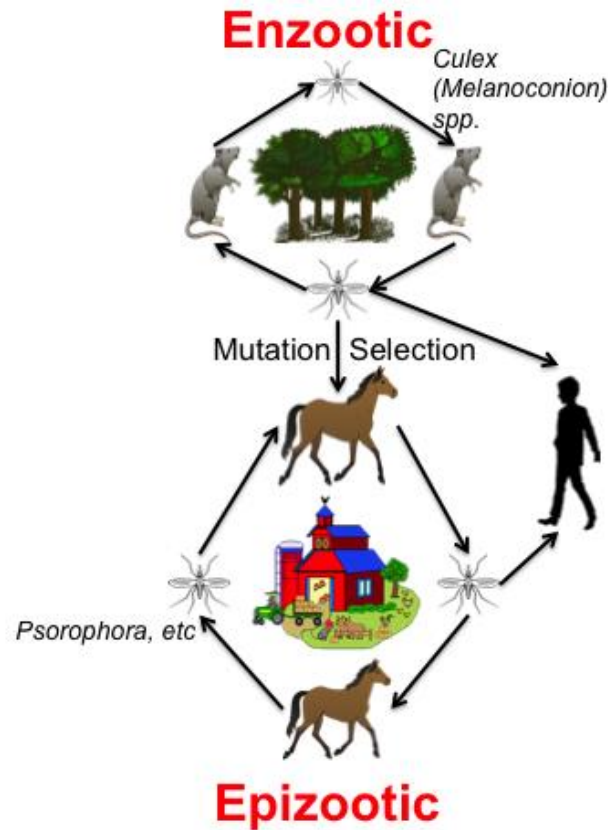
Illustration 1.6:   VEEV transmission cycle.

VEEV is primarily transmitted in an enzootic cycle between Cu. (Mel.) spp. of mosquitoes and rodents. Occasionally, a mutation will arise in the E2 glycoprotein, causing high-titer viremia in equids. This begins an epizootic cycle, which occurs between equines and various epizootic mosquito species. Humans can be infected from both enzootic and epizootic cycles, but are believed to be dead-end hosts.

Virus	Subtype	Geographic Range	Vertebrate Hosts	Mosquito vector	Human Disease	Endemic/Epizootic
VEEV	IAB	Trinidad, Peru, Colombia, Guatemala, Mexico, Texas	Horses, humans	Ae. and Ps. spp.	Yes	Epizootic
	IC	Colombia, Venezuela, Peru	Horses, humans	Ae. and Ps. spp.	Yes	Epizootic
	ID	South and Central America	Rodents	Cu. (Mel.) spp.	Yes	Endemic
	IE	Central America	Rodents, horses, humans	Cu. (Mel.) taeniopus, Ps., and Ae. spp.	Yes	Endemic, Epizootic
Everglades	II	Florida	Birds	Cu. (Mel.) spp.	Yes	Endemic
Mucambo	IIIA	South America	Unknown	Culex portesi	Yes	Endemic
Tonate	IIIB	South and Central America	Unknown	Unknown	No	Unknown
71D252	IIIC	South America	Unknown	Unknown	No	Unknown
Pixuna	IV	South America	Unknown	Unknown	No	Unknown
Cabassou	V	French Guiana	Unknown	Culex portesi	No	Unknown
Rio Negro	VI	Argentina	Unknown	Unknown	No	Unknown
Mosso das Pedras	IF	Brazil	Unknown	Cu. (Mel.) spp.	No	Unknown

Table 1.1:   VEEV serocomplex.

Table adapted from Forrester et al. (182).

IDENTIFICATION OF A LOW-FIDELITY TC-83 MUTANT

Chapter 2. Characterization of a Low-Fidelity Mutant of TC-83 and its Utility as a Live-Attenuated Vaccine[1]

INTRODUCTION

Due to the error-prone nature of the RdRp, RNA virus replication is characterized by a high mutation rate that results in increased genetic diversity of progeny viruses (337). This diversity can be utilized by the virus to evade and escape the immune system, as well as to adapt to new hosts. Maintaining the appropriate amount of virus diversity, which is typically approximately 1 mutation per genome (7) is of utmost importance to RNA virus survival within the host and during transmission. This is especially true for arboviruses, which utilize two distinct hosts to complete their transmission cycle. If the mutation rate of an RNA virus is too high, more unfit progeny will be produced due to the increased number of mutations, most of which are deleterious by chance. This results in a substantial decrease in viable genomes, and possible extinction of the viral population due to error catastrophe (338). Conversely, if the mutation rate is too low, little variation is produced, and the virus population becomes clonal and less able to adapt to diverse environments. Both scenarios reduce the overall fitness of the virus and can lead to extinction (50). This predicted lack of fitness with high or low-fidelity replication has been demonstrated experimentally with a number of viruses, including PV (66, 68), CHIKV (80, 82), WNV (83), SLEV (84), HEV 71 (72, 73, 339), FMDV (74-76, 78),

---

[1] Content of this chapter has previously been published: Kautz TF, Guerbois M, Khanipov K, Patterson EI, Langsjoen RM, Yun R, et al. Low-fidelity Venezuelan equine encephalitis virus polymerase mutants to improve live-attenuated vaccine safety and efficacy. Virus Evolution, 4(1), vey004. Reproduced with permission.

SARS CoV (89, 90, 99), FLU (87, 88), NoV (86), and CBV3 (46, 70, 71). These viruses were all subjected to treatment with nucleoside analogs such as Ribavirin or 5'Fluorouracil, which increase the mutation rate and can lead to virus extinction, or by the insertion of mutations found to change fidelity in other viruses. Virus populations circumvent extinction by developing resistance to the nucleoside analog, sometimes by developing mutations in the RdRp that either increase (high fidelity) or decrease (low-fidelity/hypermutator) RdRp fidelity (i.e. the RdRp error-rate). When compared to unpassaged, wt viruses, fidelity mutants have similar growth kinetics *in vitro*, but are attenuated *in vivo* due to the alteration of diversity produced during replication, which hampers the ability of the virus to overcome bottlenecks in the host (67, 68).

The alphavirus genus, family *Togaviridae*, contains a number of important arboviruses that are distributed worldwide. Alphaviruses are classified as either Old World or New World viruses depending on their distribution. VEEV is a New World encephalitic alphavirus that circulates continuously in an enzootic cycle in the forests and swamps of northern South America, Central America, and Mexico, typically between rodents and mosquitoes. Spillover from this cycle is believed to cause tens of thousands of dead-end human infections annually (180). Periodically, the virus emerges to cause epizootic cycles in equids, which can also spill over into humans, sometimes resulting in hundreds of thousands of infections (183, 185, 340-342). Prior to the 1960's, equine epizootics involving high fatality rates were frequently recorded in VEEV-endemic areas. Since horses remain important components of the local agricultural economies within these regions, VEEV has had a major impact on the economic output of at-risk areas (343). Recent outbreaks in both Venezuela and Mexico demonstrate the ability of VEEV to re-emerge periodically from its enzootic niche (176, 344, 345), and some earlier outbreaks spread as far north as Texas (340, 346). Independent of these natural cycles of infection, there is great concern for the use of VEEV as a biological weapon due to its

high infectivity via the aerosol route. To address this threat, multiple vaccines have been developed to protect against VEEV infection.

The first human vaccine described for VEE, TC-83, was produced following 83 serial passages of the Trinidad donkey VEEV strain (subtype IAB) in guinea pig heart cells (292). Sequencing of TC-83 revealed eleven nucleotide changes, but attenuation was attributed to only 2 of these mutations; one in the 5' UTR and one in the E2 glycoprotein gene (307, 308). The reliance of TC-83 on only two point mutations for its attenuation increases the potential for reversion during vaccination, as well as instability during manufacturing. This concern has been supported by passaging in infant mice, where TC-83 reverted in a little as three IC passages (293). The retention of mosquito infectivity adds another safety concern for transmission from vaccinees to humans or equids, and the isolation of TC-83 from wild-caught mosquitoes in 1971 during an equine vaccination campaign underscores this risk (306). Due to these concerns, as well its incomplete immunogenicity (293, 301, 347), TC-83 is only approved for equids, but it maintains investigational new drug status for at-risk military and laboratory personnel.

The presence of a high mutation rate is thought to be one reason for the persistence of RNA viruses in the environment. However, high mutation rates also have implications for LAV's such as TC-83, which typically generate long-lived immunity and are cost-effective. LAV replication has the potential to restore a virulent, wt phenotype via one or more reversions or pseudoreversions. Such events can lead to safety concerns and possible adverse events following immunization (348). However, further increasing the natural mutation rate is also hypothesized to decrease the ability of the virus to successfully revert or pseudorevert through Muller's ratchet (51, 349), by the accumulation of deleterious mutations in asexual populations (e.g. viruses) during replication in the absence of efficient recombination. Additionally, deleterious mutations can also impair the ability of fitter viruses to replicate and increase in the population (49, 50, 350). Thus, the RNA virus error rate is finely tuned to allow for optimal virus

population health while also allowing for the production of mutations, which are key for adaptation to new hosts and environments.

The present aim was designed to determine whether mutations in the TC-83 RdRp that alter virus fidelity, i.e. increasing the mutational spectrum, can attenuate the virus further, without sacrificing vaccine stability or immunogenicity. This aim will test the hypothesis that RdRp mutations identified during 5FU passaging of TC-83 will be fidelity-altering mutations, resulting in increased vaccine safety and immunogenicity in a vertebrate host. In this aim, a virus containing 3 RdRp mutations was found to slightly decrease virus fidelity, while a mutant containing 4 RdRp mutations acted much like the low-fidelity mutant, but did not have altered fidelity.

MATERIALS AND METHODS

Cell cultures and viruses

Vero (African green monkey kidney), HEK-293 (human embryonic kidney), and Baby Hamster Kidney (BHK) cells were obtained from the American Type Culture Collection (ATCC) (Bethesda, MD) and maintained in DMEM (Gibco) supplemented with 10% Fetal Bovine serum (FBS, Atlanta Biologicals), and 500µg/mL gentamycin (Corning) in a 37°C 5% CO_2 incubator. C7/10 cells were maintained in DMEM supplemented with 10% FBS, 1% Minimal Essential Medium Nonessential Amino Acids (Gibco), 1% Trypose Phosphate Broth (Sigma), and 500µg/mL gentamycin in a 30°C 5% CO_2 incubator. U4.4 cells were maintained in Mitsuhashi and Maramorosch media (Sigma) supplemented with 20% FBS, 2% Sodium Bicarbonate (7.5%) (Gibco), and 500µg/mL gentamycin in a 30°C 5% CO_2 incubator.

Virus stock generation

Viruses were rescued from a TC-83 infectious clone (307) by electroporation using BHK cells. First, 5µg of TC-83 or the other RdRp mutants was linearized using the

restriction enzyme MluI (NEB) in a 50µL volume. 5µL of each digestion was mixed with 1µL 6x gel loading dye (NEB) and run on a 1% agarose (GeneMate) TAE (Fisherbrand) gel at ca. 100V for ca. 1 hour to confirm digestion. The remainder of the linearized product was purified using phenol-chloroform extraction. To do this, 50µL of nuclease-free water (Ambion) was added to the linearized DNA, followed by the addition of 100µL of phenol-chloroform (Fisherbrand). This was vortexed and centrifuged at 16.1 *x g* for 5 minutes and the aqueous phase was transferred to a new 1.5mL tube. To this, 2µL of 5M NaCl (Ambion) and 100µL of chloroform (Fisherbrand) was added. This was vortexed and centrifuged again at 16.1 x *g* for 5 minutes. The aqueous phase was then transferred to a new 1.5mL tube, 250µL ethanol (Fisherbrand) was added, and this was stored overnight at -20°C. After the tube was centrifuged at 16.1 *x g* for 10 minutes, the ethanol was decanted and resulting pellet was washed with 300µL of 70% ethanol. Once a final 5 minutes centrifugation was complete, the ethanol was decanted and the pellet was allowed to dry for approximately 5 minutes before being reconstituted in 50µL of nuclease-free water.

In vitro transcription of the linearized DNA was performed in a 26µL volume using 2.5µL DTT (Invitrogen), 5µL 10X transcription buffer (Ambion), 2.5µL 10mM cap (NEB), 2.5µL 10mM rNTP (Roche), 5µL linearized DNA, 7µL nuclease-free water, 0.5µL RNaseOUT (Invitrogen), and 1µL of T7 (Ambion) (TC-83) or SP6 polymerase (Ambion) (RdRp mutants). This was incubated for 1 hour at 37°C and stored at -20°C overnight.

BHK cells were grown overnight in a T-150 flask to approximately 95% confluency the next day using complete media (DMEM supplemented with 10% FBS, 1% Minimal Essential Medium Nonessential Amino Acids, 1mM Sodium Pyruvate (Corning), and gentamycin. After one wash with PBS (Gibco), 0.05% trypsin-EDTA (Corning) was used to detach the cells from the flask. Once detached, 4mL of complete media was added to the cells, and this was transferred to a 15mL conical tube and

pelleted for 5 minutes at 125 $X\ g$. The media was decanted and the cells were resuspended in 7mL of cold PBS. This wash was repeated twice. Finally, the cells were resuspended in 450μL of cold PBS and stored on ice until added to 5μL of RNA from the *in vitro* transcription. This was gently mixed before being transferred to an EP cuvette with a 2mm gap (Fisherbrand). The sample was electroporated using a BTX 830 machine (Cole-Parmer) under the following conditions: 510V, 100μs pulse, 5 pulses, 184ms interval. The cuvette was left for 10 minutes at room temperature before the cells were transferred to a T-75 flask with 10mL of complete media and stored in a 37°C 5% CO_2 incubator. Every 24 hours, for 3 days, the supernatant from the flask was added to 2mL of FBS. The flask was then returned to the incubator after rehydrating the cells with fresh complete media. The supernatant was then clarified by centrifugation at 783 $X\ g$ for 5 minutes at 4°C before being transferred to new 1.5mL tubes and finally stored at -80°C. Titers of the electroporated stock virus were determined by plaque assay using Vero cells.

Plaque assay

One day prior to infection, 6-well or 12-well Vero plates were seeded using 250,000 or 500,000 cells per well respectively to ensure approximately 90% confluency the following day. Virus stocks were serially diluted 1:10 8 times using 225μL DMEM (supplemented with 2% FBS and gentamycin) and 25μL virus. This dilution series was either performed using 1.5mL tubes (using vortexing to mix) or 96 well plates (using pipetting to mix). Media was then decanted from a cell culture plate and 100μL (12-well plate) or 200μL (6-well plate) of each dilution was added to a well. This was performed in duplicate. The infected monolayers were stored in a 37°C 5% CO_2 incubator for 1 hour and were gently shaken every 15 minutes to ensure an even infection distribution. After this incubation, a 0.4% agarose overlay (1 part 2% agarose (Lonza) in filter-purified water to 4 parts DMEM supplemented with 2%FBS and gentamycin) was added to each well, and the plates were returned to the incubator. Following a 48-hour incubation, the

56

monolayers were fixed for 30 minutes using 10% formaldehyde (Fisherbrand) before the agarose plugs were removed and the monolayer was stained with 0.25% crystal violet solution (Fisherbrand). The plates were then washed with water and allowed to dry before plaques were counted.

PFU per mL was calculated using the following formula: PFU/mL=(dilution X number of plaques) (1000/amount plated), with "dilution" equaling the dilution at which the plaques were counted and "amount plated" equaling the amount of virus added when infecting the cells (i.e. 100μL for 12-well plates and 200μL for 6-well plates).

Nucleoside analog susceptibility

One day prior to infection, 24-well Vero plates were seeded using 125,000 cells per well to ensure approximately 90% confluency the following day. Cells from one well were counted the following day using a hemocytomer for MOI calculations.

Rescued viruses were tested for susceptibility to 5FU (Sigma) or Ribavirin (Sigma) in triplicate. Media was removed from the 24-well Vero plates, and replaced with 5FU or Ribavirin supplemented media (DMEM supplemented with 2% FBS, gentamycin, and 0, 10, 25, 50, 100, 200, or 300 µg/ml of 5FU or 0, 50, 100, 200, 300, or 400 µM Ribavirin) for 2 hours. The cells were then infected with 0.01 MOI of TC-83 or an RdRp mutant in a volume of 100μL and stored in a 37°C 5% CO_2 incubator. One hour post-infection, the inoculum was removed and media containing the pretreatment amount of 5FU or Ribavirin was added to the infected cells. The plates were then returned to the 37°C 5% CO_2 incubator. Cell supernatant was harvested 24 hours post-infection, supplemented with FBS to a final concentration of 20%, spun down at 3000 rpm for 5 minutes to remove cellular debris, and transferred to a new tube. These samples were stored at -80°C. Virus was titrated in duplicate using standard plaque assays.

Growth Curves – Vertebrate cells

To ensure that the inserted RdRp mutations did not interfere with viral replication, standard replication curves were conducted. One day prior to infection, 24-well Vero or HEK-293 plates were seeded using 125,000 cells per well to ensure approximately 90% confluency the following day. Cells from one well were counted the following day using a hemocytomer for MOI calculations.

Cells were infected at an MOI of 10 or 0.01 in a volume of 100μL and incubated for one hour in a 37°C 5% CO_2 incubator. After this, the cells were washed twice with PBS and overlaid with 0.5 mL of DMEM supplemented with 2% FBS and gentamycin. Virus was harvested by removing the entirety of the medium from three wells per time point. Harvested virus was supplemented with FBS to a final concentration of 20%, and clarified by centrifugation at 0.8 $X g$ for 5 min. The supernatant was then moved to a new tube and stored at -80°C. Viral titers were determined by plaque assays.

TC-83 and RdRp mutant *in vitro* passaging

One day prior to infection, 6-well plates were seeded with 500,000 Vero cells or 1,000,000 U4.4 cells. The day of the infection, one well of cells for each cell type was counted using a hemocytomer and used to determine the virus dilutions necessary for an MOI of 0.1. Once diluted, media was decanted from the 6-well cell plates and 200μL was used to infect each well. These infections were performed using two replicates per virus. Following the infection, the plate was transferred to a 37°C (Vero cells) or 30°C (U4.4 cells) 5% CO_2 incubator for 1 hour with occasional shaking. When the incubation was complete, the inoculum was removed and 2mL of DMEM supplemented with 2% FBS and gentamycin (vertebrate cells) or the standard mosquito cell media was added to each well. The plates were then returned to the appropriate 5% CO_2 incubator for 48 hours.

After the 48 hour incubation, the virus was transferred to a tube with FBS to a final concentration of 20% FBS. This was centrifuged for 5 minutes at 0.8 $X g$ and

transferred to a new tube. These tubes were stored at -80°C. Plaque assays using Vero cells were used to determine virus titer. Three total passages were performed.

Virulence assays in infant CD-1 mice

To study virulence and attenuation, six-day-old CD-1 mice (Charles Rivers Laboratories, Wilmington, MA) were inoculated IC with 10^5 PFU of virus in a volume of 20 μl, or SC with 10^5 PFU in a volume of 50 μl. Animals were weighed daily for two weeks and monitored for survival and clinical signs.

Vaccine study

7-week-old CD-1 mice were vaccinated SC with the original TC-83 virus or one of the RdRp mutants with 10^5 PFU in a volume of 50 μl, or with PBS for unvaccinated controls (n=8 per cohort). Six weeks post-vaccination, animals were challenged SC with 10^5 PFU of wt epidemic VEEV strain 3908 (179), with daily monitoring for signs of illness, survival and weight loss.

Blood samples were collected from alternating cages of vaccinated mice for 3 days post-vaccination and 4 days post-challenge for viremia detection using plaque assays, as well as 5 weeks post-vaccination for antibody measurement by PRNT. Blood was collected via the retro-orbital route with capillary tubes (Fisherbrand), which were drained into 1.5mL tubes containing 225μl DMEM supplemented with 10% FBS and gentamycin. This was stored at 4°C overnight before being centrifuged at 783 *X g* for 5 minutes. The serum was then transferred to a fresh 1.5mL tube and stored at -80°C.

Plaque reduction neutralization test (PRNT$_{80}$).

One day prior to infection, 12-well Vero plates were seeded using 250,000 cells per well to ensure approximately 90% confluency the following day.

The following day, serum samples were heat inactivated for 1 hour at 56°C. Serum samples were then diluted 1:10 in 150μl of media (DMEM supplemented with 2% FBS and gentamycin) followed by 5 additional 2-fold dilutions. 75μL of each serum dilution was then added to a 96-well plate in duplicate, and an equal amount of TC-83 diluted to 800 PFU/mL was added to this and mixed well by pipetting. A TC-83 only control (i.e. no serum) was also made to determine the un-neutralized number of plaques. The 96-well plates containing the virus/serum mixtures were then incubated for 1 hour in a 37°C 5% CO_2 incubator. After this, 12-well Vero plates were decanted, and 100μl of virus/serum mixture was added to each well. These plates were incubated at 37°C in a 5% CO_2 incubator for 1 hour. Following this, a 0.4% agarose overlay (see plaque assay protocol) was added to each well, and the plates were returned to the incubator for 48 hours. Plates were then fixed and stained as in the plaque assay protocol.

$PRNT_{80}$ cutoff values were determined by counting the number of plaques from the virus-only well and multiplying this number by 0.2. Plaques were counted for each well, and titers were determined by the cutoff value (e.g. if no neutralization $PRNT_{80} <$ 1:20, if fully neutralized $PRNT_{80} >$ 1:640).

Virus Next Generation Sequencing

VIRAL RNA EXTRACTION

Viral RNA was extracted using the Qiagen viral RNA mini kit as per the manufacturer's protocol.

LIBRARY PREPARATION

Illumina sequencing was performed by the UTMB next generation sequencing core. Viral RNA from cell culture extracts were fragmented by incubation at 94°C for 8 minutes in 19.5 μl of fragmentation buffer (Illumina, San Diego, CA). First and second strand synthesis, adapter ligation, and amplification of the library were performed using the Illumina TruSeq RNA Sample Preparation kit as per the manufacturer's protocol.

Products were fragmented using transposons, then adapter ligation and amplification of the library was performed using the Illumina TruSeq RNA Sample Preparation kit under conditions described by the manufacturer (Illumina, San Diego, CA). Samples were tracked using the "index tags" incorporated into the adapters as defined by the manufacturer.

Sequence assembly and analysis

Illumina sequencing analysis was performed by the Fofanov lab at UTMB.

QUALITY AND FILTRATION

The quality for each sample/dataset was assessed using FASTQC (351). The paired-end reads were merged for each sample and then filtered to exclude reads with unknown characters (anything other than A, T, C, G) and low quality (<15 quality score), so that only high quality reads were used during analysis. Additionally, the first 16 bases of each read were trimmed due to nucleotide bias.

REFERENCE SEQUENCE

The analysis was performed using VEEV strain TC-83, complete genome (GenBank accession #: L01443.1)(308).

VIRUS DIVERSITY ANALYSIS

To determine virus variants, each sample was run through a novel rare variant pipeline developed by the Fofanov lab. The pipeline first maps each read to the reference VEEV genome with perfect match, then unmapped reads are re-mapped with 1 mismatch and added to the final map. The 34 base long reads used in the analyses were validated as viral sequences and not host sequences by analysis of the longest subsequences shared explicitly (no mismatches allowed) and longest similar (1 mismatch allowed) between viral and host genomes. Positions in which the number of reads mapped with mismatches was higher than perfectly mapped reads or coverage was below 100 were excluded from diversity calculations. Positions with non-zero mutation frequency were considered to be

variant positions. Mutation frequency per sample was calculated by summing the per position diversities and normalizing by the number of positions for which diversity was calculated. Shannon Entropy was calculated using the equation $-[\Sigma^{s}_{i=} p\log(p)]/N$, where p equals the probability of mutation and N equals the number of base calls that can happen at a position (i.e. A, G, C, T, insertion, or deletion).

TC-83 3x and 4x backbone cloning

To rule out any differences in fitness caused by TC-83 backbone differences, the 3 or 4 RdRp mutations were inserted into the parent TC-83 plasmid. TC-83, TC-83 3x, and TC-83 4x were digested with SalI (NEB) and PspOMI (NEB) as per the manufacturer's protocol. Digestion was validated by running the entire contents of the digestion on a 1% agarose TAE gel. Bands were cut out and purified using the QIAquick Gel Extraction kit (Qiagen) as per the manufacturer's protocol. The RdRp mutations were ligated into the TC-83 plasmid using the T4 DNA ligase kit (NEB) as per the manufacturer's protocol and using a 1:3 insert to vector ratio. 4μL of the ligation was transformed using TOP10 competent cells (Invitrogen) as per the manufacturer's protocol, and 50μL of the transformation was plated on an LB-agar plate (Fisherbrand) supplemented with 100 μg/mL ampicillin (Sigma) and allowed to grow overnight in a 37°C incubator.

Colonies were picked the next morning and 8 were used to spike 5mL of LB supplemented with 100μg/mL ampicillin for miniprep processing (Clontech, as per the manufacturer's protocol) and Sanger sequencing. The primers 7246V (5'CCGTAGGAACTTCCATCATAG) and 7800C (5'CGTGGTTCTTCTTCTTCTTCC) were used to determine RdRp mutation insertion. Of the colonies positive for the RdRp mutations, one was used to spike 250mL of LB supplemented with 100μg/mL ampicillin. This was allowed to grow overnight in a 37°C incubator at 250rpm. The next morning, the bacteria were pelleted by centrifugation for 15 minutes at 2003 *X g*, and the plasmid

was purified using the NucleoBond Xtra Maxi Plus kit (Clontech). The purified plasmid stock was stored at -80°C.

Statistics

GraphPad Prism was used to perform all statistical tests, which are described in the text.

RESULTS

RdRp mutant identification and cloning.

Previous work in the lab identified three RdRp mutations during nucleoside analog passaging. Briefly, to identify mutations in the RdRp gene associated with changes in fidelity, TC-83 rescued from an infectious clone was previously used to initiate serial Vero cell passages in duplicate in the presence of Ribavirin, 5'Flurouracil (5FU), or Azacytidine (Aza). Viruses were titered using plaque assays following each passage, and diluted to an MOI of 1 plaque forming unit (PFU)/cell for each subsequent passage. Following passages 19 and 23, the RdRp gene (nsP4) was sequenced. Three mutations were identified in both 5FU passages, and all were located in the 5' end of the RdRp gene: a G5724C mutation resulting in the amino acid change G14R, an A5794G mutation resulting in the amino acid change E37G, and a G5970A mutation resulting in the amino acid change A96T (amino acid numbers refer to nsP4 residues).

The three mutations identified following the 5FU passages were cloned into the TC-83 backbone in conjunction with a high fidelity mutation that was previously identified in a related alphavirus, CHIKV (C483Y, which corresponds to position 488 in TC-83) (80). Six mutants were created (Figure 2.1A), four of which were individual mutants, and two with multiple mutations: a 3x mutant including G14R, E37G, and A96T and a 4x mutant including G14R, E37G, A96T, and C488Y. All clones were rescued by electroporation into BHK cells, and were titered using standard plaque assays on Vero

cells (352). All rescued mutants were viable, producing between 7-9 $\log_{10}$ PFU/ml following electroporation (data not shown). Due to variation in EP stock phenotypes, each figure contains information that directs to an appendix with information about the various TC-83, TC-83 3X, and TC-83 4X stocks.

Replication kinetics

As the mutants included amino acid changes in the RdRp of VEEV TC-83, the viruses were subjected to standard replication curves (Figure 2.1B-C) on Vero cells (Figure 2.1B, appendix 2 stocks 1-3). No mutants showed significant differences from TC-83 by repeated measures ANOVA. Since Vero cells are IFN-deficient, and a previous study found high fidelity PV to be attenuated in a primary cell line (67, 77), we used HEK-293 cells to examine the effects of IFN on the replication of fidelity-altered viruses. TC-83, the 3x mutant, and the 4x mutant were subjected to one-step replication curves (Figure 2.1C, appendix 2 stocks 1-3). As in Vero cells, no significant differences were observed between the viruses and their TC-83 parent.

Resistance to nucleoside analog treatment

To confirm the ability of the RdRp mutations to confer resistance to 5FU treatment (Figure 2.1D, appendix 2 stocks 8, 9, 13). Vero cells were treated with 0, 10, 25, 50, 100, 200, or 300μg/ml of 5FU and infected with parent TC-83 or an RdRp mutant using an MOI of 0.01. Repeated measures ANOVA found no significant differences between the RdRp mutants and parent TC-83 when Vero cells were treated with 0-25μg/ml 5FU. However, treatment with higher 5FU concentrations caused titers for all single RdRp mutants to drop compared to parent TC-83, demonstrating increased sensitivity to the treatment. Of note, E37G was significantly different from parent TC-83 for all of the high 5FU concentrations ($p<0.01$ for the 50μg/ml treatment, $p<0.0001$ for the 100-300μg/ml treatments). A96T was slightly more resistant, with titers significantly

64

reduced compared to parent TC-83 when cells were treated with 100-300μg/mL (p<0.0001). G14R and C488Y were the most resistant to 5FU treatment of the single mutants. Titers were only significantly reduced compared to parent TC-83 for the 200-300μg/mL treatments (p<0.5 for G14R 300μg/ml, p<0.0001 for all others). Due to the increased sensitivity of these mutants to 5FU, it was unlikely that these single mutations caused the resistance observed during the initial fidelity mutant selection.

Unlike the single RdRp mutants, TC-83 3x and 4x generally had similar or slightly higher virus titers compared to parent TC-83, suggesting increased resistance to 5FU treatment. TC-83 4x titers were significantly higher during the 50 and 100μg/mL treatments (p<0.01 and p<0.0001 respectively), and TC-83 3x titers were also significantly higher during the 100μg/mL treatment (p<0.05).

To determine if the RdRp mutants reacted similarly upon exposure to another nucleoside analog, TC-83 and the RdRp mutants were exposed to various concentrations of Ribavirin (Figure 2.1E, appendix 2 stocks 8, 9, 13). No significant difference was observed, except for the G14R mutant, which displayed increased sensitivity (p<0.01 for 100 and 300μM, p<0.001 for 400μM).

Virulence in infant mice

To assess virulence, individual TC-83 mutants were injected IC into 6-day-old CD-1 mice at a titer of ca. 5 $\log_{10}$ PFU (backtiters ranged from 1.9×10^4-2.4×10^5 per dose). Mice were weighed daily and the time of death was recorded (Figure 2.2A, appendix 2 stocks 1-3). The TC-83 3x mutant was significantly more virulent than the parent virus, with all animals succumbing by day 2 compared to TC-83, where mice began succumbing at day 3 (p≤0.05, Kaplan-Meier test). The mean time to death for parent TC-83 and all mutants except TC-83 3x was 5.36-5.54 days after infection, whereas TC-83 3x showed a mean time to death of 3.91 days.

Fidelity mutants have an impaired ability to overcome host bottlenecks, which results in reduced mortality and titer in certain organs (67-69, 99). To test this, individual mutants were injected SC into 6-day-old CD-1 mice to measure their ability to cause mortality (backtiters ranged from $6.2x10^3$-$1.35x10^5$ per dose). TC-83 3x and TC-83 4x exhibited significantly reduced mortality as reflected in survival (Kaplan-Meier test, p≤0.05) when injected SC, compared to the original TC-83, and compared with IC injection in 6-day old CD-1 mice (Figure 2.2B, appendix 2 stocks 1-3). The remaining mutants caused similar mortality to original TC-83, suggesting no change in their ability to traverse bottlenecks to cause fatal disease.

Illumina sequencing for virus population variants

EP STOCK

EP stock was sequenced using Illumina NGS to determine early differences in virus diversity. TC-83 3x and 4x were the only RdRp mutants chosen for this analysis, because they were most likely to have altered fidelity as measured by a preliminary Illumina sequencing analysis measuring the diversity of one replicate of each RdRp mutant (data not shown), as well as the phenotypic tests depicted in figures 2.1-2.2. Due to low EP stock titers (appendix 2 stock 13 was used due to the depletion of stock 12) TC-83 4x coverage was low, so it was not analyzed. Mann-Whitney U tests showed no significant differences in virus diversity for TC-83 3x when using either mutation frequency (Figure 2.3A) or Shannon Entropy (Figure 2.3B) as a measure of diversity (Appendix 2, stocks 8, 11, 12).

Interestingly, diversity hotspots (Figure 2.3 C-D) were very similar. When using a cutoff of 0.2, 18 of the 22 TC-83 variants that were above this threshold were identical to TC-83 3x, which shared 18 of its 20 most common variants with TC-83. However, while the magnitude of these hot spots was well conserved between replicates, there was some

variation between TC-83 and TC-83 3x. For example, the peaks for C10371U and C10743G were much more prominent for TC-83 than TC-83 3x.

PASSAGE 1 STOCK

To examine how different hosts in the arbovirus transmission cycle may alter virus diversity, TC-83, as well as the 3x and 4x mutants, were passaged once using primate (Vero or HEK-293) or mosquito (C7/10 or U4.4) cells (Figure 2.4, appendix 2, stocks 7, 9, 12).). Illumina sequencing showed that the 3x mutant produced a significantly higher amount of genetic diversity than parental TC-83, independent of the cell type used (Figure 2.4A). This, along with the previously discussed results, indicated that the 3x mutant is a low-fidelity variant. Interestingly, the 4x mutant did not demonstrate a significant increase or decrease in diversity compared to TC-83. Cell type had no significant effect on virus diversity, at least not after one passage. When the number of nucleotide positions containing diversity was examined (Figure 2.4B), the 3x mutant trended towards producing an increased number of positions with diversity, while the 4x mutant, again, looked much like the parent TC-83.

When examining peaks of diversity across the virus genome, some hotspots were conserved between the parent virus and RdRp mutants (Figure 2.5). These included nsP2 C2627A (Asp-Glu) and A2634Del (Met-stop), E2 U9561G (minus strand, Val-Gly), 6k C9978A (Ala-Asp), and E1 C11009A (minus strand, Arg-Ser). The parent TC-83 and, to a reduced extent, TC-83 4x both produced diversity hotspots in E1, but generally in different positions. In TC-83 4x, these consisted of C10032U (Ala-Val), U10356C (Val-Leu), and C11009A (Ala, minus strand, synonymous), while TC-83 had E1 hotspots at C10141U (Val, synonymous), C10371U (Ala-Gly), C10743G (Ala-Gly), C11009A (Ala, minus sense, synonymous), and U11269C (Asn, synonymous). Additionally, while there was no significant difference in diversity when different cell types were used (Figure

67

2.4), TC-83 3x appeared to have an increased number of diversity hotspots in C7/10 cells than the other cell types.

Furthermore, because TC-83 3x and 4x only appear to be resistant to one of the two nucleoside analogs tested (Figures 2.1 D-E), it was important to determine if this resistance is due to an alteration in the types of mutations being made by these RdRp mutants (Figure 2.4C). Indeed, both TC-83 3x and 4x produced fewer U-C mutations. As 5FU is a uracil analog and Ribavirin is not, this may explain the difference in nucleoside analog susceptibility.

PASSAGE 3 STOCK

As passage 3 stock is commonly used to decide whether an RdRp mutant is or is not a fidelity mutant (46, 68, 69, 77, 79, 89), due to the belief that the mutation rate has stabilized by this passage number (353), passage 1 stock from Vero and U4.4 cells were passaged two more times to determine changes in virus diversity (Appendix 2, stocks 7, 9, 12). While mutation frequency was significantly higher for the 3x and 4x RdRp mutants in U4.4 cells, there was no difference in Vero cells (Figure 2.6A). Additionally, while TC-83 3x exhibited consistently higher diversity as exhibited by Shannon Entropy, there was no significant difference compared to TC-83 (Figure 2.6B), likely to due to lack of statistical power. The mutation frequency of certain mutations had also changed (Figure 2.6C-D). While U-C mutations were still suppressed in the RdRp mutants in Vero cells (Figure 2.6C), after 3 passages, there was no longer any difference in U4.4 cells (Figure 2.6D). Additionally, for both cell types, U-G mutations became more frequent with TC-83 3x than the other viruses.

By passage 3, the number of high frequency variants (0.02 or higher) for all viruses had decreased (Figure 2.7), and approximately 50% of the high frequency variants were unique to the virus and passage series (40 unique variants of the 77 total variants, data not shown). Interestingly, the other 50% of the high frequency variants

were all conserved between TC-83, TC-83 3x, and TC-83 4x, with only one exception, U3559G (Val-Gly), which was found in both TC-83 3x passage series.

Immunogenicity and protection against VEEV challenge

Immunogenicity of the mutants was tested in an adult murine model previously used to test the efficacy of TC-83 (315). Adult CD-1 mice, 7 weeks of age, were vaccinated with 5 $\log_{10}$ PFU in a 50μl volume via the subcutaneous route (Appendix 2, stocks 1-3). Animals were bled on days 1-3 after vaccination and weighed daily for 1 week and then again on days 11 and 14 (Figure 2.8A). Animals exhibited no weight loss and viremia was sporadic with no significant differences among any of the viruses (repeated measures ANOVA, Table 2.1). Four weeks post-vaccination, the animals were bled to assay neutralizing antibody titers (Figure 2.8B). All vaccinated mice exhibited a strong immune response as determined by a plaque reduction neutralization test ($PRNT_{80}$). The 3x and 4x mutants produced significantly higher mean neutralizing antibody titers compared to TC-83 (one-way ANOVA, p=0.0049 and 0.0012, respectively). Following challenge at 6 weeks post-vaccination with VEEV subtype IC strain 3908, which was used previously for similar experiments (315, 316), animals were weighed daily and monitored for survival (Figure 2.8C-D). All vaccinated animals showed complete protection from weight loss and death, whereas the sham-vaccinated animals all succumbed by day 9 post-challenge.

Variation in attenuation of low-fidelity TC-83 3x EP stocks

It was recently discovered that the infectious clones for TC-83 3x and TC-83 4x were made using a combination of two different TC-83 infectious clones, resulting in 3-6 synonymous differences between these RdRp mutants and the control TC-83 used for comparison (Table 2.2). Therefore, it was important to determine that these extra mutations did not affect virus fitness. The 3 or 4 RdRp mutations were inserted into the

control TC-83 backbone, and differences in replication kinetics were measured using a 2-step Vero cell growth curve (Figure 2.9A, Appendix 2 stocks 14-16). Repeated measures ANOVA found TC-83 3x to replicate slightly higher than TC-83 at 6 HPI (p<0.0001), but there was no difference in replication after this time point. However, TC-83 4x had slightly, but significantly reduced growth at all time points (p<0.0001 for 6 and 12 HPI, p<0.01 for 24 and 48 HPI).

To ensure that the changes in infant mouse virulence were repeatable when the 3x and 4x RdRp mutants were in the same backbone as the control TC-83 (Figure 2.2A-B), 6-day-old CD-1 mice were injected IC or SC with 10^5 PFU of TC-83 3x or 4x mutants in the original (Appendix 2 stocks 8-9, 13, designated "old"), or control (Appendix 2 stocks 14-16, designated "new") TC-83 backbone, as well as the control TC-83 (Figure 2.9B-C).

IC survival curves (Figure 2.9B) were similar to those in Figure 2.2A, with most mice succumbing 5-7 days post-infection. Backtiters of the inocula ranged from 4.8-8.8x10^4 PFU per dose. As before (Figure 2.2A), neither the "old" or "new" RdRp mutants were significantly more or less virulent than TC-83 as measured by Kaplan-Meier test. This suggests that regardless of the TC-83 backbone that these RdRp mutations do not alter virulence when administered intracranially, and that the significant difference in lethality observed in Figure 2A for TC-83 3x is likely dependent on the mutant spectrum produced post-electroporation or due to host variation.

SC survival curves (Figure 2.9C) were significantly different compared to Figure 2.2B. Instead of half of the 3x and 4x mutants surviving SC inoculation, all individuals succumbed by 12 days post-infection, regardless of TC-83 backbone. Inoculum back titers ranged from 3.5x10^4 to 1.1x10^5 PFU per dose. Although all mice succumbed, there was slight variation between the cohorts. For example, while the "old" TC-83 3x cohort survived an almost identical length of time compared to the TC-83 control group, the "new" TC-83 3x cohort survived an average of 9.6 days (Kaplan-Meier, p=0.0361). The 4x RdRp mutants were similar, with the "old" backbone acting slightly more attenuated

than TC-83 (Kaplan-Meier, p=0.0054) and the "new" backbone showing no significant difference. More important than the differences in the RdRp mutant backbones was the difference between the initial SC survival curve (Figure 2.2B) and this repeat. While the "old" TC-83 3x and 4x mutants contained the same sequence and starting titer, the viruses were from different EP stocks. This and the IC survival curve results suggest that differences in the post-EP minority populations can result in variation in fidelity mutant attenuation.

DISCUSSION

Infectious diseases transmitted by arthropod vectors are difficult to control, and protecting the population via vaccination tends to be more effective than trying to control or eradicate the vector population. While LAVs tend to be cost-effective and immunogenic, LAVs have a significant Achilles' heel: the potential for reversion to wt virulence. This risk is particularly acute for RNA viruses, which replicate without proofreading, resulting in an increased ability to revert to the wt sequence or restore virulence via compensatory mutations (pseudoreversion). However, altering virus fidelity can theoretically overcome this major drawback. This approach has only been examined with fidelity mutants of poliovirus and a low-fidelity ExoN mutant of SARS-CoV (69, 99). While the high fidelity poliovirus (69) and SARS-CoV ExoN (99) mutants both demonstrated increased immunogenicity and an improved safety profile compared to the parent viruses, this was not observed for the low-fidelity poliovirus (79). However, fidelity mutants have only been generated using wt virus strains, which are unlikely to be sufficiently attenuated for vaccine use. We hypothesized that increasing the attenuation of a live-attenuated RNA virus vaccine by altering the RdRp fidelity would further improve its safety and efficacy. We addressed this by validating a series of low-fidelity mutations in a model system using the VEEV vaccine strain TC-83 to determine how this affects

the stability and attenuation. Serial passaging of TC-83 in the presence of 5FU identified 3 mutations in the RdRp, and validation showed that all three mutations were required to decrease virus replication fidelity. Additionally, we identified a 4x mutant that acted much like TC-83 3x, but showed no difference in diversity.

At present, there is no atomic resolution structure for an alphavirus RdRp, which limits our understanding of their mechanisms of fidelity alteration. However, all the mutations in the 3x mutant (G14R, E37G and A96T) were at the 5' end of the nsP4 gene, similar to the placement of the poliovirus (PV) high fidelity G64S and low-fidelity H273R substitution, which are both on the periphery of the RdRp protein rather than near the active site (67, 79, 354). For PV, the presence of the G64S mutation does not significantly alter the structure of the polymerase, but it does decrease the incorporation rate of new nucleotides (97, 355). In fact, the current theory is that this substitution simply stabilizes the polymerase rather than altering the active site. Alternatively, low-fidelity H273R PV decreases fidelity by favoring an open state of the RdRp, which decreases the duration of this fidelity checkpoint, thus increasing the likelihood of NTP misincorporation (98). The presence of the low-fidelity mutations outside of the predicted active domain of the TC-83 nsP4 gene suggests similar mechanisms might be at play, but confirmation will require an atomic resolution structure.

There are two manners in which low-fidelity mutants have been isolated, either by mutating residues found to alter fidelity in other viruses or by passaging virus in the presence of a nucleoside analog. Of the latter, three low-fidelity mutants have been identified that are resistance to at least one nucleoside analog (74, 83, 88). Our 3x and 4x fidelity mutants appear to act similarly to these low-fidelity viruses, with resistance to 5FU, but not ribavirin. When examining the mutation frequency of different mutations, the fidelity mutants produced a much lower amount of U to C transition mutations during passage 1, which would be one of the mutations expected to be selected against during 5FU passaging. This also may explain why the mutants are most resistant to 5FU when

using moderate amounts of the nucleoside analog, but then increase in susceptibility again at higher concentrations, as there is no difference in the other uracil mutation frequencies. It would be interesting to test the passage 3 U4.4 and Vero viruses to re-examine 5FU resistance, as the frequency of U to C mutations increased during U4.4 cell passaging, but not Vero cell passaged. If the decreased U-C mutation frequency is playing a role in 5FU resistance, the U4.4 passaged virus is likely to have lost any 5FU resistance.

TC-83 3x is likely a low-fidelity mutant, as evidenced by the phenotypic tests, as well as the increased genetic diversity observed using Illumina sequencing during passages 1 and 3. The 4x mutant, while exhibiting phenotypic similarities with other altered fidelity mutants, had no significant difference in virus diversity compared to the TC-83 parent, even after multiple cell culture passages. Attenuation for this RdRp mutant may be due to slightly reduced growth kinetics (Figure 2.9A), but this slight reduction is commonly observed for fidelity mutants (67, 72, 74, 76, 77, 82, 85), suggesting another mechanism. This mutant needs to be further explored to determine mechanisms of attenuation.

Also of interest is the C488Y substitution that increased replication fidelity in CHIKV, but did not affect TC-83 fidelity, although it did attenuate TC-83 in the infant mouse model. This finding is the opposite of the outcome for SINV, which exhibited low-fidelity features when a low-fidelity CHIKV mutation was inserted (82). However, SINV is more closely related to CHIKV than VEEV, so this may explain why the effects did not transfer to TC-83 even though the residue is highly conserved among alphaviruses (80).

As the TC-83 3x virus stock was passaged, differences in diversity became more apparent, suggesting that the low-fidelity phenotype is slight, but stable for this virus and increases over multiple growth cycles. Interestingly, when total genome diversity was analyzed for each construct after 1 cell culture passage, there was no significant

difference in diversity when comparing cell types. This is in contradiction to the low-fidelity CHIKV mutants, which only showed increased diversity in vertebrate, but not in mosquito cells (82). However, while no significant difference was observed in overall diversity between the cell types, TC-83 3x produced much higher peaks in diversity in C7/10 cells than was observed in other cell types or viruses. This is intriguing, because it is hypothesized that mosquitoes are drivers of diversity, likely due to the sequence specificity of the mosquito antiviral RNAi response (i.e. siRNAs), although this has only been demonstrated for West Nile virus (277, 356-358). This hypothesis does not appear to explain the increased diversity observed during the TC-83 3x C7/10 passages, because these cells lack a functional siRNA response. Additionally, no increased hotspots were observed for U4.4 cells, which do produce antiviral siRNAs. Further work is needed to determine how these diversity hotspots correspond to small RNA targeting in mosquito cells and examine the effects of the host immune response on virus populations.

Illumina sequencing uncovered many noteworthy effects during RdRp mutant growth *in vitro*. In particular, many of the minority variant hotspots were conserved for TC-83 and the 3x and 4x mutants, although the amplitude of each peak was not. Interestingly, this mutation conservation was generally conserved up to 3 passages PE, although genetic drift likely accounted for approximately 50% of the high frequency minority variants by the third passage, suggesting that further passage would lead to further diversification. Also of interest were the E1 diversity peaks identified in TC-83, but to a much less extent for the RdRp mutants. These peaks were also found in the EP stock, but greatly increased after 1 passage, and then decreased again by 3 passages. The E1 glycoprotein is responsible for the uncoating of the virus particle and escape of the genome into the cytosol. Some substitutions in the CHIKV E1 glycoprotein have been found to increase vector infectivity and transmission (28, 129, 359). Diversity in this region may be important for increased vector fitness and/or host jumps.

As our study was designed to evaluate the effectiveness of RdRp mutations that decrease fidelity in vaccines, the mutants were put through a standard challenge model previously used for different VEEV vaccines (315, 316). Mice showed no adverse effects from vaccination, viremia was consistent with that expected for TC-83, and all mice were protected against lethal challenge. Additionally, the mutants induced higher antibody titers than TC-83. Our current hypothesis for this observation is that the low-fidelity RdRp creates an increased number of defective interfering (DI) virus particles, which are well known to be strong immune stimulators (360-363). As VEEV first replicates in the draining lymph node (222), the presence of these DI particles may restrict dissemination from the draining lymph node, allowing for a greater opportunity for antigen presentation and therefore an increased immune response. This needs to be explored in future work, perhaps by labeling each virus with luciferase and imaging infected mice to determine if delayed dissemination occurs, as well as where this delay occurs.

Finally, as previous studies have shown that high fidelity PV mutations cause attenuation in mouse models by reducing dissemination to the CNS (67-69), we tested our mutants in a lethal mouse model for TC-83. The 3x and 4x RdRp mutants initially displayed equivalent virulence to parent TC-83 when injected into a single tissue that can cause lethal damage (brain) and reduced virulence when injected via a multi-tissue model (SC). However, when this experiment was repeated with virus rescued from different EP stocks, using slightly different TC-83 backbones, the 3x and 4x mutants displayed greatly increased in virulence compared to the initial SC outcome. As *in vitro* transcription is known to be error-prone (101), this suggests that minority variants randomly generated during the transcription preceding EP can have large effects on the overall virus population health, and thus virulence. Importantly, the RdRp mutants were never significantly more virulent than TC-83 when injected SC. While TC-83 is not lethal in an adult mouse model, it would be interesting to determine if the 3x and 4x mutants have consistently delayed and/or decreased dissemination compared to wt virus. This would

allow for a greater understanding of how a low-fidelity TC-83 vaccine would operate in a fully immunocompetent host.

Here, we demonstrated that the presence of low-fidelity mutations in a LAV resulted in reduced or equal virulence in an infant mouse model and increased immunogenicity in an adult mouse model, both of which are desirable properties for LAVs. However, we also observed different outcomes in low-fidelity mutant attenuation *in vivo* when different pools of virus stock were used, suggesting that the low-fidelity virus population might not be initially stable. This demonstrates that there is great need to understand the role that minority variants play in phenotypic changes in vaccine development, as changes in the mutant spectrum may significantly alter the phenotype of vaccines.
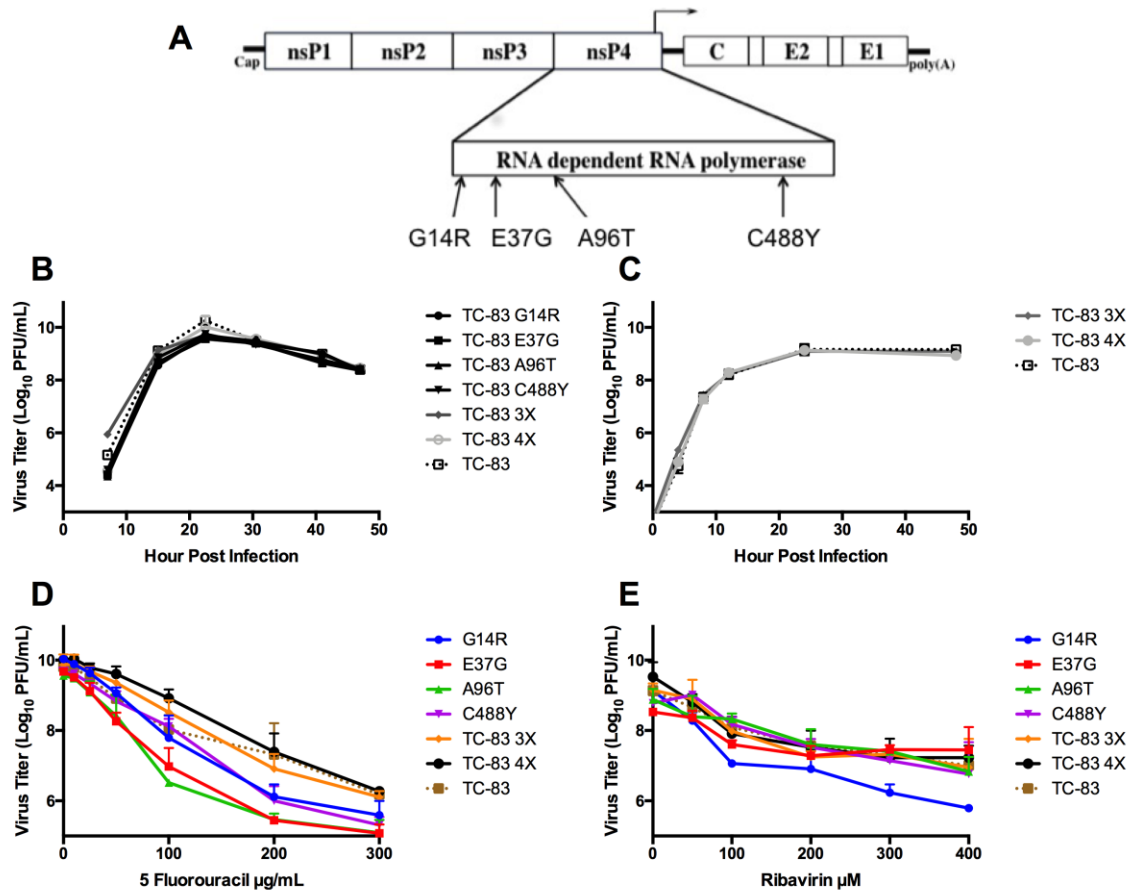
Figure 2.1: *In vitro* characterization of the TC-83 RdRp mutants.

A schematic of the TC-83 genome showing the placement of the four mutations in the RdRp gene (A). Growth curves of TC-83 and the RdRp mutants in interferon negative Vero cells (B) or interferon competent HEK-293 cells (C). Experiments were performed in triplicate and titers were determined by standard plaque assay. Two-way ANOVA was used to determine statistical significance, and bars indicate standard deviation. Resistance of TC-83 mutants to treatment by 5FU (D). Cells were treated with 0, 10, 25, 50, 100, 200, or 300 µg/ml of 5FU and infected using an MOI of 0.01; all experiments were performed in triplicate. Samples were titered by standard plaque assay. Statistical differences were determined by two-way ANOVA, and significance is detailed in the text. Resistance of TC-83 mutants to treatment by Ribavirin (E). Cells were treated with 0, 50, 100, 200, 300, or 400 µM Ribavirin and infected using an MOI of 0.01; all experiments were performed in triplicate. Samples were titered by standard plaque assay. Statistical differences were determined by two-way ANOVA, and significance is detailed in the text.
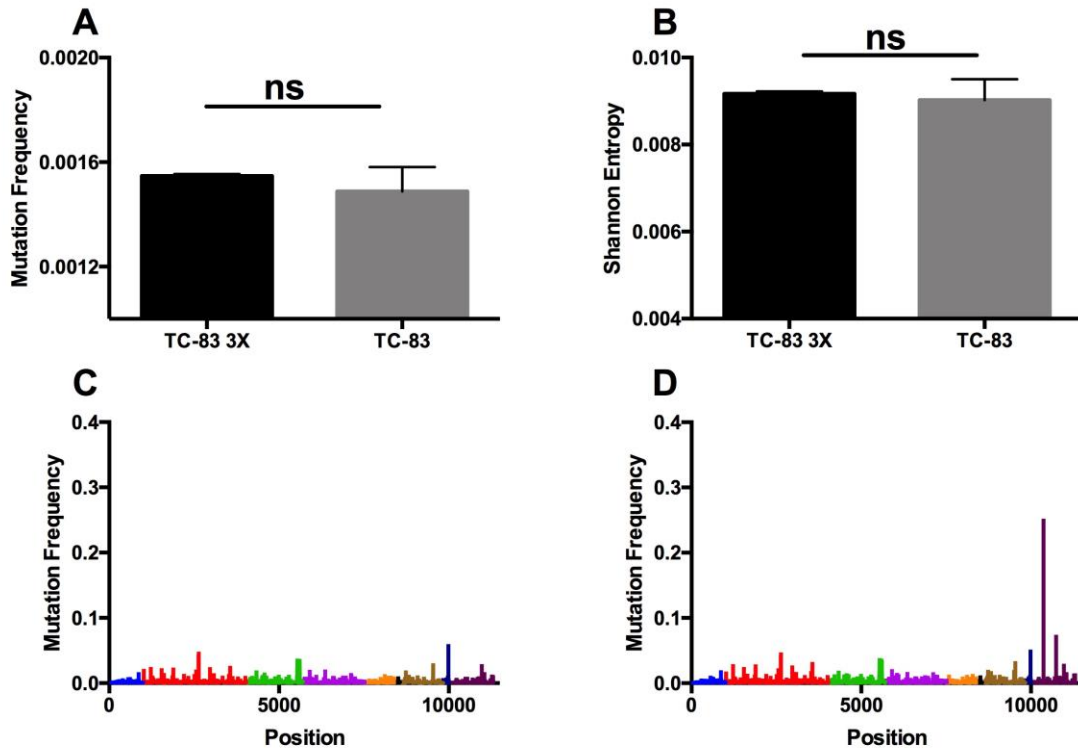
Figure 2.3: Illumina sequencing virus mutation frequency analysis of TC-83 and TC-83 3x PE using BHK cells.

Overall mutation frequency for each cell type (A). Overall Shannon Entropy for each cell type (B). Mann-Whitney U test was used to determine statistical significance, $p > 0.05$ is represented by ns. Illumina sequencing virus diversity hotspots for the coding regions of TC-83 3x (C) and TC-83 (D) PE using BHK cells. A representative replicate is pictured for each virus isolate. Genome organization is color-coded using the following: nsP1: blue, nsP2: red, nsP3: green, nsP4: purple, capsid: orange, E3: black, E2: gold, 6k: navy blue, and E1: maroon.
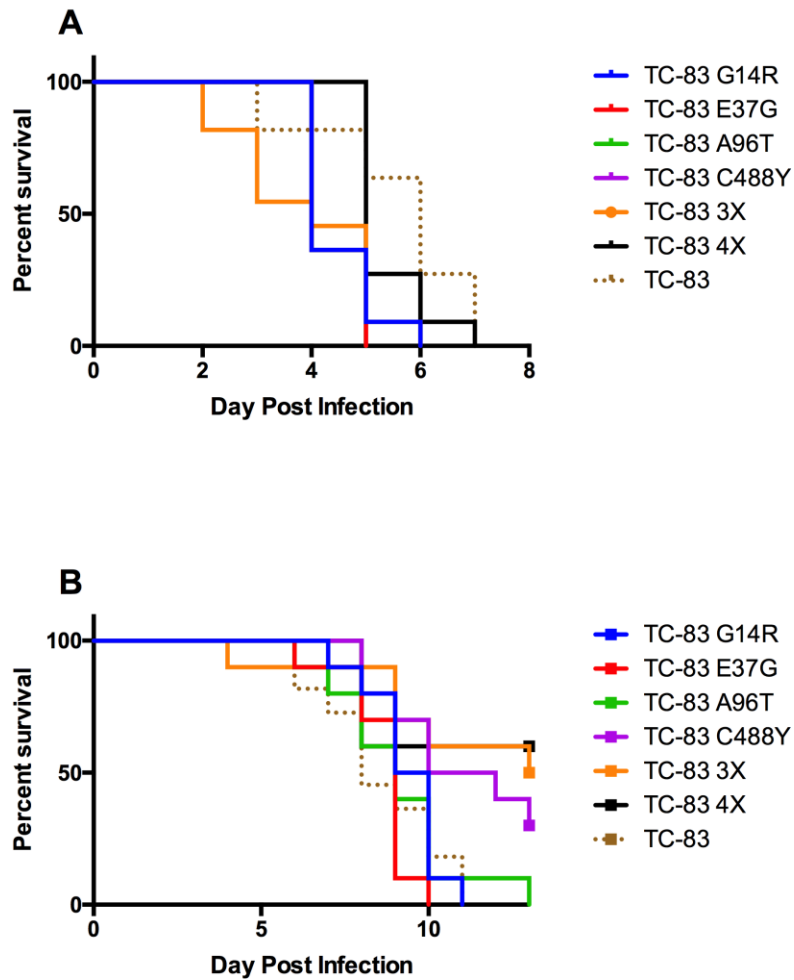
Figure 2.2:   TC-83 and RdRp mutant attenuation *in vivo*.

Survival curves for theTC-83 and the RdRp mutants in 6-day old CD-1 mice following IC injection (A) and SC injection (B) of 10^5 PFU. Statistical differences were determined using Kaplan-Meier tests, and significance is detailed in the text.
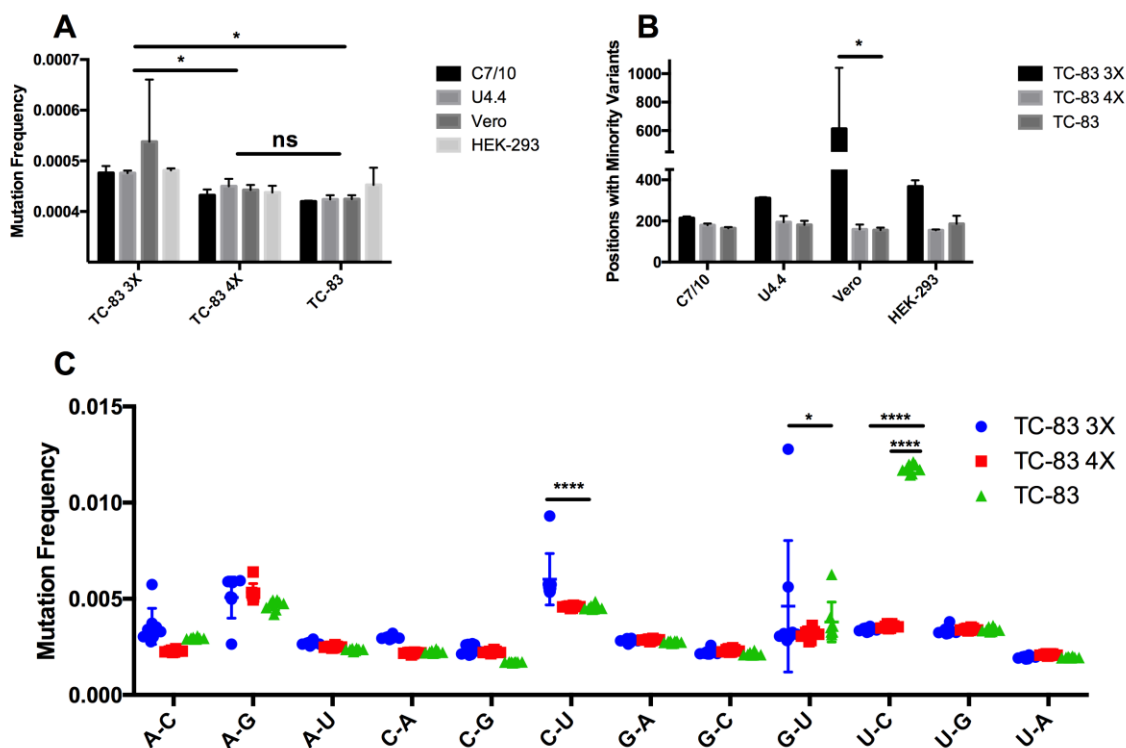
Figure 2.4:   Illumina sequencing virus mutation frequency analysis of TC-83, 3x, and 4x after 1 passage on Vero, HEK-293, C7/10, or U4.4 cells.

Overall mutation frequency for each cell type (A). Number of genomic positions with minority variants present above a frequency of 0.001 (B). Mutation frequency of different mutations (C). Two-way ANOVA was used to determine statistical significance, $p < 0.05$ is represented by *, $p < 0.01$ is represented by **, $p < 0.001$ is represented by ***, and $p < 0.0001$ is represented by ****.
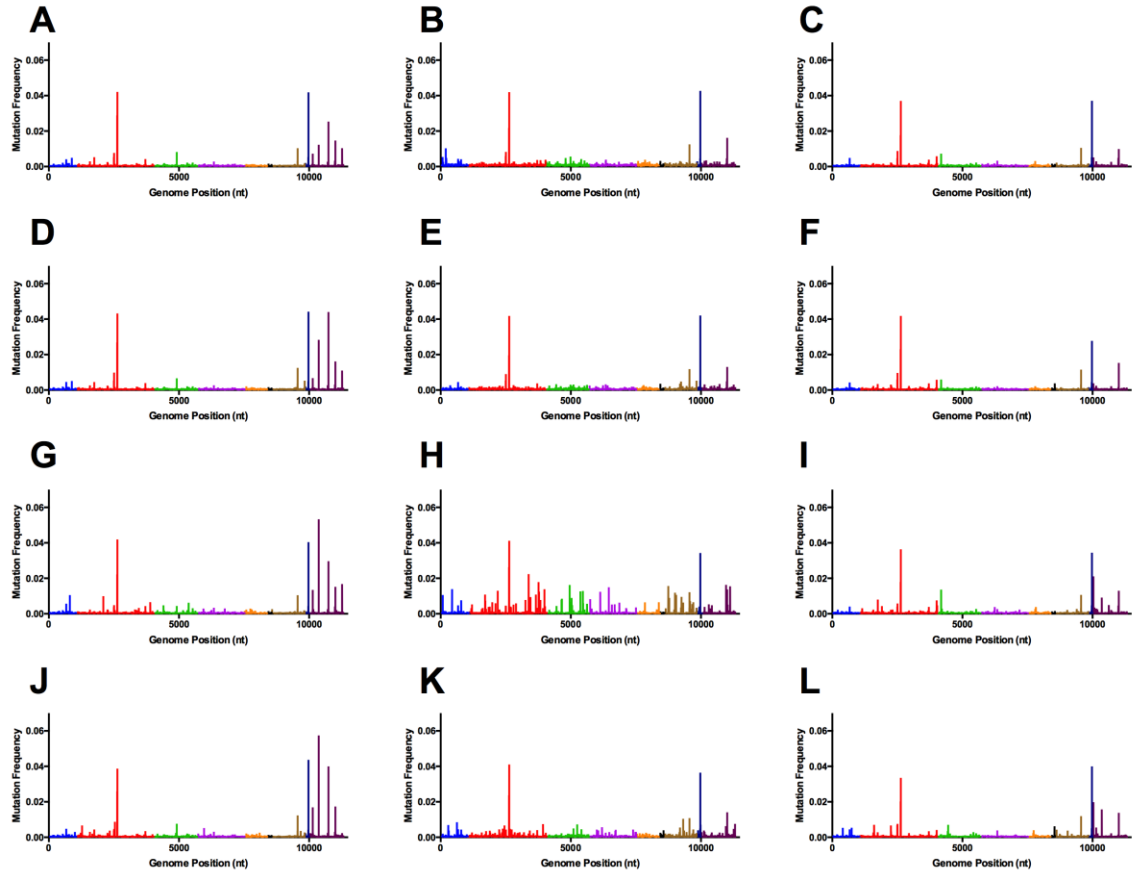
Figure 2.5:   Illumina sequencing virus diversity hotspots for the coding regions of TC-83, 3x, and 4x genomes after 1 passage on Vero, HEK-293, C7/10, or U4.4 cells.

A representative replicate is pictured for each virus isolate from each cell type. TC-83 (A, D, G, J), TC-83 3x (B, E, H, K), and TC-83 4x (C, F, I, L). Vero (A, B, C), HEK-293 (D, E, F), C7/10 (G, H, I), and U4.4 (J, K, L). Genome organization is color-coded using the following: nsP1: blue, nsP2: red, nsP3: green, nsP4: purple, capsid: orange, E3: black, E2: gold, 6k: navy blue, and E1: maroon.
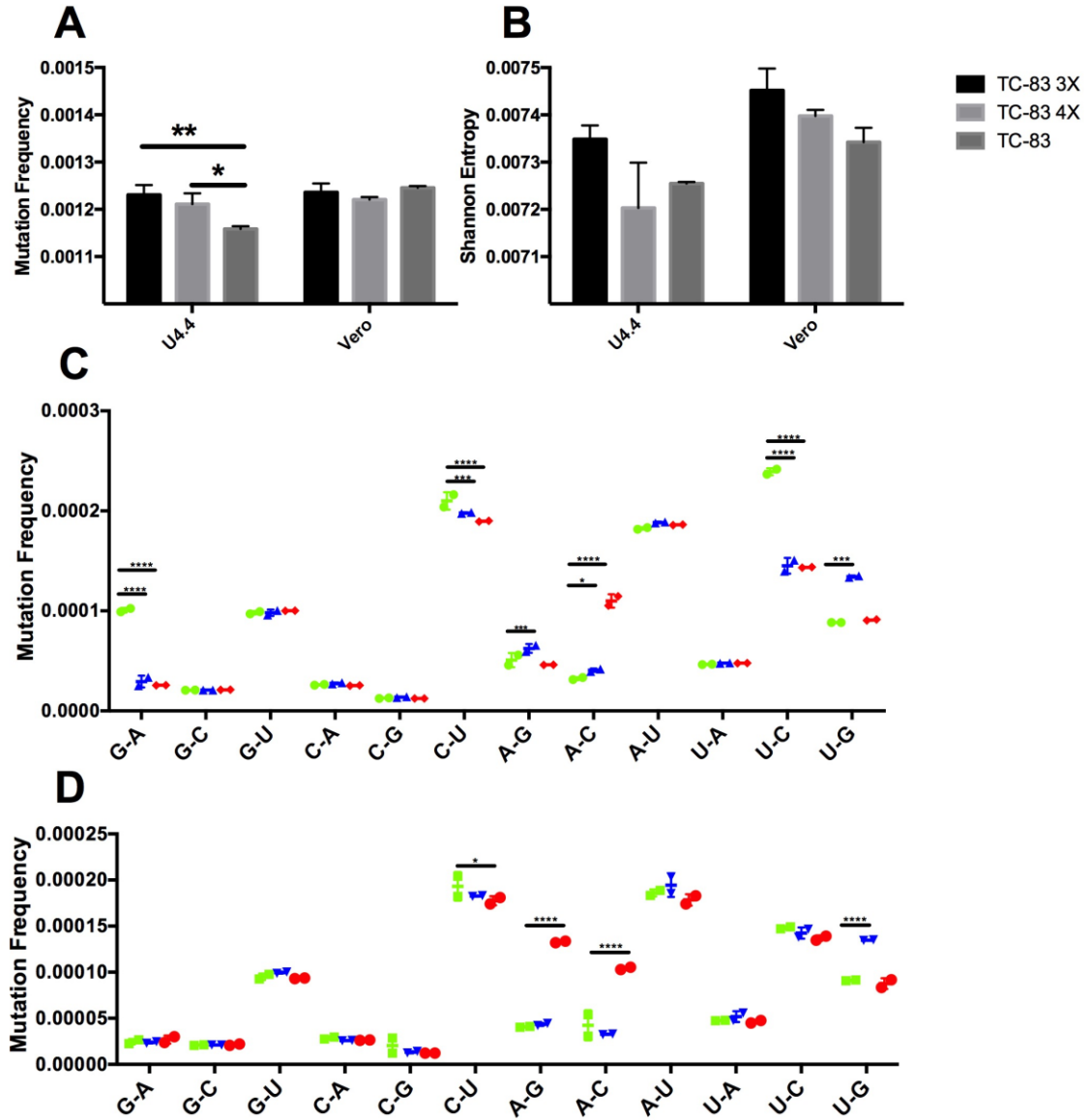
Figure 2.6: Illumina sequencing virus mutation frequency analysis of TC-83, 3x, and 4x after 3 passages on Vero or U4.4 cells.

Overall mutation frequency for each cell type (A). Overall Shannon Entropy for each cell type (B). Mutation frequency of different mutations in Vero (C) and U4.4 (D) cells. TC-83 3x: blue; TC-83 4x: green; TC-83: red. Two-way ANOVA was used to determine statistical significance, $p < 0.05$ is represented by *, $p < 0.01$ is represented by **, $p < 0.001$ is represented by ***, and $p < 0.0001$ is represented by ****.
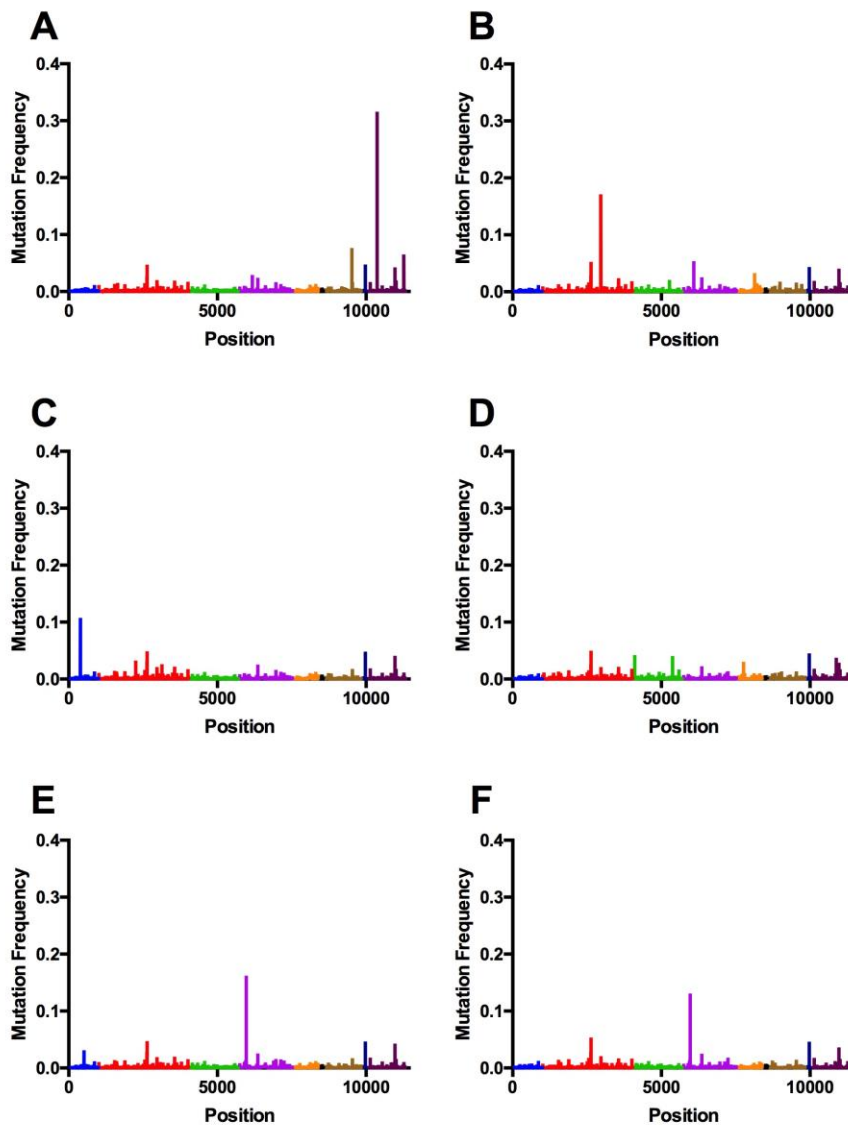
Figure 2.7: Illumina sequencing virus diversity hotspots for the coding regions of TC-83, 3x, and 4x genomes after 3 passages on Vero or U4.4 cells.

A representative replicate is pictured for each virus isolate from each cell type. TC-83 (A, B), TC-83 3x (C, D), and TC-83 4x (E, F), U4.4 (A, C, E), Vero (B, D, F). Genome organization is color-coded using the following: nsP1: blue, nsP2: red, nsP3: green, nsP4: purple, capsid: orange, E3: black, E2: gold, 6k: navy blue, and E1: maroon.
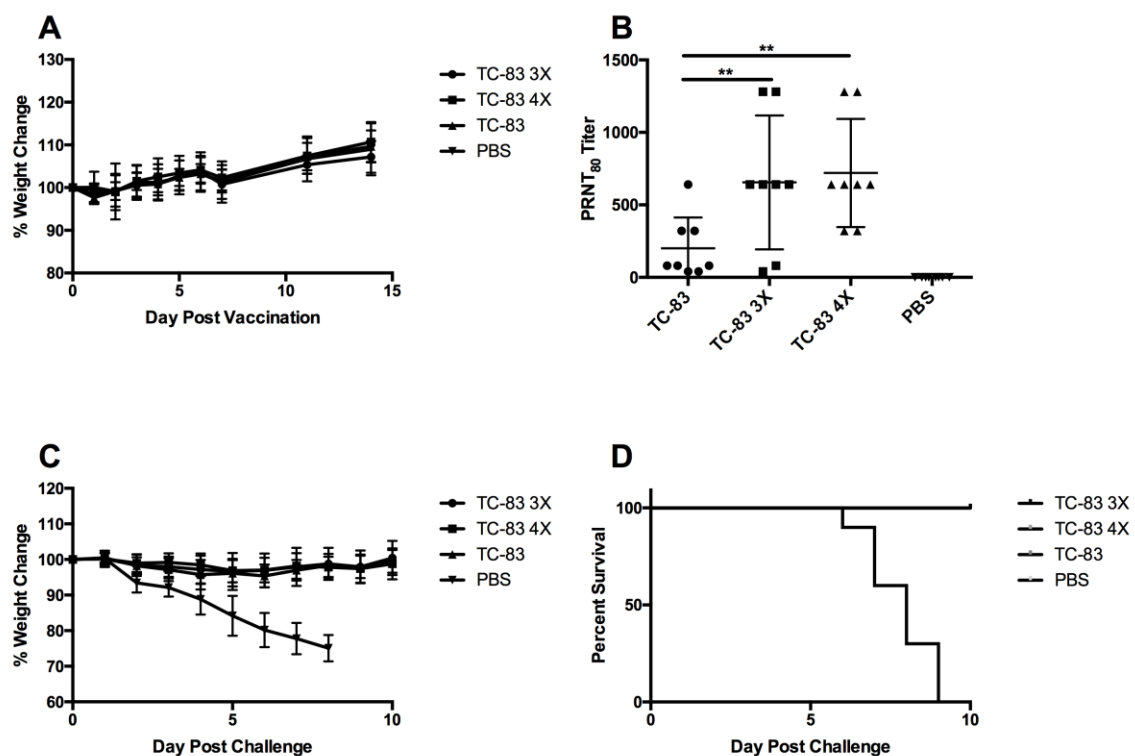
Figure 2.8:   Weight change, immunogenicity, and survival following vaccination and challenge.

Five-week old mice were injected with 10^5 PFU of TC-83, 3x, 4x, or mock in a 50ul volume (n=8 per vaccine treatment). Mice were monitored daily for percent weight change from the original weight at D0 (A). The effectiveness of the vaccine was determined by neutralizing antibody titer using serum from 6 weeks post-vaccination (B), and statistical differences were determined by two-way ANOVA, where $p<0.01$ is represented by **. Mice were challenged with 10^5 PFU of VEEV strain 3908 and were monitored for percent weight change from the original weight at D0 (C) and survival (D).

	Day 1		Day 2		Day 3	
	No. positive	Average Titer (± standard deviation)	No. positive	Average Titer (± standard deviation)	No. positive	Average Titer (± standard deviation)
TC-83 3x	5/5	2.68 (± 0.52)	2/5	2.28 (±0.21)	3/5	2.12 (± 0)
TC-83 4x	3/5	2.59 (± 0.41)	0/5	0	3/5	2.61 (± 0.59)
TC-83	4/5	2.94 (± 0.57)	1/5	2.73 (± 0)	2/5	2.47 (± 0.49)
PBS	0/5	0	0/5	0	0/5	0

Table 2.1:   Viremia titers following vaccination with TC-83, TC-83 3x, TC-83 4x, or mock.

Different cages of vaccinated mice (n=5) were bled on alternating days.

TC-83 767	TC-83 pVE IC-92	TC-83 3X	TC-83 4X
401G	401C	401G	401G
1613A	1613G	1613G	1613G
1616C	1616A	1616A	1616A
1619T	1619C	1619C	1619C
8032A	8032C	8032A	8032C
9760T	9760T	9760G	9760T
10356C	10356T	10356C	10356C
11404T	11404T+T	11404T	11404T

Table 2.2:   RdRp mutant TC-83 clone chimerization.

TC-83 3x and 4x were found to be chimeras of two different TC-83 clones in the lab: TC-83 767 and TC-83 pVE IC-92. The blue and red highlights indicate the mutations each RdRp mutant shares with one of the TC-83 clones. Mutations were synonymous, except for the T10356C mutation, which changes the amino acid from alanine to valine. For all of the experiments in this dissertation, TC-83 pVE IC-92 was used as the control TC-83.
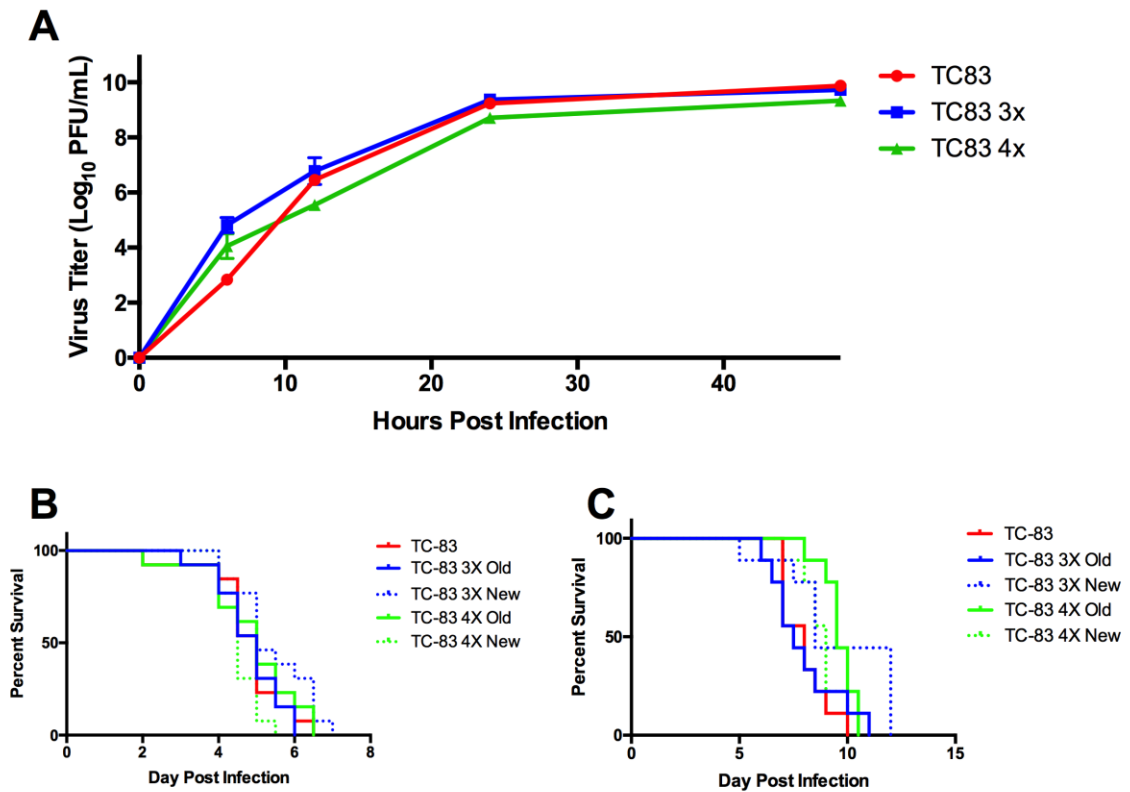
Figure 2.9:   Low-fidelity TC-83 3x variation in attenuation.

2-step growth curve in Vero cells using virus stock from clones containing the RdRp mutations in the control TC-83 backbone (A). Statistical differences were determined two-way ANOVA and are detailed in the text. Survival curves for the TC-83 mutants in 6-day old CD-1 mice following IC injection (B) and SC injection (C) of 10^5 PFU from RdRp EP stocks. "Old" denotes the original RdRp mutant clone, while "New" denotes RdRp mutants in the same backbone as the control TC-83. Statistical differences were determined using Kaplan-Meier tests and are detailed in the text.

LOW-FIDELITY TC-83 FITNESS IN THE MOSQUITO VECTOR

Chapter 3: Low-fidelity TC-83 is attenuated in the mosquito

INTRODUCTION

VEEV has been isolated from many species of mosquito, with confirmed enzootic vectors including various species of *Cu. (Mel.)* (255-259), as well as *Ps. confinnis* (252), *Ae. sollicitans* (252, 253), and *Ae. taeniorhynchus* (253, 254) during epizootic transmission. During epizootic infection, decades-old studies have found equine viremia titers to range from $10^5 - 10^8$ SMicLD$_{50}$/mL (364-366). SMicLD$_{50}$/mL is estimated to be approximately 50-850 times more sensitive than plaque assays for virulent VEEV strains (341, 365), although there is very little difference between PFU/mL and SMicLD$_{50}$/mL for TC-83 (365, 366). In horses vaccinated with TC-83, approximately 60-100% of horses produce low titer viremia, ranging from trace amounts (i.e. some suckling mice become sick but recover) to 3.7 SMicLD$_{50}$/mL (364-366).

Although these titers are low, TC-83 has been isolated from field-caught mosquitoes (306), suggesting that the vaccine is able to enter a transmission cycle. This is especially concerning due to the high levels of TC-83 reversion and pseudoreversion (292, 295), which could potentially initiate an epizootic outbreak. As our low-fidelity TC-83 3x mutant produces identical viremias post-vaccination of mice in comparison to TC-83, it is important to know if this mutant is more restricted in the mosquito vector than the original TC-83. As other arbovirus fidelity mutants are attenuated *in vitro* and *in vivo* in the mosquito (80, 82, 83), we hypothesize that TC-83 3x will be more attenuated than TC-83 in the mosquito vector.

METHODS

Cell cultures

Vero (African green monkey kidney) cells were obtained from the American Type Culture Collection (Bethesda, MD) and maintained in DMEM (Gibco) supplemented with 10% Fetal Bovine serum (FBS, Atlanta Biologicals), and 500μg/mL gentamycin (Corning) in a 37°C 5% CO_2 incubator. C7/10 and C6/36 mosquito cells were maintained in DMEM supplemented with 10% Fetal Bovine serum, 1% Minimal Essential Medium Nonessential Amino Acids (Gibco), 1% Trypose Phosphate Broth (Sigma), and 500μg/mL gentamycin in a 30°C 5% CO_2 incubator. U4.4 cells were maintained in Mitsuhashi and Maramorosch media (Sigma) supplemented with 20% FBS, 2% Sodium Bicarbonate (7.5%) (Gibco), and 500μg/mL gentamycin in a 30°C 5% CO_2 incubator.

Plaque assay

One day prior to infection, 6-well or 12-well Vero plates were plated using 250,000 or 500,000 cells per well respectively to ensure approximately 90% confluency the following day. Virus stocks were diluted 1:10 8 times using 225μL DMEM (supplemented with 2% FBS and gentamycin) and 25μL virus. If no plaques were observed for an isolate, then the plaque assay was repeated using 100 μL of undiluted sample, resulting in a limit of detection of 10 PFU/mL. This dilution series was either performed using 1.5mL tubes (using vortexing to mix) or 96 well plates (using pipetting to mix). Media was then decanted from a cell culture plate and 100μL (12-well plate) or 200μL (6-well plate) of each dilution was added to a well. This was performed in duplicate. The infected monolayers were stored in a 37°C 5% CO_2 incubator for 1 hour and were gently shaken every 15 minutes to ensure an even infection distribution. After this incubation, a 0.4% agarose overlay (1 part 2% agarose (Lonza) in filter-purified water to 4 parts DMEM supplemented with 2%FBS and gentamycin) was added to each well, and the plates were returned to the incubator. Following a 48 hour incubation, the monolayers were fixed for 30 minutes using 10% formaldehyde (Fisherbrand) before the

agarose plugs were removed and the monolayer was stained with 0.25% crystal violet solution (Fisherbrand). The plates were then washed with water and allowed to dry before plaques were counted.

PFU per mL was calculated using the following formula: PFU/mL=(dilution X number of plaques) (1000/amount plated), with "dilution" equaling the dilution at which the plaques were counted and "amount plated" equaling the amount of virus added when infecting the cells (i.e. 100μL for 12-well plates and 200μL for 6-well plates).

Mosquito infections

F1 generation *Ae. taeniorhynchus* mosquitoes were infected with TC-83 or TC-83 3x mixed 1:1 with defibrinated sheep blood (Colorado Serum Co.) to a final titer of 10^5 PFU/mL in 4mL total. *Ae. sollicitans* mosquitoes also from a UTMB insectary colony were infected with TC-83 or TC-83 3x mixed 1:1 with defibrinated sheep blood to a final titer of 10^7 PFU/mL in 4mL total.

2-3 mL of the virus/blood mixture was pipetted into a Hemotek reservoir enclosed in mouse skin. Two cohorts of 50 mosquitoes per virus were allowed to feed for 30 minutes before being transferred to a -20°C freezer until paralyzed. Mosquitoes that had failed to feed were discarded. Those that fed were incubated for 9 (*Ae. sollicitans)* or 10 (*Ae. taeniorhynchus*) days at 27°C before being harvested. Heads and bodies were removed and stored in separate tubes containing a steel bead as well as 125μl DMEM supplemented with 10% FBS, gentamycin, and 0.25μg/mL fungizone (Gibco). Mosquitoes were homogenized using a TissueLyser II (Qiagen) for 5 minutes at 26 beats/second, and then centrifuged for 5 minutes at 3.3 *X g*. Supernatant was transferred to a fresh tube and stored at -80°C. Plaque assays were used to determine virus titer.

Growth Curves

The day of the infection, U4.4 or C7/10 mosquito cells were counted using a hemocytomer and diluted to 10^6 cells/mL. Depending on the number of samples needed for each experimental condition, a certain volume of the cells was aliquoted into a 50mL tube with a single tube for each condition.

The cells were centrifuged for 2 minutes at 783 X g and 4°C. Media was decanted, and the cells were infected with an MOI of 10 or 0.01 by resuspension in 500μL of the appropriate media for the cell type (see "cell cultures"). The infected cells were incubated for one hour in a 30°C 5% CO_2 incubator with gentle mixing every 10 minutes. After this, the cells were centrifuged for 2 minutes at 783 X g and 4°C and the inoculum was aspirated from the pellet and discarded. Following this, the cells were resuspended in 5mL of PBS and centrifuged for 2 minutes at 783 X g and 4°C. After this wash step was repeated, the cells were resuspended in the initial volume of media and 0.5mL/well was aliquoted into a 24-well plate and returned to the 30°C 5% CO_2 incubator.

Virus was harvested by removing the entirety of the medium from three wells per time point (independent measures). During the dependent measures growth curve, media was replaced after each harvest. Harvested virus was supplemented with FBS to a final concentration of 20%, and clarified by centrifugation at 0.8 X g for 5 min. The supernatant was transferred to a new tube and stored at -80°C. Viral titers were determined by plaque assays on Vero cells, as described above.

Enoxacin treatment of mosquito cells

The day of the infection, media was removed from T-150 flasks of U4.4 or C6/36 mosquito cells and replaced with the 15mL of the appropriate media for the cell type (see "cell cultures") supplemented with 25 or 50μM Enoxacin (Sigma). After a 2 hour incubation in a 30°C 5% CO_2 incubator, the cells were counted using a hemocytomer and diluted to 10^6 cells/mL. Depending on the number of samples needed for each

experimental condition, a certain volume of the cells was aliquoted into a 50mL tube with a single tube for each condition.

The cells were centrifuged for 2 minutes at 783 *X g* and 4°C. Media was decanted, and the cells were infected with an MOI of 10 or 0.01 by resuspension in 500μL of the appropriate media for the cell type. The infected cells were incubated for one hour in a 30°C 5% CO_2 incubator with gentle mixing every 10 minutes. After this, the cells were centrifuged for 2 minutes at 783 *X g* and 4°C and the inoculum was aspirated from the pellet and discarded. Following this, the cells were resuspended in 5mL of PBS and centrifuged for 2 minutes at 783 *X g* and 4°C. After this wash step was repeated, the cells were resuspended in the initial volume of media supplemented with 25 or 50μM Enoxacin. 0.5mL of this cellular suspension was aliquoted into a 24-well plate and returned to the 30°C 5% CO_2 incubator.

Virus was harvested by removing the entirety of the medium from three wells per time point. Harvested virus was supplemented with FBS to a final concentration of 20%, and clarified by centrifugation at 0.8 *X g* for 5 min. The supernatant was transferred to a new tube and stored at -80°C. Viral titers were determined by plaque assays.

Sanger sequencing of TC-83 RdRp mutations

To determine if the TC-83 3x virus that was able to grow well during the 2-step mosquito cells growth curve may have reverted any of the RdRp mutations, sequencing was performed.

Virus RNA was extracted from the positive virus samples using the QIAamp Viral RNA Minikit as per the manufacturer's protocol and stored at -80°C. Using 3μl of this RNA, the Superscript III RT PCR kit (Invitrogen) was used to generate cDNA by adding 5μl nuclease-free water, 1μl dNTPs (NEB), and 1μl random hexamers. This was incubated at 65°C for 5 minutes and placed on ice for 2 minutes. Following these incubations, 4μl $MgCl_2$, 2μl 10X RT buffer, 2μl DTT, 1μl RNase OUT, and 1μl SSIII

enzyme was added to the first tube and incubated for 10 minutes at room temperature, followed by 43°C for 90 minutes, and finally 50°C for 10 minutes. This was stored at - 20°C.

High fidelity Phusion PCR (NEB) was used to generate approximately two, 1.5kb amplicons that encompassed the RdRp mutations. In a PCR tube, 2.5μl of cDNA was added to 10μl 5X buffer, 1μl dNTPs, 1μl forward primer (20μM), 1μl reverse primer (20μM), 32μl nuclease-free water, 2μl MgCl$_2$, and 0.5μl Phusion polymerase. The amplicon primers were as follows: 4937V+6579C and 6207V+7800C. The PCRs were amplified using a 98°C hot start for 30 seconds, followed by 35 cycles of a 10 second, 98°C denaturation, a 10 second 60°C anneal, and a 1.5 minute elongation at 72°C.

Following PCR amplification, amplicons were visualized by running the entire contents of the reaction on a 1% agarose gel in TAE buffer. The bands were excised and purified using the QIAquick Gel Extraction kit as per the manufacturer's protocol. DNA was eluted into 35μl of nuclease-free water and stored at -20°C.

Sequencing reactions were prepared by adding 1μL of a 2μM primer (4937V, 5200C, 5500V, 5750C, 6000V, or 6579C for the first amplicon and 6207V, 6750V, 7000C, 7250V, or 7800C for the second amplicon) (Table 3.1) to 5μL DNA, 2μL 5X sequencing buffer, and 2μL BigDye (Applied Biosystems). The sequencing reactions were amplified using a 96°C hot start for 2 minutes, followed by 30 cycles of a 10 second 96°C denaturation, a 5 second 50°C anneal, and a 4 minute elongation at 60°C. Following this, sequencing reactions were purified using Performa spin columns (EdgeBio) as per the manufacturer's protocol, and loaded onto the Applied Biosystems 3500 Genetic Analyzer sequencer. Sequences were analyzed using Sequencher version 5.0.1.

RESULTS

Mosquitoes are refractory to TC-83 infection

Although TC-83 was previously isolated from a pool of field-caught *Ps. confinnis* mosquitoes (306), these mosquitoes were not available for infection. Instead, other VEEV vectors were tested for susceptibility to TC-83.

First, *Ae. taeniorhynchus* mosquitoes were allowed to feed on a blood meal spiked with 10^5 PFU/mL of TC-83 or TC-83 3x (Appendix 2, stocks 1-2). Of the 100 mosquitoes allowed to feed per virus, approximately half of these mosquitoes became engorged. After a 10-day incubation, however, none of the mosquitoes that survived were positive for infection as measured by CPE assay on Vero cells (data not shown).

Later, *Ae. sollicitans* mosquitoes were allowed to blood feed using a higher dose of 10^7 PFU/mL (Appendix 2, stocks 4-5). Of the approximately 100 mosquitoes that were allowed to feed per virus (Table 3.2), roughly half of the mosquitoes became engorged, and 23 (TC-83) or 18 (TC-83 3x) survived the 9-day incubation period. Of these, only 4 mosquitoes became infected per virus, with one or two mosquitoes experiencing a disseminated infection. There was no significant difference in the body or head titers of the TC-83 or TC-83 3x infected mosquitoes (Figure 3.1).

Attenuated growth of low-fidelity TC-83 *in vitro*

Due to the high number of mosquito infections that would be required to further study infection *in vivo*, as well as the unnaturally high titers required for infection, *in vitro* studies were carried out to further determine differences in the mosquito host between TC-83 and the low-fidelity TC-83 3x.

One-step growth curves were performed in various mosquito cells to determine differences in the single-cell life cycle kinetics of the viruses (Figure 3.2). As expected, TC-83 was able to grow to higher titers in C6/36 and C7/10 cells, which lack a functional siRNA pathway, than in U4.4 mosquito cells, which produce antiviral siRNAs (272) (Figure 3.2 A-D). We hypothesized that these siRNAs would play a role in attenuating low-fidelity TC-83 due to the sequence specificity of RNAi. Interestingly, TC-83 3x was

attenuated in all of the tested mosquito cells. These results were repeatable (Figure 3.2A-B (Appendix 2, stocks 1-2) versus Figure 3.2C-D (Appendix 2, stocks 1-2). The observed attenuation of TC-83 3x was not due to the RdRp mutations altering temperature sensitivity, as Vero cells infected with TC-83 or TC-83 3x at 30°C showed no significant differences in virus titer (Figure 3.2 E-F, Appendix 2 stocks 8-9).

During 2-step growth curves, which measure differences in growth kinetics that may need several lifecycles to become apparent, TC-83 growth was slightly, but not significantly attenuated in U4.4 versus C7/10 mosquito cells. The low-fidelity mutant, however, struggled to produce infectious virus, with many isolates measuring completely negative by standard plaque assay. Independent samples were taken for each time point, so samples negative for infectious virus resulted in very large error bars (Figure 3.3A, Appendix 2 stocks 1-2). When these virus negative samples were removed (Figure 3.3 B), the growth kinetics more closely reflected the 1-step growth curve results (Figure 3.2 A&C). Sanger sequencing of successful TC-83 3x virus showed that none of fidelity-altering mutations reverted.

To determine if the virus extinction results in Figure 3.3 were due to fluctuating release of the virus or an overall failure of the infecting virus to cause a productive infection, 2-step growth curves were performed in parallel using 10 replicates of TC-83 3x per cell type. For this experiment, media was collected and replaced at every time point. In C7/10 cells (Figure 3.4A, Appendix 2 stocks 4-5), 4 of the 10 replicates did not produce any infectious virus as measured by plaque assays, while the remainder of the replicates all grew at a normal rate once virus began to be produced. The U4.4 replicates acted similarly to the C7/10 cell infection (Figure 3.4B). Interestingly, at 24 HPI the titer dipped for many of the U4.4 replicates, with the lowest-titer replicate driven to extinction by 48 HPI.

Unfortunately, efforts to better understand this attenuation were stalled when a new TC-83 3x EP stock failed to exhibit this attenuation phenotype, even after multiple

95

infections (data not shown, Appendix 2 stocks 9-10). As two prior EP stocks exhibited this attenuated phenotype (Appendix 2 stocks 2 and 5), this suggests that the *in vitro* mosquito cell attenuation results from the most EP recent stock are the exception rather than the norm.

Enoxacin treatment has no effect on TC-83 growth *in vitro*

Mosquito cells were treated with enoxacin, a fluoroquinolone shown to enhance the RNAi response (367, 368), to determine if enhancement of RNAi would further attenuate the low-fidelity TC-83 mutant. No effect was observed when cells were treated with 50 or 100μM enoxacin and infected with an MOI of 10 (Figure 3.5, Appendix 2 stocks 1-2).

When treated with 50μM enoxacin and infected with an MOI of 0.01 (Appendix 2, stocks 1-2), no difference was observed for untreated cells infected with TC-83 (Figure 3.6 A&C). The extreme differences in virus titer observed during low MOI TC-83 3x infection also occurred when cells were treated with enoxacin (Figure 3.6 A&C), with enoxacin perhaps contributing to a lack of virus growth in U4.4 cells (Figure 3.7).

DISCUSSION

For a mosquito to be considered an arbovirus vector, it must be known to interact with and take blood meals from the vertebrate host in question, have multiple mosquito isolates from nature that are positive for virus infection, and be experimentally demonstrated to be competent for infection and transmission (369, 370). Based upon this definition, TC-83 has not been proven to be transmissible by a mosquito vector, as it has only been isolated once in the wild (306) and mosquitoes are only easily infected via IT injection (371). Our *in vivo* results suggest that the probability of a natural mosquito infection with TC-83 is low. For example, although *Ae. sollicitans* mosquitoes typically

exhibit high VEEV infection rates (253), these mosquitoes were difficult to infect with TC-83 even when using bloodmeal titers 10,000-fold higher than those expected from a vaccinated horse (304, 366).

However, on the off chance that a mosquito does become infected with TC-83, our *in vitro* results suggest that the low-fidelity TC-83 mutant will be more attenuated in the vector than the original vaccine. This is not surprising as other fidelity arbovirus mutants are also attenuated in the mosquito vector (80, 82, 83). However, the mechanisms behind this attenuation are not well understood. A recent paper found low-fidelity SINV to be attenuated in *Drosophila* due to the increased number of defective viral genomes being produced during infection, causing increased stimulation of the RNAi response (372). Due to the similarities between this mutant and ours, it is likely that our low-fidelity mutant is also attenuated in a similar fashion.

Because RNAi does not play a significant antiviral role in the vertebrate host, where no difference between fidelity mutants and parent virus is observed *in vitro*, this suggests that RNAi is playing the predominant role in fidelity mutant attenuation in mosquito cells. As altering the virus fidelity changes the RNA sequences produced during virus replication, we hypothesized that the antiviral RNAi response in the mosquito was decreasing low-fidelity TC-83 3x replication fitness. To better understand if this response is why fidelity mutants are attenuated *in vitro* in mosquito cells, we attempted to enhance the RNAi response using the fluoroquinolone, enoxacin. In our hands, enoxacin did not appear to have any effect on virus growth for either TC-83 or TC-83 3x. This may be because enoxacin has only been previously examined in mammalian cells (367, 368), suggesting that the mechanism of action for this drug is not conserved in mosquitoes. Future work examining the small RNA repertoire in mosquito cells is needed to better understand the interaction of our low-fidelity virus with the RNAi response.

Primer name	Primer sequence (5' to 3')
4937V	TACTGGTGTGCAGAAGATCC
5263C	GATGCRTGAGGAATGGACC
5538V	ATTWCTAGGGAGGAGCTCGAGG
5637C	CTCRAACTCCTCTCTTGTAATCAC
6579C	TTGTTCCTGGAGTCACTTTCAC
6474V	AAATTAAAAGGACCAAARGCTG
6980V	GATGAAATCYGGGATGTTCC
7037C	TCTCTTAACACTCTGCTTGCG
7203V	GCGCCYTATTTYTGTGGAG
7800C	CGTGGTTCTTCTTCTTCTTCC

Table 3.1:   PCR and sequencing primers.

 "V" designates primer sequences complementary to the virus sequence (i.e. positive-sense), while "C" designates primer sequences that bind to the minus-sense strand.

	TC-83	TC-83 3X
Number Fed/Total	47/96	57/101
Number Survived	23	18
CPE + Bodies	4	4
CPE + Heads	2	1

Table 3.2:   *Ae. sollicitans* mosquito infection.

Ae sollicitans mosquitoes were allowed to feed on an infectious blood meal containing 10^7 PFU of TC-83 or TC-83 3x. Mosquitoes were harvested after 10 days, and CPE assays were used to determine infection status.
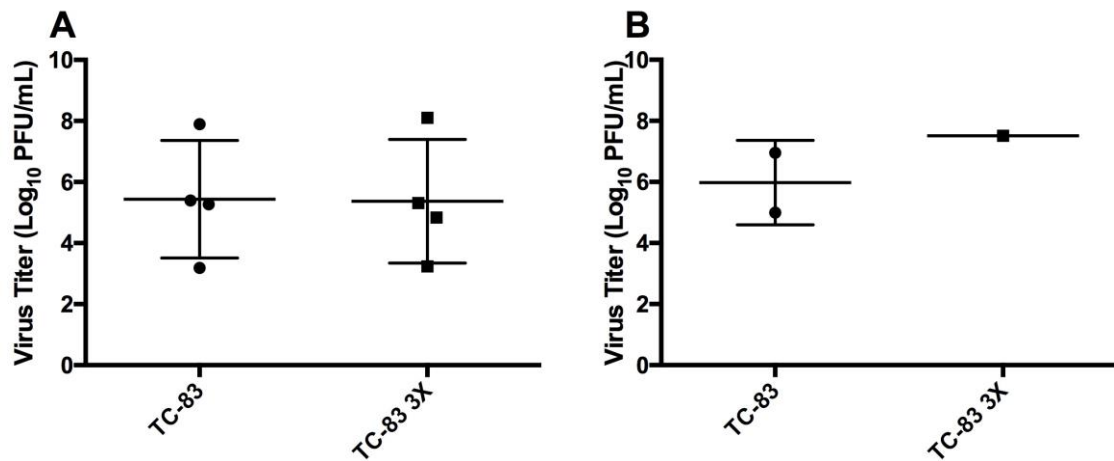
Figure 3.1: *Ae. sollicitans* body and head titers.

Ae. sollicitans mosquitoes were allowed to feed on an infectious blood meal containing 10^7 PFU of TC-83 or TC-83 3x. Mosquitoes were harvested after 10 days, and plaque assays were used to determine the body (A) and head (B) titers of CPE+ mosquitoes. Student's t-test found no significant differences in body titers.
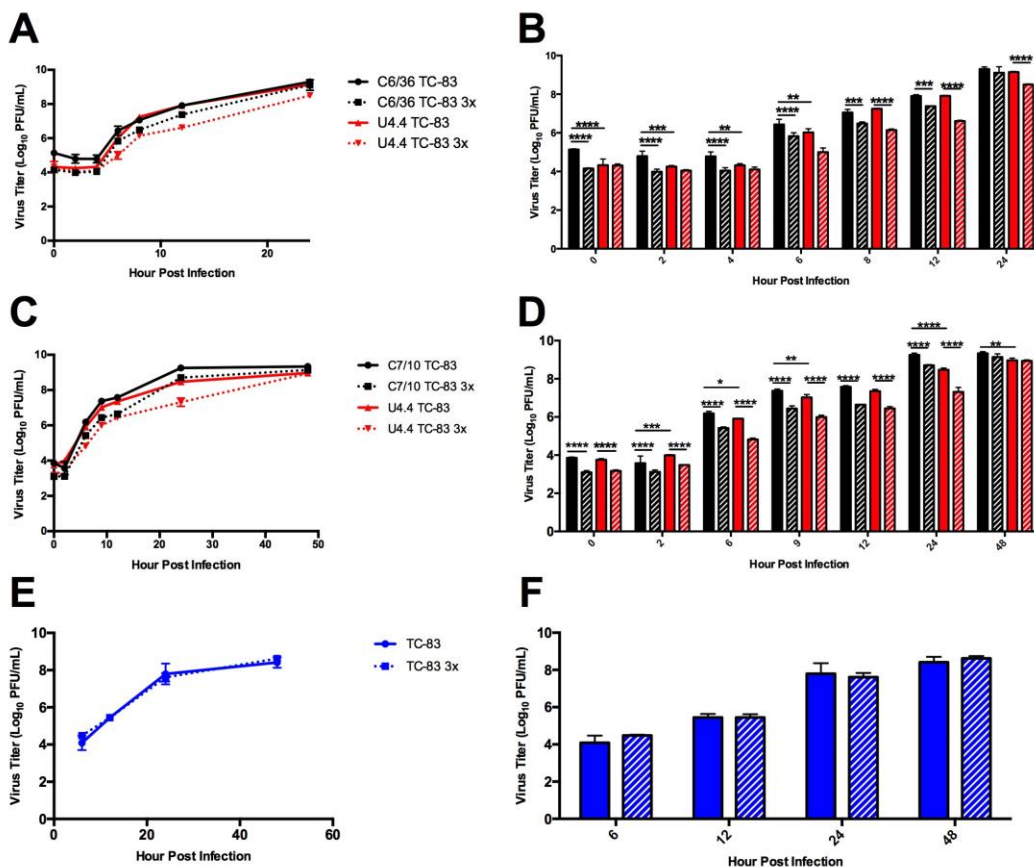
Figure 3.2: Mosquito cell 1-step growth curves.

C6/36 and U4.4 mosquitoes cells were infected with an MOI of 10 of TC-83 or TC-83 3x (A, B). Repeat infection of C7/10 and U4.4 mosquito cells infected with an MOI of 10 of TC-83 or TC-83 3x (C, D). Vero cells infected with at MOI of 10 at 30C (E, F). Infections were performed in triplicate and plaque assayed in duplicate. Error bars show standard deviation. Two-way ANOVA was performed. Significance is displayed in B, D, and F. $p < 0.05$ designated by *, $p < 0.01$ designated by **, . $p < 0.001$ designated by ***, $p < 0.0001$ designated by ****.
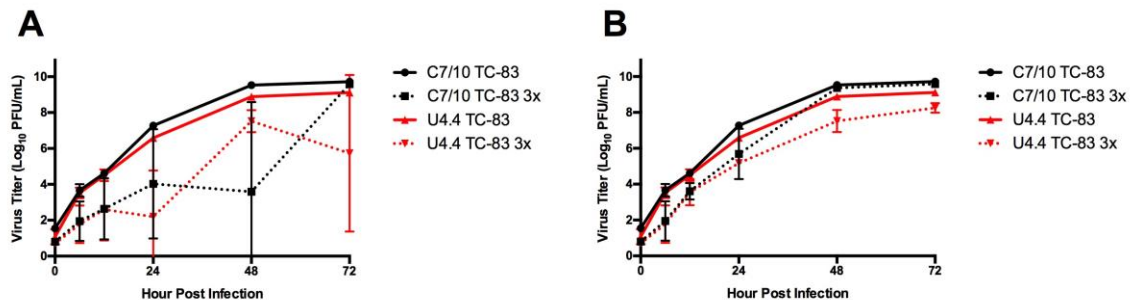
Figure 3.3:   Mosquito cell 2-step growth curves.

U4.4 (A, B, C, D) and C7/10 (A, B, E, F) mosquito cells were infected with TC-83 or TC-83 3x using an MOI of 0.01. Many of the isolates were negative for infectious virus, resulting in large error bars (A, C, E). To better visualize the infectious titers produced, isolates negative for virus were removed (B, D, F). Plaque assays were performed in duplicate. Error bars show standard deviation.
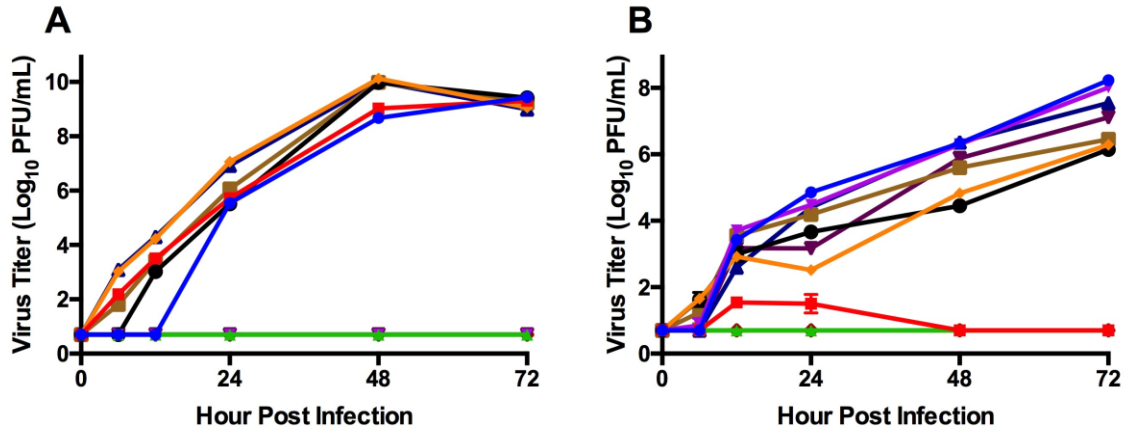
Figure 3.4:   Repeated measure TC-83 3x mosquito cell infection.

To determine how the virus titer changes over time in mosquito cells, C7/10 (A) and U4.4 (B) were infected in replicates of 10 using an MOI of 0.01. Plaque assays were performed in duplicate. Error bars show standard deviation.
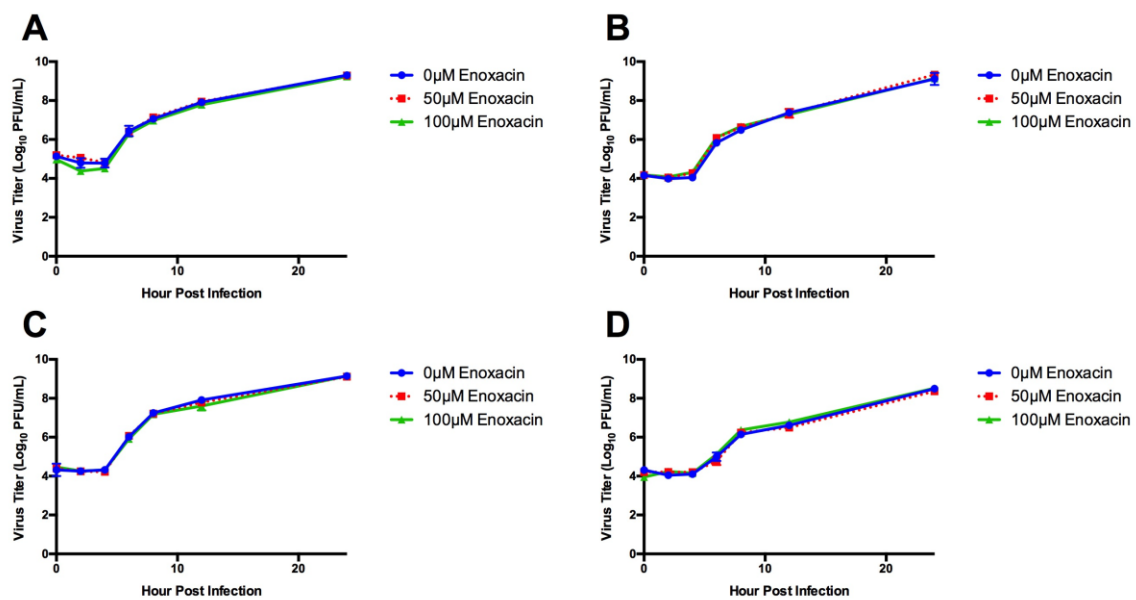
Figure 3.5:   Enoxacin does not protect mosquito cells against high MOI TC-83 infection.

C6/36 cells infected with TC-83 (A) or TC-83 3x (B). U4.4 cells infected with TC-83 (C) or TC-83 3x (D). Mosquito cells were treated with enoxacin or mock, and infections were performed in triplicate using an MOI of 10. Plaque assays were performed in duplicate. Repeated measures ANOVA found no significant difference. Error bars show standard deviation.
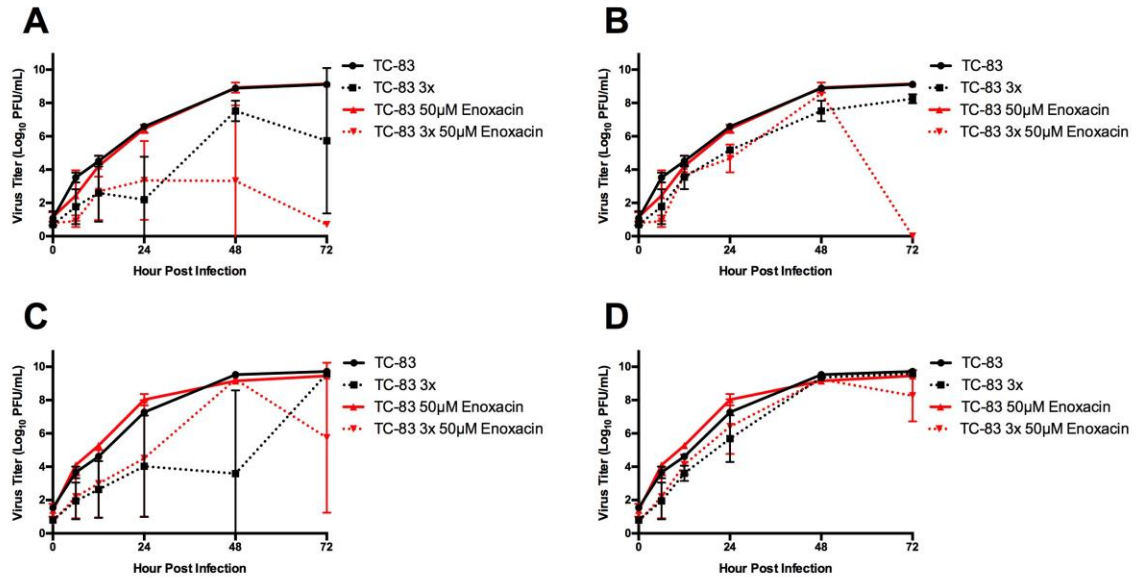
Figure 3.6:   Enoxacin treated mosquito cells during a low MOI infection.

U4.4 (A, B) and C7/10 (C, D) mosquito cells were treated with enoxacin or mock and infected with TC-83 or TC-83 3x using an MOI of 0.01. Many of the isolates were negative for infectious virus, resulting in large error bars (A, C). To better visualize the infectious titers produced, isolates negative for virus were removed (B, D). Plaque assays were performed in duplicate. Error bars show standard deviation.
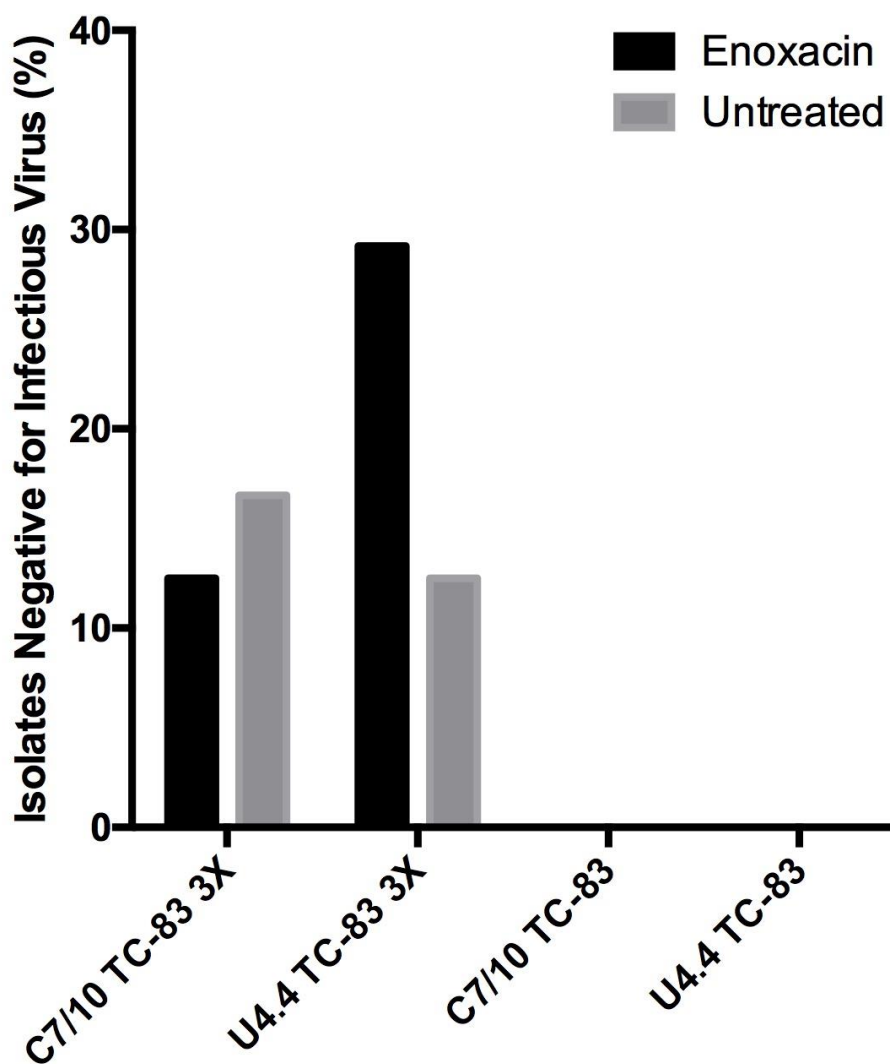
Figure 3.7:   Percentage of virus extinctions in mosquito cells.

During 2-step C7/10 and U4.4 mosquito cell growth curves, a significant number of TC-83 3x infected cells failed to produce infectious virus.

VACCINE STABILITY

Chapter 4: Low-fidelity TC-83 genetic and phenotypic stability[2]

INTRODUCTION

Although LAVs are immunogenic and relatively easy to manufacture, there is the potential for reversion and restoration of virulence. Unfortunately, due to their error-prone RdRp (7), RNA virus LAVs carry the highest risk of reversion or pseudoreversion. For example, the global eradication of PV is nearly complete, largely due to the success of the live-attenuated Sabin vaccine (373). However, this vaccine has also been the source of sporadic cases of vaccine-derived polio, which occasionally result in outbreaks (373-376). Recombination with other enteroviruses (374, 376) and back-mutations (374, 375) of the attenuating mutations have both been described as mechanisms for this reversion, with low vaccination coverage increasing this risk (373). Due to stability issues such as these, as well as the ever-increasing threshold for what constitutes a safe vaccine, it is highly important to test LAVs for their genetic and phenotypic stability. As our RdRp mutant is low-fidelity, it is even more critical to closely examine and determine if this vaccine candidate is at higher risk of reversion compared to TC-83, which itself is notoriously unstable and known to rapidly increase in virulence (292, 295).

While some previously described low-fidelity mutants, such as the alphaviruses CHIKV and SINV, have been shown to be prone to reversion (82), other low-fidelity mutants, such as the ExoN mutant of SARS-CoV are quite stable (99). The mechanisms behind this difference in stability are unknown, although it may be due to the number of

---

[2] Content of this chapter has previously been published: Kautz TF, Guerbois M, Khanipov K, Patterson EI, Langsjoen RM, Yun R, et al. Low-fidelity Venezuelan equine encephalitis virus polymerase mutants to improve live-attenuated vaccine safety and efficacy. Virus Evolution, 4(1), vey004. Reproduced with permission.

fidelity altering mutations; CHIKV and SINV are only one mutation away from reversion, while the SARS-CoV ExoN mutant is six mutations away. As low-fidelity TC-83 exhibited unstable phenotypes in the studies described in the previous two chapters, we hypothesize that the likelihood of reversion or pseudoreversion is rather high, much like the low-fidelity CHIKV and SINV mutants. During this aim, genetic stability (i.e. reversion of the TC-83 attenuating mutations and/or low-fidelity mutations) was measured *in vitro* and *in vivo*, while changes in virulence were assessed *in vivo*.

METHODS

Cell culture

Vero (African green monkey kidney), HEK-293 (human embryonic kidney), MRC-5 (human fetal lung fibroblast), and Baby Hamster Kidney (BHK) cells were obtained from the American Type Culture Collection (ATCC) (Bethesda, MD) and maintained in DMEM (Gibco) supplemented with 10% Fetal Bovine serum (FBS, Atlanta Biologicals), and 500μg/mL gentamycin (Corning) in a 37°C 5% CO_2 incubator. C7/10 cells were maintained in DMEM supplemented with 10% Fetal Bovine serum, 1% Minimal Essential Medium Nonessential Amino Acids (Gibco), 1% Trypose Phosphate Broth (Sigma), and 500μg/mL gentamycin in a 30°C 5% CO_2 incubator. U4.4 cells were maintained in Mitsuhashi and Maramorosch media (Sigma) supplemented with 20% FBS, 2% Sodium Bicarbonate (7.5%) (Gibco), and 500μg/mL gentamycin in a 30°C 5% CO_2 incubator.

Virus stock generation

Viruses were rescued from a TC-83 infectious clone (307) by electroporation using BHK cells. First, 5μg of TC-83 or the other RdRp mutants was linearized using the restriction enzyme MluI (NEB) in a 50μL volume. 5μL of each digestion was mixed with 1μL 6el loading dye (NEB) and run on a 1% agarose (GeneMate) TAE (Fisherbrand) gel

at ca. 100V for ca. 1 hour to confirm digestion. The remainder of the linearized product was purified using a NucleoSpin PCR Clean-up and Gel Extraction kit (Clontech) as per the manufacturer's protocol.

In vitro transcription of the linearized DNA was performed in a 26μL volume using 2.5μL DTT (Invitrogen), 5μL 10X transcription buffer (Ambion), 2.5μL 10mM cap (NEB), 2.5μL 10mM rNTP (Roche), 250ng linearized DNA, XμL nuclease-free water up to a final volume of 26μL, 0.5μL RNaseOUT (Invitrogen), and 1μL of T7 (Ambion) (TC-83) or SP6 polymerase (Ambion) (RdRp mutants for mouse passaging and *in vitro* transmission cycle passaging). This was incubated for 1 hour at 37°C and stored at -20°C overnight.

BHK cells were grown overnight in a T-150 flask to approximately 95% confluency the next day using complete media (DMEM supplemented with 10% FBS, 1% Minimal Essential Medium Nonessential Amino Acids, 1mM Sodium Pyruvate (Corning), and gentamycin. After one wash with with PBS (Gibco), 0.05% trypsin-EDTA (Corning) was used to detach the cells from the flask. Once detached, 4mL of complete media was added to the cells, and this was transferred to a 15mL conical tube and pelleted for 5 minutes at 125 *X g*. The media was decanted and the cells were resuspended in 7mL of cold PBS. This was wash repeated twice. Finally, the cells were resuspended in 450μL of cold PBS and stored on ice until added to 5μL of RNA from the *in vitro* transcription. This was gently mixed before being transferred to an electroporation cuvette with a 2mm gap (Fisherbrand). The sample was electroporated using a BTX 830 machine under the following conditions: 510V, 100μs pulse, 5 pulses, 184ms interval. The cuvette was left for 10 minutes at room temperature before the cells were transferred to a T-75 flask with 10mL of complete media and stored in a 37°C 5% CO_2 incubator. To collect, the supernatant from the flask was added to 2mL of FBS. The flask was then returned to the incubator after rehydrating the cells with fresh complete media. The supernatant was then clarified by centrifugation at 783 *X g* for 5 minutes at

4°C before being transferred to new 1.5mL tubes and finally stored at -80°C. Titers of the EP stock virus were determined by plaque assay using Vero cells.

Plaque assay

One day prior to infection, 6-well or 12-well Vero plates were plated using 250,000 or 500,000 cells per well respectively to ensure approximately 90% confluency the following day. Virus stocks were diluted 1:10 8 times using 225µL DMEM (supplemented with 2% FBS and gentamycin) and 25µL virus. This dilution series was either performed using 1.5mL tubes (using vortexing to mix) or 96 well plates (using pipetting to mix). Media was then decanted from a cell culture plate and 100µL (12-well plate) or 200µL (6-well plate) of each dilution was added to a well. This was performed in duplicate. The infected monolayers were stored in a 37°C 5% CO_2 incubator for 1 hour and were gently shaken every 15 minutes to ensure an even infection distribution. After this incubation, a 0.4% agarose overlay (1 part 2% agarose (Lonza) in filter-purified water to 4 parts DMEM supplemented with 2%FBS and gentamycin) was added to each well, and the plates were returned to the incubator. Following a 48 hour incubation, the monolayers were fixed for 30 minutes using 10% formaldehyde (Fisherbrand) before the agarose plugs were removed and the monolayer was stained with 0.25% crystal violet solution (Fisherbrand). The plates were then washed with water and allowed to dry before plaques were counted.

PFU per mL was calculated using the following formula: PFU/mL=(dilution X number of plaques) (1000/amount plated), with "dilution" equaling the dilution at which the plaques were counted and "amount plated" equaling the amount of virus added when infecting the cells (i.e. 100µL for 12-well plates and 200µL for 6-well plates).

Illumina NGS for EP stock generation and mouse passaging

Viral RNA was extracted using the Qiagen viral RNA mini kit as per the manufacturer's protocol.

LIBRARY PREPARATION

Illumina sequencing was performed by the UTMB sequencing core. Viral RNA from cell culture extracts were fragmented by incubation at 94°C for 8 minutes in 19.5 μl of fragmentation buffer (Illumina, San Diego, CA). First and second strand synthesis, adapter ligation, and amplification of the library were performed using the Illumina TruSeq RNA Sample Preparation kit as per the manufacturer's protocol. For virus isolates from animals, PCR was first done using sequence-specific primers tiled across the VEEV genome to provide amplified products of approximately 1.5kb in size that were used for library generation. Products were fragmented using transposons, then adapter ligation and amplification of the library was performed using the Illumina TruSeq RNA Sample Preparation kit under conditions described by the manufacturer (Illumina, San Diego, CA). Samples were tracked using the "index tags" incorporated into the adapters as defined by the manufacturer.

Sequence assembly and analysis

Illumina sequencing analysis was performed by the Fofanov lab at UTMB.

QUALITY AND FILTRATION

The quality for each sample/dataset was assessed using FASTQC (351). The paired-end reads were merged for each sample and then filtered to exclude reads with unknown characters (anything other than A, T, C, G) and low quality (<15 quality score), so that only high quality reads were used during analysis. Additionally, the first 16 bases of each read were trimmed due to nucleotide bias.

The analysis was performed using VEEV strain TC-83, complete genome (GenBank accession #: L01443.1) (308).

VIRUS DIVERSITY ANALYSIS

To analyze the variant hotspots, each sample was run through a novel rare variant pipeline (available upon request). The pipeline first maps each read to the reference VEEV genome with perfect match, then unmapped reads are re-mapped with 1 mismatch and added to the final map. The 34 base long reads used in the analyses were validated as viral sequences and not host sequences by analysis of the longest subsequences shared explicitly (no mismatches allowed) and longest similar (1 mismatch allowed) between viral and host genomes. Positions in which the number of reads mapped with mismatches was higher than perfectly mapped reads or coverage was below 100 were excluded from diversity calculations. Mutation frequency per sample was calculated by summing the per position diversities and normalizing by the number of positions for which diversity was calculated. Shannon Entropy was calculated using the equation $-[\Sigma^{s}_{i=} p\log(p)]/N$, where p equals the probability of mutation and N equals the number of base calls that can happen at a position (i.e. A, G, C, T, insertion, or deletion).

Cloning

TC-83 GFP

TC-83 containing GFP under the control of a second subgenomic promoter was provided by the Weaver lab at UTMB (Figure 6.1C). TC-83 GFP and TC-83 3x were digested using the restriction enzymes PspOMI (NEB) and PpuMI (NEB) as per the manufacturer's protocol. The digestion was validated by running the entire contents of the digestion on a 1% agarose TAE gel. Bands were cut out and purified using the QIAquick Gel Extraction kit (Qiagen) as per the manufacturer's protocol. The TC-83

GFP genome containing the GFP gene was ligated with the TC-83 3x genome containing the RdRp mutations using a T4 DNA ligase kit (NEB) as per the manufacturer's protocol at a 1:3 insert to vector ratio. 4μL of the ligation was transformed using TOP10 competent cells (Invitrogen) as per the manufacturer's protocol, and 50μL of the transformation was plated on an LB-agar plate supplemented with 100μg/mL ampicillin and allowed to grow overnight in a 37°C incubator.

Colonies were picked the next morning and tested for GFP insertion using the GoTaq green PCR master mix (Promega) as per the manufacturer's protocol, with the primers 6705V (5'GCHGTCCTGCTTCCGAAC) and 7800C (5'CGTGGTTCTTCTTCTTCTTCC) used to determine GFP insertion. Of the colonies positive for the insert, one was used to spike 250mL of LB supplemented with 100μg/mL ampicillin. This was allowed to grow overnight in a 37°C incubator at 250rpm. The next morning, the bacteria were pelleted by centrifugation for 15 minutes at 2003 X g, and the plasmid was purified using a Plasmid Maxi kit (Qiagen). The purified plasmid stock was stored at -80°C.

TC-83 RT-QPCR CONTROL PLASMID

To determine RNA copy number, a control plasmid containing a portion of TC-83 complementary to the real time PCR primers was needed. TC-83 plasmid DNA and the pBluescript II (SK+) plasmid (Stratagene) were digested with XBaI (NEB) and BamHI (NEB) as per the manufacturer's protocol, generating an approximately 1.6kb fragment of TC-83 for insertion. The digestion was validated by running its entire contents on a 1% agarose TAE gel. Bands were cut out and purified using the QIAquick Gel Extraction kit (Qiagen) as per the manufacturer's protocol. The 1.6kb TC-83 genome fragment was ligated with the pBluescript II (SK+) plasmid using the T4 DNA ligase kit (NEB) as per the manufacturer's protocol and using a 1:3 insert to vector ratio. 4μL of the ligation was transformed using TOP10 competent cells (Invitrogen) as per the manufacturer's

protocol, and 50μL of the transformation was plated on an LB-agar plate (Fisherbrand) supplemented with 100μg/mL ampicillin (Sigma) and allowed to grow overnight in a 37°C incubator.

Colonies were picked the next morning and tested for TC-83 fragment insertion using the GoTaq green PCR master mix (Promega) as per the manufacturer's protocol. The primers M13 forward (5'GTAAAACGACGGCCAGT) and M13 reverse (5'CAGGAAACAGCTATGAC) primers were used to determine TC-83 insertion. Of the colonies positive for the insert, one was used to spike 250mL of LB supplemented with 100μg/mL ampicillin. This was allowed to grow overnight in a 37°C incubator at 250rpm. The next morning, the bacteria were pelleted by centrifugation for 15 minutes at 2003 X g, and the plasmid was purified using the NucleoBond Xtra Maxi Plus kit (Clontech). The purified plasmid stock was stored at -80°C.

RT-qPCR for TC-83 RNA copy number

COPY NUMBER STANDARD

To prepare the copy number standard (see "TC-83 RT-qPCR control plasmid"), 1μg of the plasmid was digested using SphI (NEB) according to the manufacturer's protocol. The digested plasmid was cleaned using the ClonTech PCR-cleanup kit as per the manufacturer's protocol, and transcribed using the MaxiScript T7 kit (Ambion), also using the manufacturer's protocol. Once transcribed, the plasmid DNA was digested using the DNA-free DNA removal kit (Invitrogen) and the RNA was further purified using the RNAqueous total RNA isolation kit (Ambion), both according to the manufacturer's protocol. Finally, linearization, transcription, DNase I treatment, and further purification of the copy number standard were visualized for confirmation of each step using a 1% agarose TAE gel. Copy number was calculated using a DS-11 spectrophotometer (DeNovix) to quantify the amount of RNA per microliter. An online calculator (http://endmemo.com/bio/dnacopynum.php) used this and the transcript length

(1,723bp) to determine the RNA copy number per microliter. Following this, the RNA was diluted to 2×10^{10} copies per μL in 20μL aliquots and stored in a cold block at -20°C. RNA was only freeze-thawed once before being discarded.

RT-QPCR

Viral RNA was extracted using the ZR Viral RNA minikit (Zymo) as per the manufacturer's protocol and eluted in 15μL nuclease free water. This was stored on ice as the rest of the reaction was prepared.

A standard curve of the above RNA standard was made to total 8, 10-fold dilutions in nuclease-free water (5μL RNA mixed with 45μL nuclease-free water). Pipetting was used to mix between each dilution. This was stored on ice while the master mix was prepared.

Real time PCR primers were designed to amplify a portion of the nsP3 gene. The forward (4840F 5-ATG CCA TGA CTC CAG AAA GAG-3) and reverse (4981R 5-GGT GAG AAC AAT ATA GGC TGG G-3) primers were diluted to 20μM stocks in nuclease-free water, whereas the FAM tagged probe (4926P 5- /56-FAM/ ACT TCG GCA ATG GAA AGG ATG AGC A/3BHQ_1/ -3) was diluted to a 5μM stock, also in nuclease-free water. A master mix of reagents was made using 0.5μL of the 40X TaqMan RT enzyme, 10uL 2X RT-PCR mix, 0.9μL 4840F stock primer, 0.9μL 2981R stock primer, 1uL 4840F stock probe, and 1.7μL nuclease-free water per sample (TaqMan RNA-to Ct 1-Step kit, Applied Biosystems). This was vortexed to mix and stored on ice.

To set up the PCR, 10μL of viral RNA, standard, or nuclease-free water (as a non-template control) was added to each well in every other column of a 96-well Real Time PCR plate (Applied Biosystems). To this, 30μL of the above master mix was added, and a multichannel pipet was used to mix. After thorough mixing, 20μL from each well was transferred to the adjacent well and the plate was sealed with optical tape (Applied Biosystems). After the plate was centrifuged at 125 *X g* for 1 minute, it was loaded into

the QuantStudio 6 Flex Real Time PCR System (Applied Biosystems), which was run using a 15 minute RT step at 48°C, followed by a 10 minute hot start at 95°C, and lastly 40 cycles consisting of a 15 second denaturation at 95°C and 1 minute annealing and elongation step at 60°C. Following the run, the copy number calculated using the RNA standard was converted to RNA copy number per mL.

TC-83 *in vitro* passaging: GFP

One day prior to infection, a 6-well plate was seeded with 500,000 Vero cells. The day of infection, TC-83 GFP or TC-83 3x GFP (low-fidelity TC-83) was diluted 10,000-fold for an MOI of approximately 0.5. Once diluted, media was decanted from the 6-well Vero cell plate and 200μL of diluted virus was used to infect each well. These infections were performed using three replicates per virus. After this, the plate was transferred to a 37°C 5% CO_2 incubator for 1 hour with occasional shaking. When the incubation was complete, the inoculum was removed and 2mL of DMEM supplemented with 2% FBS and gentamycin was added to each well. The plates were then returned to the 37°C 5% CO_2 incubator.

After a 24 hour incubation, the cell supernatant was removed and transferred to a tube with FBS to a final concentration of 20% FBS. This was centrifuged for 5 minutes at 0.8 X g and transferred to a new tube. These tubes were stored at -80°C. Plaque assays were used to determine virus titer. Ten total passages were performed.

To determine PFU:GFP, plaque assays were performed as per the usual protocol. After 48 hours, the cells were visualized under a fluorescent microscope and florescent plaques were counted. Following this, the cells were fixed and stained following the standard plaque assay protocol, and the number of plaques were counted. The number of GFP to PFU plaques was then calculated as a ratio to determine the amount of GFP florescence lost over the course of passaging.

Illumina NGS for GFP passaging

VIRAL RNA EXTRACTION

Viral RNA was extracted using the Zymo Direct-zol RNA mini kit as per the manufacturer's protocol. 100ng of RNA was used for each ClickSeq library.

CLICKSEQ LIBRARY PREPARATION

ClickSeq (65) was used instead of the traditional Illumina library procedures to avoid the errant recombination that frequently occurs during the typical fragmentation and ligation steps. Instead of RNA fragmentation, SSIII RT-PCR (Invitrogen) is performed using random hexamers attached to an Illumina p7 adapter sequence. In addition to this, azido-NTPs, which cause chain-termination, are added to the NTPs at a 1:35 ratio. In a manner similar to Sanger sequencing, this results in cDNA strands of various sizes. Following this, a modified 5'-hexynyl Illumina sequencing adapter was click-ligated onto the N-terminus of the cDNA strands using a copper-catalyzed azide-alkyne cycloaddition. The cDNA was then purified using a Zymo DNA clean column and amplified using 18 cycles of OneTaq (NEB) PCR, resulting in the removal of the triazole group linking the cDNA fragment to the 3' Illumina sequencing adapter. Following another Zymo DNA clean column purification, the samples were visualized on an agarose gel. cDNA libraries between 400-700bp were excised and purified using the Zymo Research Gel Recovery kit. Sequencing was performed by the UTMB sequencing core using an Illumina NextSeq 550.

Sequence assembly and analysis

Illumina ClickSeq sequencing analysis was performed by the Routh lab at UTMB.

Cutadapt was used to remove adaptor sequences. Following this, FASTX toolkit was used to remove the random hexamer sequences generated during cDNA synthesis, as well as sequences with a PHRED score below 20.

REFERENCE SEQUENCE

The analysis was performed using VEEV strain TC-83 GFP, complete genome.

VIRUS RECOMBINATION ANALYSIS

Bowtie was used to align the virus sequences to the reference genome, with up to one allowed mismatch. Those sequences that did not align using Bowtie were processed using ViReMa, a recombination mapper, to determine the incidence of recombination. These reads were normalized to the average number of reads aligning to the virus genome.

Infant mouse passaging and virulence

Six-day-old CD-1 mice (Charles Rivers, Wilmington, MA) were inoculated IC with 10^4 PFU of virus in a volume of 20µl. After 48 hours, brains were removed, weighed, and transferred to a tube with a steel bead. Media (DMEM supplemented with 10% FBS and gentamycin) was added to a produce final concentration of 10% weight to volume. Brains were homogenized using a TissueLyser II (Qiagen) for 5 minutes at 26 beats/second, and then spun down for 5 minutes at 3.3 *X g*. Supernatant was transferred to a fresh tube and stored at -80°C. Plaque assays were used to determine virus titer. This information was used to dilute the virus for the next passage. 10 passages were performed in total.

Following passages 5 and 10, 6-day-old CD-1 mice were challenged SC with 10^5 PFU or PBS in a volume of 50 μl. Animals were weighed daily for two weeks and monitored for survival.

Virus full genome Sanger sequencing

Virus RNA was extracted from the homogenized mouse brains using the QIAamp Viral RNA Minikit as per the manufacturer's protocol and stored at -80°C. Using 3μl of this RNA, the Superscript III RT PCR kit (Invitrogen) was used to generate cDNA by adding 5μl nuclease-free water, 1μl dNTPs (NEB), and 1μl random hexamers. This was incubated at 65°C for 5 minutes and placed on ice for 2 minutes. Following these incubations, 4μl MgCl$_2$, 2μl 10X RT buffer, 2μl DTT, 1μl RNase OUT, and 1μl SSIII enzyme was added to the first tube and incubated for 10 minutes at room temperature, followed by 43°C for 90 minutes, and finally 50°C for 10 minutes. This was stored at -20°C.

High fidelity Phusion PCR (NEB) was used to generate approximately 1.5kb amplicons that tiled the entire TC-83 genome. In a PCR tube, 2.5μl of cDNA was added to 10μl 5X buffer, 1μl dNTPs, 1μl forward primer (20μM), 1μl reverse primer (20μM), 32μl nuclease-free water, 2μl MgCl$_2$, and 0.5μl Phusion polymerase. The amplicon primers were as follows: 1V+1512C, 1210V+2874C, 2440V+4014C, 3725V+5263C, 4937V+6579C, 6207V+7800C, 7246V+9047C, 8443V+10281C, and 9883V+11422C. The PCR reactions were amplified using a 98°C hot start for 30 seconds, followed by 35 cycles of a 10 second 98°C denaturation, a 10 second 60°C anneal, and a 1.5 minute elongation at 72°C.

Following PCR amplification, amplicons were visualized by running the entire contents of the reaction on a 1% agarose gel in TAE buffer. The bands were excised and purified using the QIAquick Gel Extraction kit as per the manufacturer's protocol. DNA was eluted into 35μl of nuclease-free water and stored at -20°C.

Sequencing reactions were prepared by adding 1μL of a 2μM primer (Table 4.1) to 5μL DNA, 2μL 5X sequencing buffer, and 2μL BigDye (Applied Biosystems). The sequencing reactions were amplified using a 96°C hot start for 2 minutes, followed by 30 cycles of a 10 second 96°C denaturation, a 5 second 50°C anneal, and a 4 minute elongation at 60°C. Following this, sequencing reactions were purified using Performa spin columns (EdgeBio) as per the manufacturer's protocol, and loaded onto the Applied Biosystems 3500 Genetic Analyzer sequencer. Sequences were analyzed using Sequencher version 5.0.1.

Statistics

GraphPad Prism was used to perform all statistical tests, which are described in the text.

RESULTS

Phenotypic variation in EP stock

Work in previous chapters suggested that differences in virus EP stock led to differences in phenotypes, both *in vivo* (Chapter 2) and *in vitro* (Chapter 3). To further examine this, EP stocks of TC-83 and TC-83 3x were generated independently in triplicate (Illustration 4.1). The TC-83 3x that was used for this experiment only contained the three low-fidelity RdRp mutations. After each clone was linearized, purified, and transcribed, virus RNA was electroporated into BHK cells and collected at 32 and 56 HPE.

At 32 HPE (Figure 4.1 A&B) and 56 HPE (not shown), no significant differences in CPE were observed between the two viruses or EP replicates. The titers from 56 HPE was slightly higher for all virus stocks, so these were selected for further characterization. There was no significant difference in virus titer as measured by plaque assay (Figure

4.1C) or RT-qPCR (Figure 4.1D), and thus no significant difference in specific infectivity (i.e. the ratio of infectious virus to virus RNA copy number).

In the prior studies described in chapter 3, TC-83 3x was attenuated in mosquito cells at a low MOI when using two different EP stocks, but this attenuation was lost when using a third stock. However, the control TC-83 was always infectious when using this MOI. To determine if there were differences in mosquito cell attenuation for these new EP stocks, mosquito cells were infected using an MOI of 0.01 using 10 replicates, and supernatant collected at 24HPI was tested for infectious virus using a CPE assay. In stark contrast to the results described in chapter 3, all EP stocks generated for this experiment were attenuated, regardless of fidelity (Figure 4.1E). Additionally, there was no significant difference in the percentage of replicates negative for infectious virus.

Illumina sequencing for virus variants during EP stock generation

To determine the changes in virus diversity and minority variants that occurred when preparing clone-derived TC-83 and TC-83 3x, Illumina NGS was used to sequence each step of the EP procedure (Illustration 4.1). Equal amounts of linearized and purified virus clone DNA were used for each *in vitro* transcription, with 5μL of the transcription product used for EP, as per standard protocol. There was no significant difference in virus diversity for TC-83 and TC-83 3x during any EP step. However, TC-83 3x trended towards producing higher EP stock diversity, with p-values approaching the 0.05 significance cut-off (Figures 4.2 A&C). Strikingly, however, the amount of virus diversity produced by the EP replicates varied enough to cause overlap in the diversity observed for individual TC-83 and TC-83 3x replicates.

Overall diversity at one EP procedure step did not correlate with diversity at a later step (Figures 4.2 B&D). In contrast to this, the number of high frequency minority variants grew during each sequencing step (Figures 4.2 E&F). There was no difference in the number of high frequency minority variants between TC-83 and TC-83 3x until the

EP step, where TC-83 3x generated significantly more variants (Mann-Whitney U, p<0.01) (Figure 4.2E). Additionally, while high conservation in the location and amplitude of mutation hotspots for the DNA and *in vitro* transcription stocks was observed in Figures 4.3-4.4, there was clearly more variation in the EP stocks, especially for TC-83 3x.

Interestingly, while 13-66% of high frequency DNA minority variants were later found in the *in vitro* transcription stocks, 80-93% of high frequency *in vitro* transcription minority variants were also found in the EP virus stock (Tables 4.2-4.3). These variants were almost entirely conserved between each EP stock, regardless of RdRp fidelity. However, these conserved mutations only comprised 67% of the high frequency TC-83 3x EP mutations and 76% of those identified for TC-83. Of the remaining mutations, the majority were unique to each stock, with only 22% of TC-83 and 10% of TC-83 3x high frequency mutations found in another EP stock. Additionally, some variants were only found in high amounts in one step, but not another. For example, A7653C was found at a high frequency in all DNA stocks, but was not found in high amounts during transcription and EP. Additionally, T2507+T or T2507A was found in all transcription stocks at high levels, but not during EP.

Illumina sequencing of EP stocks to determine mechanisms of *in vitro* mosquito attenuation

As all of the EP stocks generated during this chapter were attenuated in mosquito cells when using a low MOI (Figure 4.1E), these stocks were compared to the TC-83 and TC-83 3x EP stocks that were not attenuated in Chapter 3. There was no significant difference in overall virus diversity between attenuated and unattenuated EP stocks (Figure 4.5 A-B) or in the number of high frequency mutations (Figure 4.5 C). Of these diversity hotspots, 62% of the variants were shared between attenuated and unattenuated virus stocks (data not shown). The remainder of these variants was diverse, with no high

frequency variants specific to either *in vitro* phenotype. Additionally, while some small differences were observed in the mutation frequencies of the attenuated versus unattenuated stocks, none were severe enough to explain the phenotypic changes (Figure 4.5 D-E). Thus, no clear differences in virus diversity or the variants required for a successful infection of mosquito cells at a low MOI were found.

Rapid loss of GFP florescence during low-fidelity TC-83 passaging

To examine reporter gene stability, three independent replicates of TC-83 and low-fidelity TC-83 3x GFP were passaged 10 times on Vero cells using an approximate MOI of 0.5. Over the course of this passaging, reduced GFP expression for low-fidelity TC-83 3x was observed beginning at passage 4 (Figure 4.6B). In contrast, GFP loss was not observed for the TC-83 replicates until passage 8 (Figure 4.6A).

To quantify this loss, the number of fluorescent plaques was compared to the number of plaques for passages 5-10 (Figure 4.7). Until passage 10, almost every TC-83 plaque was fluorescent, and the largest PFU:GFP difference was approximately 1:30, which was only observed for one replicate during the final passage. On the other hand, all low-fidelity TC-83 replicates experienced an approximately 500-1500-fold decrease in fluorescence by passage 10, orders of magnitude higher than the ratios observed for the TC-83 GFP passaging replicates. As a low-fidelity SINV mutant was found to produce DI particles at high rates (64, 372), we hypothesized that low-fidelity TC-83 was also recombining at higher rates than TC-83, resulting in rapid GFP gene removal.

Low-fidelity TC-83 GFP gene removal is enhanced

ClickSeq was used to generate Illumina sequencing libraries, allowing the frequency of virus deletion mutants to be quantified. All three TC-83 GFP replicates contained minority deletion variants that were able to selectively remove the GFP reporter gene by passage 10 (Figure 4.8). Deletion inside the GFP gene was higher than

for any other gene, even as soon as passage 1. In support of our hypothesis, low-fidelity TC-83 GFP was much more efficient at removing the GFP gene, as the frequency of deletions within GFP gene were far higher than those of TC-83 GFP (Figure 4.9).

The first replicate of each virus was chosen for further analysis, as these both had median levels of decreased GFP florescence in Figure 4.7. Interestingly, for both viruses, peak recombination appeared in the middle of the GFP gene, and slowly spread out over the course of passaging to the entire gene (Figure 4.10). TC-83 3x was efficiently removing the entire GFP fragment by passage 3, while TC-83 needed until passage 8 to reach similar levels of GFP removal. This clearly demonstrated that TC-83 3x is much more efficient at recombination than TC-83.

Genetic stability *in vivo*

The low-fidelity TC-83 3x mutant and TC-83 were subjected to 10 serial intracranial passages in infant mice to determine if compensatory mutations accumulated *in vivo* (Appendix 2, stocks 1-2). To assess changes in virulence during passaging, passage 5 and 10 virus was injected subcutaneously into 6-day-old mice. TC-83 and TC-83 3x both gained virulence by passage 5 compared to their unpassaged counterparts in Figure 2.2 (Kaplan-Meier test, p≤0.0001) (Figure 4.11A). Figure 2.2 was chosen for statistical comparison, as the same stocks were used for both of these experiments. At passage 5, the 3x mutant reached virulence equivalent to that of the original, unpassaged TC-83 with no significant difference in time to death. Interestingly, no significant changes in virulence occurred between passage 5 and 10 for either virus. This indicates that TC-83 3x can only reach virulence equivalent to unpassaged TC-83 and is unable to increase in virulence past that point.

Illumina sequencing for virus variants following *in vivo* passaging

Illumina sequencing following mouse brain passage 5 showed an increase in diversity for the low-fidelity mutant relative to previous *in vitro* results (Figure 4.11B). Curiously, while diversity hotspots increased for TC-83 3x, the 6k hotspot observed after cell culture passage in Chapter 2 (Figures 2.3, 2.5 & 2.7) was greatly reduced for both passage 5 viruses (Figure 4.11 D&E). Although a different EP stock was used for infant mice passaging than the stock used to determine virus diversity during Chapter 2 (Figures 2.3-7), TC-83 3x still exhibited fewer U-C mutations (Figure 2.4), suggesting that this may be a stable phenotype for low-fidelity TC-83.

While TC-83 3x was more diverse than the parent TC-83 as measured by Illumina virus sequencing, fewer revertents occurred at the E2 mutation required for TC-83 attenuation (Figure 4.11C) (307). Due to the position of the 5'UTR attenuation mutation, coverage was too low to assess true differences in the potential for this site to also revert, but no reads contained the revertent mutation for either virus. Following passage 10 in mouse brains, Sanger sequencing was used to identify several SNPs (Table 4.4). TC-83 and TC-83 3x each produced 2 SNPs following 10 infant mouse passages. None of these SNPs reverted the TC-83 mutations that cause attenuation or the inserted RdRp mutations. Additionally, no convergent mutations were found in all passage series.

DISCUSSION

To ascertain the genetic and phenotype stability of our low-fidelity variant, we subjected TC-83 and TC-83 3x to various tests designed to examine stability when the viruses are first generated, as well as after multiple *in vitro* and *in vivo* growth cycles. Contrary to our initial hypothesis, the genetic stability of TC-83 3x is quite stable, with no evidence of reversion in any of our genetic stability assays. However, some variation was discovered.

Errors are generated during each step of the Illumina NGS procedure and form up to 1% of detected variants (377). To correct for these errors, numerous biological controls

(e.g. CirSeq (378), DNA clone controls (379), primer IDs (380)) as well as *in silico* programs (e.g. DeepSNV (379), ShoRAH (381), PredictHaplo (382), etc.) have been developed. These methods are not perfect. For example, while some biological controls account for PCR errors, these also fail to control for errors generated during the error-prone RT-step (i.e. infectious DNA clone controls (379), primer IDs (380)). Unfortunately, protocols that are able to control for RT errors also require high amounts of input RNA, making widespread use of these techniques unrealistic (378). Additionally, even when coverage is high and mapping is accurate, *in silico* approaches can either be too conservative, causing true variants to be missed, or too lax, resulting in a lack of precision (377). Variant callers can balance these two extremes by using various statistical models to predict expected variant error. However, unknown biases commonly result in greater than expected fluctuations in variants.

The EP sequencing data summarized in Tables 4.2-4.3 suggest that our rare virus variant pipeline is liberal when identifying these variants, which due to the difficulty of calling rare virus variants accurately is not surprising. For example, all of the high frequency DNA variants were biased towards either the negative or positive sense strands, which is indicative of sequencing artifacts (379). This was true even when only reads with a quality score of 30 or above were used (data not shown). Interestingly, some of these sequencing artifacts, such as T9988A-G, were also found in high proportions in the transcription and EP stock, suggesting that there was high Illumina sequencing bias for these variants or that, indeed, these are true variants. While there was a link in the variants identified during all three EP stock steps, the variants in the transcription step were positively correlated with those that appeared in the EP. These may also be sequencing artifacts. However, as *in vitro* transcription is known to be error-prone, generating approximately the same error as an RdRp (101), and because these variants were much less common in the plasmid stock, this suggests that the errors that occur during *in vitro* transcription are largely carried over into the EP virus stock population.

Intriguingly, the errors generated during *in vitro* transcription largely form the common high frequency variants found in the different EP stocks. As this experient only examined T7 promoted clone sequences, it would be interesting to use different RNA polymerases during *in vitro* transcription to examine how this might alter the variants that occur during EP, as well as the effects this may have on virus fitness.

Continuing the trend of inconsistency, all EP stocks generated during this subaim were sensitive to low MOI mosquito cell infection, regardless of RdRp fidelity. These attenuated stocks were compared to previously generated stocks that grew well in mosquito cells at a low MOI. However, no differences were identified. This suggests that factors beyond those measured here are responsible for the mosquito cell phenotype instability observed here and in chapter 3. Importantly, however, each EP stock exhibited slightly different amounts of overall diversity and was composed of a unique repertoire of high frequency virus variants, especially for low-fidelity TC-83, showing that EP stocks are not the same. In the future, it would be interesting to test these different EP stocks for variation in growth kinetics and/or *in vivo* (i.e. infant mice LD_{50}) to determine differences in virulence, as it is not well understood how specific minority variants may contribute to different phenotypes.

Previous research using a low-fidelity variant of SINV found that it also produced an overabundance of DI particles relative to the original virus when passaged using a high MOI (64). To determine if this was also true for our fidelity mutant, we passaged TC-83 GFP and TC-83 3x GFP ten times in Vero cells. However, a low MOI was used for a more accurate representation of virus recombination. Until recently, it was not feasible to observe recombination variants that naturally occur in virus populations due to the high amounts of recombination artifacts generated by typical Illumina sequencing library procedures (65). However, due to the ClickSeq method of generating libraries (65), it has now become possible to observe the regions in the virus genome most prone to recombination. It is important to understand where virus recombination occurs, not

only to understand the role of recombination in virus evolution, but also to comprehend how RNA viruses remove inserted genes, such as reporter genes used to visualize or quantify virus infection (i.e. GFP, luciferase). Reporter gene instability is a common phenomenon for RNA viruses, resulting in rapid loss of the reporter gene both *in vitro* (383-387) and *in vivo* (383, 385, 386). Understanding the frequency of reporter gene removal, as well as where removal is most likely to occur, at the level of the entire virus population will aid in the design of reporter genes with increased stability.

We found conserved regions of recombination in the genome, as well as a slow, but persistent removal of GFP that was highly specific to only the inserted gene. Additionally, low-fidelity TC-83 3x was much more efficient at removing the extraneous GFP gene, suggesting recombination and fidelity for low-fidelity alphavirus RdRp mutants may be closely entwined (64). This also implies that experiments requiring reporter genes may not be very stable when using these low-fidelity constructs. Future experiments need to examine recombination differences in an unaltered genome to better understand the subtle changes in recombination that naturally occur.

Finally, to ensure that our observations from the *in vitro* data were consistent with virus behavior *in vivo*, TC-83 and TC-83 3x were passaged IC in infant mice. Perhaps counterintuitively, the 3x hyper mutator variant, while undergoing an initial increase in virulence during *in vivo* passaging, only reverted to the same level of virulence as unpassaged TC-83. This is likely due to an increased amount of unfit virions (e.g. defective interfering particles), which hamper wt virus virulence, as well as the inability of the 3x mutant to revert the inserted RdRp mutations. Also, the passage 10 results for each virus were very similar to the passage 5 data, which demonstrates that the low-fidelity mutant exhibits decreased risk of reversion to wt virulence compared to the original TC-83. While promising, this experiments bears repeating in the future to ensure that these results are consistently observed.

Overall, we have shown our TC-83 3x mutant to be genetically stable, with no reversion of the RdRp or TC-83 attenuating mutation, although not always phenotypically stable. Importantly, TC-83 3x was much less prone to reversion *in vivo*, which has always been problematic for TC-83 (292, 295), suggesting that our low-fidelity mutant is still an improvement over the original vaccine.

Primer name	Primer sequence (5' to 3')
1V	ATGGGCGGCGCATGAG
510C	TAGAGGCTWGTCGGTCCGTCAAC
722V	CATTCTTAGGAAGAAGTATTTGAAAC
1263C	ACTGTCTRTCTCGTAGTCCTAGTGG
1512C	ATCGGCTGCGCACTTAGC
1210V	AGGCRTTTGCTAGGTGGG
1671V	GGYTTGATAAAGGTTACCAGC
1779C	CACTATGACTTGTTCAGCGAG
2265C	TTTYTTGGCGCTYACCAC
2520C	CGTGGTTAAAATGCACTTTCAG
2814C	TTGTACCGAACGGCATACAC
2240V	CGCTCATAGCCATYATAAGAC
3024C	TCMGGTCTCTCCAAGATGTG
3207V	TGCGTKAGGTTCTTTGGAC
3525C	TGCCCTTCAGTTTGCTGAC
3768C	GGATTCAGATGCAGRCAAGC
4014C	CAWCCGGCTTCGTGGAG
3725V	GTGTGAAGATCATGCTATTAAGC
4192V	AAGCGCGRCTGGTCAAAG
4515C	TCDGAKATGCATATCTCCTCCAC
4689V	GAAATTAATGCCATGTGGC
5263C	GATGCRTGAGGAATGGACC
4937V	TACTGGTGTGCAGAAGATCC
5226V	TGTTGCAAGTCGAGGCAG
5538V	ATTWCTAGGGAGGAGCTCGAGG
5793C	GGCATACGAAATCTCCAATTC
5966V	GAAGGCAGAMGGAAAAGTGG
6579C	TTGTTCCTGGAGTCACTTTCAC
6207V	CGCAGYTTTCCAAAGAAAC
6705V	GCHGTCCTGCTTCCGAAC
7037C	TCTCTTAACACTCTGCTTGCG
7203V	GCGCCYTATTTYTGTGGAG
7800C	CGTGGTTCTTCTTCTTCTTCC
7426V	CCGTAGGAACTTCCATCATAG
7701V	ACCTGACGTTCAAGCAACG
8049C	TTCTTCGTCTTRAGTGCGG
8204V	GGTGCCGAAAGGAGTTGG
8763C	GTTCCGTGCATGTCATACC
9047C	TGCATCTCGACATABGCTCC
8443V	ACCAATTTGCTAYGACAGAAAAC
8954V	TTTAATCCTGTAGGCAGAGAAC
9581C	GGGTGCTGTTTCCTGTGC
9885V	TCTGGATTCAATTGCTGATCC
10281C	TTCTCAGTGTCGCARAAGC

10215V	ACAGGCCTGATGAACAGTG
10794C	AGTTTTCGGCGCGAATGG
11422C	GAAATATTAAAAACAAAATCCGATTYG

Table 4.1:   Sequencing primers.

Primers used during the PCR amplification and sequencing of virus isolated TC-83 or TC-83 3x infected infant mice brain. "V" designates primer sequences complementary to the virus sequence (i.e. positive-sense), while "C" designates primer sequences that bind to the minus-sense strand.
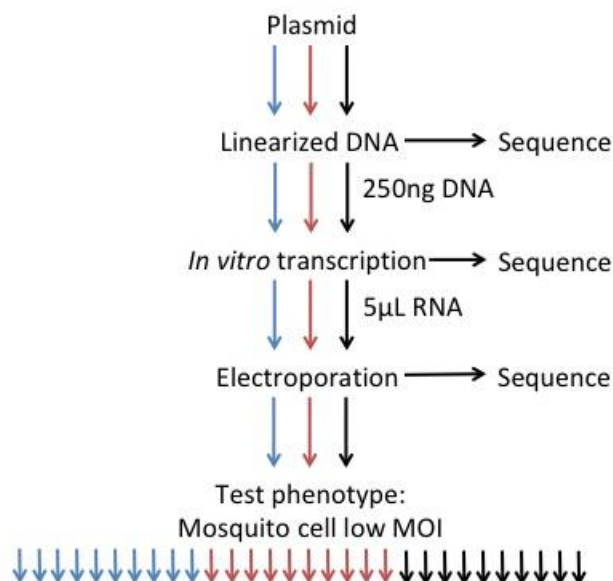
Illustration 4.1.   EP stock variability experiment.

To test differences in EP stocks, three independent EP replicates were each generated for TC-83 and TC-83 3x. First, 5μg of TC-83 or TC-83 3x was linearized using the restriction enzyme MluI. After purification, 250ng of this DNA was used to generate RNA copies of the virus genome. 5μL of this RNA was then electroporated into BHK cells to generate infectious virus. The linearized DNA, in vitro transcribed RNA, and EP stock RNA were sequenced using an Illumina NextSeq 550 to test for differences in diversity and minority variants. To test for differences in EP stock phenotypes, C7/10 mosquito cells were infected at an MOI of 0.01 using 10 replicates of each EP stock. Following a 24-hour incubation, the supernatant of the infected C7/10 cells was collected, clarified, and used to infect Vero cells. If Vero cell CPE was observed for all 10 replicates of an EP stock, the stock was considered to be unattenuated. However, if any of the 10 replicates failed to produce CPE in Vero cells, the EP stock was considered to be attenuated. In this illustration, blue represents replicate 1, red represents replicate 2, and black represents replicate 3.
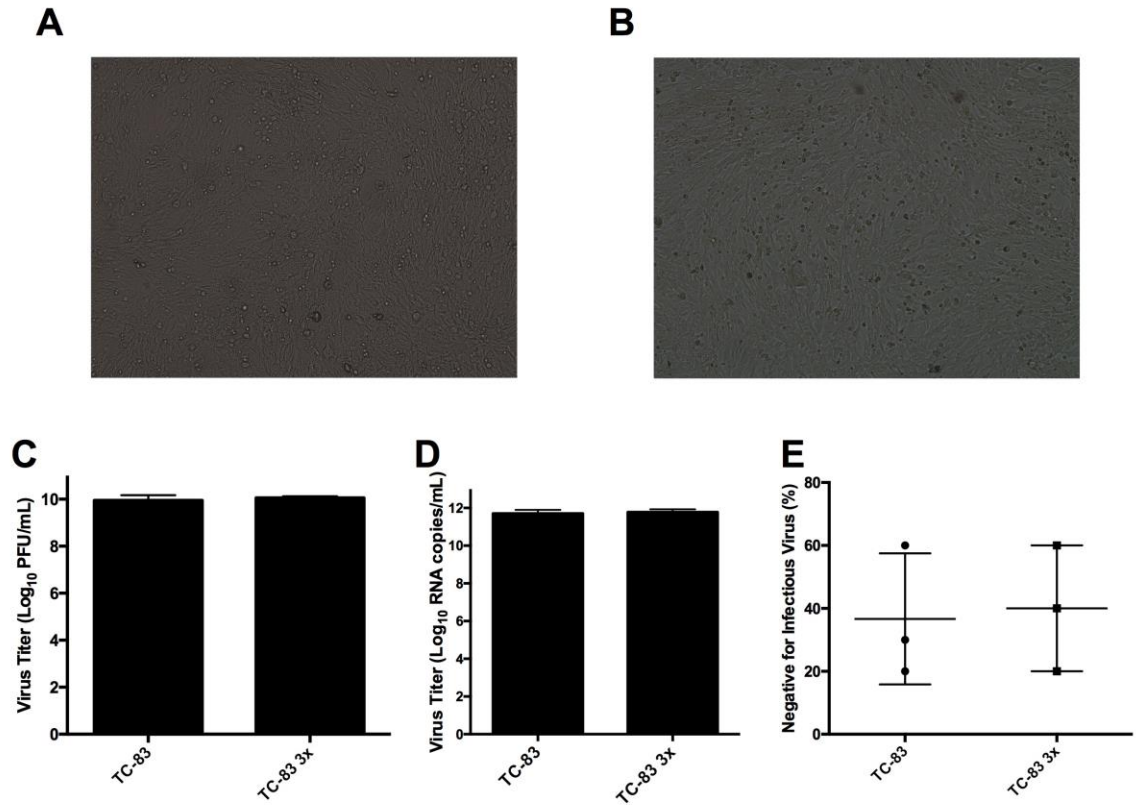
Figure 4.1:   Variation in EP stock phenotype.

BHK cells were EP in triplicate with TC-83 or TC-83 3x. At 32 HPE there was no difference in the CPE produced by TC-83 (A) or TC-83 3x (B). Using an unpaired t-test, no significant difference in virus titers as measured using plaque assay (C) or RNA copy number using RT-qPCR (D). Mosquito cells were infected with an MOI of 0.01 using TC-83 or TC-83 3x from the electroporation stocks (E). No significant difference in low MOI mosquito cell infectivity was observed using an unpaired t-test.
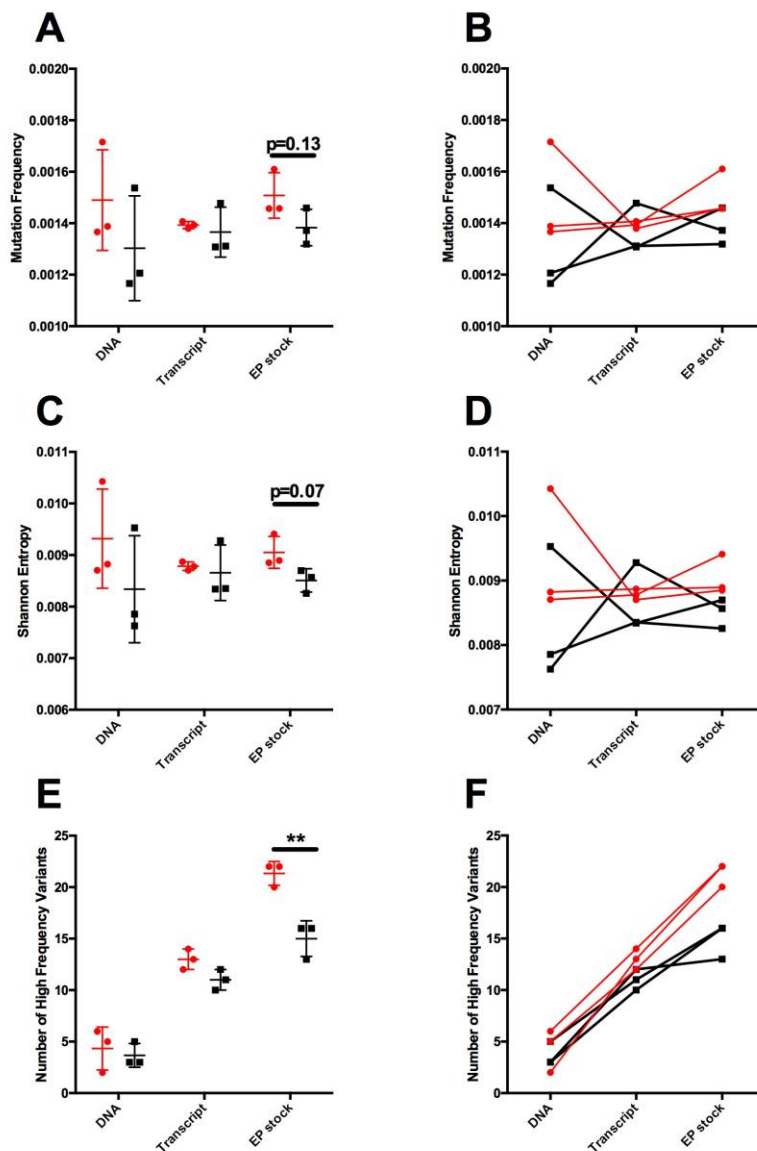
Figure 4.2:   Illumina sequencing virus mutation frequency analysis of TC-83 and TC-83
              3x PE using BHK cells.

Differences in overall mutation frequency between TC-83 and TC-83 3x after DNA
linearization, in vitro transcription, and EP (A). Changes in the mutation frequency of
each replicate after DNA linearization, in vitro transcription, and EP (B). Differences in
overall Shannon Entropy between TC-83 and TC-83 3x after DNA linearization, in vitro
transcription, and EP (C). Changes in the Shannon Entropy of each replicate after DNA
linearization, in vitro transcription, and EP (D). Number of high frequency mutations
(cut-off=0.02) for TC-83 and TC-83 3x after DNA linearization, in vitro transcription,
and EP (E). Number of high frequency mutations (cut-off=0.02) of each replicate after
DNA linearization, in vitro transcription, and EP (F). Mann-Whitney U test was used to
determine statistical significance, $p < 0.01$ is represented by **. TC-83 3x data points are
in red, while TC-83 data points are in black.

134
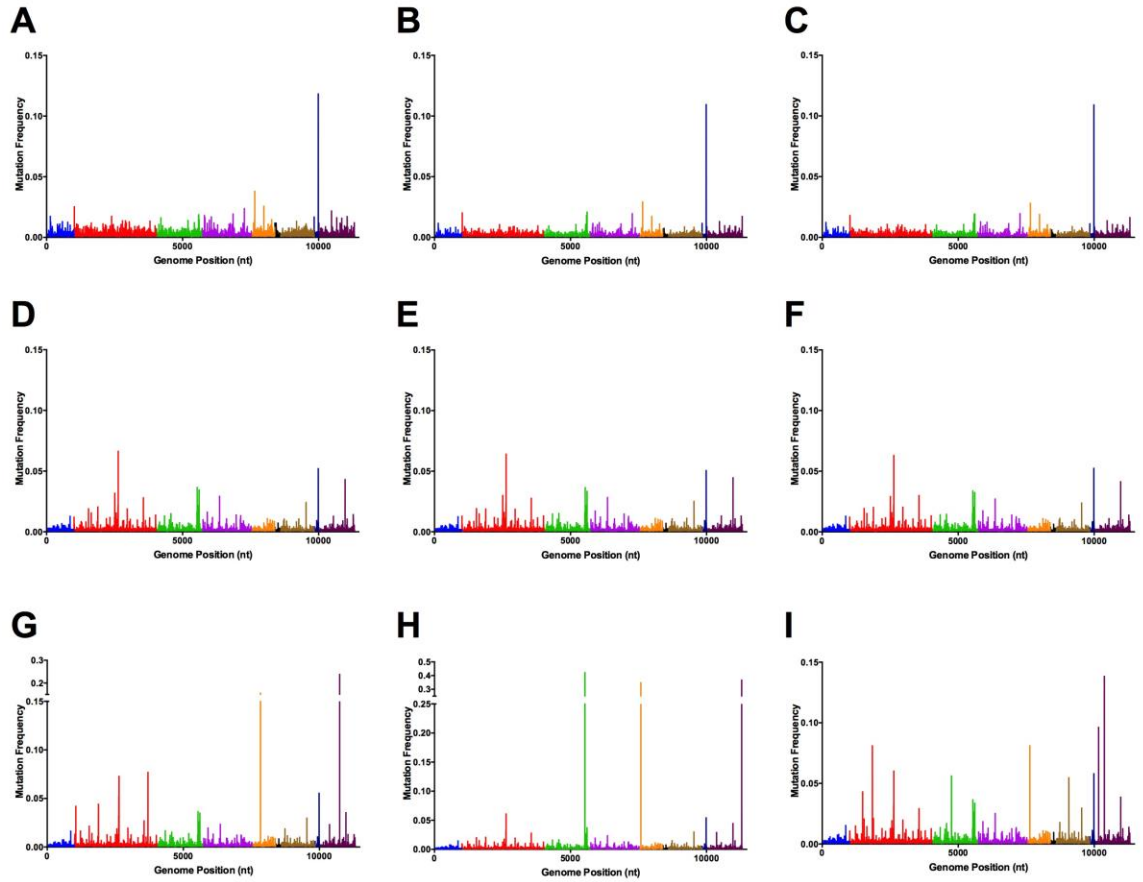
Figure 4.3: Illumina sequencing virus diversity hotspots for the coding regions of three TC-83 3x replicates.

Purified, linearized DNA replicate 1 (A), Purified, linearized DNA replicate 2 (B), Purified, linearized DNA replicate 3 (C). In vitro transcription replicate 1 (D), In vitro transcription replicate 2 (E), In vitro transcription replicate 3 (F). EP stock replicate 1 (G), EP stock replicate 2 (H), EP stock replicate 3 (I). Genome organization is color-coded using the following: nsP1: blue, nsP2: red, nsP3: green, nsP4: purple, capsid: orange, E3: black, E2: gold, 6k: navy blue, and E1: maroon.

DNA R1	TX R1	EP R1	DNA R2	TX R2	EP R2	DNA R3	TX R3	EP R3
A1021C (-)	A1885G (-)	A1053T (+/-)	A1021C (-)	T2507+T (+)	A1543G (-)	A7653C (+)	A1885G (-)	A1488C (+/-)
A7270C (+)	T2507+T (+)	A1543G (-)	C5609A (-)	G2627+G (-)	A1885G (-)	T9988A-G (-)	T2507+T (+)	A1543G (-)
A7653C (+)	G2627+G (-)	C1883T (+/-)	A7270C (+)	A2634del (+)	G2627+G (-)		G2627+G (-)	A1846C (+/-)
A7989C (-)	A2634del (+)	G2627+G (-)	A7653C (+)	A3559G (-)	A2634del (+)		A2634del (+)	A1885G (-)
T9988A-G (-)	A3559G (-)	A2634del (+	T9988A-G (-)	C5540A (+)	A2966G (-)		A2966G (-)	G2627+G (-)
A10476C (-)	C5540A (+)	G2638A (+/-)		C5555A (+)	A3559G (-)		A3559G (-)	A2634del (+)
	C5555A (+)	A2966G (-)		A5589C-G (-)	A5530G (+/-)		C5540A (+)	A2966G (-)
	A5589C-G (-)	A3559G (-)		C5609A (-)	C5540A (+)		A5589C-G (-)	A3559G (-)
	A5593C (-)	A3701T (+/-)		C6360T (-)	A5589C-G (-)		C5609A (-)	A4754G (+/-)
	C5609A (-)	C5540A (+)		A9539G (-)	A5593C (-)		C6360T (-)	C5540A (+)
	C6360T (-)	C5555A (+)		T9988A-G (-)	C5609A (-)		A9539G (-)	C5555A (+)
	A9539G (-)	A5589C-G (-)		A10973G (-)	A5908G (-)		T9988A-G (-)	A5589C-G (-)
	T9988A-G (-)	A5593C (-)			C6360T (-)		A10973G (-)	A5593C (-)
	A10973G (-)	C5609A (-)			A7589G (+/-)			C5609A (-)
		A5908G (-)			A9539G (-)			C6360T (-)
		C6360T (-)			T9988A-G (-)			C7634A (+/-)
		A7836C (+/-)			C10371T (+/-)			C9068A (+/-)
		A9539G (-)			A10973G (-)			A9539G (-)
		T9988A-G (-)			C11295G (+/-)			T9988A-G (-)
		C10371T (+/-			C11296+T (+)			G10161T (+/-)
		C10743G (+/-)						C10371T (+/-
		A10973G (-)						A10973G (-)

Table 4.2:   High frequency variants (≥0.02) for the coding region of TC-83 3x.

If a variant was found to be present in more than one EP step (i.e. DNA, TX, or EP) for a replicate, this nt position was highlighted. R1: replicate 1, R2: replicate 2, R3: replicate 3, TX: in vitro transcription, del: deletion, +: insertion. Genome strand bias: positive (+), minus (-), or both (+/-) is indicated in the parentheses.
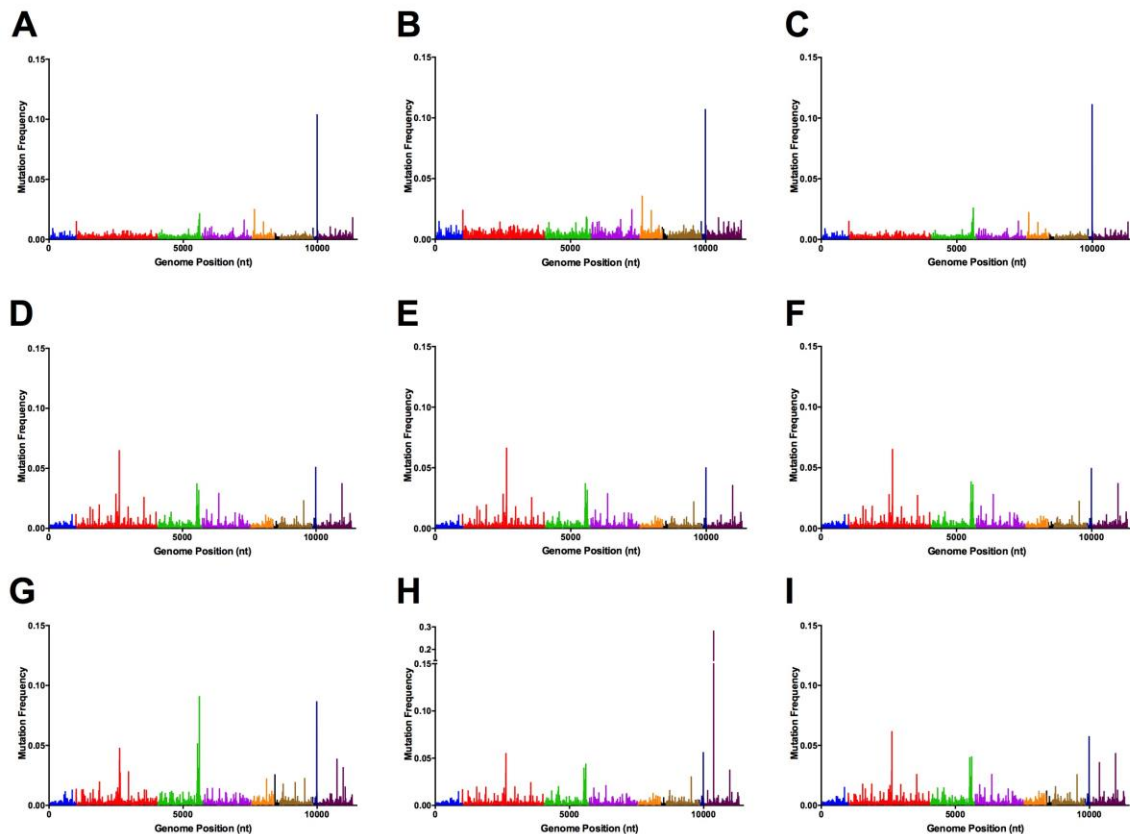
Figure 4.4:   Illumina sequencing virus diversity hotspots for the coding regions of three TC-83 replicates.

Purified, linearized DNA replicate 1 (A), Purified, linearized DNA replicate 2 (B), Purified, linearized DNA replicate 3 (C). In vitro transcription replicate 1 (D), In vitro transcription replicate 2 (E), In vitro transcription replicate 3 (F). EP stock replicate 1 (G), EP stock replicate 2 (H), EP stock replicate 3 (I). Genome organization is color-coded using the following: nsP1: blue, nsP2: red, nsP3: green, nsP4: purple, capsid: orange, E3: black, E2: gold, 6k: navy blue, and E1: maroon.

DNA R1	TX R1	EP R1	DNA R2	TX R2	EP R2	DNA R3	TX R3	EP R3
C5609G (-)	T2507A (+)	C2627A (+/-)	A1021C (-)	T2507+T (+)	A1543G (-)	C5609G (-)	T2507+T (+)	C2627+G (-)
A7653C (+)	A2634del(+)	A2634del(+)	A7270C (+)	A2634del (+)	C2627A (+)	A7653C (+)	A2634del (+)	A2634del (+)
T9988A-G (-)	A3559G (-)	A2654G (+/-)	A7653C (+)	A3559G (-)	A2634del (+)	T9988A-G (-)	A3559G (-)	A3559G (-)
	C5540A (+)	A2966G (-)	A7989C (-)	C5540A (+/-)	A2966G (-)		G5528A-T (+/-)	C5540A (+)
	C5555A (+)	G5528A (+/-)	T9988A-G (-)	C5555A (+)	A3559G (-)		C5540A (+)	C5555A (+)
	C5609A (-)	C5540A (+)		A5589C-G (-)	T4592C (+/-)		C5555A (+)	A5589C-G (-)
	C6360T (-)	C5555A (+)		C5609A (-)	C5540A (+/-)		A5589C-G (-)	A5593C (-)
	A9539G (-)	A5589C-G (-)		C6360T (-)	C5555A (+)		C5609G (-)	C5609G (-)
	T9988A-G (-)	A5593C (-)		A9539G (-)	A5589C-G (-)		C6360T (-)	C6360T (-)
	A10973G (-)	C5609A (-)		T9988A-G (-)	A5593C (-)		A9539G (-)	A9539G (-)
		C8116T (-)		A10973G (-)	C5609A (-)		T9988A-G (-)	T9988A-G (-)
		C8428A (+/-)			C6360T (-)		A10973G (-)	C10371T (+/-)
		A9539G (-)			A9539G (-)			A10973G (-)
		T9988A-G (-)			T9988A-G (-)			
		T10744A (+/-)			C10371T (+/-)			
		A10973G (-)			A10973G (-)			

Table 4.3:   High frequency variants (≥0.02) for the coding region of TC-83.

If a variant was found to be present in more than one EP step (i.e. DNA, TX, or EP) for a replicate, this nt position was highlighted. R1: replicate 1, R2: replicate 2, R3: replicate 3, TX: in vitro transcription, del: deletion, +: insertion. Genome strand bias: positive (+), minus (-), or both (+/-) is indicated in the parentheses.
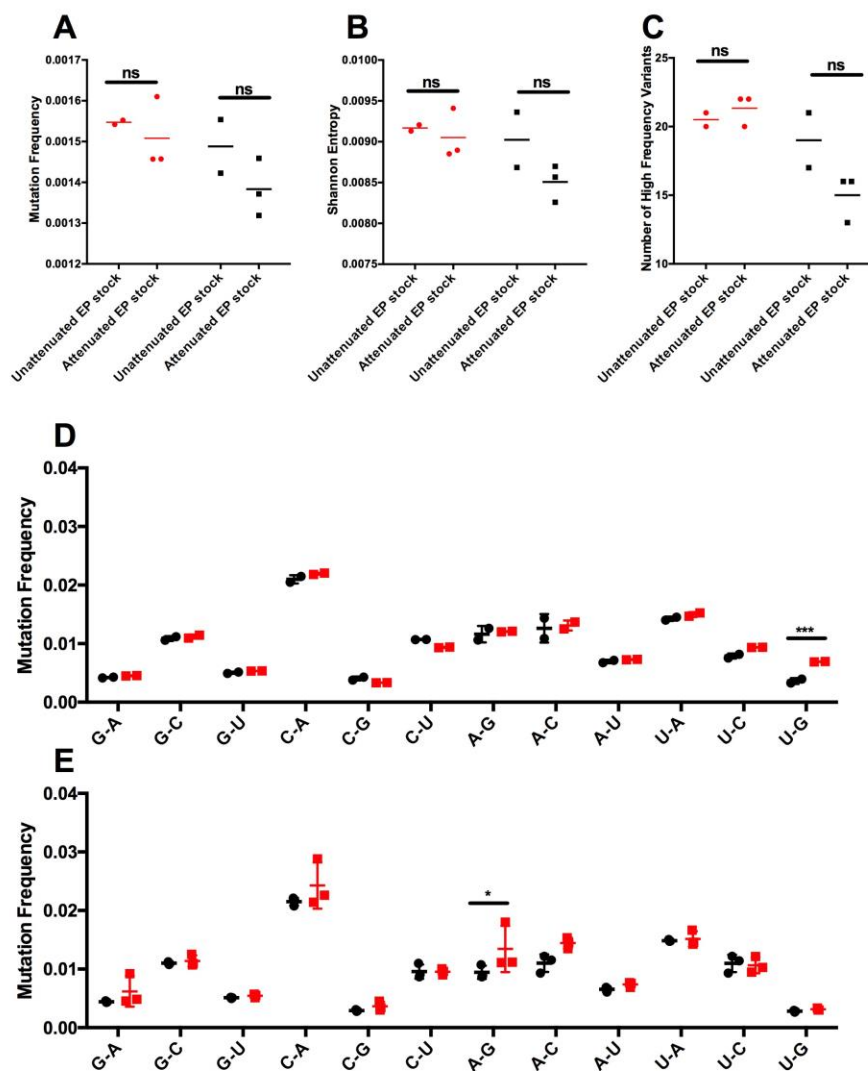
Figure 4.5:   Correlation of genetic and phenotypic differences in EP stocks.

EP stock from chapter 2, which was not attenuated in mosquito cells, was compared to TC-83 and TC-83 3x EP stock that was attenuated to determine differences between the EP stocks. Differences in overall mutation frequency between attenuated and unattenuated TC-83 and TC-83 3x stocks (A). Differences in overall Shannon Entropy between attenuated and unattenuated TC-83 and TC-83 3x stocks (B). Number of high frequency mutations (cut-off=0.02) for TC-83 and TC-83 3x after DNA linearization, in vitro transcription, and EP (E). Differences in the number of high frequency mutations (cut-off=0.02) between attenuated and unattenuated TC-83 and TC-83 3x stocks (C). Mann-Whitney U test was used to determine statistical significance for A-C. Mutation frequency of different mutations for unattenuated (D) and attenuated (E) TC-83 and TC-83 3x. Two-way ANOVA was used to determine statistical significance for D-E. TC-83 3x data points are in red, while TC-83 data points are in black. $p > 0.05$ is represented by ns, $p < 0.05$ is represented by *, $p < 0.01$ is represented by **, $p < 0.001$ is represented by ***.
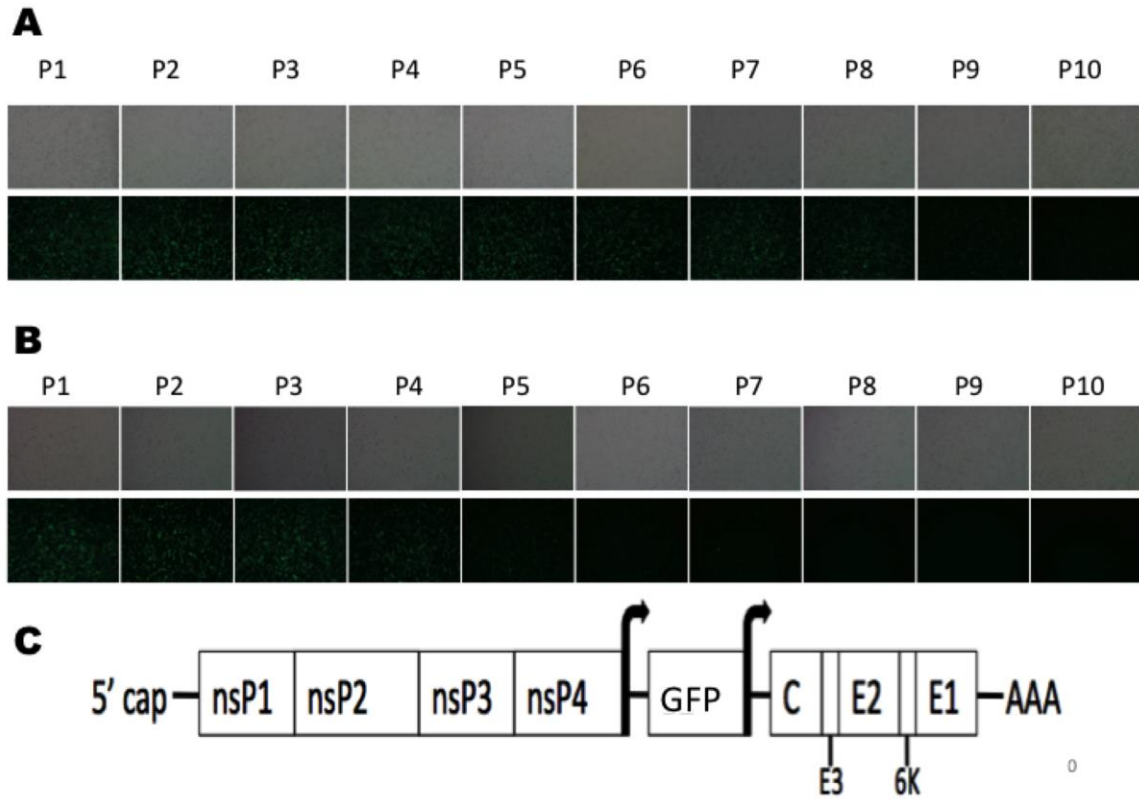
Figure 4.6: Loss of GFP fluorescence during passage.

Vero cells were infected with TC-83 GFP (A) or low-fidelity TC-83 GFP (B) over the course of 10 virus passages. A representative replicate for each virus is depicted. Upper panels show brightfield microscopy images, while lower panels show GFP florescence. P: passage. Genome schematic of TC-83 GFP (C).
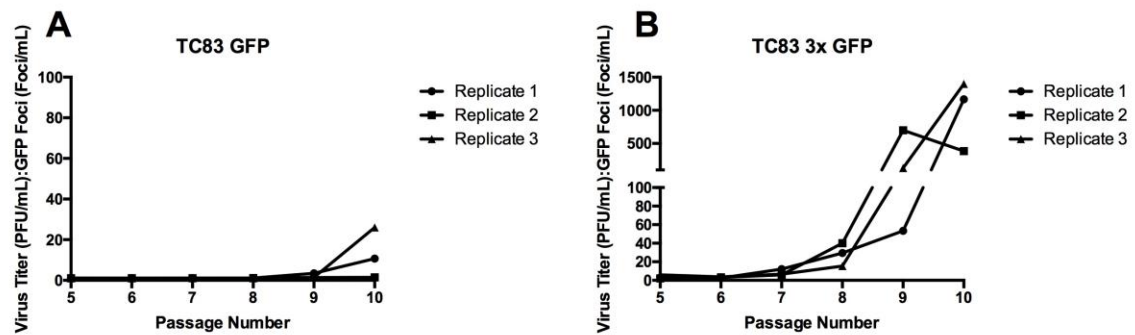
Figure 4.7:   Loss of GFP fluorescence during passage.

The ratio of PFU:GFP foci was determined to estimate the loss of GFP florescence for TC-83 GFP (A) and low-fidelity TC-83 GFP (B). Replicate 1: circle, replicate 2: square, replicate 3: triangle.
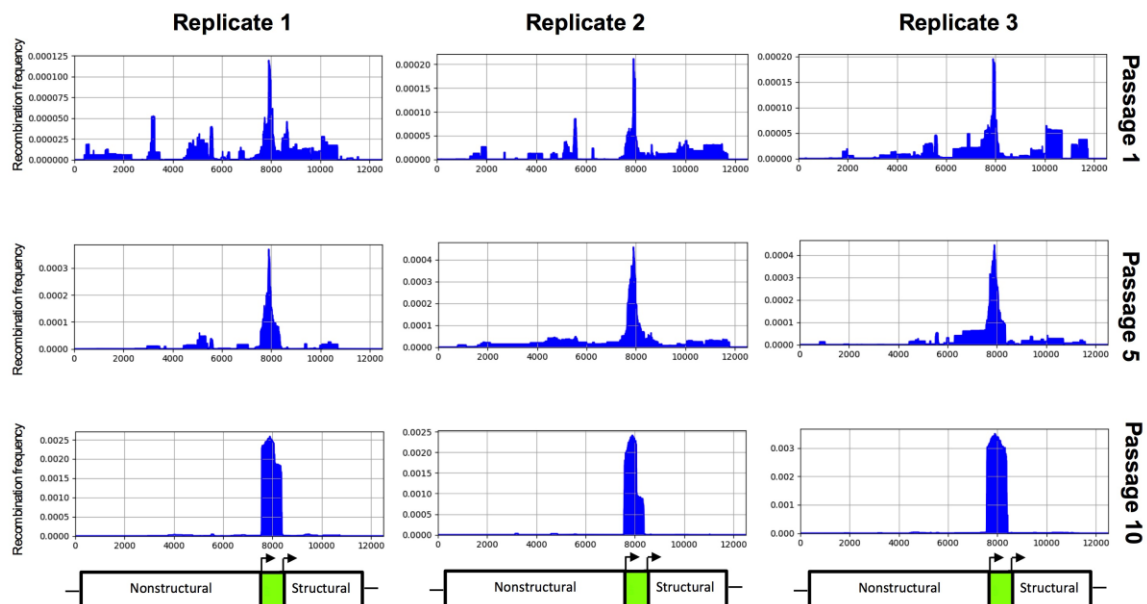
Figure 4.8:   ViReMa recombination results for TC-83 GFP.

Passages 1, 5, and 10 are shown for each TC-83 GFP replicate. The x-axis shows genome position, while the y-axis shows the recombination frequency (i.e. normalized to the total reads that map to TC-83 GFP). Below the recombination charts, a schematic shows the approximate location of the nsP, GFP, and structural genes.
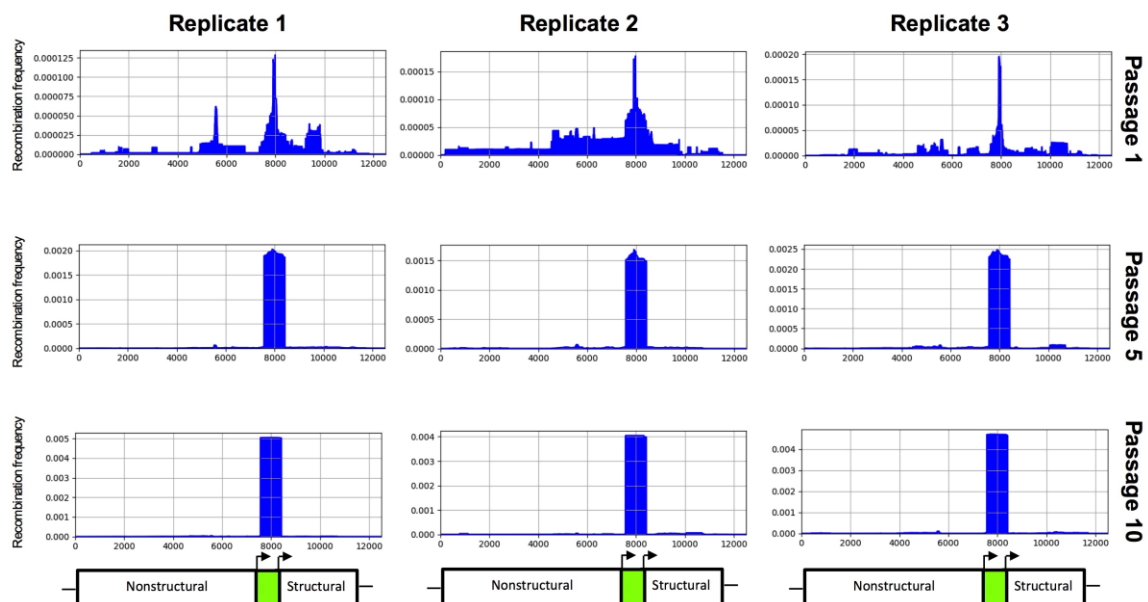
Figure 4.9:   ViReMa recombination results for TC-83 3x GFP.

Passages 1, 5, and 10 are shown for each TC-83 3x GFP replicate. The x-axis shows genome position, while the y-axis shows the recombination frequency (i.e. normalized to the total reads that map to TC-83 3x GFP). Below the recombination charts, a schematic shows the approximate location of the nsP, GFP, and structural genes.
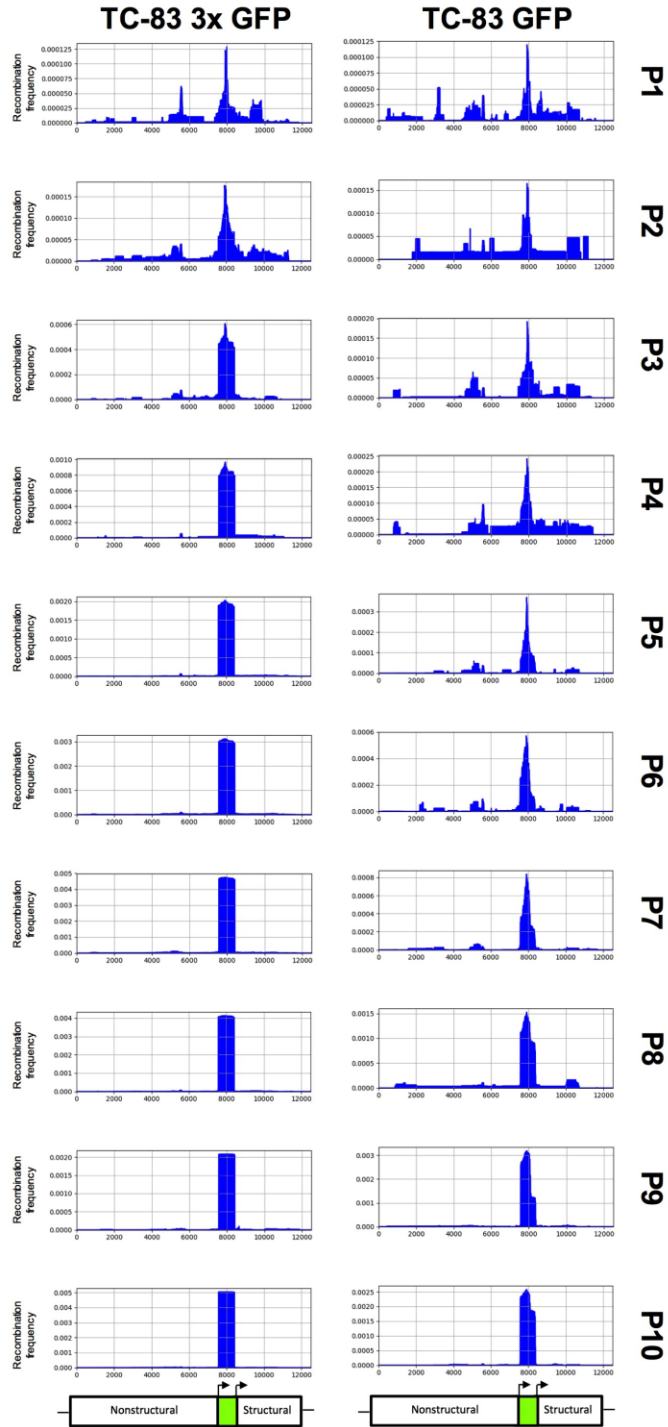
Figure 4.10: ViReMa recombination results for TC-83 GFP and TC-83 3x GFP.

Each passage of the first replicate of TC-83 GFP and TC-83 3x GFP was sequenced using ClickSeq libraries and analyzed using ViReMa. The x-axis shows genome position, while the y-axis shows the recombination frequency (i.e. normalized to the total reads that map to TC-83 3x GFP). Below the recombination charts, a schematic shows the approximate location of the nsP, GFP, and structural genes. "P" represents passage.

144
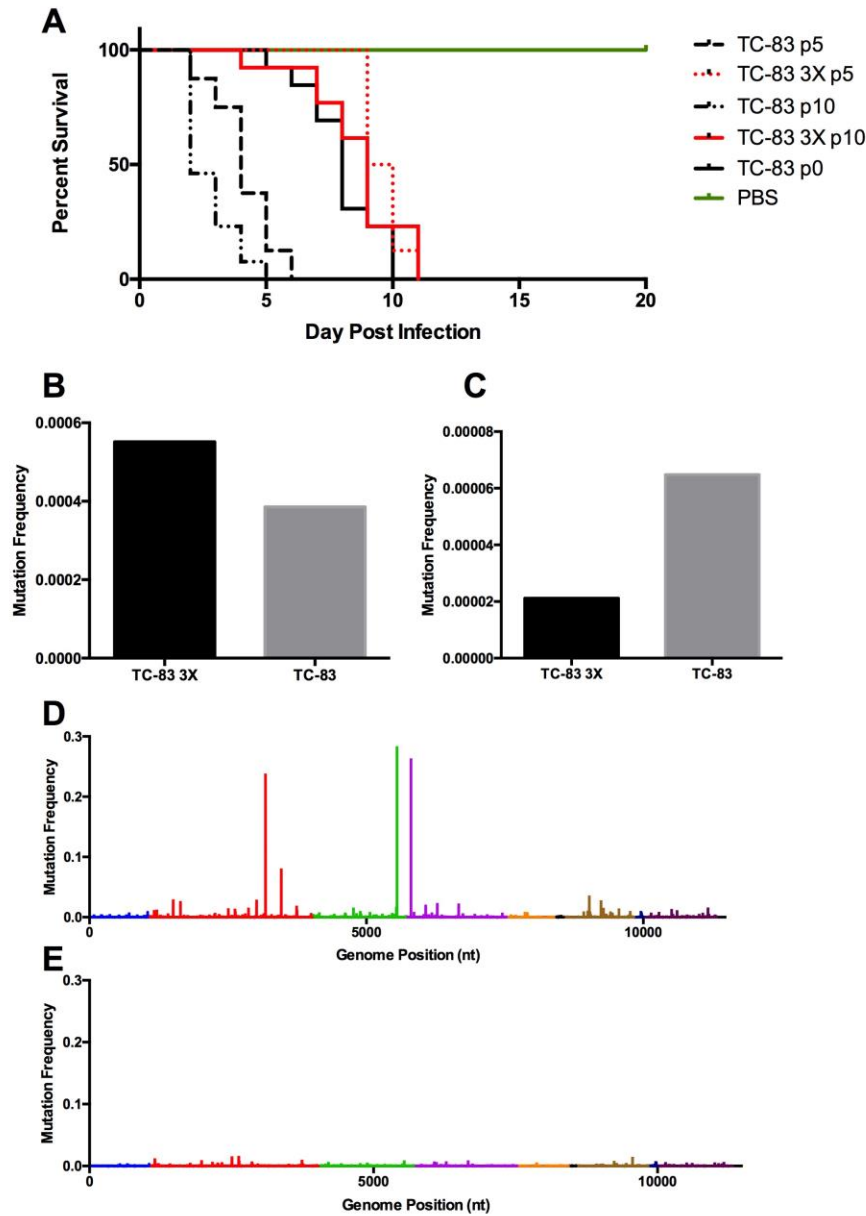
Figure 4.11: *In vivo* genetic and phenotypic stability.

Survival of 6-day old CD-1 mice following SC injection with 10^5 PFU in a 50ul volume of passage 0, 5, or 10 TC-83 or TC-83 3x from infant mouse intracranial passages (A). Statistical differences were determined using Kaplan-Meier tests, and significance is detailed in the text. Illumina sequencing diversity analysis was used to determine changes in virus diversity of passage 5 TC-83 or TC-83 3x in infant mice (B). Mutation reversion frequency of the E2 8922 mutation required for TC-83 attenuation (C). Illumina sequencing virus diversity hotspots for the coding regions of TC-83 (D) and TC-83 3x (E) genomes after 5 intracranial passages. Genome organization is color-coded using the following: nsP1: blue, nsP2: red, nsP3: green, nsP4: purple, capsid: orange, E3: black, E2: gold, 6k: navy blue, and E1: maroon.

145

		Amino Acid Change	TC-83 3X	TC-83
nsP2	C3179T		X	
nsP4	T7208C			X
E2	A8805T	D-L	X	
3'UTR	C11386T			X

Table 4.4:   Changes in nucleotide sequence following p10 in mouse brains as verified by Sanger sequencing.

WHAT IS A FIDELITY MUTANT?

Chapter 5. Discussion

In this dissertation, a low-fidelity TC-83 was found to improve upon the unaltered TC-83 in a variety of ways. For example, this mutant enhanced the neutralizing antibody response when used as a vaccine, decreased virulence in an infant mouse model, decreased replication *in vitro* in mosquito cells, was genetically stable, and was unable to increase in virulence on par with TC-83 when passaged in infant mice. However, when some of these assays were repeated, such as the infant mouse virulence experiments and low MOI mosquito cell infections, phenotypes were not reproduced, likely due to differences in EP stocks. While frustrating, this is a common problem in science, referred to as the replication crisis (388). This is especially concerning for the vaccine candidate described in this dissertation, as these inconsistent outcomes represent a significant barrier against the development of fidelity mutants as live-attenuated vaccine. These inconsistencies necessitate further consideration of the putative characteristics of a virus fidelity mutant.

DEFINING A FIDELITY MUTANT

The most basic definition of a RNA virus fidelity mutant is a virus that produces more or less error when replicating relative to unaltered virus. While identifying a fidelity mutant may appear straightforward, it can be difficult to link certain mutations to changes in fidelity. Additionally, questions arise that are difficult to answer. For example, is a virus a fidelity mutant if it is not high or low-fidelity for all mutation types? For half of the mutation types? As long as the overall balance is consistently higher or lower than the control virus? While this may be less of a concern for fidelity mutants that are resistant to

multiple types of nucleoside analogs, this is important to know for fidelity mutants that only display resistance to one type (78).

As the low-fidelity TC-83 discussed during this dissertation displays inconsistent changes in the frequency of certain mutations, these questions must be asked. The answer likely depends on the purpose of the project. For example, if the goal is to cause further attenuation of a vaccine, this is not likely to be important as long as the attenuation is stable. However, this knowledge is important if a vaccine phenotype is not stable or when asking basic science questions. Unfortunately, the frequency of different mutations is not available for most fidelity mutants, and the majority of those mutants for which this is available either find an imbalance in different types of mutation (74, 79, 83) or do not provide enough information to determine this (63, 88).

ARE SOME FIDELITY MUTANTS ACTUALLY KINETIC MUTANTS?

Theoretically, fidelity mutants should not be attenuated *in vitro*, because changes in fidelity should not be detrimental to virus replication (353). The lack of a growth defect is a desirable characteristic for a LAV, as this is one less barrier against production of the vaccine. This is especially true for a vaccine such as TC-83, which grows to very high titers. However, many fidelity mutants do grow slightly slower than wt virus (72, 76, 82, 85, 389), especially in primary vertebrate cells (67, 77) and mosquito cells (82-84). While the mechanisms behind this slight attenuation are not well understood, this suggests that in a more complex environment, such as those found *in vivo*, that fidelity mutants may essentially behave as kinetics mutants (67). As fidelity mutants commonly display lower titers and tissue restriction *in vivo* (46, 68, 69, 73, 80, 82, 86, 339), perhaps the lower titers produced by fidelity mutants act as a bottlenecks, producing a virus population without the correct mutant spectrum to infect the same number of tissues as wt virus. Additionally, a drop in the virus titer due to slightly lower replication kinetics likely makes the infection easier for the host to control, which could be a confounding

factor in the attenuation commonly observed for fidelity mutants. This begs the question of whether fidelity and kinetics can ever truly be separated.

Newer technologies may aid in determining the differences between fidelity and replication, if they do indeed exist. For example, measuring the incorporation of 1-2 nt, as is common in sym/sub replication kinetics experiments, is not an accurate depiction of virus replication, which requires the RdRp to replicate not one, but thousands of nts. A new technique, known as magnetic tweezers, addresses this by attaching a coverslip to one strand of an approximately 3kb dsRNA molecule and a magnetic bead to the other (390, 391). As the RdRp replicates the RNA, this releases the beaded RNA strand from the anchored RNA strand, allowing the magnetic bead to migrate upwards towards a magnet. The longer the distance between the coverslip and the magnet, the more efficient the RdRp is at replication. Sym/sub replication studies have shown low-fidelity viruses to be fast, but inaccurate nt incorporators (18, 46, 77, 83). However, magnetic tweezers have shown that low-fidelity PV H273R also displays an increased number of pause events, which are associated with the incorporation of incorrect nts (390). This suggests that low-fidelity polymerases are prone to stuttering when replicating, which may have impacts on other polymerase-associated events, such as recombination. Understanding the role of processivity and its ties to fidelity is one step towards closing the gap of knowledge between what is observed during very simple measures of virus replication, such as sym/sub replication, and what is observed in cell culture and animals.

For some viruses, such as those in the alphavirus genus, the RdRp is unstable, and thus fine measurements of RdRp replication kinetics are not possible. Single-cell sequencing presents an exciting alternative, while also offering a better understanding of the fate of each virus-infected cell (392-394). Interestingly, when low-fidelity H273R PV was examined using this technique, it was found to cause a reduced number of infections compared to wt virus, as well as delayed replication initiation (392). However, H273R was able to replicate quickly enough to reach peak titer at the same time at wt PV. This

experiment confirmed what had been measured using the sym/sub system (79), suggesting that some of the measurements that once required cell-free systems to assay can now be performed in cells. This also improves upon the more standard biochemical and growth curve kinetics assays by allowing for the measurement of thousands of infections at the same time in replicate, instead of only examining a composite. However, as these techniques are relatively new, this type of analysis is not yet widely available.

FIDELITY MUTANT STABILITY

As John Allen Paulos once said, "uncertainty is the only certainty there is," (395) which seems to be especially true of RNA virus fidelity mutants. While fidelity mutants exhibit certain trends, like attenuation in one environment versus another, these do not appear to always be stable. During studies described in chapters 2-4 of this dissertation, there were multiple *in vivo* and *in vitro* examples of inconsistent TC-83 phenotypes with no clear explanation as to the reason for this instability. This is not entirely surprising, as RNA virus fitness landscapes are hypothesized to be turbulent (20, 22), and there is a paucity of methods to aid in the prediction of these landscapes. When examining the literature, most fidelity mutants have only been characterized in the paper showcasing their discovery, and those that have appeared in more than one publication are used to examine something novel. Occasionally, however, assays are repeated, and these commonly show inconsistent fidelity and/or phenotypes, as described below.

The high-fidelity HEV71 mutants were first described by Sadeghipour et al. in a pair of concurrent papers (72, 339). While G64R, G64T, and S264L RdRp mutations were all able to increase HEV71 fidelity *in vitro* (72), only S264L caused attenuation *in vivo* when using 5-day-old BALB/c mice, which have an intact IFN response (339). However, when these mutants were later examined in a slightly different virus backbone that was not murine-adapted, G64R was approximately 3-fold less virulent than S264L when using 10-day-old AG129 mice (IFN-receptor deficient), which itself was 37-fold

less virulent than the control virus (73). This is odd, because these results suggest that small changes to the HEV71 backbone can cause dramatic changes in virulence. However, if the highly conserved PV G64 residue is able to increase fidelity in a distantly related enterovirus such as HEV71, this is not likely to be the cause of differences in virulence. Alternatively, changing the mouse model may have resulted in decreased G64R virulence in AG129 mice. However, as PV G64S (67, 68) and other fidelity mutants (46, 71, 75-80, 82, 86, 87) are attenuated in mice with intact IFN, it would therefore be predicted that the HEV71 G64R mutant would also be attenuated in the BALB/c model. Thus, there is no clear explanation for why the HEV71 G64R mutant would behave so differently in the hands of different labs.

The most famous and highly studied fidelity mutant, high-fidelity PV G64S, is not immune to incongruent results. The first study to examine PV G64S in $vivo$ infected cohorts of 10-week-old PVR mice IM with $5x10^6$ PFU of G64S or wt PV (67). Of the 25 mice per cohort, approximately 10 G64S PV mice exhibited no symptoms over the course of infection, while only 5 of the mice infected with wt PV exhibited no symptoms. While it was stated that fewer deaths were recorded for G64S infected mice, this data was not shown. In contrast to this, Vignuzzi et al. (68) found that 100% of 8-week-old PVR mice infected IM with 10^7 PFU of G64S were able to survive infection, suggesting that this G64S was more attenuated than it was in the initial in $vivo$ virulence study (67). Vignuzzi et al. also used this experiment to calculate LD_{50} values, which were $1.2x10^6$ PFU for wt PV and $3.9x10^8$ PFU for G64S, a 325-fold difference. These are the exact same LD_{50} values published in a later paper also by the Vignuzzi lab (69). This alone would not be too concerning as both papers demonstrated that G64S PV was more attenuated in $vivo$ than wt PV. However, a recent dissertation (396) reported complete hind limb paralysis in all mice (which mice cannot recover from) when 4-6-week-old PVR mice were infected IM with 10^7 PFU of G64S, as well as no difference in the LD_{50} values for G64S versus wt PV. Intriguingly, for this group, G64S was only more attenuated than wt PV

when 5-week-old mice were infected IP. This report was further reinforced by the most recent paper to examine G64S virulence, which also found 5-week-old PVR mice infected IM with 10^7 PFU of this mutant or wt PV to succumb to infection at identical rates (63). There was also no difference in the LD_{50} values. Xiao et al. suggested that this difference may be due to age, as the wt PV LD_{50} for 8-week old mice in this study was 10^7 PFU versus $5x10^5$ PFU for 5-week-old mice. However, it is unknown how this translates to high-fidelity G64S PV, and does not explain why the LD_{50} values would be so similar for wt PV and G64S. Again, as seen for HEV71, fairly large differences in phenotypes were observed when different labs examined this fidelity mutant.

The inconsistency observed for *in vivo* attenuation with HEV71, PV, and our TC-83 mutant suggest that this is a prevalent occurrence for fidelity mutants. This is concerning, as one of the best pieces of evidence for the theory of virus quasispecies is the original high-fidelity PV study by Vignuzzi et al., which demonstrated that it was the overall diversity of the quasispecies that caused virulence, not any one mutation (see "Poliovirus" in the introduction). Perhaps it is not surprising that *in vivo* attenuation is inconsistent, as it is hypothesized that high fidelity viruses will be less likely, not entirely unable, to produce the mutants necessary for different tasks (e.g. IFN evasion, host switching). This is supported by recent studies that have correlated specific minority variant mutations to increases in virus fitness (204, 397). Additionally, while low-fidelity viruses are hypothesized to overproduce deleterious, interfering mutants, perhaps some stocks harbor more interfering mutants than others, while others may generate high fitness mutations due to random chance, leading to differences in attenuation.

While the mechanism(s) behind this variation in attenuation *in vivo* have yet to be determined, a study by Xiao et al. hints that PV is able to overcome increased fidelity by using recombination, suggesting that recombination may be playing a compensating role for other fidelity mutants (91). Additionally, as suggested by Xiao et al., the age of the mouse could explain the severe changes in attenuation, although this may be specific to

152

PV G64S. If so, this is of large concern for vaccine development, as this suggests that, at best, only certain human populations would benefit from the increased vaccine attenuation, or at worst, that there would be no discernable difference between vaccines with or without altered fidelity. This needs to be examined closely to determine exactly what is causing these changes in virulence and if these mechanisms are conserved between different fidelity mutants. At minimum, this suggests that separate LD_{50}s should be performed for each altered fidelity mutant stock to ensure consistent attenuation.

Additionally, the diversity of fidelity mutants can be somewhat inconsistent. For example, the mutation frequency of high-fidelity CHIKV C483Y was initially determined to be approximately 1.4-fold higher than wt virus (80). Five independent EP stocks for each virus were used to determine these mutation frequencies, and, interestingly, there was large overlap of the mutation frequency error bars between the two viruses, similar to our EP results in Chapter 4. Later publications that used C483Y as a control found no difference in the mutation frequencies generated by C483Y or wt CHIKV (81, 82), which may explain why the TC-83 C488Y mutant examined in Chapter 2 had no effect on virus fidelity. Interestingly, the mutation frequency per 10^4 nt was slightly higher for wt CHIKV in the initial study compared to more recent papers (5.1 versus 4.4 and 4.4), as well as slightly lower for C483Y (3.6 versus 4.1 and 4.2), suggesting that slight fluctuations in both the wt and RdRp mutant stock can reduce or entirely ablate significant differences in replication fidelity. Alternatively, this change in the CHIKV C483Y mutation frequency is perhaps explained by an nsP2 mutation, G641D, which was found during the initial high-fidelity CHIKV identification (80) and later shown to also increase CHIKV fidelity (81). It would be interesting to determine the occurrence of this nsP2 mutation in different CHIKV C483Y EP stocks, and whether the appearance of this mutation in the minority variant population is correlated with decreased mutation frequencies. Importantly, while the flux in this CHIKV mutant's replication fidelity is likely one of the more egregious examples, some degree of mutation frequency flexibility

is probably to be expected due to differences in mutation frequency measurements, random chance, and other unknown variables (Figure 5.1).

Unfortunately, for many fidelity mutants we may never know what aspects are or are not repeatable, as the majority of fidelity mutants have not been closely and repeatedly examined. This is problematic, as outcomes from experiments using putative fidelity mutants are being used to draw significant conclusions regarding RNA virus evolution (37, 372). Without a thorough understanding of the shortcoming of each proposed fidelity mutant, however, their use is likely to lead to ambiguous and misrepresentative results. Thus, it is now important for the fidelity mutant field to take a step backwards to truly assess what it means for a virus to display altered fidelity.

USING FIDELITY MUTANTS AS VACCINES

As described above, the inconsistent attenuation observed with fidelity mutant viruses suggests that fidelity mutants are not yet ready for mainstream use as vaccine candidates. If the outcome of virus recovery is variable and leads to major shifts in the observed phenotype for a fidelity mutant, despite the same consensus level mutations being present, this creates a significant barrier for developing a controlled manufacturing process. At minimum, correlates of attenuation need to be developed by generating many pools of virus stock, establishing a correlate of protection (e.g. a significantly lower LD_{50} in a mouse model), and sequencing these stocks to determine minority sequences associated with attenuation or virulence. It would also be important to passage these stocks to guarantee stability of the vaccine genotype and phenotype and reduce adverse events following vaccination.

Perhaps our low-fidelity TC-83 vaccine candidate could be further improved upon by further attenuation beyond the E2 and 5'UTR mutations responsible for its initial attenuation. For example, inserting our low-fidelity mutations into a closely related VEEV vaccine candidate (e.g. V3526 (311)) could result in a more consistently

154

attenuated vaccine candidate. It may also be interesting to explore differences in vaccine attenuation caused by different methods of preparing virus stocks. As shown in chapter 4, minority variants created during *in vitro* transcription are largely retained in the EP stock. Different plasmid promoters (e.g. T7, SP6, CMV) and the repercussions of these on virus stock genotypes and phenotypes should be explored in future work. Using a CMV promoter would be especially interesting, because this would allow for the delivery of the vaccine candidate as a plasmid via a gene gun, as described in the overall introduction. This method of vaccine delivery would eliminate the errors generated during the *in vitro* transcription step necessitated by our EP virus stocks and would streamline the manufacturing process.

While using fidelity mutants as vaccines held such large promise during the initial high fidelity poliovirus studies, the work described in this dissertation and elsewhere suggests that this method of virus attenuation is only workable if attenuated viruses are used as the backbones for these mutants. There is some historical evidence for this, as the vaccine for yellow fever, 17D, is believed to be a safe and effective vaccine based upon multiple attenuation mutations as well as a high fidelity polymerase. Perhaps in the future the instability exhibited by our low-fidelity vaccine candidate, as well as other fidelity mutants, will be overcome, allowing for these fidelity mutants to be used as vaccines. Until then, however, fidelity mutants will remain as a tool for basic science, at least when used in a well-controlled setting.
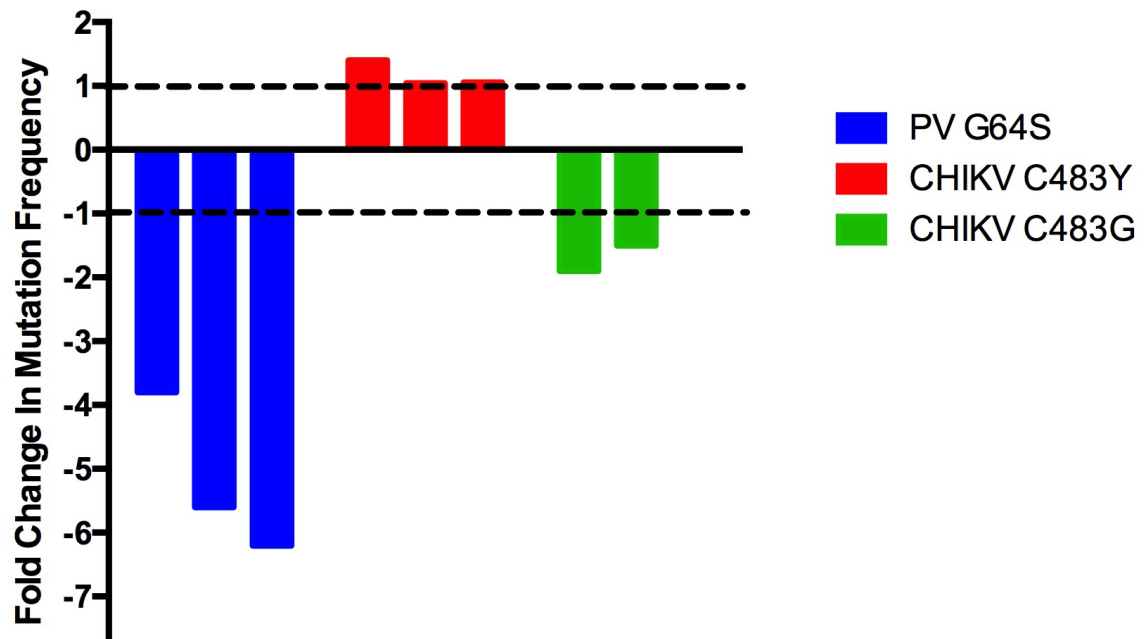
Figure 5.1:   Variation in fidelity mutant mutation frequencies.

Variation in the mutation frequency of unaltered virus versus: high-fidelity PV G64S (68, 69, 79), high-fidelity CHIKV C483Y (80-82), or low-fidelity CHIKV C483G (81, 82). Dashed lines indicate equal levels of mutation frequency for control and fidelity mutant viruses.

APPENDIX 1. VEEV TRANSMISSION CYCLE *IN VITRO*

No work has examined genetic/phenotypic stability of arbovirus fidelity mutants in a transmission cycle. To better understand how TC-83 and the low-fidelity mutant adapt when confronted with alternating animal and vector environments, these viruses were serially passaged in duplicate using mosquito cells, vertebrate cells, or cycling between the two. Also, to determine if any adaptive changes occurred while virus was passaged in cells with functional cellular immunity, interferon competent (MRC-5) or incompetent (Vero) vertebrate cells were used alongside siRNA competent (U4.4) or incompetent (C7/10) mosquito cells (Illustration 6.1).

METHODS

Cell culture

Vero (African green monkey kidney), HEK-293 (human embryonic kidney), MRC-5 (human fetal lung fibroblast), and Baby Hamster Kidney (BHK) cells were obtained from the American Type Culture Collection (ATCC) (Bethesda, MD) and maintained in DMEM (Gibco) supplemented with 10% Fetal Bovine serum (FBS, Atlanta Biologicals), and 500μg/mL gentamycin (Corning) in a 37°C 5% CO_2 incubator. C7/10 cells were maintained in DMEM supplemented with 10% Fetal Bovine serum, 1% Minimal Essential Medium Nonessential Amino Acids (Gibco), 1% Trypose Phosphate Broth (Sigma), and 500μg/mL gentamycin in a 30°C 5% CO_2 incubator. U4.4 cells were maintained in Mitsuhashi and Maramorosch media (Sigma) supplemented with 20% FBS, 2% Sodium Bicarbonate (7.5%) (Gibco), and 500μg/mL gentamycin in a 30°C 5% CO_2 incubator.

Plaque assay

One day prior to infection, 6-well or 12-well Vero plates were plated using 250,000 or 500,000 cells per well respectively to ensure approximately 90% confluency the following day. Virus stocks were diluted 1:10 8 times using 225μL DMEM (supplemented with 2% FBS and gentamycin) and 25μL virus. This dilution series was either performed using 1.5mL tubes (using vortexing to mix) or 96 well plates (using pipetting to mix). Media was then decanted from a cell culture plate and 100μL (12-well plate) or 200μL (6-well plate) of each dilution was added to a well. This was performed in duplicate. The infected monolayers were stored in a 37°C 5% CO_2 incubator for 1 hour and were gently shaken every 15 minutes to ensure an even infection distribution. After this incubation, a 0.4% agarose overlay (1 part 2% agarose (Lonza) in filter-purified water to 4 parts DMEM supplemented with 2%FBS and gentamycin) was added to each well, and the plates were returned to the incubator. Following a 48 hour incubation, the monolayers were fixed for 30 minutes using 10% formaldehyde (Fisherbrand) before the agarose plugs were removed and the monolayer was stained with 0.25% crystal violet solution (Fisherbrand). The plates were then washed with water and allowed to dry before plaques were counted.

PFU per mL was calculated using the following formula: PFU/mL=(dilution X number of plaques) (1000/amount plated), with "dilution" equalling the dilution at which the plaques were counted and "amount plated" equalling the amount of virus added when infecting the cells (i.e. 100μL for 12-well plates and 200μL for 6-well plates).

TC-83 passaging

One day prior to infection, 6-well plates were seeded with 500,000 Vero or MRC-5 vertebrate cells or 1,000,000 U4.4 or C7/10 mosquito cells. The day of the infection, one well of cells for each cell type was counted using a hemocytomer and used to determine the virus dilutions necessary for an MOI of 0.1. Once diluted, media was decanted from the 6-well Vero cell plate and 200μL was used to infect each well. These

infections were performed using two replicates per virus. Following the infection, the plate was transferred to a 37°C (vertebrate cells) or 30°C (mosquito cells) 5% CO_2 incubator for 1 hour with occasional shaking. When the incubation was complete, the inoculum was removed and 2mL of DMEM supplemented with 2% FBS and gentamycin (vertebrate cells) or the standard mosquito cell media was added to each well. The plates were then returned to the appropriate 5% CO_2 incubator for 24 hours.

After the 48 hour incubation, the virus was transferred to a tube with FBS to a final concentration of 20% FBS. This was centrifuged for 5 minutes at 0.8 X g and transferred to a new tube. These tubes were stored at -80°C. Plaque assays using Vero cells were used to determine virus titer. Six total passages were performed.

To determine changes in plaque size over the course of passaging, plaque assays were preformed as per the usual protocol. All TC-83 plates were done in one batch, while all the TC-83 3x plates were done in another batch to insure that differences in cell confluency would not act as a confounding variable for differences in plaque size. After 48 hours, the cells were fixed and stained following the usual plaque assay protocol, and a picture was taken using an iPhone 6 (Apple) of each plate. The plaque size of 10 plaques per virus group was measured using the Dew ADI16 program.

RT-qPCR for TC-83 RNA copy number

COPY NUMBER STANDARD

To prepare the copy number standard (see "TC-83 RT-qPCR control plasmid"), 1μg of the plasmid was digested using SphI (NEB) according to the manufacturer's protocol. The digested plasmid was cleaned using the ClonTech PCR-cleanup kit as per the manufacturer's protocol, and transcribed using the MaxiScript T7 kit (Ambion), also using the manufacturer's protocol. Once transcribed, the plasmid DNA was digested using the DNA-free DNA removal kit (Invitrogen) and the RNA was further purified using the RNAqueous total RNA isolation kit (Ambion), both according to the

manufacturer's protocol. Finally, linearization, transcription, DNase I treatment, and further purification of the copy number standard were visualized for confirmation of each step using a 1% agarose TAE gel. Copy number was calculated using a DS-11 spectrophotometer (DeNovix) to quantify the amount of RNA per microliter. An online calculator (http://endmemo.com/bio/dnacopynum.php) used this and the transcript length (1,723bp) to determine the RNA copy number per microliter. Following this, the RNA was diluted to $2x10^{10}$ copies per μL in 20μL aliquots and stored in a cold block at -20°C. RNA was only freeze-thawed once before being discarded.

RT-qPCR

Viral RNA was extracted using the ZR Viral RNA minikit (Zymo) as per the manufacturer's protocol and eluted in 15μL nuclease free water. This was stored on ice as the rest of the reaction was prepared.

A standard curve of the above RNA standard was made to total 8, 10-fold dilutions in nuclease-free water (5μL RNA mixed with 45μL nuclease-free water). Pipetting was used to mix between each dilution. This was stored on ice while the master mix was prepared.

Real time PCR primers were designed to amplify a portion of the nsP3 gene. The forward (4840F 5-ATG CCA TGA CTC CAG AAA GAG-3) and reverse (4981R 5-GGT GAG AAC AAT ATA GGC TGG G-3) primers were diluted to 20μM stocks in nuclease-free water, whereas the FAM tagged probe (4926P 5- /56-FAM/ ACT TCG GCA ATG GAA AGG ATG AGC A/3BHQ_1/ -3) was diluted to a 5μM stock, also in nuclease-free water. A master mix of reagents was made using 0.5μL of the 40X TaqMan RT enzyme, 10uL 2X RT-PCR mix, 0.9μL 4840F stock primer, 0.9μL 2981R stock primer, 1uL 4840F stock probe, and 1.7μL nuclease-free water per sample (TaqMan RNA-to Ct 1-Step kit, Applied Biosystems). This was vortexed to mix and stored on ice.

To set up the PCR, 10μL of viral RNA, standard, or nuclease-free water (as a non-template control) was added to each well in every other column of a 96-well Real Time PCR plate (Applied Biosystems). To this, 30μL of the above master mix was added, and a multichannel pipet was used to mix. After thorough mixing, 20μL from each well was transferred to the adjacent well and the plate was sealed with optical tape (Applied Biosystems). After the plate was centrifuged at 125 *X g* for 1 minute, it was loaded into the QuantStudio 6 Flex Real Time PCR System (Applied Biosystems), which was run using a 15 minute RT step at 48°C, followed by a 10 minute hot start at 95°C, and lastly 40 cycles consisting of a 15 second denaturation at 95°C and 1 minute annealing and elongation step at 60°C. Following the run, the copy number calculated using the RNA standard was converted to RNA copy number per mL.

Illumina NGS for TC-83 *in vitro* passaging: Transmission cycle

VIRAL RNA EXTRACTION

Viral RNA was extracted using the Zymo Direct-zol RNA mini kit as per the manufacturer's protocol. 100ng of RNA was used for each ClickSeq library.

CLICKSEQ LIBRARY PREPARATION

ClickSeq was used instead of the traditional Illumina library procedures to avoid the errant recombination that frequently occurs during the typical fragmentation and ligation steps. Instead of RNA fragmentation, SSIII RT-PCR (Invitrogen) is performed using random hexamers attached to an Illumina p7 adapter sequence. In addition to this, azido-NTPs, which cause chain-termination, are added to the NTPs at a 1:35 ratio. In a manner similar to Sanger sequencing, this results in cDNA strands of various sizes. Following this, a modified 5'-hexynyl Illumina sequencing adapter was click-ligated onto the N-terminus of the cDNA strands using a copper-catalyzed azide-alkyne cycloaddition. The cDNA was then purified using a Zymo DNA clean column and

amplified using 18 cycles of OneTaq (NEB) PCR, resulting in the removal of the triazole group linking the cDNA fragment to the 3' Illumina sequencing adapter. Following another Zymo DNA clean column purification, the samples were visualized on an agarose gel. cDNA libraries between 400-700bp were excised and purified using the Zymo Research Gel Recovery kit. Sequencing was performed by the UTMB sequencing core using an Illumina NextSeq 550.

Sequence assembly and analysis

Illumina ClickSeq sequencing analysis was performed by the Fofanov lab at UTMB.

QUALITY AND FILTRATION

The quality for each sample/dataset was assessed using FASTQC (351). The paired-end reads were merged for each sample and then filtered to exclude reads with unknown characters (anything other than A, T, C, G) and low quality (<15 quality score), so that only high quality reads were used during analysis. Additionally, the first 16 bases of each read were trimmed due to nucleotide bias.

REFERENCE SEQUENCE

The analysis was performed using VEEV strain TC-83, complete genome (GenBank accession #: L01443.1) (308).

VIRUS DIVERSITY ANALYSIS

To analyze the variant hotspots, each sample was run through a novel rare variant pipeline (available upon request). The pipeline first maps each read to the reference VEEV genome with perfect match, then unmapped reads are re-mapped with 1 mismatch and added to the final map. The 34 base long reads used in the analyses were validated as viral sequences and not host sequences by analysis of the longest subsequences shared

explicitly (no mismatches allowed) and longest similar (1 mismatch allowed) between viral and host genomes. Positions in which the number of reads mapped with mismatches was higher than perfectly mapped reads or coverage was below 100 were excluded from diversity calculations. Mutation frequency per sample was calculated by summing the per position diversities and normalizing by the number of positions for which diversity was calculated. Shannon Entropy was calculated using the equation $-[\Sigma^{s}_{i=}\, p\log(p)]/N$, where p equals the probability of mutation and N equals the number of base calls that can happen at a position (i.e. A, G, C, T, insertion, or deletion).

Those sequences that did not align using Bowtie were processed using ViReMa, a recombination mapper, to determine the incidence of recombination. These reads were normalized to the average number of reads aligning to the virus genome.

Statistics

GraphPad Prism was used to perform all statistical tests, which are described in the text.

RESULTS

Titers during passaging

During passaging in C7/10 and U4.4 mosquito cells, TC-83 3x virus titer was almost always lower than the parent virus (Figure 6.1 A&B), as was also observed during Chapter 3. Virus titers in the serially passaged vertebrate cell lines were stable, with little difference between TC-83 3x and TC-83 (Figure 6.1 C&D). The alternating passages (Figure 6.1 E&F) were a mixture of these two observations, with TC-83 3x titers dropping slightly during the mosquito cell passages (passages 2, 4, and 6) and rebounding during vertebrate cell passages (passages 1, 3, and 5). Except for the U4.4 TC-83 and TC-83 3x passages, no other passage series showed a consistently significant change in titer by PFU or RNA quantity from the first passage as measured by Kruskal-Wallis.

163

Of interest, the specific infectivity results suggest that TC-83 3x acted more like a low-fidelity mutant in the cell lines without an intact immune response (Figure 6.2 B, D, F), with a higher amount of RNA produced than infectious virus. This seemed to stabilize over the course of passaging, with higher passage numbers of TC-83 3x consistently producing lower specific infectivity values than TC-83. No consistent differences in specific infectivity were observed when TC-83 and TC-83 3x were passaged in the intact immunity cell lines (Figure 6.2 A, C, E).

During passaging, some of the passage series began to produce smaller plaques (Figures 6.3-6.5). When these plaques were measured, one of the TC-83 3x C6/36 passage replicates as well as a TC-83 U4.4 replicate (with the other replicate trending) produced significantly smaller plaques compared to the first passage (Figure 6.5). Because this only occurred in the mosquito cell passages, this suggested that these virus passages were possibly losing fitness in vertebrate cells, as these are what were used for plaque assays.

Genetic Stability

To understand the genetic changes that occurred during passaging, passages 1 and 6 from every passaging condition were prepped using ClickSeq and sequenced using an Illumina NextSeq. Due to low coverage, the first U4.4 passages were not analyzed further.

No SNPs occurred during any of the passage series. For all passage series, changes in mutation frequency (Figure 6.5) and Shannon entropy (Figure 6.6) were small, with no overt pattern of changes in diversity based upon RdRp fidelity or cell type. This was also observed for the number of high frequency variants (Figure 6.7).

The TC-83 3x RdRp mutations were very stable, ranging from a mutation frequency of 0.000048-0.0024 in the final passage (data not shown). Unlike the *in vivo* results in Chapter 4, TC-83 3x produced a small proportion of revertants at the E2

attenuating position, while TC-83 did not produce any. The low amount of TC-83 revertants may have been due to lower coverage at that position, with TC-83 retaining an average coverage of 4639±2200, while the average TC-83 3x coverage was 7450±2626. Additionally, although coverage was low at the 3'UTR attenuating mutation (equal to 183±140), neither TC-83 nor TC-83 3x reverted at this position (data not shown).

DISCUSSION

As in other microevolution studies designed to examine the trade-off hypothesis (192-202), the results for these passaging conditions were largely inconclusive, at least after only 6 passages. As changes in fitness were not directly measured (e.g. a competition assay), it is unknown if changes in fitness occurred. However, some of the TC-83 and TC-83 3x mosquito passages began to produce significantly smaller plaques over the course of passaging, which has previously been observed for mosquito cell adapted SINV (398) and EEEV (193). It would be interesting to compete and compare these small plaque passage series against passage series that did not result in significantly smaller plaque sizes to validate the presumed fitness changes.

Similar to other studies that have examined arbovirus microevolution (194, 197, 200), no consensus sequence changes occurred during any of the passage series. However, this does not necessarily mean that no fitness gains occurred, as changes in the minority virus population have been implicated in increased virus fitness (204, 397). Additionally, the changes in virus diversity over the course of passaging were fairly small. In contrast to the specific infectivity results, which suggested stabilization of the low-fidelity phenotype in the immune incompetent cell passages, there was no apparent difference in the virus diversity produced by TC-83 versus TC-83 3x. Perhaps this is due to the ClickSeq library protocol (65), which uses the relatively low-fidelity Taq polymerase (399) to generate its Illumina sequencing libraries. This may ablate the small changes in diversity typically seen for the TC-83 3x mutant. In the future, we need to

directly compare the differences in diversity generated during ClickSeq library preparation versus the standard protocol to ensure that ClickSeq is not obscuring changes in virus fidelity.
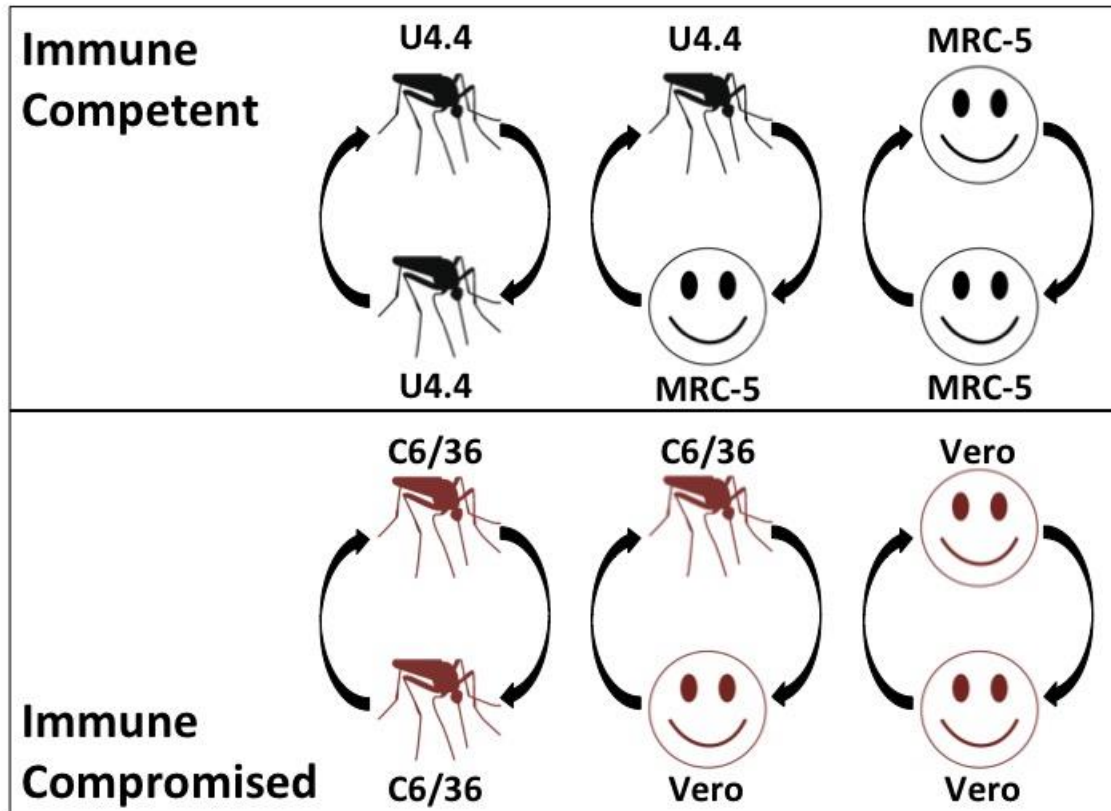
Illustration 6.1.   In vitro transmission cycle.

To determine differences caused by mosquito and vertebrate cell lines, TC-83 and TC-83 3x were passaged 6 times in duplicate using an MOI of 0.1. Additionally, cell lines with different antiviral immune properties were used to determine how these factors affect the two viruses. U4.4 mosquito cells have an active siRNA response, while C6/36 cells do not. On the other hand, MRC-5 cells can produce and respond to IFN, while Vero cells are not able to produce IFN. During alternating transmission cycles, the passages began using the vertebrate cell lines (i.e. Vero and MRC-5).
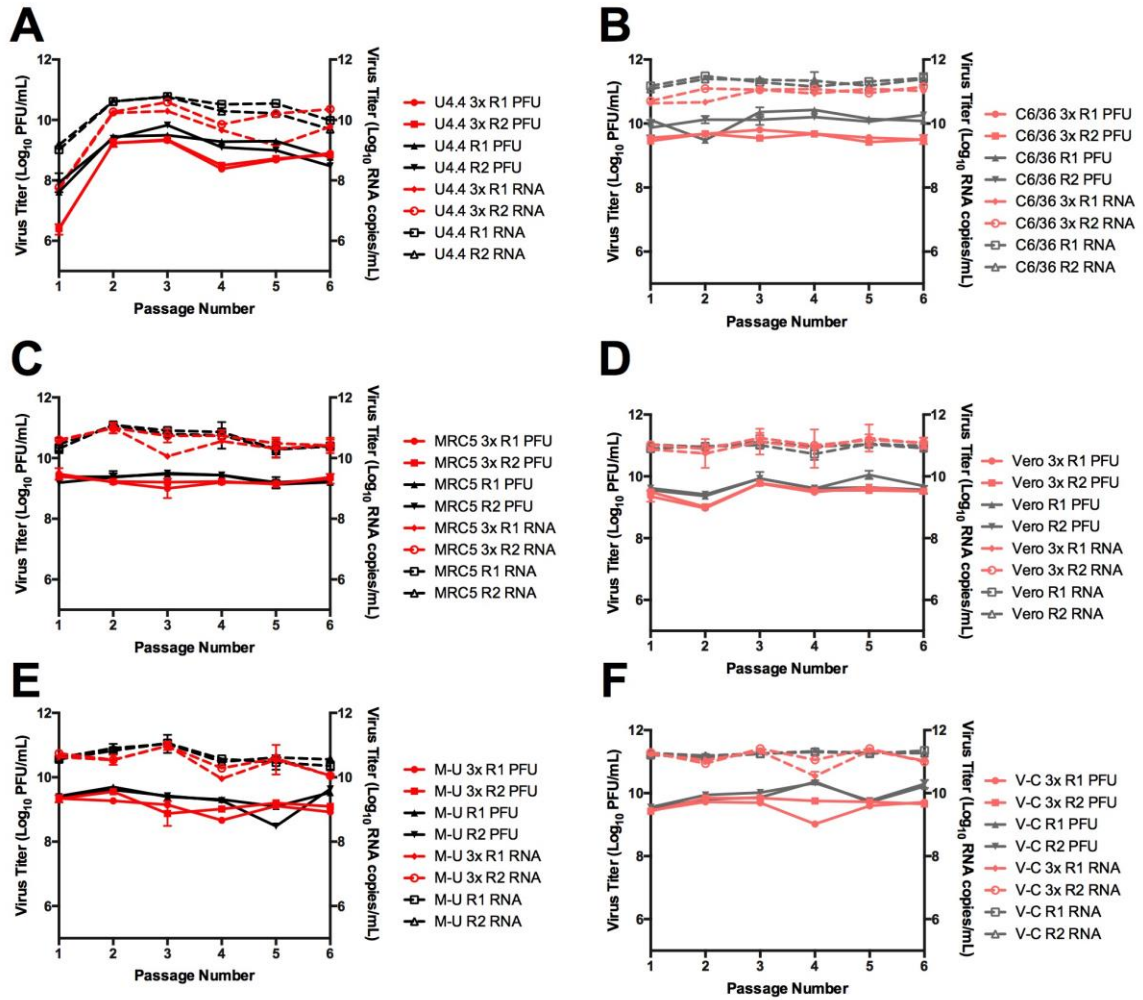
Figure 6.1:   Virus titer during passaging.

Changes in plaque assay (left y-axis) and RNA copy number (right y-axis) during passaging in U4.4 (A), C6/36 (B), MRC-5 (C), Vero (D), M-U (E), and V-C (F). M-U denotes alternating passage between MRC-5 and U4.4 cells. V-C denotes alternating passage between Vero and C6/36 cells. 3x denotes TC-83 3x. R1 denotes replicate 1, while R2 denotes replicate 2.
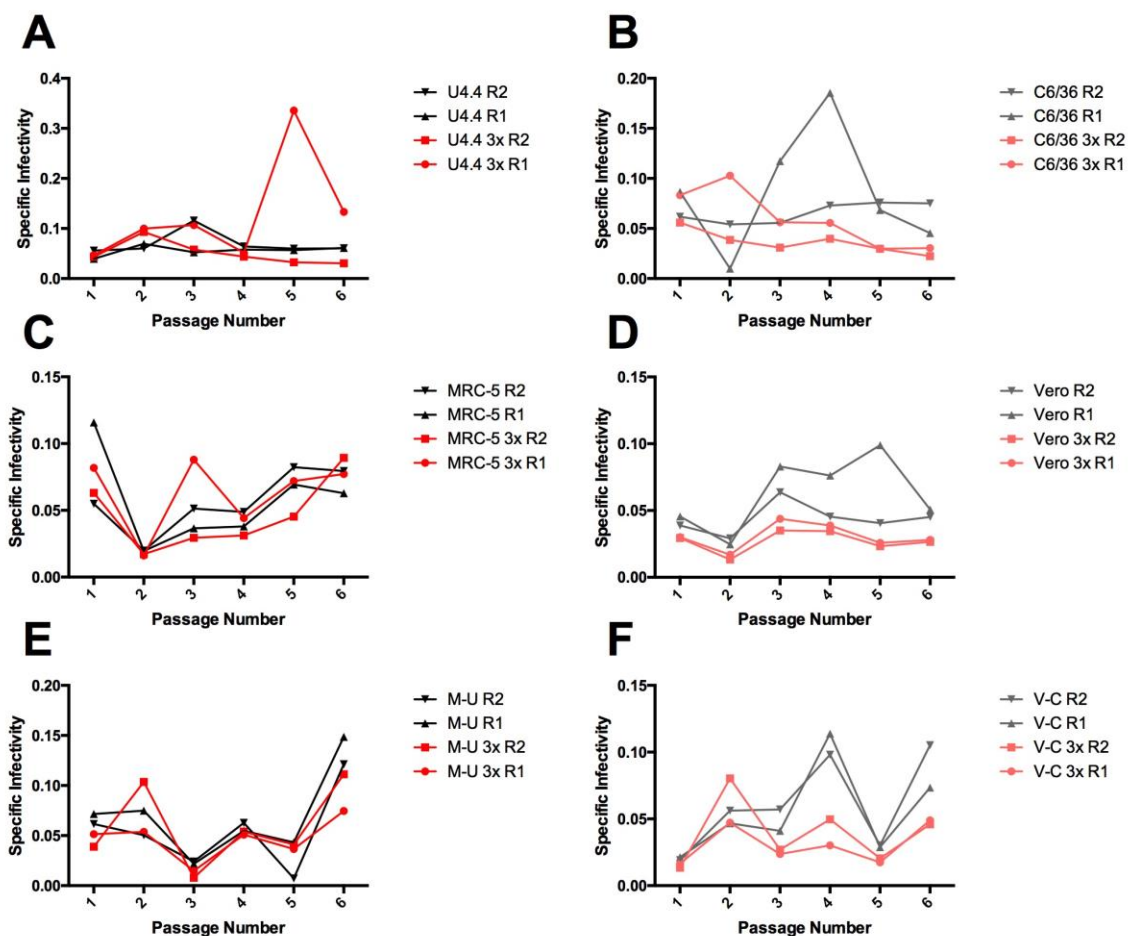
Figure 6.2: Specific infectivity during virus passaging.

Changes in specific infectivity (plaque assay:RNA copy number) during passaging in U4.4 (A), C6/36 (B), MRC-5 (C), Vero (D), M-U (E), and V-C (F). M-U denotes alternating passage between MRC-5 and U4.4 cells. V-C denotes alternating passage between Vero and C6/36 cells. 3x denotes TC-83 3x. R1 denotes replicate 1, while R2 denotes replicate 2.
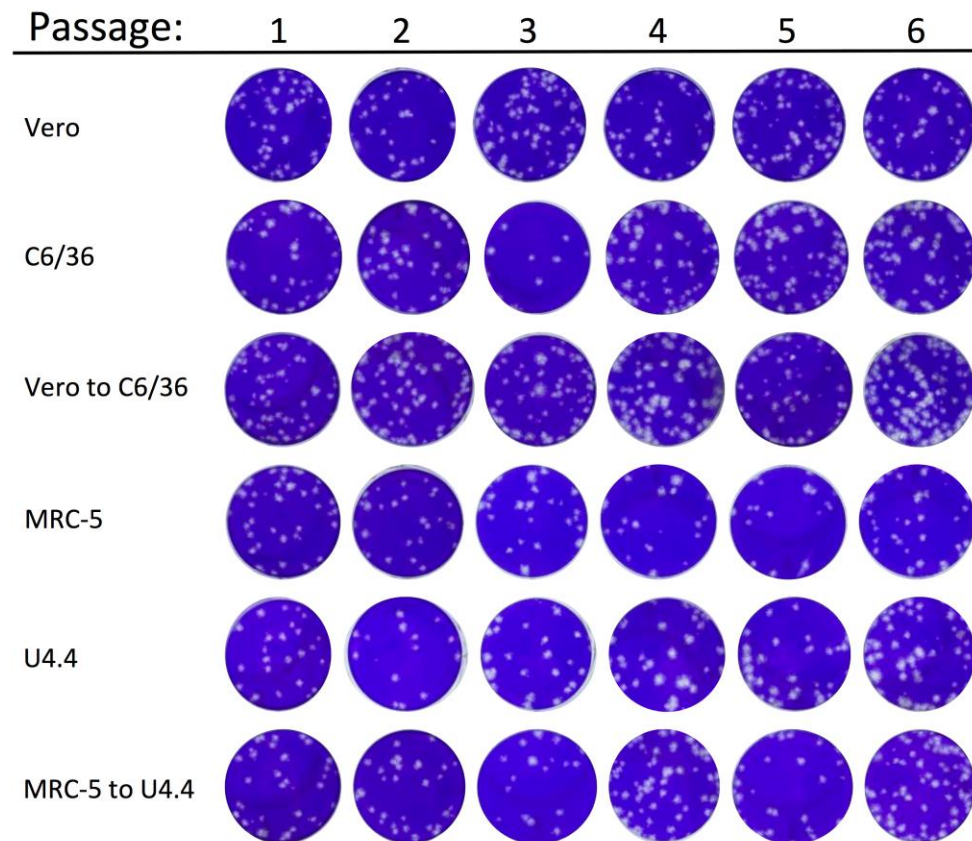
Figure 6.3:   TC-83 3x plaque size during passaging.

Pictures of TC-83 3x replicate 1 plaques for each passage series.
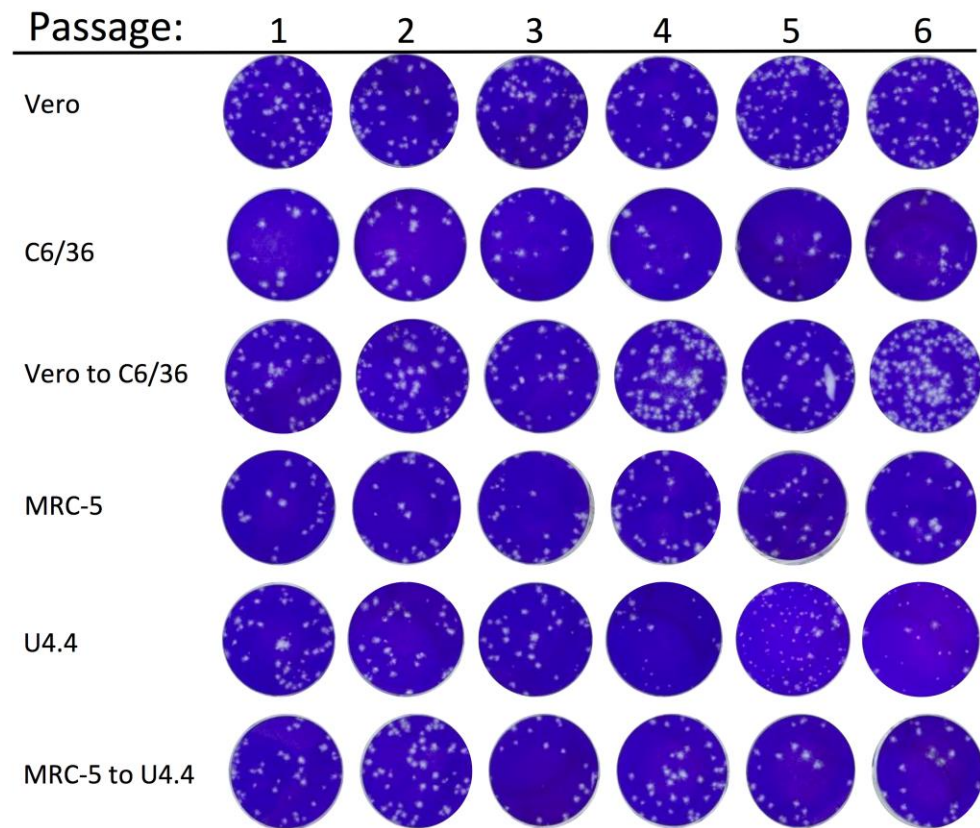
Figure 6.4:   TC-83 plaque size during passaging.

Pictures of TC-83 replicate 1 plaques for each passage series.
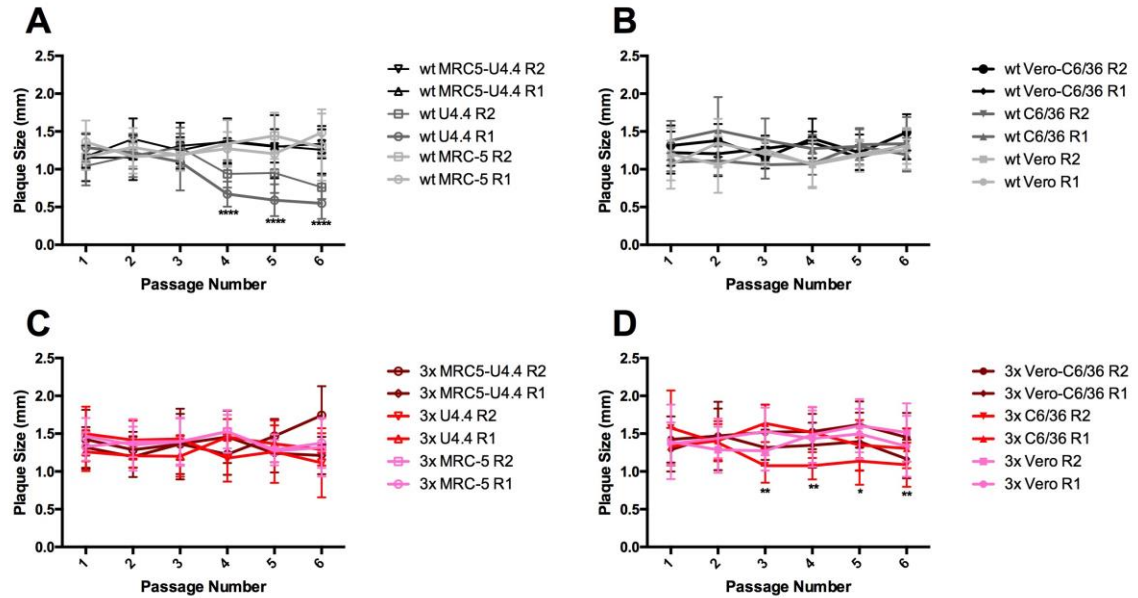
Figure 6.5:   Plaque size during passaging.

Changes in TC-83 (A, B) and TC-83 3x (C, D) plaque size during passaging in immune competent (A, C) and immune compromised (B, D) cell lines. 3x denotes TC-83 3x. R1 denotes replicate 1, while R2 denotes replicate 2.
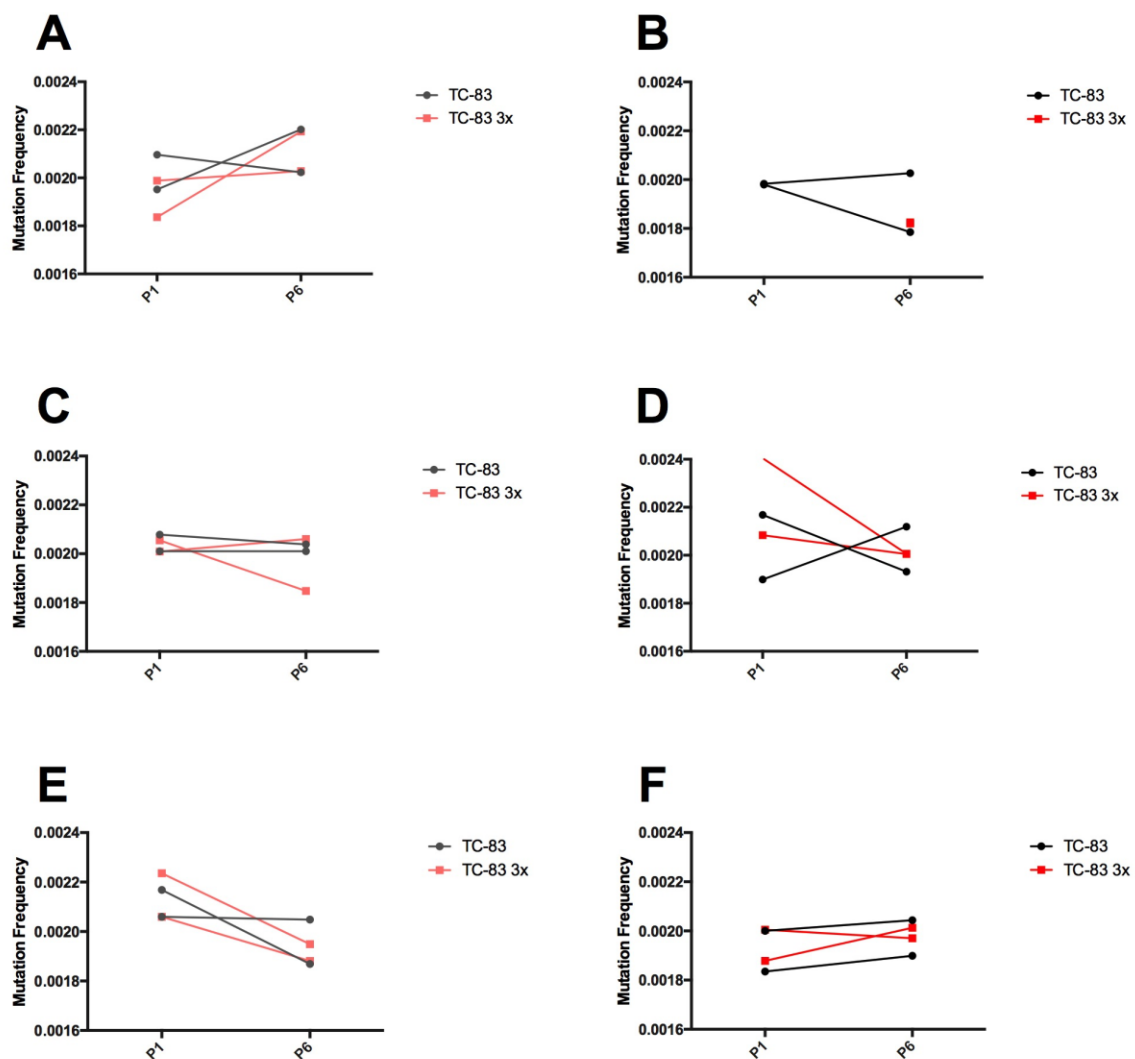
Figure 6.6:   Mutation frequency during passaging.

Changes in mutation frequency during passaging in C6/36 (A), U4.4 (B), Vero (C), MRC-5 (D), V-C (E), and M-U (F). M-U denotes alternating passage between MRC-5 and U4.4 cells. V-C denotes alternating passage between Vero and C6/36 cells. 3x denotes TC-83 3x. P1 denotes passage 1, while P6 denotes passage 6. U4.4 p1 was not included due to low coverage.
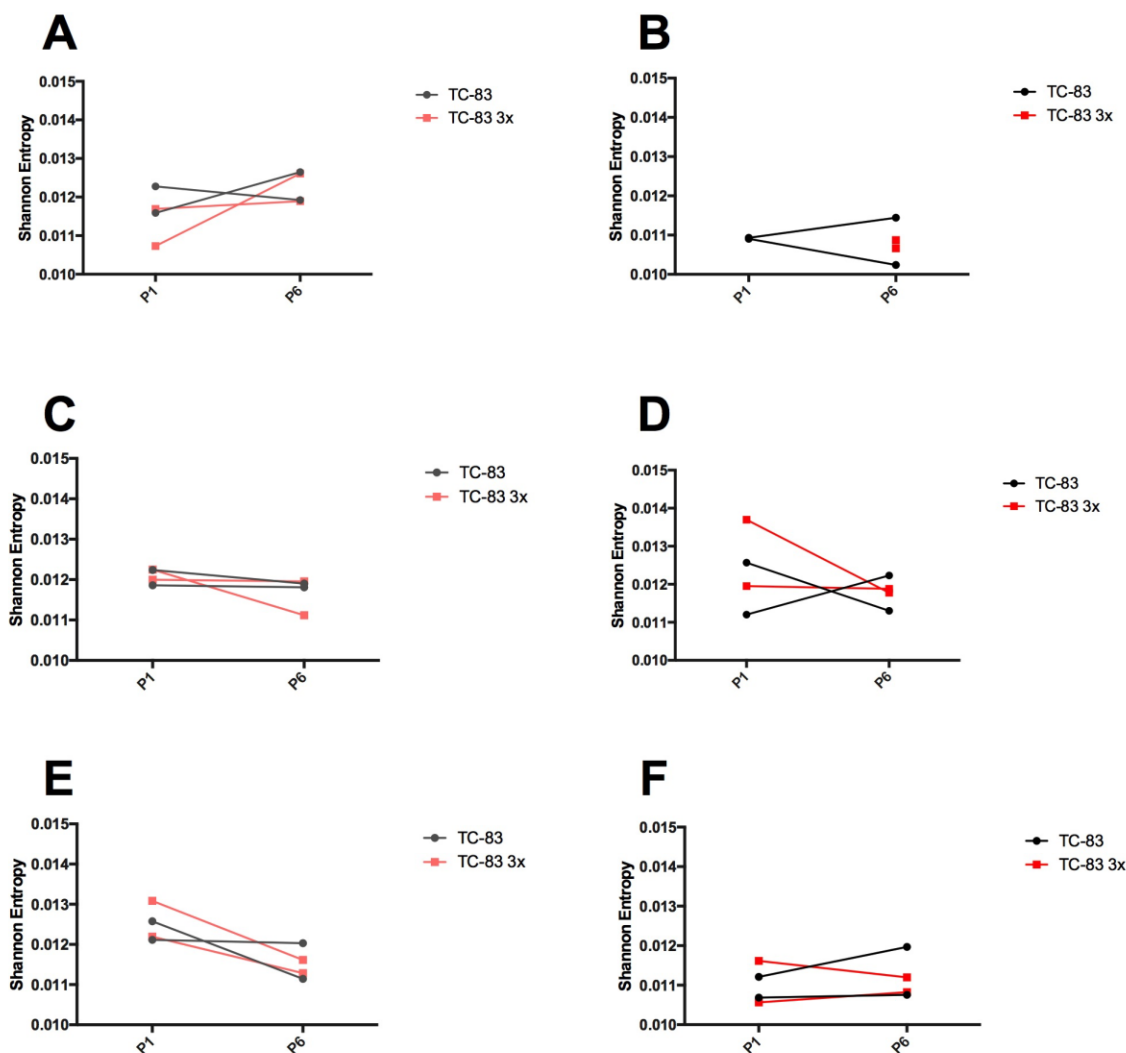
Figure 6.7:   Shannon entropy during passaging.

Changes in Shannon entropy during passaging in C6/36 (A), U4.4 (B), Vero (C), MRC-5 (D), V-C (E), and M-U (F). M-U denotes alternating passage between MRC-5 and U4.4 cells. V-C denotes alternating passage between Vero and C6/36 cells. 3x denotes TC-83 3x. P1 denotes passage 1, while P6 denotes passage 6. U4.4 p1 was not included due to low coverage.
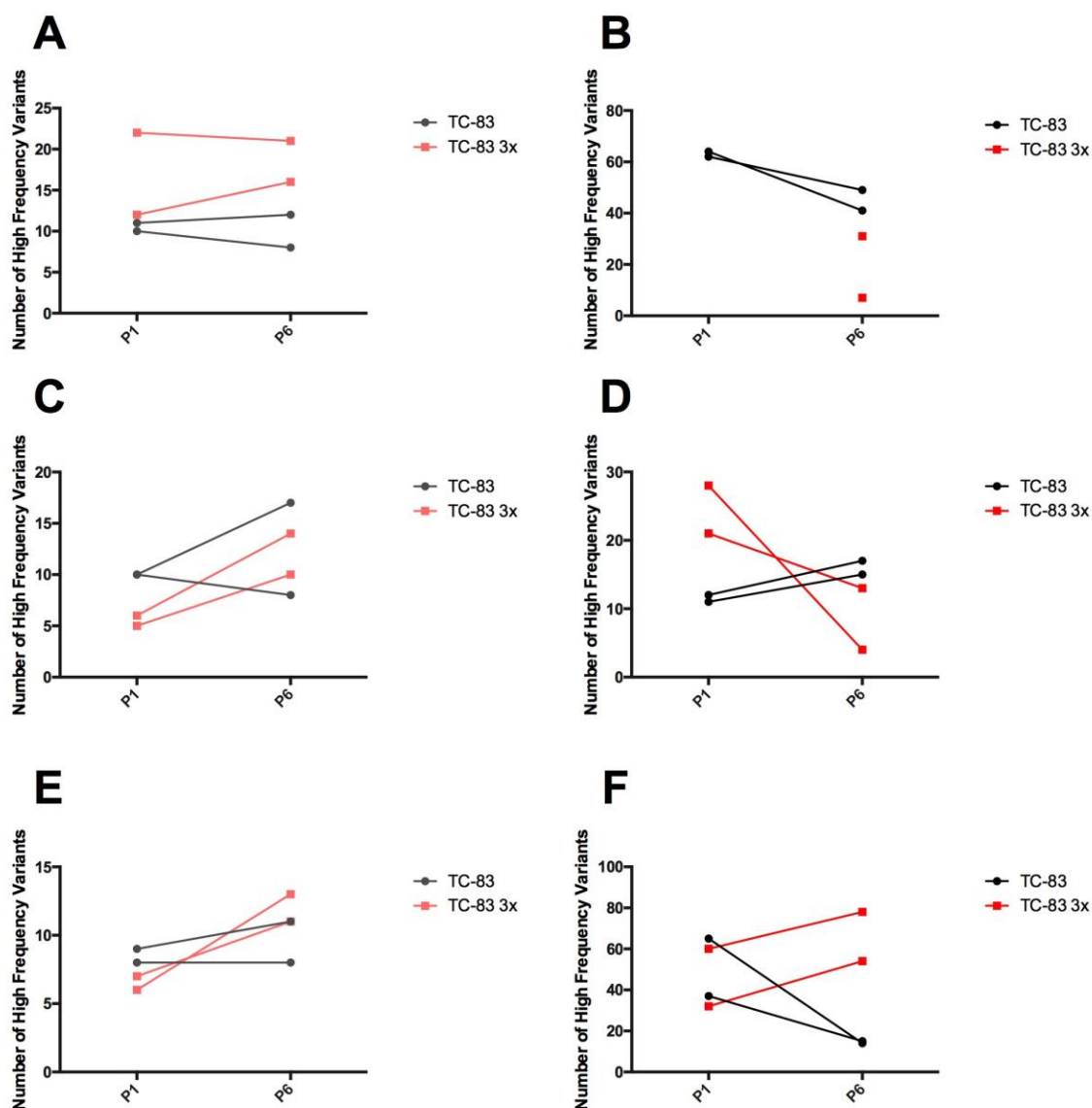
Figure 6.8: High frequency variants during passaging.

Changes in the number of high frequency variants (>0.2) during passaging in C6/36 (A), U4.4 (B), Vero (C), MRC-5 (D), V-C (E), and M-U (F). M-U denotes alternating passage between MRC-5 and U4.4 cells. V-C denotes alternating passage between Vero and C6/36 cells. 3x denotes TC-83 3x. P1 denotes passage 1, while P6 denotes passage 6. U4.4 p1 was not included due to low coverage.
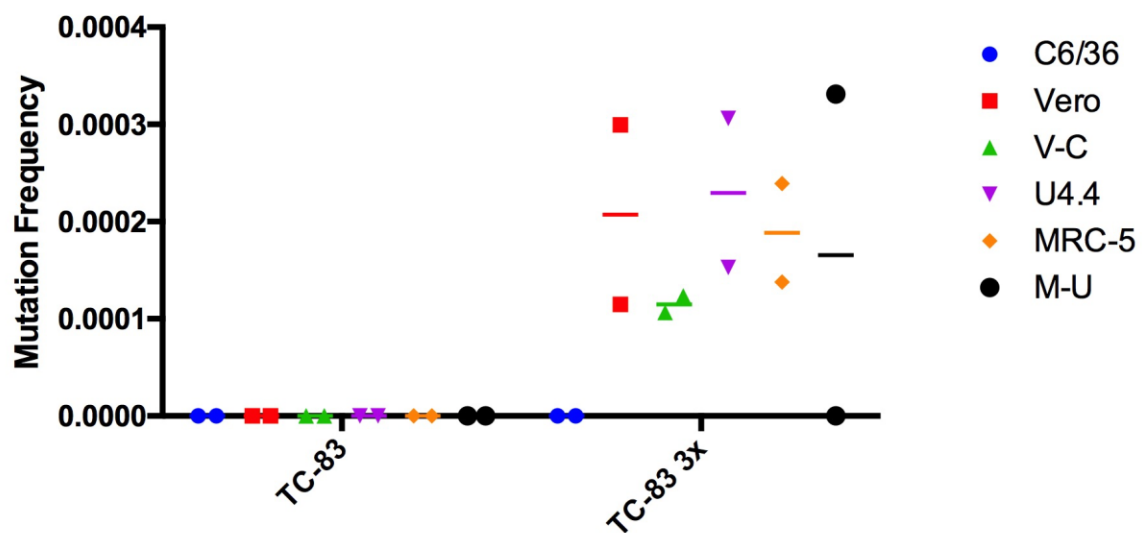
Figure 6.9:   E2 attenuation reversion.

Reversion of the E2 G8922C mutation that is responsible for TC-83 attenuation.

As different stocks of viruses used for this dissertation demonstrated different phenotypes in chapter 2-4, it was evident that the results for each experiment needed to be considered in terms of the specific virus stock used. Unfortunately, there is no deep sequencing data for most of these stocks, because each vial of stock virus was discarded after use in an experiment and none were saved from these earlier stocks. This appendix contains the known information for each virus stock used in the experiments described in earlier chapters. The methods for this chapter were included in chapters 2-4.

RESULTS AND DISCUSSION

Virus Stocks

While titer varied post-electroporation as measured by plaque assay, there were no significant differences between electroporation titer and the studied phenotypes (Table 7.1). Future stock will incorporate NGS analysis and various phenotypic tests (e.g. attenuation in an infant mouse model) to tease apart differences in virus stock attenuation.

Number	Virus	Hour Post-Electroporation	Stock Titer (PFU/mL)	Infant Mouse Attenuation	Mosquito Cell Attenuation
1	TC-83	36	1.95×10^9	No	No
2	TC-83 3X	36	5.75×10^9	Yes	Yes
3	TC-83 4X	36	3.53×10^6	Yes	n/a
4	TC-83	36	1.43×10^{10}	n/a	No
5	TC-83	36	8.25×10^9	n/a	Yes
6	TC-83	48	2.1×10^8	n/a	n/a
7	TC-83	48	1.15×10^9	n/a	n/a
8	TC-83	72	2.7×10^8	No	n/a
9	TC-83 3X	24	4.15×10^9	No	No
10	TC-83 3X	48	4.2×10^9	n/a	No
11	TC-83 3X	72	1.7×10^8	n/a	n/a
12	TC-83 4X	48	2.85×10^5	n/a	n/a
13	TC-83 4X	72	1.15×10^8	No	n/a
14	TC-83	48	1.95×10^9	No	n/a
15	TC-83 3X	48	1.75×10^9	No	n/a
16	TC-83 4X	48	2.2×10^9	No	n/a

Table 7.1:   Virus stocks used in this dissertation.

The virus stocks used in this dissertation are listed above. Infant mouse attenuation refers to attenuation in a SC infant mouse model compared to TC-83. Mosquito cell attenuation refers to the lack of infection when mosquito cells were infected at a low MOI.

References

1.   Anthony SJ, Epstein JH, Murray KA, Navarrete-Macias I, Zambrana-Torrelio CM, Solovyov A, et al. A strategy to estimate unknown viral diversity in mammals. MBio. 2013 Sep 3;4(5):e00598-13.
2.   Li CX, Shi M, Tian JH, Lin XD, Kang YJ, Chen LJ, et al. Unprecedented genomic diversity of RNA viruses in arthropods reveals the ancestry of negative-sense RNA viruses. Elife. 2015 Jan 29;4.
3.   Shi M, Lin XD, Tian JH, Chen LJ, Chen X, Li CX, et al. Redefining the invertebrate RNA virosphere. Nature. 2016 Nov 23.
4.   Zhang YZ, Shi M, Holmes EC. Using Metagenomics to Characterize an Expanding Virosphere. Cell. 2018 Mar 8;172(6):1168-72.
5.   Gago S, Elena SF, Flores R, Sanjuan R. Extremely high mutation rate of a hammerhead viroid. Science. 2009 Mar 6;323(5919):1308.
6.   Drake JW, Holland JJ. Mutation rates among RNA viruses. Proceedings of the National Academy of Sciences of the United States of America. 1999 Nov 23;96(24):13910-3.
7.   Sanjuan R, Nebot MR, Chirico N, Mansky LM, Belshaw R. Viral mutation rates. Journal of virology. 2010 Oct;84(19):9733-48.
8.   Jenkins GM, Rambaut A, Pybus OG, Holmes EC. Rates of molecular evolution in RNA viruses: a quantitative phylogenetic analysis. J Mol Evol. 2002 Feb;54(2):156-65.
9.   Drake JW. The distribution of rates of spontaneous mutation over viruses, prokaryotes, and eukaryotes. Ann N Y Acad Sci. 1999 May 18;870:100-7.
10.   Kumar S, Subramanian S. Mutation rates in mammalian genomes. Proceedings of the National Academy of Sciences of the United States of America. 2002 Jan 22;99(2):803-8.
11.   Bruenn JA. A structural and primary sequence comparison of the viral RNA-dependent RNA polymerases. Nucleic acids research. 2003 Apr 1;31(7):1821-9.
12.   Gong P, Peersen OB. Structural basis for active site closure by the poliovirus RNA-dependent RNA polymerase. Proceedings of the National Academy of Sciences of the United States of America. 2010 Dec 28;107(52):22505-10.
13.   Choi KH, Rossmann MG. RNA-dependent RNA polymerases from Flaviviridae. Curr Opin Struct Biol. 2009 Dec;19(6):746-51.
14.   Butcher SJ, Grimes JM, Makeyev EV, Bamford DH, Stuart DI. A mechanism for initiating RNA-dependent RNA polymerization. Nature. 2001 Mar 8;410(6825):235-40.
15.   Moustafa IM, Shen H, Morton B, Colina CM, Cameron CE. Molecular dynamics simulations of viral RNA polymerases link conserved and correlated motions of functional elements to fidelity. J Mol Biol. 2011 Jul 1;410(1):159-81.
16.   Shu B, Gong P. Structural basis of viral RNA-dependent RNA polymerase catalysis and translocation. Proceedings of the National Academy of Sciences of the United States of America. 2016 Jul 12;113(28):E4005-14.

17.   Yang X, Smidansky ED, Maksimchuk KR, Lum D, Welch JL, Arnold JJ, et al. Motif D of viral RNA-dependent RNA polymerases determines efficiency and fidelity of nucleotide addition. Structure. 2012 Sep 5;20(9):1519-27.
18.   Liu X, Yang X, Lee CA, Moustafa IM, Smidansky ED, Lum D, et al. Vaccine-derived mutation in motif D of poliovirus RNA-dependent RNA polymerase lowers nucleotide incorporation fidelity. The Journal of biological chemistry. 2013 Nov 8;288(45):32753-65.
19.   Eigen M. Selforganization of matter and the evolution of biological macromolecules. Naturwissenschaften. 1971 Oct;58(10):465-523.
20.   Lauring AS, Andino R. Quasispecies theory and the behavior of RNA viruses. PLoS pathogens. 2010;6(7):e1001005.
21.   Holland J, Spindler K, Horodyski F, Grabau E, Nichol S, VandePol S. Rapid evolution of RNA genomes. Science. 1982 Mar 26;215(4540):1577-85.
22.   Eigen M. Error catastrophe and antiviral strategy. Proceedings of the National Academy of Sciences of the United States of America. 2002 Oct 15;99(21):13374-6.
23.   Orr HA. Fitness and its role in evolutionary genetics. Nat Rev Genet. 2009 Aug;10(8):531-9.
24.   Shan C, Xie X, Muruato AE, Rossi SL, Roundy CM, Azar SR, et al. An Infectious cDNA Clone of Zika Virus to Study Viral Virulence, Mosquito Transmission, and Antiviral Inhibitors. Cell host & microbe. 2016 Jun 8;19(6):891-900.
25.   Stapleford KA, Coffey LL, Lay S, Borderia AV, Duong V, Isakov O, et al. Emergence and transmission of arbovirus evolutionary intermediates with epidemic potential. Cell host & microbe. 2014 Jun 11;15(6):706-16.
26.   Stern A, Yeh MT, Zinger T, Smith M, Wright C, Ling G, et al. The Evolutionary Pathway to Virulence of an RNA Virus. Cell. 2017 Mar 23;169(1):35-46 e19.
27.   Tsetsarkin KA, Chen R, Yun R, Rossi SL, Plante KS, Guerbois M, et al. Multi-peaked adaptive landscape for chikungunya virus evolution predicts continued fitness optimization in Aedes albopictus mosquitoes. Nature communications. 2014;5:4084.
28.   Tsetsarkin KA, Chen R, Leal G, Forrester N, Higgs S, Huang J, et al. Chikungunya virus emergence is constrained in Asia by lineage-specific adaptive landscapes. Proceedings of the National Academy of Sciences of the United States of America. 2011 May 10;108(19):7872-7.
29.   Hinkley T, Martins J, Chappey C, Haddad M, Stawiski E, Whitcomb JM, et al. A systems analysis of mutational effects in HIV-1 protease and reverse transcriptase. Nat Genet. 2011 May;43(5):487-9.
30.   Biebricher CK, Eigen M. The error threshold. Virus Res. 2005 Feb;107(2):117-27.
31.   Wilke CO, Wang JL, Ofria C, Lenski RE, Adami C. Evolution of digital organisms at high mutation rates leads to survival of the flattest. Nature. 2001 Jul 19;412(6844):331-3.
32.   Bergstrom CT, McElhany P, Real LA. Transmission bottlenecks as determinants of virulence in rapidly evolving pathogens. Proceedings of the National Academy of Sciences of the United States of America. 1999 Apr 27;96(9):5095-100.
33.   Crotty S, Maag D, Arnold JJ, Zhong W, Lau JY, Hong Z, et al. The broad-spectrum antiviral ribonucleoside ribavirin is an RNA virus mutagen. Nat Med. 2000 Dec;6(12):1375-9.

34.   Grande-Perez A, Lazaro E, Lowenstein P, Domingo E, Manrubia SC. Suppression of viral infectivity through lethal defection. Proceedings of the National Academy of Sciences of the United States of America. 2005 Mar 22;102(12):4448-52.
35.   Crotty S, Cameron CE, Andino R. RNA virus error catastrophe: direct molecular test by using ribavirin. Proceedings of the National Academy of Sciences of the United States of America. 2001 Jun 5;98(12):6895-900.
36.   Lee CH, Gilbertson DL, Novella IS, Huerta R, Domingo E, Holland JJ. Negative effects of chemical mutagenesis on the adaptive behavior of vesicular stomatitis virus. Journal of virology. 1997 May;71(5):3636-40.
37.   Moratorio G, Henningsson R, Barbezange C, Carrau L, Borderia AV, Blanc H, et al. Attenuation of RNA viruses by redirecting their evolution in sequence space. Nat Microbiol. 2017 Jun 5;2:17088.
38.   Vignuzzi M, Stone JK, Andino R. Ribavirin and lethal mutagenesis of poliovirus: molecular mechanisms, resistance and biological implications. Virus Res. 2005 Feb;107(2):173-81.
39.   Wray SK, Gilbert BE, Noall MW, Knight V. Mode of action of ribavirin: effect of nucleotide pool alterations on influenza virus ribonucleoprotein synthesis. Antiviral research. 1985 Feb;5(1):29-37.
40.   Wray SK, Gilbert BE, Knight V. Effect of ribavirin triphosphate on primer generation and elongation during influenza virus transcription in vitro. Antiviral research. 1985 Feb;5(1):39-48.
41.   Zhou S, Liu R, Baroudy BM, Malcolm BA, Reyes GR. The effect of ribavirin and IMPDH inhibitors on hepatitis C virus subgenomic replicon RNA. Virology. 2003 Jun 5;310(2):333-42.
42.   Robins RK, Revankar GR, McKernan PA, Murray BK, Kirsi JJ, North JA. The importance of IMP dehydrogenase inhibition in the broad spectrum antiviral activity of ribavirin and selenazofurin. Adv Enzyme Regul. 1985;24:29-43.
43.   Bougie I, Bisaillon M. The broad spectrum antiviral nucleoside ribavirin as a substrate for a viral RNA capping enzyme. The Journal of biological chemistry. 2004 May 21;279(21):22124-30.
44.   Fang SH, Hwang LH, Chen DS, Chiang BL. Ribavirin enhancement of hepatitis C virus core antigen-specific type 1 T helper cell response correlates with the increased IL-12 level. J Hepatol. 2000 Nov;33(5):791-8.
45.   Longley DB, Harkin DP, Johnston PG. 5-fluorouracil: mechanisms of action and clinical strategies. Nat Rev Cancer. 2003 May;3(5):330-8.
46.   Gnadig NF, Beaucourt S, Campagnola G, Borderia AV, Sanz-Ramos M, Gong P, et al. Coxsackievirus B3 mutator strains are attenuated in vivo. Proceedings of the National Academy of Sciences of the United States of America. 2012 Aug 21;109(34):E2294-303.
47.   Duarte EA, Clarke DK, Moya A, Elena SF, Domingo E, Holland J. Many-trillionfold amplification of single RNA virus particles fails to overcome the Muller's ratchet effect. Journal of virology. 1993 Jun;67(6):3620-3.
48.   Manrubia SC, Escarmis C, Domingo E, Lazaro E. High mutation rates, bottlenecks, and robustness of RNA viral quasispecies. Gene. 2005 Mar 14;347(2):273-82.

49.	Duarte E, Clarke D, Moya A, Domingo E, Holland J. Rapid fitness losses in mammalian RNA virus clones due to Muller's ratchet. Proceedings of the National Academy of Sciences of the United States of America. 1992 Jul 1;89(13):6015-9.

50.	Escarmis C, Lazaro E, Arias A, Domingo E. Repeated bottleneck transfers can lead to non-cytocidal forms of a cytopathic virus: implications for viral extinction. J Mol Biol. 2008 Feb 15;376(2):367-79.

51.	Chao L. Fitness of RNA virus decreased by Muller's ratchet. Nature. 1990 Nov 29;348(6300):454-5.

52.	Lazaro E, Escarmis C, Perez-Mercader J, Manrubia SC, Domingo E. Resistance of virus to extinction on bottleneck passages: study of a decaying and fluctuating pattern of fitness loss. Proceedings of the National Academy of Sciences of the United States of America. 2003 Sep 16;100(19):10830-5.

53.	Ruiz-Jarabo CM, Arias A, Baranowski E, Escarmis C, Domingo E. Memory in viral quasispecies. Journal of virology. 2000 Apr;74(8):3543-7.

54.	Wilke CO, Novella IS. Phenotypic mixing and hiding may contribute to memory in viral quasispecies. BMC Microbiol. 2003 Jun 9;3:11.

55.	Salter JD, Bennett RP, Smith HC. The APOBEC Protein Family: United by Structure, Divergent in Function. Trends Biochem Sci. 2016 Jul;41(7):578-94.

56.	Sheehy AM, Gaddis NC, Choi JD, Malim MH. Isolation of a human gene that inhibits HIV-1 infection and is suppressed by the viral Vif protein. Nature. 2002 Aug 8;418(6898):646-50.

57.	Simon-Loriere E, Holmes EC. Why do RNA viruses recombine? Nat Rev Microbiol. 2011 Jul 4;9(8):617-26.

58.	Simmonds P. Recombination and selection in the evolution of picornaviruses and other Mammalian positive-stranded RNA viruses. Journal of virology. 2006 Nov;80(22):11124-40.

59.	Taucher C, Berger A, Mandl CW. A trans-complementing recombination trap demonstrates a low propensity of flaviviruses for intermolecular recombination. Journal of virology. 2010 Jan;84(1):599-611.

60.	Huang AS, Baltimore D. Defective viral particles and viral disease processes. Nature. 1970 Apr 25;226(5243):325-7.

61.	Roux L, Simon AE, Holland JJ. Effects of defective interfering viruses on virus replication and pathogenesis in vitro and in vivo. Adv Virus Res. 1991;40:181-211.

62.	Li D, Lott WB, Lowry K, Jones A, Thu HM, Aaskov J. Defective interfering viral particles in acute dengue infections. PloS one. 2011 Apr 29;6(4):e19447.

63.	Xiao Y, Rouzine IM, Bianco S, Acevedo A, Goldstein EF, Farkov M, et al. RNA Recombination Enhances Adaptability and Is Required for Virus Spread and Virulence. Cell host & microbe. 2016 Apr 13;19(4):493-503.

64.	Poirier EZ, Mounce BC, Rozen-Gagnon K, Hooikaas PJ, Stapleford KA, Moratorio G, et al. Low-Fidelity Polymerases of Alphaviruses Recombine at Higher Rates To Overproduce Defective Interfering Particles. Journal of virology. 2015 Dec 16;90(5):2446-54.

65.	Routh A, Head SR, Ordoukhanian P, Johnson JE. ClickSeq: Fragmentation-Free Next-Generation Sequencing via Click Ligation of Adaptors to Stochastically Terminated 3'-Azido cDNAs. J Mol Biol. 2015 Aug 14;427(16):2610-6.

66.   Pfeiffer JK, Kirkegaard K. A single mutation in poliovirus RNA-dependent RNA polymerase confers resistance to mutagenic nucleotide analogs via increased fidelity. Proceedings of the National Academy of Sciences of the United States of America. 2003 Jun 10;100(12):7289-94.

67.   Pfeiffer JK, Kirkegaard K. Increased fidelity reduces poliovirus fitness and virulence under selective pressure in mice. PLoS pathogens. 2005 Oct;1(2):e11.

68.   Vignuzzi M, Stone JK, Arnold JJ, Cameron CE, Andino R. Quasispecies diversity determines pathogenesis through cooperative interactions in a viral population. Nature. 2006 Jan 19;439(7074):344-8.

69.   Vignuzzi M, Wendt E, Andino R. Engineering attenuated virus vaccines by controlling replication fidelity. Nat Med. 2008 Feb;14(2):154-61.

70.   Levi LI, Gnadig NF, Beaucourt S, McPherson MJ, Baron B, Arnold JJ, et al. Fidelity variants of RNA dependent RNA polymerases uncover an indirect, mutagenic activity of amiloride compounds. PLoS pathogens. 2010;6(10):e1001163.

71.   McDonald S, Block A, Beaucourt S, Moratorio G, Vignuzzi M, Peersen OB. Design of a Genetically Stable High Fidelity Coxsackievirus B3 Polymerase That Attenuates Virus Growth in Vivo. The Journal of biological chemistry. 2016 Jul 1;291(27):13999-4011.

72.   Sadeghipour S, Bek EJ, McMinn PC. Ribavirin-resistant mutants of human enterovirus 71 express a high replication fidelity phenotype during growth in cell culture. Journal of virology. 2013 Feb;87(3):1759-69.

73.   Meng T, Kwang J. Attenuation of human enterovirus 71 high-replication-fidelity variants in AG129 mice. Journal of virology. 2014 May;88(10):5803-15.

74.   Arias A, Arnold JJ, Sierra M, Smidansky ED, Domingo E, Cameron CE. Determinants of RNA-dependent RNA polymerase (in)fidelity revealed by kinetic analysis of the polymerase encoded by a foot-and-mouth disease virus mutant with reduced sensitivity to ribavirin. Journal of virology. 2008 Dec;82(24):12346-55.

75.   Zeng J, Wang H, Xie X, Yang D, Zhou G, Yu L. An increased replication fidelity mutant of foot-and-mouth disease virus retains fitness in vitro and virulence in vivo. Antiviral research. 2013 Oct;100(1):1-7.

76.   Xie X, Wang H, Zeng J, Li C, Zhou G, Yang D, et al. Foot-and-mouth disease virus low-fidelity polymerase mutants are attenuated. Arch Virol. 2014 Oct;159(10):2641-50.

77.   Rai DK, Diaz-San Segundo F, Campagnola G, Keith A, Schafer EA, Kloc A, et al. Attenuation of Foot-and-Mouth Disease Virus by Engineered Viral Polymerase Fidelity. Journal of virology. 2017 Aug 1;91(15).

78.   Zeng J, Wang H, Xie X, Li C, Zhou G, Yang D, et al. Ribavirin-resistant variants of foot-and-mouth disease virus: the effect of restricted quasispecies diversity on viral virulence. Journal of virology. 2014 Apr;88(8):4008-20.

79.   Korboukh VK, Lee CA, Acevedo A, Vignuzzi M, Xiao Y, Arnold JJ, et al. RNA virus population diversity, an optimum for maximal fitness and virulence. The Journal of biological chemistry. 2014 Oct 24;289(43):29531-44.

80.   Coffey LL, Beeharry Y, Borderia AV, Blanc H, Vignuzzi M. Arbovirus high fidelity variant loses fitness in mosquitoes and mice. Proceedings of the National Academy of Sciences of the United States of America. 2011 Sep 20;108(38):16038-43.

81.   Stapleford KA, Rozen-Gagnon K, Das PK, Saul S, Poirier EZ, Blanc H, et al. Viral Polymerase-Helicase Complexes Regulate Replication Fidelity To Overcome Intracellular Nucleotide Depletion. Journal of virology. 2015 Nov;89(22):11233-44.

82.   Rozen-Gagnon K, Stapleford KA, Mongelli V, Blanc H, Failloux AB, Saleh MC, et al. Alphavirus mutator variants present host-specific defects and attenuation in mammalian and insect models. PLoS pathogens. 2014 Jan;10(1):e1003877.

83.   Van Slyke GA, Arnold JJ, Lugo AJ, Griesemer SB, Moustafa IM, Kramer LD, et al. Sequence-Specific Fidelity Alterations Associated with West Nile Virus Attenuation in Mosquitoes. PLoS pathogens. 2015 Jun;11(6):e1005009.

84.   Griesemer SB, Kramer LD, Van Slyke GA, Pata JD, Gohara DW, Cameron CE, et al. Mutagen resistance and mutation restriction of St. Louis encephalitis virus. The Journal of general virology. 2017 Feb;98(2):201-11.

85.   Tian D, Meng XJ. Amino acid residues Ala283 and His421 in the RNA-dependent RNA polymerase of porcine reproductive and respiratory syndrome virus play important roles in viral ribavirin sensitivity and quasispecies diversity. The Journal of general virology. 2016 Jan;97(1):53-9.

86.   Arias A, Thorne L, Ghurburrun E, Bailey D, Goodfellow I. Norovirus Polymerase Fidelity Contributes to Viral Transmission In Vivo. mSphere. 2016 Sep-Oct;1(5).

87.   Cheung PP, Watson SJ, Choy KT, Fun Sia S, Wong DD, Poon LL, et al. Generation and characterization of influenza A viruses with altered polymerase fidelity. Nature communications. 2014 Sep 3;5:4794.

88.   Pauly MD, Lyons DM, Fitzsimmons WJ, Lauring AS. Epistatic Interactions within the Influenza A Virus Polymerase Complex Mediate Mutagen Resistance and Replication Fidelity. mSphere. 2017 Jul-Aug;2(4).

89.   Eckerle LD, Lu X, Sperry SM, Choi L, Denison MR. High fidelity of murine hepatitis virus replication is decreased in nsp14 exoribonuclease mutants. Journal of virology. 2007 Nov;81(22):12135-44.

90.   Graepel KW, Lu X, Case JB, Sexton NR, Smith EC, Denison MR. Proofreading-Deficient Coronaviruses Adapt for Increased Fitness over Long-Term Passage without Reversion of Exoribonuclease-Inactivating Mutations. MBio. 2017 Nov 7;8(6).

91.   Xiao Y, Dolan PT, Goldstein EF, Li M, Farkov M, Brodsky L, et al. Poliovirus intrahost evolution is required to overcome tissue-specific innate immune responses. Nature communications. 2017 Aug 29;8(1):375.

92.   Gorbalenya AE, Enjuanes L, Ziebuhr J, Snijder EJ. Nidovirales: evolving the largest RNA virus genome. Virus Res. 2006 Apr;117(1):17-37.

93.   Eckerle LD, Becker MM, Halpin RA, Li K, Venter E, Lu X, et al. Infidelity of SARS-CoV Nsp14-exonuclease mutant virus replication is revealed by complete genome sequencing. PLoS pathogens. 2010 May 6;6(5):e1000896.

94.   Cameron CE, Moustafa IM, Arnold JJ. Fidelity of Nucleotide Incorporation by the RNA-Dependent RNA Polymerase from Poliovirus. Enzymes. 2016;39:293-323.

95.   Yang X, Liu X, Musser DM, Moustafa IM, Arnold JJ, Cameron CE, et al. Triphosphate Reorientation of the Incoming Nucleotide as a Fidelity Checkpoint in Viral RNA-dependent RNA Polymerases. The Journal of biological chemistry. 2017 Mar 3;292(9):3810-26.

96.   Gohara DW, Arnold JJ, Cameron CE. Poliovirus RNA-dependent RNA polymerase (3Dpol): kinetic, thermodynamic, and structural analysis of ribonucleotide selection. Biochemistry. 2004 May 11;43(18):5149-58.
97.   Arnold JJ, Vignuzzi M, Stone JK, Andino R, Cameron CE. Remote site control of an active site fidelity checkpoint in a viral RNA-dependent RNA polymerase. The Journal of biological chemistry. 2005 Jul 8;280(27):25706-16.
98.   Moustafa IM, Korboukh VK, Arnold JJ, Smidansky ED, Marcotte LL, Gohara DW, et al. Structural dynamics as a contributor to error-prone replication by an RNA-dependent RNA polymerase. The Journal of biological chemistry. 2014 Dec 26;289(52):36229-48.
99.   Graham RL, Becker MM, Eckerle LD, Bolles M, Denison MR, Baric RS. A live, impaired-fidelity coronavirus vaccine protects in an aged, immunocompromised mouse model of lethal disease. Nat Med. 2012 Dec;18(12):1820-6.
100.   Theiler M, Smith HH. The Effect of Prolonged Cultivation in Vitro Upon the Pathogenicity of Yellow Fever Virus. J Exp Med. 1937 May 31;65(6):767-86.
101.   Pugachev KV, Guirakhoo F, Ocran SW, Mitchell F, Parsons M, Penal C, et al. High fidelity of yellow fever virus RNA polymerase. Journal of virology. 2004 Jan;78(2):1032-8.
102.   Beck A, Tesh RB, Wood TG, Widen SG, Ryman KD, Barrett AD. Comparison of the live attenuated yellow fever vaccine 17D-204 strain to its virulent parental strain Asibi by deep sequencing. The Journal of infectious diseases. 2014 Feb 1;209(3):334-44.
103.   Seligman SJ, Gould EA. Live flavivirus vaccines: reasons for caution. Lancet. 2004 Jun 19;363(9426):2073-5.
104.   Lindsey NP, Rabe IB, Miller ER, Fischer M, Staples JE. Adverse event reports following yellow fever vaccination, 2007-13. J Travel Med. 2016 May;23(5).
105.   Mayer SV, Tesh RB, Vasilakis N. The emergence of arthropod-borne viral diseases: A global prospective on dengue, chikungunya and zika fevers. Acta Trop. 2017 Feb;166:155-63.
106.   Tulman ER, Delhon GA, Ku BK, Rock DL. African swine fever virus. Curr Top Microbiol Immunol. 2009;328:43-87.
107.   Powers AM, Brault AC, Shirako Y, Strauss EG, Kang W, Strauss JH, et al. Evolutionary relationships and systematics of the alphaviruses. Journal of virology. 2001 Nov;75(21):10118-31.
108.   Forrester NL, Palacios G, Tesh RB, Savji N, Guzman H, Sherman M, et al. Genome-scale phylogeny of the alphavirus genus suggests a marine origin. Journal of virology. 2012 Mar;86(5):2729-38.
109.   Strauss JH, Strauss EG. The alphaviruses: gene expression, replication, and evolution. Microbiol Rev. 1994 Sep;58(3):491-562.
110.   Fuller SD, Berriman JA, Butcher SJ, Gowen BE. Low pH induces swiveling of the glycoprotein heterodimers in the Semliki Forest virus spike complex. Cell. 1995 Jun 2;81(5):715-25.
111.   Cheng RH, Kuhn RJ, Olson NH, Rossmann MG, Choi HK, Smith TJ, et al. Nucleocapsid and glycoprotein organization in an enveloped virus. Cell. 1995 Feb 24;80(4):621-30.

112. Paredes AM, Brown DT, Rothnagel R, Chiu W, Schoepp RJ, Johnston RE, et al. Three-dimensional structure of a membrane-containing virus. Proceedings of the National Academy of Sciences of the United States of America. 1993 Oct 1;90(19):9095-9.

113. Gaedigk-Nitschko K, Schlesinger MJ. The Sindbis virus 6K protein can be detected in virions and is acylated with fatty acids. Virology. 1990 Mar;175(1):274-81.

114. Lusa S, Garoff H, Liljestrom P. Fate of the 6K membrane protein of Semliki Forest virus during virus assembly. Virology. 1991 Dec;185(2):843-6.

115. Li L, Jose J, Xiang Y, Kuhn RJ, Rossmann MG. Structural changes of envelope proteins during alphavirus fusion. Nature. 2010 Dec 2;468(7324):705-8.

116. Klimstra WB, Nangle EM, Smith MS, Yurochko AD, Ryman KD. DC-SIGN and L-SIGN can act as attachment receptors for alphaviruses and distinguish between mosquito cell- and mammalian cell-derived viruses. Journal of virology. 2003 Nov;77(22):12022-32.

117. Mayor S, Pagano RE. Pathways of clathrin-independent endocytosis. Nat Rev Mol Cell Biol. 2007 Aug;8(8):603-12.

118. Bernard KA, Klimstra WB, Johnston RE. Mutations in the E2 glycoprotein of Venezuelan equine encephalitis virus confer heparan sulfate interaction, low morbidity, and rapid clearance from blood of mice. Virology. 2000 Oct 10;276(1):93-103.

119. Heil ML, Albee A, Strauss JH, Kuhn RJ. An amino acid substitution in the coding region of the E2 glycoprotein adapts Ross River virus to utilize heparan sulfate as an attachment moiety. Journal of virology. 2001 Jul;75(14):6303-9.

120. Klimstra WB, Ryman KD, Johnston RE. Adaptation of Sindbis virus to BHK cells selects for use of heparan sulfate as an attachment receptor. Journal of virology. 1998 Sep;72(9):7357-66.

121. Gardner CL, Ebel GD, Ryman KD, Klimstra WB. Heparan sulfate binding by natural eastern equine encephalitis viruses promotes neurovirulence. Proceedings of the National Academy of Sciences of the United States of America. 2011 Sep 20;108(38):16026-31.

122. DeTulleo L, Kirchhausen T. The clathrin endocytic pathway in viral infection. EMBO J. 1998 Aug 17;17(16):4585-93.

123. Doxsey SJ, Brodsky FM, Blank GS, Helenius A. Inhibition of endocytosis by anti-clathrin antibodies. Cell. 1987 Jul 31;50(3):453-63.

124. Kielian M, Helenius A. pH-induced alterations in the fusogenic spike protein of Semliki Forest virus. J Cell Biol. 1985 Dec;101(6):2284-91.

125. Omar A, Koblet H. Semliki Forest virus particles containing only the E1 envelope glycoprotein are infectious and can induce cell-cell fusion. Virology. 1988 Sep;166(1):17-23.

126. Sanz MA, Rejas MT, Carrasco L. Individual expression of sindbis virus glycoproteins. E1 alone promotes cell fusion. Virology. 2003 Jan 20;305(2):463-72.

127. Kolokoltsov AA, Fleming EH, Davey RA. Venezuelan equine encephalitis virus entry mechanism requires late endosome formation and resists cell membrane cholesterol depletion. Virology. 2006 Apr 10;347(2):333-42.

128. Lu YE, Cassese T, Kielian M. The cholesterol requirement for sindbis virus entry and exit and characterization of a spike protein region involved in cholesterol dependence. Journal of virology. 1999 May;73(5):4272-8.

129.	Tsetsarkin KA, Vanlandingham DL, McGee CE, Higgs S. A single mutation in chikungunya virus affects vector specificity and epidemic potential. PLoS pathogens. 2007 Dec;3(12):e201.

130.	Volk SM, Chen R, Tsetsarkin KA, Adams AP, Garcia TI, Sall AA, et al. Genome-scale phylogenetic analyses of chikungunya virus reveal independent emergences of recent epidemics and various evolutionary rates. Journal of virology. 2010 Jul;84(13):6497-504.

131.	Coffey LL, Forrester N, Tsetsarkin K, Vasilakis N, Weaver SC. Factors shaping the adaptive landscape for arboviruses: implications for the emergence of disease. Future Microbiol. 2013 Feb;8(2):155-76.

132.	Rubach JK, Wasik BR, Rupp JC, Kuhn RJ, Hardy RW, Smith JL. Characterization of purified Sindbis virus nsP4 RNA-dependent RNA polymerase activity in vitro. Virology. 2009 Feb 5;384(1):201-8.

133.	Hardy RW, Rice CM. Requirements at the 3' end of the sindbis virus genome for efficient synthesis of minus-strand RNA. Journal of virology. 2005 Apr;79(8):4630-9.

134.	Thal MA, Wasik BR, Posto J, Hardy RW. Template requirements for recognition and copying by Sindbis virus RNA-dependent RNA polymerase. Virology. 2007 Feb 5;358(1):221-32.

135.	Ahola T, Kaariainen L. Reaction in alphavirus mRNA capping: formation of a covalent complex of nonstructural protein nsP1 with 7-methyl-GMP. Proceedings of the National Academy of Sciences of the United States of America. 1995 Jan 17;92(2):507-11.

136.	Spuul P, Salonen A, Merits A, Jokitalo E, Kaariainen L, Ahola T. Role of the amphipathic peptide of Semliki forest virus replicase protein nsP1 in membrane association and virus replication. Journal of virology. 2007 Jan;81(2):872-83.

137.	Hardy WR, Strauss JH. Processing the nonstructural polyproteins of sindbis virus: nonstructural proteinase is in the C-terminal half of nsP2 and functions both in cis and in trans. Journal of virology. 1989 Nov;63(11):4653-64.

138.	Das PK, Merits A, Lulla A. Functional cross-talk between distant domains of chikungunya virus non-structural protein 2 is decisive for its RNA-modulating activity. The Journal of biological chemistry. 2014 Feb 28;289(9):5635-53.

139.	Li C, Debing Y, Jankevicius G, Neyts J, Ahel I, Coutard B, et al. Viral Macro Domains Reverse Protein ADP-Ribosylation. Journal of virology. 2016 Oct 1;90(19):8478-86.

140.	Cristea IM, Rozjabek H, Molloy KR, Karki S, White LL, Rice CM, et al. Host factors associated with the Sindbis virus RNA-dependent RNA polymerase: role for G3BP1 and G3BP2 in virus replication. Journal of virology. 2010 Jul;84(13):6720-32.

141.	Frolova E, Gorchakov R, Garmashova N, Atasheva S, Vergara LA, Frolov I. Formation of nsP3-specific protein complexes during Sindbis virus replication. Journal of virology. 2006 Apr;80(8):4122-34.

142.	Kim DY, Reynaud JM, Rasalouskaya A, Akhrymuk I, Mobley JA, Frolov I, et al. New World and Old World Alphaviruses Have Evolved to Exploit Different Components of Stress Granules, FXR and G3BP Proteins, for Assembly of Viral Replication Complexes. PLoS pathogens. 2016 Aug;12(8):e1005810.

143.   de Groot RJ, Rumenapf T, Kuhn RJ, Strauss EG, Strauss JH. Sindbis virus RNA polymerase is degraded by the N-end rule pathway. Proceedings of the National Academy of Sciences of the United States of America. 1991 Oct 15;88(20):8967-71.
144.   O'Reilly EK, Kao CC. Analysis of RNA-dependent RNA polymerase structure and function as guided by known polymerase structures and computer predictions of secondary structure. Virology. 1998 Dec 20;252(2):287-303.
145.   Pietila MK, Hellstrom K, Ahola T. Alphavirus polymerase and RNA replication. Virus Res. 2017 Apr 15;234:44-57.
146.   Rupp JC, Jundt N, Hardy RW. Requirement for the amino-terminal domain of sindbis virus nsP4 during virus infection. Journal of virology. 2011 Apr;85(7):3449-60.
147.   Tomar S, Hardy RW, Smith JL, Kuhn RJ. Catalytic core of alphavirus nonstructural protein nsP4 possesses terminal adenylyltransferase activity. Journal of virology. 2006 Oct;80(20):9962-9.
148.   Li ML, Lin YH, Simmonds HA, Stollar V. A mutant of Sindbis virus which is able to replicate in cells with reduced CTP makes a replicase/transcriptase with a decreased Km for CTP. Journal of virology. 2004 Sep;78(18):9645-51.
149.   Lin YH, Yadav P, Ravatn R, Stollar V. A mutant of Sindbis virus that is resistant to pyrazofurin encodes an altered RNA polymerase. Virology. 2000 Jun 20;272(1):61-71.
150.   Barton DJ, Sawicki SG, Sawicki DL. Solubilization and immunoprecipitation of alphavirus replication complexes. Journal of virology. 1991 Mar;65(3):1496-506.
151.   Li G, Rice CM. The signal for translational readthrough of a UGA codon in Sindbis virus RNA involves a single cytidine residue immediately downstream of the termination codon. Journal of virology. 1993 Aug;67(8):5062-7.
152.   Vasiljeva L, Merits A, Golubtsov A, Sizemskaja V, Kaariainen L, Ahola T. Regulation of the sequential processing of Semliki Forest virus replicase polyprotein. The Journal of biological chemistry. 2003 Oct 24;278(43):41636-45.
153.   Sawicki DL, Sawicki SG. Short-lived minus-strand polymerase for Semliki Forest virus. Journal of virology. 1980 Apr;34(1):108-18.
154.   Lemm JA, Rumenapf T, Strauss EG, Strauss JH, Rice CM. Polypeptide requirements for assembly of functional Sindbis virus replication complexes: a model for the temporal regulation of minus- and plus-strand RNA synthesis. EMBO J. 1994 Jun 15;13(12):2925-34.
155.   Frolova EI, Gorchakov R, Pereboeva L, Atasheva S, Frolov I. Functional Sindbis virus replicative complexes are formed at the plasma membrane. Journal of virology. 2010 Nov;84(22):11679-95.
156.   Froshauer S, Kartenbeck J, Helenius A. Alphavirus RNA replicase is located on the cytoplasmic surface of endosomes and lysosomes. J Cell Biol. 1988 Dec;107(6 Pt 1):2075-86.
157.   Melancon P, Garoff H. Processing of the Semliki Forest virus structural polyprotein: role of the capsid protease. Journal of virology. 1987 May;61(5):1301-9.
158.   Garoff H, Simons K, Dobberstein B. Assembly of the Semliki Forest virus membrane glycoproteins in the membrane of the endoplasmic reticulum in vitro. J Mol Biol. 1978 Oct 5;124(4):587-600.
159.   Bonatti S, Migliaccio G, Blobel G, Walter P. Role of signal recognition particle in the membrane assembly of Sindbis viral glycoproteins. Eur J Biochem. 1984 May 2;140(3):499-502.

160.   Liljestrom P, Garoff H. Internally located cleavable signal sequences direct the formation of Semliki Forest virus membrane proteins from a polyprotein precursor. Journal of virology. 1991 Jan;65(1):147-54.

161.   Marquardt T, Helenius A. Misfolding and aggregation of newly synthesized proteins in the endoplasmic reticulum. J Cell Biol. 1992 May;117(3):505-13.

162.   Mulvey M, Brown DT. Formation and rearrangement of disulfide bonds during maturation of the Sindbis virus E1 glycoprotein. Journal of virology. 1994 Feb;68(2):805-12.

163.   Knight RL, Schultz KL, Kent RJ, Venkatesan M, Griffin DE. Role of N-linked glycosylation for sindbis virus infection and replication in vertebrate and invertebrate systems. Journal of virology. 2009 Jun;83(11):5640-7.

164.   Zhang W, Mukhopadhyay S, Pletnev SV, Baker TS, Kuhn RJ, Rossmann MG. Placement of the structural proteins in Sindbis virus. Journal of virology. 2002 Nov;76(22):11645-58.

165.   Mulvey M, Brown DT. Assembly of the Sindbis virus spike protein complex. Virology. 1996 May 1;219(1):125-32.

166.   Sjoberg M, Lindqvist B, Garoff H. Activation of the alphavirus spike protein is suppressed by bound E3. Journal of virology. 2011 Jun;85(11):5644-50.

167.   Zhang X, Fugere M, Day R, Kielian M. Furin processing and proteolytic activation of Semliki Forest virus. Journal of virology. 2003 Mar;77(5):2981-9.

168.   de Curtis I, Simons K. Dissection of Semliki Forest virus glycoprotein delivery from the trans-Golgi network to the cell surface in permeabilized BHK cells. Proceedings of the National Academy of Sciences of the United States of America. 1988 Nov;85(21):8052-6.

169.   Barth BU, Suomalainen M, Liljestrom P, Garoff H. Alphavirus assembly and entry: role of the cytoplasmic tail of the E1 spike subunit. Journal of virology. 1992 Dec;66(12):7560-4.

170.   Beck CE, Wyckoff RW. Venezuelan Equine Encephalomyelitis. Science. 1938 Dec 2;88(2292):530.

171.   Kubes V, Rios FA. The Causative Agent of Infectious Equine Encephalomyelitis in Venezuela. Science. 1939 Jul 7;90(2323):20-1.

172.   Quiroz E, Aguilar PV, Cisneros J, Tesh RB, Weaver SC. Venezuelan equine encephalitis in Panama: fatal endemic disease and genetic diversity of etiologic viral strains. PLoS neglected tropical diseases. 2009 Jun 30;3(6):e472.

173.   Weaver SC, Ferro C, Barrera R, Boshell J, Navarro JC. Venezuelan equine encephalitis. Annual review of entomology. 2004;49:141-74.

174.   Johnson KM, Martin DH. Venezuelan equine encephalitis. Advances in veterinary science and comparative medicine. 1974;18(0):79-116.

175.   Paessler S, Weaver SC. Vaccines for Venezuelan equine encephalitis. Vaccine. 2009 Nov 5;27 Suppl 4:D80-5.

176.   Oberste MS, Fraire M, Navarro R, Zepeda C, Zarate ML, Ludwig GV, et al. Association of Venezuelan equine encephalitis virus subtype IE with two equine epizootics in Mexico. The American journal of tropical medicine and hygiene. 1998 Jul;59(1):100-7.

177.   R B Zehmer PBD, W D Sudia, C H Calisher, G E Sather, R L Parker. Venezuelan equine encephalitis epidemic in Texas, 1971. Health Serv Rep. 1974;89(3):5.

178.   Rivas F, Diaz LA, Cardenas VM, Daza E, Bruzon L, Alcala A, et al. Epidemic Venezuelan equine encephalitis in La Guajira, Colombia, 1995. The Journal of infectious diseases. 1997 Apr;175(4):828-32.
179.   Navarro JC, Medina G, Vasquez C, Coffey LL, Wang E, Suarez A, et al. Postepizootic persistence of Venezuelan equine encephalitis virus, Venezuela. Emerging infectious diseases. 2005 Dec;11(12):1907-15.
180.   Aguilar PV, Estrada-Franco JG, Navarro-Lopez R, Ferro C, Haddow AD, Weaver SC. Endemic Venezuelan equine encephalitis in the Americas: hidden under the dengue umbrella. Future Virol. 2011;6(6):721-40.
181.   Young NA, Johnson KM. Antigenic variants of Venezuelan equine encephalitis virus: their geographic distribution and epidemiologic significance. American journal of epidemiology. 1969 Mar;89(3):286-307.
182.   Forrester NL, Wertheim JO, Dugan VG, Auguste AJ, Lin D, Adams AP, et al. Evolution and spread of Venezuelan equine encephalitis complex alphavirus in the Americas. PLoS neglected tropical diseases. 2017 Aug;11(8):e0005693.
183.   Anishchenko M, Bowen RA, Paessler S, Austgen L, Greene IP, Weaver SC. Venezuelan encephalitis emergence mediated by a phylogenetically predicted viral mutation. Proceedings of the National Academy of Sciences of the United States of America. 2006 Mar 28;103(13):4994-9.
184.   Greene IP, Paessler S, Austgen L, Anishchenko M, Brault AC, Bowen RA, et al. Envelope glycoprotein mutations mediate equine amplification and virulence of epizootic venezuelan equine encephalitis virus. Journal of virology. 2005 Jul;79(14):9128-33.
185.   Brault AC, Powers AM, Holmes EC, Woelk CH, Weaver SC. Positively charged amino acid substitutions in the e2 envelope glycoprotein are associated with the emergence of venezuelan equine encephalitis virus. Journal of virology. 2002 Feb;76(4):1718-30.
186.   Brault AC, Powers AM, Weaver SC. Vector infection determinants of Venezuelan equine encephalitis virus reside within the E2 envelope glycoprotein. Journal of virology. 2002 Jun;76(12):6387-92.
187.   Brault AC, Powers AM, Ortiz D, Estrada-Franco JG, Navarro-Lopez R, Weaver SC. Venezuelan equine encephalitis emergence: enhanced vector infection from a single amino acid substitution in the envelope glycoprotein. Proceedings of the National Academy of Sciences of the United States of America. 2004 Aug 3;101(31):11344-9.
188.   Weaver SC, Bellew LA, Rico-Hesse R. Phylogenetic analysis of alphaviruses in the Venezuelan equine encephalitis complex and identification of the source of epizootic viruses. Virology. 1992 Nov;191(1):282-90.
189.   Steele KE, Twenhafel NA. REVIEW PAPER: pathology of animal models of alphavirus encephalitis. Veterinary pathology. 2010 Sep;47(5):790-805.
190.   Wilson DS, Yoshimura J. On the Coexistence of Specialists and Generalists. Am Nat. 1994 Oct;144(4):692-707.
191.   Kassen R. The experimental evolution of specialists, generalists, and the maintenance of diversity. J Evolution Biol. 2002 Mar;15(2):173-90.
192.   Weaver SC, Brault AC, Kang W, Holland JJ. Genetic and fitness changes accompanying adaptation of an arbovirus to vertebrate and invertebrate cells. Journal of virology. 1999 May;73(5):4316-26.

193.   Cooper LA, Scott TW. Differential evolution of eastern equine encephalitis virus populations in response to host cell type. Genetics. 2001 Apr;157(4):1403-12.

194.   Greene IP, Wang E, Deardorff ER, Milleron R, Domingo E, Weaver SC. Effect of alternating passage on adaptation of sindbis virus to vertebrate and invertebrate cells. Journal of virology. 2005 Nov;79(22):14253-60.

195.   Vasilakis N, Deardorff ER, Kenney JL, Rossi SL, Hanley KA, Weaver SC. Mosquitoes put the brake on arbovirus evolution: experimental evolution reveals slower mutation accumulation in mosquito than vertebrate cells. PLoS pathogens. 2009 Jun;5(6):e1000467.

196.   Moutailler S, Roche B, Thiberge JM, Caro V, Rougeon F, Failloux AB. Host alternation is necessary to maintain the genome stability of rift valley fever virus. PLoS neglected tropical diseases. 2011 May;5(5):e1156.

197.   Ciota AT, Lovelace AO, Ngo KA, Le AN, Maffei JG, Franke MA, et al. Cell-specific adaptation of two flaviviruses following serial passage in mosquito cell culture. Virology. 2007 Jan 20;357(2):165-74.

198.   Coffey LL, Vignuzzi M. Host alternation of chikungunya virus increases fitness while restricting population diversity and adaptability to novel selective pressures. Journal of virology. 2011 Jan;85(2):1025-35.

199.   Coffey LL, Vasilakis N, Brault AC, Powers AM, Tripet F, Weaver SC. Arbovirus evolution in vivo is constrained by host alternation. Proceedings of the National Academy of Sciences of the United States of America. 2008 May 13;105(19):6970-5.

200.   Ciota AT, Jia Y, Payne AF, Jerzak G, Davis LJ, Young DS, et al. Experimental passage of St. Louis encephalitis virus in vivo in mosquitoes and chickens reveals evolutionarily significant virus characteristics. PloS one. 2009 Nov 17;4(11):e7876.

201.   Deardorff ER, Fitzpatrick KA, Jerzak GV, Shi PY, Kramer LD, Ebel GD. West Nile virus experimental evolution in vivo and the trade-off hypothesis. PLoS pathogens. 2011 Nov;7(11):e1002335.

202.   Ciota AT, Lovelace AO, Jia Y, Davis LJ, Young DS, Kramer LD. Characterization of mosquito-adapted West Nile virus. The Journal of general virology. 2008 Jul;89(Pt 7):1633-42.

203.   Jerzak GV, Brown I, Shi PY, Kramer LD, Ebel GD. Genetic diversity and purifying selection in West Nile virus populations are maintained during host switching. Virology. 2008 May 10;374(2):256-60.

204.   Patterson EI, Khanipov K, Rojas MM, Kautz TF, Rockx-Brouwer D, Golovko G, et al. Mosquito bottlenecks alter viral mutant swarm in a tissue and time-dependent manner with contraction and expansion of variant positions and diversity. Virus Evol. 2018 Jan;4(1):vey001.

205.   Hahn CS, Lustig S, Strauss EG, Strauss JH. Western equine encephalitis virus is a recombinant virus. Proceedings of the National Academy of Sciences of the United States of America. 1988 Aug;85(16):5997-6001.

206.   Weaver SC, Kang W, Shirako Y, Rumenapf T, Strauss EG, Strauss JH. Recombinational history and molecular evolution of western equine encephalomyelitis complex alphaviruses. Journal of virology. 1997 Jan;71(1):613-23.

207.   Weiss BG, Schlesinger S. Recombination between Sindbis virus RNAs. Journal of virology. 1991 Aug;65(8):4017-25.

208. Raju R, Subramaniam SV, Hajjou M. Genesis of Sindbis virus by in vivo recombination of nonreplicative RNA precursors. Journal of virology. 1995 Dec;69(12):7391-401.

209. Berglund P, Sjoberg M, Garoff H, Atkins GJ, Sheahan BJ, Liljestrom P. Semliki Forest virus expression system: production of conditionally infectious recombinant particles. Biotechnology (N Y). 1993 Aug;11(8):916-20.

210. Hajjou M, Hill KR, Subramaniam SV, Hu JY, Raju R. Nonhomologous RNA-RNA recombination events at the 3' nontranslated region of the Sindbis virus genome: hot spots and utilization of nonviral sequences. Journal of virology. 1996 Aug;70(8):5153-64.

211. Vasilakis N, Falvey D, Gangolli SS, Coleman J, Kowalski J, Udem SA, et al. Transfection-independent production of alphavirus replicon particles based on poxvirus expression vectors. Nat Biotechnol. 2003 Aug;21(8):932-5.

212. Pushko P, Parker M, Ludwig GV, Davis NL, Johnston RE, Smith JF. Replicon-helper systems from attenuated Venezuelan equine encephalitis virus: expression of heterologous genes in vitro and immunization against heterologous pathogens in vivo. Virology. 1997 Dec 22;239(2):389-401.

213. Kaariainen L, Pettersson RF, Keranen S, Lehtovaara P, Soderlund H, Ukkonen P. Multiple structurally related defective-interfering RNAs formed during undiluted passages of Semliki forest virus. Virology. 1981 Sep;113(2):686-97.

214. Eaton BT. Evidence for the synthesis of defection interfering particles by Aedes albopictus cells persistently infected with Sindbis virus. Virology. 1977 Apr;77(2):843-8.

215. Lehtovaara P, Soderlund H, Keranen S, Pettersson RF, Kaariainen L. 18S defective interfering RNA of Semliki Forest virus contains a triplicated linear repeat. Proceedings of the National Academy of Sciences of the United States of America. 1981 Sep;78(9):5353-7.

216. Monroe SS, Schlesinger S. Common and distinct regions of defective-interfering RNAs of Sindbis virus. Journal of virology. 1984 Mar;49(3):865-72.

217. Forrester NL, Guerbois M, Adams AP, Liang X, Weaver SC. Analysis of intrahost variation in Venezuelan equine encephalitis virus reveals repeated deletions in the 6-kilodalton protein gene. Journal of virology. 2011 Sep;85(17):8709-17.

218. Petterson E, Stormoen M, Evensen O, Mikalsen AB, Haugland O. Natural infection of Atlantic salmon (Salmo salar L.) with salmonid alphavirus 3 generates numerous viral deletion mutants. The Journal of general virology. 2013 Sep;94(Pt 9):1945-54.

219. Petterson E, Guo TC, Evensen O, Mikalsen AB. Experimental piscine alphavirus RNA recombination in vivo yields both viable virus and defective viral RNA. Sci Rep. 2016 Nov 2;6:36317.

220. Coffey LL, Carrara AS, Paessler S, Haynie ML, Bradley RD, Tesh RB, et al. Experimental Everglades virus infection of cotton rats (Sigmodon hispidus). Emerging infectious diseases. 2004 Dec;10(12):2182-8.

221. Carrara AS, Coffey LL, Aguilar PV, Moncayo AC, Da Rosa AP, Nunes MR, et al. Venezuelan equine encephalitis virus infection of cotton rats. Emerging infectious diseases. 2007 Aug;13(8):1158-65.

222. MacDonald GH, Johnston RE. Role of dendritic cell targeting in Venezuelan equine encephalitis virus pathogenesis. Journal of virology. 2000 Jan;74(2):914-22.

223.   Grieder FB, Davis NL, Aronson JF, Charles PC, Sellon DC, Suzuki K, et al. Specific restrictions in the progression of Venezuelan equine encephalitis virus-induced disease resulting from single amino acid changes in the glycoproteins. Virology. 1995 Feb 1;206(2):994-1006.

224.   Davis NL, Grieder FB, Smith JF, Greenwald GF, Valenski ML, Sellon DC, et al. A molecular genetic approach to the study of Venezuelan equine encephalitis virus pathogenesis. Archives of virology Supplementum. 1994;9:99-109.

225.   Grieder FB, Nguyen HT. Virulent and attenuated mutant Venezuelan equine encephalitis virus show marked differences in replication in infection in murine macrophages. Microb Pathog. 1996 Aug;21(2):85-95.

226.   Charles PC, Walters E, Margolis F, Johnston RE. Mechanism of neuroinvasion of Venezuelan equine encephalitis virus in the mouse. Virology. 1995 Apr 20;208(2):662-71.

227.   Vogel P, Abplanalp D, Kell W, Ibrahim MS, Downs MB, Pratt WD, et al. Venezuelan equine encephalitis in BALB/c mice: kinetic analysis of central nervous system infection following aerosol or subcutaneous inoculation. Arch Pathol Lab Med. 1996 Feb;120(2):164-72.

228.   Steele KE, Davis KJ, Stephan K, Kell W, Vogel P, Hart MK. Comparative neurovirulence and tissue tropism of wild-type and attenuated strains of Venezuelan equine encephalitis virus administered by aerosol in C3H/HeN and BALB/c mice. Veterinary pathology. 1998 Sep;35(5):386-97.

229.   Hart MK, Pratt W, Panelo F, Tammariello R, Dertzbaugh M. Venezuelan equine encephalitis virus vaccines induce mucosal IgA responses and protection from airborne infection in BALB/c, but not C3H/HeN mice. Vaccine. 1997 Mar;15(4):363-9.

230.   Hart MK, Caswell-Stephan K, Bakken R, Tammariello R, Pratt W, Davis N, et al. Improved mucosal protection against Venezuelan equine encephalitis virus is induced by the molecularly defined, live-attenuated V3526 vaccine candidate. Vaccine. 2000 Jul 1;18(26):3067-75.

231.   Gleiser CA, Gochenour WS, Jr., Berge TO, Tigertt WD. The comparative pathology of experimental Venezuelan equine encephalomyelitis infection in different animal hosts. The Journal of infectious diseases. 1962 Jan-Feb;110:80-97.

232.   Reed DS, Glass PJ, Bakken RR, Barth JF, Lind CM, da Silva L, et al. Combined alphavirus replicon particle vaccine induces durable and cross-protective immune responses against equine encephalitis viruses. Journal of virology. 2014 Oct;88(20):12077-86.

233.   Danes L, Rychterova V, Kufner J, Hruskova J. The role of the olfactory route on infection of the respiratory tract with Venezuelan equine encephalomyelitis virus in normal and operated Macaca rhesus monkeys. II. Results of histological examination. Acta Virol. 1973 Jan;17(1):57-60.

234.   Reed DS, Lind CM, Sullivan LJ, Pratt WD, Parker MD. Aerosol infection of cynomolgus macaques with enzootic strains of venezuelan equine encephalitis viruses. The Journal of infectious diseases. 2004 Mar 15;189(6):1013-7.

235.   Spotts DR, Reich RM, Kalkhan MA, Kinney RM, Roehrig JT. Resistance to alpha/beta interferons correlates with the epizootic and virulence potential of Venezuelan equine encephalitis viruses and is determined by the 5' noncoding region and glycoproteins. Journal of virology. 1998 Dec;72(12):10286-91.

236.   Anishchenko M, Paessler S, Greene IP, Aguilar PV, Carrara AS, Weaver SC. Generation and characterization of closely related epizootic and enzootic infectious cDNA clones for studying interferon sensitivity and emergence mechanisms of Venezuelan equine encephalitis virus. Journal of virology. 2004 Jan;78(1):1-8.

237.   Couderc T, Chretien F, Schilte C, Disson O, Brigitte M, Guivel-Benhassine F, et al. A mouse model for Chikungunya: young age and inefficient type-I interferon signaling are risk factors for severe disease. PLoS pathogens. 2008 Feb 8;4(2):e29.

238.   Frolov I, Akhrymuk M, Akhrymuk I, Atasheva S, Frolova EI. Early events in alphavirus replication determine the outcome of infection. Journal of virology. 2012 May;86(9):5055-66.

239.   Jahrling PB, Navarro E, Scherer WF. Interferon induction and sensitivity as correlates to virulence of Venezuelan encephalitis viruses for hamsters. Arch Virol. 1976;51(1-2):23-35.

240.   Jordan GW. Interferon sensitivity of Venezuelan equine encephalomyelitis virus. Infect Immun. 1973 Jun;7(6):911-7.

241.   Powers AM, Brault AC, Kinney RM, Weaver SC. The use of chimeric Venezuelan equine encephalitis viruses as an approach for the molecular identification of natural virulence determinants. Journal of virology. 2000 May;74(9):4258-63.

242.   Fox JM, Long F, Edeling MA, Lin H, van Duijl-Richter MKS, Fong RH, et al. Broadly Neutralizing Alphavirus Antibodies Bind an Epitope on E2 and Inhibit Entry and Egress. Cell. 2015 Nov 19;163(5):1095-107.

243.   Kam YW, Lum FM, Teo TH, Lee WW, Simarmata D, Harjanto S, et al. Early neutralizing IgG response to Chikungunya virus in infected patients targets a dominant linear epitope on the E2 glycoprotein. EMBO Mol Med. 2012 Apr;4(4):330-43.

244.   Rabinowitz SG, Adler WH. Host defenses during primary Venezuelan equine encephalomyelitis virus infection in mice. I. Passive transfer of protection with immune serum and immune cells. J Immunol. 1973 May;110(5):1345-53.

245.   Calisher CH, Berardi VP, Muth DJ, Buff EE. Specificity of immunoglobulin M and G antibody responses in humans infected with eastern and western equine encephalitis viruses: application to rapid serodiagnosis. J Clin Microbiol. 1986 Feb;23(2):369-72.

246.   Griffin DE. Roles and reactivities of antibodies to alphaviruses. Seminars in Virology. 1995 August 1995;6(4):249-55.

247.   Yun NE, Peng BH, Bertke AS, Borisevich V, Smith JK, Smith JN, et al. CD4+ T cells provide protection against acute lethal encephalitis caused by Venezuelan equine encephalitis virus. Vaccine. 2009 Jun 19;27(30):4064-73.

248.   Paessler S, Yun NE, Judy BM, Dziuba N, Zacks MA, Grund AH, et al. Alpha-beta T cells provide protection against lethal encephalitis in the murine model of VEEV infection. Virology. 2007 Oct 25;367(2):307-23.

249.   Bennett AM, Lescott T, Phillpotts RJ. Improved protection against Venezuelan equine encephalitis by genetic engineering of a recombinant vaccinia virus. Viral immunology. 1998;11(3):109-17.

250.   Taylor K, Kolokoltsova O, Ronca SE, Estes M, Paessler S. Live, Attenuated Venezuelan Equine Encephalitis Virus Vaccine (TC83) Causes Persistent Brain Infection in Mice with Non-functional alphabeta T-Cells. Front Microbiol. 2017;8:81.

251.   Smith DR, Adams AP, Kenney JL, Wang E, Weaver SC. Venezuelan equine encephalitis virus in the mosquito vector Aedes taeniorhynchus: infection initiated by a small number of susceptible epithelial cells and a population bottleneck. Virology. 2008 Mar 1;372(1):176-86.

252.   Sudia WD, McLean RG, Newhouse VF, Johnston JG, Miller DL, Trevino H, et al. Epidemic Venezuelan equine encephalitis in North America in 1971: vertebrate field studies. American journal of epidemiology. 1975 Jan;101(1):36-50.

253.   Turell MJ, Ludwig GV, Beaman JR. Transmission of Venezuelan equine encephalomyelitis virus by Aedes sollicitans and Aedes taeniorhynchus (Diptera: Culicidae). Journal of medical entomology. 1992 Jan;29(1):62-5.

254.   Kramer LD, Scherer WF. Vector competence of mosquitoes as a marker to distinguish Central American and Mexican epizootic from enzootic strains of Venezuelan encephalitis virus. The American journal of tropical medicine and hygiene. 1976 Mar;25(2):336-46.

255.   Cupp EW, Scherer WF, Ordonez JV. Transmission of Venezuelan encephalitis virus by naturally infected Culex (Melanoconion) opisthopus. The American journal of tropical medicine and hygiene. 1979 Nov;28(6):1060-3.

256.   Weaver SC, Scherer WF, Taylor CA, Castello DA, Cupp EW. Laboratory vector competence of Culex (Melanoconion) cedecei for sympatric and allopatric Venezuelan equine encephalomyelitis viruses. The American journal of tropical medicine and hygiene. 1986 May;35(3):619-23.

257.   Ferro C, Boshell J, Moncayo AC, Gonzalez M, Ahumada ML, Kang W, et al. Natural enzootic vectors of Venezuelan equine encephalitis virus, Magdalena Valley, Colombia. Emerging infectious diseases. 2003 Jan;9(1):49-54.

258.   Chamberlain RW, Sudia WD, Work TH, Coleman PH, Newhouse VF, Johnston JG, Jr. Arbovirus studies in south Florida, with emphasis on Venezuelan equine encephalomyelitis virus. American journal of epidemiology. 1969 Feb;89(2):197-210.

259.   Galindo P, Grayson MA. Culex (Melanoconion) aikenii: natural vector in Panama of endemic Venezuelan encephalitis. Science. 1971 May 7;172(3983):594-5.

260.   Connelly NAACR. Aedes taeniorhynchus. Featured creatures 2014 [cited 2018 March 5]; Available from: http://entnemdept.ufl.edu/creatures/AQUATIC/aedes_taeniorhynchus.htm

261.   Smith DR, Aguilar PV, Coffey LL, Gromowski GD, Wang E, Weaver SC. Venezuelan equine encephalitis virus transmission and effect on pathogenesis. Emerging infectious diseases. 2006 Aug;12(8):1190-6.

262.   Scherer WF, Cupp EW, Lok JB, Brenner RJ, Ordonez JV. Intestinal threshold of an enzootic strain of Venezuelan encephalitis virus in Culex (Melanoconion) taeniopus mosquitoes and its implications to vector competency and vertebrate amplifying hosts. The American journal of tropical medicine and hygiene. 1981 Jul;30(4):862-9.

263.   Kenney JL, Adams AP, Gorchakov R, Leal G, Weaver SC. Genetic and anatomic determinants of enzootic Venezuelan equine encephalitis virus infection of Culex (Melanoconion) taeniopus. PLoS neglected tropical diseases. 2012;6(4):e1606.

264.   Forrester NL, Guerbois M, Seymour RL, Spratt H, Weaver SC. Vector-borne transmission imposes a severe bottleneck on an RNA virus population. PLoS pathogens. 2012 Sep;8(9):e1002897.

265.   Blair CD. Mosquito RNAi is the major innate immune pathway controlling arbovirus infection and transmission. Future microbiology. 2011 Mar;6(3):265-77.
266.   Galiana-Arnoux D, Dostert C, Schneemann A, Hoffmann JA, Imler JL. Essential function in vivo for Dicer-2 in host defense against RNA viruses in drosophila. Nature immunology. 2006 Jun;7(6):590-7.
267.   Elbashir SM, Lendeckel W, Tuschl T. RNA interference is mediated by 21- and 22-nucleotide RNAs. Genes & development. 2001 Jan 15;15(2):188-200.
268.   Okamura K, Ishizuka A, Siomi H, Siomi MC. Distinct roles for Argonaute proteins in small RNA-directed RNA cleavage pathways. Genes & development. 2004 Jul 15;18(14):1655-66.
269.   Rand TA, Ginalski K, Grishin NV, Wang X. Biochemical identification of Argonaute 2 as the sole protein required for RNA-induced silencing complex activity. Proceedings of the National Academy of Sciences of the United States of America. 2004 Oct 5;101(40):14385-9.
270.   Horwich MD, Li C, Matranga C, Vagin V, Farley G, Wang P, et al. The Drosophila RNA methyltransferase, DmHen1, modifies germline piRNAs and single-stranded siRNAs in RISC. Current biology : CB. 2007 Jul 17;17(14):1265-72.
271.   Saito K, Sakaguchi Y, Suzuki T, Suzuki T, Siomi H, Siomi MC. Pimet, the Drosophila homolog of HEN1, mediates 2'-O-methylation of Piwi- interacting RNAs at their 3' ends. Genes & development. 2007 Jul 1;21(13):1603-8.
272.   Morazzani EM, Wiley MR, Murreddu MG, Adelman ZN, Myles KM. Production of virus-derived ping-pong-dependent piRNA-like small RNAs in the mosquito soma. PLoS pathogens. 2012 Jan;8(1):e1002470.
273.   Scott JC, Brackney DE, Campbell CL, Bondu-Hawkins V, Hjelle B, Ebel GD, et al. Comparison of dengue virus type 2-specific small RNAs from RNA interference-competent and -incompetent mosquito cells. PLoS neglected tropical diseases. 2010;4(10):e848.
274.   Hess AM, Prasad AN, Ptitsyn A, Ebel GD, Olson KE, Barbacioru C, et al. Small RNA profiling of Dengue virus-mosquito interactions implicates the PIWI RNA pathway in anti-viral defense. BMC Microbiol. 2011 Feb 28;11:45.
275.   Goic B, Stapleford KA, Frangeul L, Doucet AJ, Gausson V, Blanc H, et al. Virus-derived DNA drives mosquito vector tolerance to arboviral infection. Nature communications. 2016 Sep 1;7:12410.
276.   Parameswaran P, Sklan E, Wilkins C, Burgon T, Samuel MA, Lu R, et al. Six RNA viruses and forty-one hosts: viral small RNAs and modulation of small RNA repertoires in vertebrate and invertebrate systems. PLoS pathogens. 2010 Feb 12;6(2):e1000764.
277.   Brackney DE, Beane JE, Ebel GD. RNAi targeting of West Nile virus in mosquito midguts promotes virus diversification. PLoS pathogens. 2009 Jul;5(7):e1000502.
278.   ter Brake O, von Eije KJ, Berkhout B. Probing the sequence space available for HIV-1 evolution. Aids. 2008 Sep 12;22(14):1875-7.
279.   Soldan SS, Plassmeyer ML, Matukonis MK, Gonzalez-Scarano F. La Crosse virus nonstructural protein NSs counteracts the effects of short interfering RNA. Journal of virology. 2005 Jan;79(1):234-44.

280.   Gitlin L, Stone JK, Andino R. Poliovirus escape from RNA interference: short interfering RNA-target recognition and implications for therapeutic approaches. Journal of virology. 2005 Jan;79(2):1027-35.

281.   Konishi M, Wu CH, Kaito M, Hayashi K, Watanabe S, Adachi Y, et al. siRNA-resistance in treated HCV replicon cells is correlated with the development of specific HCV mutations. Journal of viral hepatitis. 2006 Nov;13(11):756-61.

282.   Siu RW, Fragkoudis R, Simmonds P, Donald CL, Chase-Topping ME, Barry G, et al. Antiviral RNA interference responses induced by Semliki Forest virus infection of mosquito cells: characterization, origin, and frequency-dependent functions of virus-derived small interfering RNAs. Journal of virology. 2011 Mar;85(6):2907-17.

283.   Souza-Neto JA, Sim S, Dimopoulos G. An evolutionary conserved function of the JAK-STAT pathway in anti-dengue defense. Proceedings of the National Academy of Sciences of the United States of America. 2009 Oct 20;106(42):17841-6.

284.   Xi Z, Ramirez JL, Dimopoulos G. The Aedes aegypti toll pathway controls dengue virus infection. PLoS pathogens. 2008 Jul 4;4(7):e1000098.

285.   Vaidyanathan R, Scott TW. Apoptosis in mosquito midgut epithelia associated with West Nile virus infection. Apoptosis. 2006 Sep;11(9):1643-51.

286.   Girard YA, Schneider BS, McGee CE, Wen J, Han VC, Popov V, et al. Salivary gland morphology and virus transmission during long-term cytopathologic West Nile virus infection in Culex mosquitoes. The American journal of tropical medicine and hygiene. 2007 Jan;76(1):118-28.

287.   Wang H, Gort T, Boyle DL, Clem RJ. Effects of manipulating apoptosis on Sindbis virus infection of Aedes aegypti mosquitoes. Journal of virology. 2012 Jun;86(12):6546-54.

288.   Randall R, Mills, J. W., Engel, L. L. Immunization of laboratory workers with purified Venezuelan equine encephalomyelitis vaccine. Jour Immunol. 1949;65:313-8.

289.   Smith DG, Katz, H. H., Wagner, J. C. Venezuelan equine encephalomyelitis. Preparation and evaluation of a partially purified vaccine. Bact Proc. 1954;59.

290.   W. D. Tigertt WGD. Studies on the virus of Venezuelan equine encephalomyelitis in Trinidad, W.I.I. The 1943-1944 epizootic. Am J Trop Med Hyg. 1962;11:822-34.

291.   Sutton LS, Brooke CC. Venezuelan equine encephalomyelitis due to vaccination in man. J Am Med Assoc. 1954 Aug 21;155(17):1473-6.

292.   Berge TO, Banks IS, Tigertt WD. ATTENUATION OF VENEZUELAN EQUINE ENCEPHALOMYELITIS VIRUS BY IN VITRO CULTIVATION IN GUINEA-PIG HEART CELLS 1. American journal of epidemiology. 1961;73(2):209-18.

293.   McKinney RW, Berge TO, Sawyer WD, Tigertt WD, Crozier D. Use of an Attenuated Strain of Venezuelan Equine Encephalomyelitis Virus for Immunization in Man. The American journal of tropical medicine and hygiene. 1963 Jul;12:597-603.

294.   Ludwig GV, Turell MJ, Vogel P, Kondig JP, Kell WK, Smith JF, et al. Comparative neurovirulence of attenuated and non-attenuated strains of Venezuelan equine encephalitis virus in mice. The American journal of tropical medicine and hygiene. 2001 Jan-Feb;64(1-2):49-55.

295.   Calisher CH, Maness KC. Virulence of Venezuelan equine encephalomyelitis virus subtypes for various laboratory hosts. Appl Microbiol. 1974 Nov;28(5):881-4.

296.   Jahrling PB, Stephenson EH. Protective efficacies of live attenuated and formaldehyde-inactivated Venezuelan equine encephalitis virus vaccines against aerosol challenge in hamsters. J Clin Microbiol. 1984 Mar;19(3):429-31.

297.   Phillpotts RJ, Wright AJ. TC-83 vaccine protects against airborne or subcutaneous challenge with heterologous mouse-virulent strains of Venezuelan equine encephalitis virus. Vaccine. 1999 Feb 26;17(7-8):982-8.

298.   Spertzel RO, Crabbs CL, Vaughn RE. Transplacental transmission of Venezuelan equine encephalomyelitis virus in mice. Infect Immun. 1972 Sep;6(3):339-43.

299.   Cole FE, Jr., Pedersen CE, Jr., Robinson DM. Early protection in hamsters immunized with attenuated Venezuelan equine encephalomyelitis vaccine. Appl Microbiol. 1972 Oct;24(4):604-8.

300.   Pratt WD, Gibbs P, Pitt ML, Schmaljohn AL. Use of telemetry to assess vaccine-induced protection against parenteral and aerosol infections of Venezuelan equine encephalitis virus in non-human primates. Vaccine. 1998 May-Jun;16(9-10):1056-64.

301.   Alevizatos AC, McKinney RW, Feigin RD. Live, attenuated Venezuelan equine encephalomyelitis virus vaccine. I. Clinical effects in man. The American journal of tropical medicine and hygiene. 1967 Nov;16(6):762-8.

302.   Burke DS, Ramsburg HH, Edelman R. Persistence in humans of antibody to subtypes of Venezuelan equine encephalomyelitis (VEE) virus after immunization with attenuated (TC-83) VEE virus vaccine. The Journal of infectious diseases. 1977 Sep;136(3):354-9.

303.   Pittman PR, Makuch RS, Mangiafico JA, Cannon TL, Gibbs PH, Peters CJ. Long-term duration of detectable neutralizing antibodies after administration of live-attenuated VEE vaccine and following booster vaccination with inactivated VEE vaccine. Vaccine. 1996 Mar;14(4):337-43.

304.   Eddy GA, Martin DH, Reeves WC, Johnson KM. Field studies of an attenuated Venezuelan equine encephalomyelitis vaccine (strain TC-83). Infect Immun. 1972 Feb;5(2):160-3.

305.   Fine DL, Roberts BA, Teehee ML, Terpening SJ, Kelly CL, Raetz JL, et al. Venezuelan equine encephalitis virus vaccine candidate (V3526) safety, immunogenicity and efficacy in horses. Vaccine. 2007 Feb 26;25(10):1868-76.

306.   Pedersen CE, Jr., Robinson DM, Cole FE, Jr. Isolation of the vaccine strain of Venezuelan equine encephalomyelitis virus from mosquitoes in Louisiana. American journal of epidemiology. 1972 May;95(5):490-6.

307.   Kinney RM, Chang GJ, Tsuchiya KR, Sneider JM, Roehrig JT, Woodward TM, et al. Attenuation of Venezuelan equine encephalitis virus strain TC-83 is encoded by the 5'-noncoding region and the E2 envelope glycoprotein. Journal of virology. 1993 Mar;67(3):1269-77.

308.   Kinney RM, Johnson BJ, Welch JB, Tsuchiya KR, Trent DW. The full-length nucleotide sequences of the virulent Trinidad donkey strain of Venezuelan equine encephalitis virus and its attenuated vaccine derivative, strain TC-83. Virology. 1989 May;170(1):19-30.

309.   Kulasegaran-Shylini R, Thiviyanathan V, Gorenstein DG, Frolov I. The 5'UTR-specific mutation in VEEV TC-83 genome has a strong effect on RNA replication and subgenomic RNA synthesis, but not on translation of the encoded proteins. Virology. 2009 Apr 25;387(1):211-21.

310.   White LJ, Wang JG, Davis NL, Johnston RE. Role of alpha/beta interferon in Venezuelan equine encephalitis virus pathogenesis: effect of an attenuating mutation in the 5' untranslated region. Journal of virology. 2001 Apr;75(8):3706-18.

311.   Pratt WD, Davis NL, Johnston RE, Smith JF. Genetically engineered, live attenuated vaccines for Venezuelan equine encephalitis: testing in animal models. Vaccine. 2003 Sep 8;21(25-26):3854-62.

312.   Rao V, Hinz ME, Roberts BA, Fine D. Environmental hazard assessment of Venezuelan equine encephalitis virus vaccine candidate strain V3526. Vaccine. 2004 Jun 30;22(20):2667-73.

313.   Martin SS, Bakken RR, Lind CM, Garcia P, Jenkins E, Glass PJ, et al. Evaluation of formalin inactivated V3526 virus with adjuvant as a next generation vaccine candidate for Venezuelan equine encephalitis virus. Vaccine. 2010 Apr 19;28(18):3143-51.

314.   Volkova E, Frolova E, Darwin JR, Forrester NL, Weaver SC, Frolov I. IRES-dependent replication of Venezuelan equine encephalitis virus makes it highly attenuated and incapable of replicating in mosquito cells. Virology. 2008 Jul 20;377(1):160-9.

315.   Guerbois M, Volkova E, Forrester NL, Rossi SL, Frolov I, Weaver SC. IRES-driven expression of the capsid protein of the Venezuelan equine encephalitis virus TC-83 vaccine strain increases its attenuation and safety. PLoS neglected tropical diseases. 2013;7(5):e2197.

316.   Rossi SL, Guerbois M, Gorchakov R, Plante KS, Forrester NL, Weaver SC. IRES-based Venezuelan equine encephalitis vaccine candidate elicits protective immunity in mice. Virology. 2013 Mar 15;437(2):81-8.

317.   Rossi SL, Russell-Lodrigue KE, Killeen SZ, Wang E, Leal G, Bergren NA, et al. IRES-Containing VEEV Vaccine Protects Cynomolgus Macaques from IE Venezuelan Equine Encephalitis Virus Aerosol Challenge. PLoS neglected tropical diseases. 2015 May;9(5):e0003797.

318.   Paessler S, Fayzulin RZ, Anishchenko M, Greene IP, Weaver SC, Frolov I. Recombinant sindbis/Venezuelan equine encephalitis virus is highly attenuated and immunogenic. Journal of virology. 2003 Sep;77(17):9278-86.

319.   Atasheva S, Kim DY, Frolova EI, Frolov I. Venezuelan equine encephalitis virus variants lacking transcription inhibitory functions demonstrate highly attenuated phenotype. Journal of virology. 2015 Jan;89(1):71-82.

320.   Weaver SC, Pfeffer M, Marriott K, Kang W, Kinney RM. Genetic evidence for the origins of Venezuelan equine encephalitis virus subtype IAB outbreaks. The American journal of tropical medicine and hygiene. 1999 Mar;60(3):441-8.

321.   Martin SS, Bakken RR, Lind CM, Garcia P, Jenkins E, Glass PJ, et al. Comparison of the immunological responses and efficacy of gamma-irradiated V3526 vaccine formulations against subcutaneous and aerosol challenge with Venezuelan equine encephalitis virus subtype IAB. Vaccine. 2010 Jan 22;28(4):1031-40.

322.   Greenway TE, Eldridge JH, Ludwig G, Staas JK, Smith JF, Gilley RM, et al. Induction of protective immune responses against Venezuelan equine encephalitis (VEE) virus aerosol challenge with microencapsulated VEE virus vaccine. Vaccine. 1998 Aug;16(13):1314-23.

323.   Hodgson LA, Ludwig GV, Smith JF. Expression, processing, and immunogenicity of the structural proteins of Venezuelan equine encephalitis virus from recombinant baculovirus vectors. Vaccine. 1999 Mar 5;17(9-10):1151-60.

324.   Phillpotts RJ, O'Brien L, Appleton RE, Carr S, Bennett A. Intranasal immunisation with defective adenovirus serotype 5 expressing the Venezuelan equine encephalitis virus E2 glycoprotein protects against airborne challenge with virulent virus. Vaccine. 2005 Feb 18;23(13):1615-23.

325.   Calisher CH, Sasso DR, Sather GE. Possible evidence for interference with Venezuelan equine encephalitis virus vaccination of equines by pre-existing antibody to Eastern or Western Equine encephalitis virus, or both. Appl Microbiol. 1973 Oct;26(4):485-8.

326.   McClain DJ, Pittman PR, Ramsburg HH, Nelson GO, Rossi CA, Mangiafico JA, et al. Immunologic interference from sequential administration of live attenuated alphavirus vaccines. The Journal of infectious diseases. 1998 Mar;177(3):634-41.

327.   Erasmus JH, Seymour RL, Kaelber JT, Kim DY, Leal G, Sherman MB, et al. Novel Insect-Specific Eilat Virus-Based Chimeric Vaccine Candidates Provide Durable, Mono- and Multivalent, Single-Dose Protection against Lethal Alphavirus Challenge. Journal of virology. 2018 Feb 15;92(4).

328.   Riemenschneider J, Garrison A, Geisbert J, Jahrling P, Hevey M, Negley D, et al. Comparison of individual and combination DNA vaccines for B. anthracis, Ebola virus, Marburg virus and Venezuelan equine encephalitis virus. Vaccine. 2003 Sep 8;21(25-26):4071-80.

329.   Dupuy LC, Richards MJ, Reed DS, Schmaljohn CS. Immunogenicity and protective efficacy of a DNA vaccine against Venezuelan equine encephalitis virus aerosol challenge in nonhuman primates. Vaccine. 2010 Oct 28;28(46):7345-50.

330.   Dupuy LC, Locher CP, Paidhungat M, Richards MJ, Lind CM, Bakken R, et al. Directed molecular evolution improves the immunogenicity and protective efficacy of a Venezuelan equine encephalitis virus DNA vaccine. Vaccine. 2009 Jun 24;27(31):4152-60.

331.   Bounds CE, Terry FE, Moise L, Hannaman D, Martin WD, De Groot AS, et al. An immunoinformatics-derived DNA vaccine encoding human class II T cell epitopes of Ebola virus, Sudan virus, and Venezuelan equine encephalitis virus is immunogenic in HLA transgenic mice. Hum Vaccin Immunother. 2017 Dec 2;13(12):2824-36.

332.   Dupuy LC, Richards MJ, Ellefsen B, Chau L, Luxembourg A, Hannaman D, et al. A DNA vaccine for venezuelan equine encephalitis virus delivered by intramuscular electroporation elicits high levels of neutralizing antibodies in multiple animal models and provides protective immunity to mice and nonhuman primates. Clin Vaccine Immunol. 2011 May;18(5):707-16.

333.   Hannaman D, Dupuy LC, Ellefsen B, Schmaljohn CS. A Phase 1 clinical trial of a DNA vaccine for Venezuelan equine encephalitis delivered by intramuscular or intradermal electroporation. Vaccine. 2016 Jun 30;34(31):3607-12.

334.   Tretyakova I, Lukashevich IS, Glass P, Wang E, Weaver S, Pushko P. Novel vaccine against Venezuelan equine encephalitis combines advantages of DNA immunization and a live attenuated vaccine. Vaccine. 2013 Feb 4;31(7):1019-25.

335.   de la Higuera I, Ferrer-Orta C, de Avila AI, Perales C, Sierra M, Singh K, et al. Molecular and Functional Bases of Selection against a Mutation Bias in an RNA Virus. Genome Biol Evol. 2017 May 1;9(5):1212-28.

336.   Schrödinger L. The PyMOL Molecular Graphics System. 1.8.4.0 ed; 2016.

337.   Domingo E, Escarmis C, Lazaro E, Manrubia SC. Quasispecies dynamics and RNA virus extinction. Virus Res. 2005 Feb;107(2):129-39.

338.   Manrubia SC, Domingo E, Lazaro E. Pathways to extinction: beyond the error threshold. Philos Trans R Soc Lond B Biol Sci. 2010 Jun 27;365(1548):1943-52.

339.   Sadeghipour S, McMinn PC. A study of the virulence in mice of high copying fidelity variants of human enterovirus 71. Virus Res. 2013 Sep;176(1-2):265-72.

340.   Sudia WD, Newhouse VF, Beadle ID, Miller DL, Johnston JG, Jr., Young R, et al. Epidemic Venezuelan equine encephalitis in North America in 1971: vector studies. American journal of epidemiology. 1975 Jan;101(1):17-35.

341.   Wang E, Bowen RA, Medina G, Powers AM, Kang W, Chandler LM, et al. Virulence and viremia characteristics of 1992 epizootic subtype IC Venezuelan equine encephalitis viruses and closely related enzootic subtype ID strains. The American journal of tropical medicine and hygiene. 2001 Jul;65(1):64-9.

342.   Weaver SC, Anishchenko M, Bowen R, Brault AC, Estrada-Franco JG, Fernandez Z, et al. Genetic determinants of Venezuelan equine encephalitis emergence. Archives of virology Supplementum. 2004(18):43-64.

343.   T.E. Walton MAG. Venezuelan equine encephalocyelitis. 1 ed. Boca Raton, Florida: CRC Press; 1988.

344.   Rico-Hesse R, Weaver SC, de Siger J, Medina G, Salas RA. Emergence of a new epidemic/epizootic Venezuelan equine encephalitis virus in South America. Proceedings of the National Academy of Sciences of the United States of America. 1995 Jun 6;92(12):5278-81.

345.   Weaver SC, Salas R, Rico-Hesse R, Ludwig GV, Oberste MS, Boshell J, et al. Re-emergence of epidemic Venezuelan equine encephalomyelitis in South America. VEE Study Group. Lancet. 1996 Aug 17;348(9025):436-40.

346.   Lord RD. History and geographic distribution of Venezuelan equine encephalitis. Bull Pan Am Health Organ. 1974;8(2):100-10.

347.   Engler RJ, Mangiafico JA, Jahrling P, Ksiazek TG, Pedrotti-Krueger M, Peters CJ. Venezuelan equine encephalitis-specific immunoglobulin responses: live attenuated TC-83 versus inactivated C-84 vaccine. J Med Virol. 1992 Dec;38(4):305-10.

348.   Roukens AH, Visser LG. Yellow fever vaccine: past, present and future. Expert Opin Biol Ther. 2008 Nov;8(11):1787-95.

349.   Muller HJ. The Relation of Recombination to Mutational Advance. Mutat Res. 1964 May;106:2-9.

350.   Escarmis C, Davila M, Domingo E. Multiple molecular pathways for fitness recovery of an RNA virus debilitated by operation of Muller's ratchet. J Mol Biol. 1999 Jan 15;285(2):495-505.

351.   Hoffmann S, Otto C, Kurtz S, Sharma CM, Khaitovich P, Vogel J, et al. Fast mapping of short sequences with mismatches, insertions and deletions using index structures. PLoS Comput Biol. 2009 Sep;5(9):e1000502.

352.   B.J. Beaty CHC, R.E. Shope. Arboviruses. 7 ed. Washington DC: American Public Health Association; 1995.

353.   Beaucourt S, Borderia AV, Coffey LL, Gnadig NF, Sanz-Ramos M, Beeharry Y, et al. Isolation of fidelity variants of RNA viruses and characterization of virus mutation frequency. Journal of visualized experiments : JoVE. 2011 Jun 16(52).

354.   Campagnola G, McDonald S, Beaucourt S, Vignuzzi M, Peersen OB. Structure-function relationships underlying the replication fidelity of viral RNA-dependent RNA polymerases. Journal of virology. 2015 Jan;89(1):275-86.
355.   Marcotte LL, Wass AB, Gohara DW, Pathak HB, Arnold JJ, Filman DJ, et al. Crystal structure of poliovirus 3CD protein: virally encoded protease and precursor to the RNA-dependent RNA polymerase. Journal of virology. 2007 Apr;81(7):3583-96.
356.   Brackney DE, Schirtzinger EE, Harrison TD, Ebel GD, Hanley KA. Modulation of flavivirus population diversity by RNA interference. Journal of virology. 2015 Apr;89(7):4035-9.
357.   Grubaugh ND, Smith DR, Brackney DE, Bosco-Lauth AM, Fauver JR, Campbell CL, et al. Experimental evolution of an RNA virus in wild birds: evidence for host-dependent impacts on population structure and competitive fitness. PLoS pathogens. 2015 May;11(5):e1004874.
358.   Grubaugh ND, Fauver JR, Ruckert C, Weger-Lucarelli J, Garcia-Luna S, Murrieta RA, et al. Mosquitoes Transmit Unique West Nile Virus Populations during Each Feeding Episode. Cell Rep. 2017 Apr 25;19(4):709-18.
359.   Vazeille M, Moutailler S, Coudrier D, Rousseaux C, Khun H, Huerre M, et al. Two Chikungunya isolates from the outbreak of La Reunion (Indian Ocean) exhibit different patterns of infection in the mosquito, Aedes albopictus. PloS one. 2007 Nov 14;2(11):e1168.
360.   Dimmock NJ, Kennedy SI. Prevention of death in Semliki Forest virus-infected mice by administration of defective-interfering Semliki Forest virus. The Journal of general virology. 1978 May;39(2):231-42.
361.   Mercado-Lopez X, Cotter CR, Kim WK, Sun Y, Munoz L, Tapia K, et al. Highly immunostimulatory RNA derived from a Sendai virus defective viral genome. Vaccine. 2013 Nov 19;31(48):5713-21.
362.   Sun Y, Jain D, Koziol-White CJ, Genoyer E, Gilbert M, Tapia K, et al. Immunostimulatory Defective Viral Genomes from Respiratory Syncytial Virus Promote a Strong Innate Antiviral Response during Infection in Mice and Humans. PLoS pathogens. 2015 Sep;11(9):e1005122.
363.   Tapia K, Kim WK, Sun Y, Mercado-Lopez X, Dunay E, Wise M, et al. Defective viral genomes arising in vivo provide critical danger signals for the triggering of lung antiviral immunity. PLoS pathogens. 2013 Oct;9(10):e1003703.
364.   Dietz WH, Jr., Alvarez O, Jr., Martin DH, Walton TE, Ackerman LJ, Johnson KM. Enzootic and epizootic Venezuelan equine encephalomyelitis virus in horses infected by peripheral and intrathecal routes. The Journal of infectious diseases. 1978 Mar;137(3):227-37.
365.   Henderson BE, Chappell WA, Johnston JG, Jr., Sudia WD. Experimental infection of horses with three strains of Venezuelan equine encephalomyelitis virus. I. Clinical and virological studies. American journal of epidemiology. 1971 Mar;93(3):194-205.
366.   Walton TE, Alvarez O, Jr., Buckwalter RM, Johnson KM. Experimental infection of horses with enzootic and epizootic strains of Venezuelan equine encephalomyelitis virus. The Journal of infectious diseases. 1973 Sep;128(3):271-82.
367.   Zhang Q, Zhang C, Xi Z. Enhancement of RNAi by a small molecule antibiotic enoxacin. Cell Res. 2008 Oct;18(10):1077-9.

368.   Shan G, Li Y, Zhang J, Li W, Szulwach KE, Duan R, et al. A small molecule enhances RNA interference and promotes microRNA processing. Nat Biotechnol. 2008 Aug;26(8):933-40.
369.   Roundy CM, Azar SR, Brault AC, Ebel GD, Failloux AB, Fernandez-Salas I, et al. Lack of evidence for Zika virus transmission by Culex mosquitoes. Emerg Microbes Infect. 2017 Oct 18;6(10):e90.
370.   Wilson AJ, Morgan ER, Booth M, Norman R, Perkins SE, Hauffe HC, et al. What is a vector? Philos Trans R Soc Lond B Biol Sci. 2017 May 5;372(1719).
371.   Turell MJ, Ludwig GV, Kondig J, Smith JF. Limited potential for mosquito transmission of genetically engineered, live-attenuated Venezuelan equine encephalitis virus vaccine candidates. The American journal of tropical medicine and hygiene. 1999 Jun;60(6):1041-4.
372.   Poirier EZ, Goic B, Tome-Poderti L, Frangeul L, Boussier J, Gausson V, et al. Dicer-2-Dependent Generation of Viral DNA from Defective Genomes of RNA Viruses Modulates Antiviral Immunity in Insects. Cell host & microbe. 2018 Mar 14;23(3):353-65 e8.
373.   Wringe A, Fine PE, Sutter RW, Kew OM. Estimating the extent of vaccine-derived poliovirus infection. PloS one. 2008;3(10):e3433.
374.   Kew O, Morris-Glasgow V, Landaverde M, Burns C, Shaw J, Garib Z, et al. Outbreak of poliomyelitis in Hispaniola associated with circulating type 1 vaccine-derived poliovirus. Science. 2002 Apr 12;296(5566):356-9.
375.   Cuervo NS, Guillot S, Romanenkova N, Combiescu M, Aubert-Combiescu A, Seghier M, et al. Genomic features of intertypic recombinant sabin poliovirus strains excreted by primary vaccinees. Journal of virology. 2001 Jul;75(13):5740-51.
376.   Yang CF, Naguib T, Yang SJ, Nasr E, Jorba J, Ahmed N, et al. Circulation of endemic type 2 vaccine-derived poliovirus in Egypt from 1983 to 1993. Journal of virology. 2003 Aug;77(15):8366-77.
377.   Posada-Cespedes S, Seifert D, Beerenwinkel N. Recent advances in inferring viral diversity from high-throughput sequencing data. Virus Res. 2017 Jul 15;239:17-32.
378.   Acevedo A, Brodsky L, Andino R. Mutational and fitness landscapes of an RNA virus revealed through population sequencing. Nature. 2014 Jan 30;505(7485):686-90.
379.   Gerstung M, Beisel C, Rechsteiner M, Wild P, Schraml P, Moch H, et al. Reliable detection of subclonal single-nucleotide variants in tumour cell populations. Nature communications. 2012 May 1;3:811.
380.   Jabara CB, Jones CD, Roach J, Anderson JA, Swanstrom R. Accurate sampling and deep sequencing of the HIV-1 protease gene using a Primer ID. Proceedings of the National Academy of Sciences of the United States of America. 2011 Dec 13;108(50):20166-71.
381.   Zagordi O, Bhattacharya A, Eriksson N, Beerenwinkel N. ShoRAH: estimating the genetic diversity of a mixed sample from next-generation sequencing data. BMC bioinformatics. 2011;12:119.
382.   Giallonardo FD, Topfer A, Rey M, Prabhakaran S, Duport Y, Leemann C, et al. Full-length haplotype reconstruction to infer the structure of heterogeneous virus populations. Nucleic acids research. 2014 Aug;42(14):e115.

383.   Brault AC, Foy BD, Myles KM, Kelly CL, Higgs S, Weaver SC, et al. Infection patterns of o'nyong nyong virus in the malaria-transmitting mosquito, Anopheles gambiae. Insect Mol Biol. 2004 Dec;13(6):625-35.

384.   Sun C, Gardner CL, Watson AM, Ryman KD, Klimstra WB. Stable, high-level expression of reporter proteins from improved alphavirus expression vectors to track replication and dissemination during encephalitic and arthritogenic disease. Journal of virology. 2014 Feb;88(4):2035-46.

385.   Tsetsarkin K, Higgs S, McGee CE, De Lamballerie X, Charrel RN, Vanlandingham DL. Infectious clones of Chikungunya virus (La Reunion isolate) for vector competence studies. Vector Borne Zoonotic Dis. 2006 Winter;6(4):325-37.

386.   Reuther P, Gopfert K, Dudek AH, Heiner M, Herold S, Schwemmle M. Generation of a variety of stable Influenza A reporter viruses by genetic engineering of the NS gene segment. Sci Rep. 2015 Jun 12;5:11346.

387.   Pierson TC, Diamond MS, Ahmed AA, Valentine LE, Davis CW, Samuel MA, et al. An infectious West Nile virus that expresses a GFP reporter gene. Virology. 2005 Mar 30;334(1):28-40.

388.   Baker M. 1,500 scientists lift the lid on reproducibility. Nature. 2016 May 26;533(7604):452-4.

389.   Sierra M, Airaksinen A, Gonzalez-Lopez C, Agudo R, Arias A, Domingo E. Foot-and-mouth disease virus mutant with decreased sensitivity to ribavirin: implications for error catastrophe. Journal of virology. 2007 Feb;81(4):2012-24.

390.   Dulin D, Arnold JJ, van Laar T, Oh HS, Lee C, Perkins AL, et al. Signatures of Nucleotide Analog Incorporation by an RNA-Dependent RNA Polymerase Revealed Using High-Throughput Magnetic Tweezers. Cell Rep. 2017 Oct 24;21(4):1063-76.

391.   Dulin D, Cui TJ, Cnossen J, Docter MW, Lipfert J, Dekker NH. High Spatiotemporal-Resolution Magnetic Tweezers: Calibration and Applications for DNA Dynamics. Biophys J. 2015 Nov 17;109(10):2113-25.

392.   Guo F, Li S, Caglar MU, Mao Z, Liu W, Woodman A, et al. Single-Cell Virology: On-Chip Investigation of Viral Infection Dynamics. Cell Rep. 2017 Nov 7;21(6):1692-704.

393.   Combe M, Garijo R, Geller R, Cuevas JM, Sanjuan R. Single-Cell Analysis of RNA Virus Infection Identifies Multiple Genetically Diverse Viral Genomes within Single Infectious Units. Cell host & microbe. 2015 Oct 14;18(4):424-32.

394.   Schulte MB, Andino R. Single-cell analysis uncovers extensive biological noise in poliovirus replication. Journal of virology. 2014 Jun;88(11):6205-12.

395.   Paulos JA. A mathematician plays the stock market. New York: Basic Books; 2003.

396.   Lee CA. Viral Polymerase Mechanism-Based Strategies for Viral Attenuation and Vaccine Development [Dissertation]. State College, PN: Pennsylvania State University; 2015.

397.   Borderia AV, Isakov O, Moratorio G, Henningsson R, Aguera-Gonzalez S, Organtini L, et al. Group Selection and Contribution of Minority Variants during Virus Adaptation Determines Virus Fitness and Phenotype. PLoS pathogens. 2015 May;11(5):e1004838.

398.   Karpf AR, Lenches E, Strauss EG, Strauss JH, Brown DT. Superinfection exclusion of alphaviruses in three mosquito cell lines persistently infected with Sindbis virus. Journal of virology. 1997 Sep;71(9):7119-23.

399.   McInerney P, Adams P, Hadi MZ. Error Rate Comparison during Polymerase Chain Reaction by DNA Polymerase. Mol Biol Int. 2014;2014:287430.

NAME: Tiffany Faye Kautz

PRESENT POSITION AND ADDRESS:

Predoctoral Research Fellow
University of Texas Medical Branch at Galveston
Department of Microbiology and Immunology
4.104 Keiller Building
301 University Blvd.
Galveston, TX 77555-0609
Email: tfkautz@utmb.edu

BIOGRAPHICAL: Date of Birth: 09/30/1987
                     Birthplace: Manteca, CA
                     Father: Douglas Dean Kautz
                     Mother: Sherilyn Ann Kautz
                     Citizenship: USA

EDUCATION:

08/2012 to present   **Predoctoral Research Fellow**
                     Department of Microbiology and Immunology
                     The University of Texas Medical Branch, Galveston, TX

05/2011-05/2012   **Masters of Science in Biotechnology**
                     New Mexico State University, Las Cruces, NM

08/2006-05/2011   **Bachelor's of Science in Genetics**, *Honors*
                     New Mexico State University, Las Cruces, NM

08/2006-05/2011   **Bachelor's of Arts in Psychology**, *Honors*
                     New Mexico State University, Las Cruces, NM

PROFESSIONAL AND TEACHING EXPERIENCE:
Professional Experience:
08/2013 to present   **Predoctoral Research Fellow**, Department of Microbiology and
                     Immunology, University of Texas Medical Branch, Galveston, TX
                     Mentor: Naomi Forrester

Project: Develop and characterize fidelity variants of arboviruses, such as Venezuelan equine encephalitis virus and chikungunya virus.
Project: Examine the ability of low-fidelity versions of live-attenuated vaccines for Venezuelan equine encephalitis virus to increase vaccine safety and enhance immunogenicity.
Project: Examine the stability of low-fidelity mutations in a transmission cycle.

08/2013 to present **Predoctoral Research Fellow**, Department of Microbiology and Immunology, University of Texas Medical Branch, Galveston, TX
Mentor: Scott Weaver
Project: Tested human serum and mosquitoes from Mexico, Colombia, and the Dominican Republic for the presence of chikungunya virus and analyzed these for genetic evidence of chikungunya virus adaptation to the secondary chikungunya virus mosquito vector, *Aedes albopictus*.

05/2011-05/2012 **Graduate Research Assistant**, Department of Biology, New Mexico State University, Las Cruces, NM
Mentor: Kathryn Hanley
Project: Examined the effects of sylvatic dengue virus infection in the dengue virus reservoir species *Chlorocebus sabaeus* (African green monkey).

01/2010-05/2011 **Undergraduate Research Assistant**, Department of Biology, New Mexico State University, Las Cruces, NM
Mentor: Kathryn Hanley
Project: Used siRNA mediated knockdown to study quasispecies diversity in dengue virus.
Project: Examined how dengue virus competition in *Aedes aegypti* mosquitoes affected the ability of sylvatic and endemic dengue virus strains to disseminate.
Project: Determined differences in sialome composition in wild birds in New Mexico to determine relative risk for different types of influenza infection.

07/2009-12/2009 **Undergraduate Research Assistant**, Department of Psychology, New Mexico State University, Las Cruces, NM
Mentor: Jim Kroger
Project: Used EEG technology to examine the role of the prefrontal cortex in maintaining attention.

09/2008-08/2010 **Undergraduate Research Assistant**, Department of Agriculture, New Mexico State University, Las Cruces, NM
Mentor: Willis Fedio

Project: Improvement of detection methods for *E. coli O157:H7*, *Listeria*, and *Salmonella* in various food products for the FDA.

06/2008-08/2008   **Undergraduate Student Researcher**, Bioscience Division, Los Alamos National Laboratories, Los Alamos, NM
Mentor: Norman Doggett
Project: Built a collection of bacteria representing different taxonomic groups for use in PCR assay testing and validation.

09/2007-05/2009   **Howard Hughes Scholar**, Department of Psychology, New Mexico State University, Las Cruces, NM
Mentor: Melissa Guynn
Project: Used cognitive psychology techniques to better understand prospective memory.

Teaching Experience:
09/2014-12/2014   **Facilitator**, Biochemistry
University of Texas Medical Branch, Galveston, NM

Training and Supervision of Undergraduate, Graduate and Medical Students
09/2015-02/2016   Zachary Ahmed, High School Student

06/2015-07/2015   Juan David Rodas Gonzalez, Visiting Scientist

02/2015-03/2015   Esteban Diaz Gonzalez, Graduate Student

02/2015-03/2015   Iliana Malo Garcia, Visiting Scientist

11/2015-04/2015   Dawn Auguste, Volunteer

11/2014-01/2015   Nicolas Ruiz, Medical School Student

11/2014-01/2015   Johnae Snell, Medical School Student

11/2014-01/2015   Russell Purpura, Medical School Student

11/2014-01/2015   Aidan Deleon, Medical School Student

09/2014-05/2015   Rose Coleman, High School Student

06/2014-08/2014   Ellie Lewis, Undergraduate Student

GRANT SUPPORT:

09/2014-08/2016   McLaughlin Predoctoral Grant

09/2016-08/2017   Tropical Diseases T32 Predoctoral Grant

MEMBERSHIPS IN SCIENTIFIC SOCIETIES:

National:

12/2013 to present	Student Member, American Society of Tropical Medicine and Hygiene (ASTMH)
08/2015 to present	Student Member, American Association for the Advancement of Science (AAAS)
02/2016 to present	Student Member, American Society for Virology (ASV)

HONORS AND AWARDS

04/2017	Travel award to IDEAS workshop on Evolutionary Causes and Consequences of Arbovirus Emergence, IDEAS
03/2017	McLaughlin Symposium Poster Award, UTMB
05/2016	Department of Pathology Annual Trainee Research Day Poster Award, UTMB
04/2016	ASV Student Travel Award, ASV
11/2015	Cary and Kay Cooper Scholarship Fund, UTMB
08/2015	AAAS/Science Program for Excellence in Science, UTMB
04/2015	Preventative Medicine and Community Health Poster Award, UTMB
11/2014	Sealy Center for Vaccine Development Travel Award, UTMB
04/2014	McLaughlin Symposium Poster Award, UTMB
12/2013	Am J Trop Med Hyg Student Subscription, UTMB
08/2012	McLaughlin Scholar, UTMB
03/2012	NMSU Arts and Sciences Travel Award, NMSU
08/2006	Tiscowitz Scholarship, NMSU

COMMUNITY SERVICE AND ACTIVITIES:

05/2016 to 10/2017	Student representative for the Microbiology and Immunology curriculum committee. Galveston, TX.
08/2014 to 05/2016	Mentor for BENCH program designed to expose Ball High School students to basic research techniques and the scientific method. Galveston, TX.
05/2014 to present	Member of UTMB biodefense journal club
01/2014	Science fair judge for students at Odyssey Academy. Galveston, TX.
03/2012-05/2012	Facilitator for Minority Biomedical Research Support-Research Initiative for Scientific Enhancement (MBRS-RISE).
09/2007-07/2012	Volunteer, Humane Society, Las Cruces, NM.

BIBLIOGRAPHY:
Poster Presentations:

1. <u>Kautz, T.F.</u>; Coleman, R.; Kanipov, K.; Guerbois, M.; Yun, R.; Fofanov, Y.; Weaver, S.C.; Forrester, N.L. Low-fidelity arbovirus vaccine stability. 36th annual American Society for Virology conference. June 2017. Madison, Wisconsin.
2. <u>Kautz, T.F.</u>; Khanipov, K.; Guerbois, M.; Patterson, E.I.; Yun, R.; Langsjoen, R.M.; Alcorn, M.D.; Fofanov, F.; Weaver, S.C.; Forrester, N.L. Characterization of a low-fidelity arbovirus and implications for live attenuated vaccine efficacy and stability. Department of Pathology Annual Trainee 23rd Annual Research Day. May 2017. Galveston, TX.
3. <u>Kautz, T.F.</u>; Khanipov, K.; Guerbois, M.; Patterson, E.I.; Yun, R.; Langsjoen, R.M.; Alcorn, M.D.; Fofanov, F.; Weaver, S.C.; Forrester, N.L. Characterization of a low-fidelity arbovirus and implications for live attenuated vaccine efficacy and stability. McLaughlin Symposium. March 2017. Galveston, TX.
4. <u>Kautz, T.F.</u>; Rojas, M.; Patterson, E.I.; Auguste, D.A.; Fofanov, Y.; Weaver, S.C.; Forrester, N.L. High fidelity TC-83 has reduced growth rate in RNAi competent mosquito cells. Department of Pathology Annual Trainee 22nd Annual Research Day. May 2016. Galveston, TX.
5. <u>Kautz, T.F.</u>; Rojas, M.; Patterson, E.I.; Auguste, D.A.; Fofanov, Y.; Weaver, S.C.; Forrester, N.L. High fidelity TC-83 has reduced growth rate in RNAi competent mosquito cells. Positive-Strand RNA Viruses Keystone Symposium. May 2016. Austin, TX.
6. <u>Kautz, T.F.</u>; Rojas, M.; Patterson, E.I.; Auguste, D.A.; Fofanov, Y.; Weaver, S.C.; Forrester, N.L. High fidelity TC-83 has reduced growth rate in RNAi competent mosquito cells. McLaughlin Symposium. April 2016. Galveston, TX.

7. <u>Kautz, T.F.</u>; Díaz-González, E.E.; Erasmus, J.H.; Auguste, A.J.; Rubinstein, R.J.; Watson, K.E.; Malo-García, I.R.; Langsjoen, R.M.; Patterson E.I; Auguste, D.I.; Ruiz, N.; Gerhardt, R.; Snell, J.D.; Chavez, C.; Deleon, A.; Purpura, R.; Coleman, R.; Forrester, N.L.; Sanchez-Casas, R.M.; Hernández-Ávila, M.; Alpuche-Aranda, C.M.; Kiaty Figueroa, L.A.; Dacso, M.M.; Fernández-Salas, I.; Weaver, S.C. Chikungunya virus identified as cause of massive febrile illness outbreak in the Dominican Republic and Mexico. 64rd Annual Meeting of the American Society of Tropical Medicine and Hygiene, Philadelphia, PA. October 2015.
8. <u>Kautz, T.F.</u>; Díaz-González, E.E.; Erasmus, J.H.; Auguste, A.J.; Rubinstein, R.J.; Watson, K.E.; Malo-García, I.R.; Langsjoen, R.M.; Patterson E.I; Auguste, D.I.; Ruiz, N.; Gerhardt, R.; Snell, J.D.; Chavez, C.; Deleon, A.; Purpura, R.; Coleman, R.; Forrester, N.L.; Sanchez-Casas, R.M.; Hernández-Ávila, M.; Alpuche-Aranda, C.M.; Kiaty Figueroa, L.A.; Dacso, M.M.; Fernández-Salas, I.; Weaver, S.C. Chikungunya virus identified as cause of massive febrile illness outbreak in the Dominican Republic and Mexico. 4th Annual Global Health Education Symposium. October 2015.

9. <u>Kautz, T.F.</u>; Diaz-Gonzalez, E.E.; Erasmus, J.H.; Malo-Garcia, I.R.; Langsjoen, R.M.; Patterson, E.I.; Auguste, D.I.; Forrester, N.L.; Sanchez-Casas, R.M.; Hernandez-Avila, M.; Alpuche-Aranda, C.M.; Weaver, S.C.; Fernandez-Salas, I. Chikungunya virus in Chiapas, Mexico. 34th annual American Society for Virology conference. July 2015. London, Ontario, Canada.

10. <u>Kautz, T.F.</u>; Patterson, E.I.; Auguste, D.A.; Guerbois, M.; Kong, F.; Yun, R.; Langsjoen, R.M.; Spratt, H.; Luxon, B.; Weaver, S.C.; Forrester, N.L. High fidelity TC-83 has reduced growth rate in RNAi competent mosquito cells. Pathology Research Training Day Symposium. May 2015. Galveston, TX.
11. <u>Kautz, T.F.</u>; Diaz-Gonzalez, E.E.; Erasmus, J.H.; Malo-Garcia, I.R.; Langsjoen, R.M.; Patterson, E.I.; Auguste, D.I.; Forrester, N.L.; Sanchez-Casas, R.M.; Hernandez-Avila, M.; Alpuche-Aranda, C.M.; Weaver, S.C.; Fernandez-Salas, I. Autochthonous transmission of chikungunya virus during an outbreak of febrile illness in Chiapas, Mexico. Preventative Medicine and Community Public Health Symposium. April 2015. Galveston, TX.
12. <u>Kautz, T.F.</u>; Diaz-Gonzalez, E.E.; Erasmus, J.H.; Malo-Garcia, I.R.; Langsjoen, R.M.; Patterson, E.I.; Auguste, D.I.; Forrester, N.L.; Sanchez-Casas, R.M.; Hernandez-Avila, M.; Alpuche-Aranda, C.M.; Weaver, S.C.; Fernandez-Salas, I. Autochthonous transmission of chikungunya virus during an outbreak of febrile illness in Chiapas, Mexico. McLaughlin Symposium. March 2015. Galveston, TX.
13. <u>Kautz, T.F.</u>; Guerbois, M.; Kong, F.; Yun R.; Langsjoen, R.M.; Alcorn, M.D.; Spratt, H.; Luxon, B.; Weaver, S.C.; Forrester, N.L. High fidelity mutations in the vaccine TC-83 increase immunogenicity and attenuation. McLaughlin Symposium. March 2014. Galveston, TX.
14. <u>Kautz, T.F.</u>; Vasilakis N.; Weaver, S.C.; Brown, M.A.; Marx, P.A.; Hanley, K.A. Sylvatic dengue virus serotype 2 infection in the African Green Monkey. New Mexico-IDeA Networks of Biomedical Research Excellence (NM-INBRE) Annual Symposium. March 2012. Santa Fe, NM.
15. <u>Kautz, T.F.</u>; Vasilakis N.; Weaver, S.C.; Brown, M.A.; Marx, P.A.; Hanley, K.A. Sylvatic dengue virus serotype 2 infection in the African Green Monkey. Rio Grande Branch of the American Society for Microbiology (RGASM) Annual Meeting. February 2012. Las Cruces, NM.

16. <u>Kautz, T.F.;</u> Doggett, N. Building a collection of bacteria representing different taxonomic groups for use in PCR assay testing and validation. Los Alamos National Laboratory Student Symposium. August 2008. Los Alamos, NM.

<u>Oral presentations:</u>

1. <u>Kautz, T.F</u>.; Khanipov, K.; Jaworski, E.; Guerbois, M.; Patterson, E.I.; Yun, R.; Langsjoen, R.M.; Fofanov, F.; Weaver, S.C.; Forrester, N.L. Low-fidelity Venezuelan Equine Encephalitis Virus Stability. Microbiology and Immunology Student Research Update Seminar, University of Texas Medical Branch, Galveston, TX. October 2017.
2. <u>Kautz, T.F</u>.; Khanipov, K.; Guerbois, M.; Patterson, E.I.; Yun, R.; Langsjoen, R.M.; Alcorn, M.D.; Fofanov, F.; Weaver, S.C.; Forrester, N.L. Down the rabbit hole: Unexpected bottlenecks during high fidelity VEEV infection of mosquito cells. Microbiology and Immunology Student Research Update Seminar, University of Texas Medical Branch, Galveston, TX. October 2016.
3. <u>Kautz, T.F</u>.; Rojas, M.; Patterson, E.I.; Auguste, D.A.; Fofanov, Y.; Weaver, S.C.; Forrester, N.L. High fidelity TC-83 has reduced growth rate in RNAi competent mosquito cells. 35th annual American Society for Virology conference. June 2016. Blacksburg, Virginia.

4. <u>Kautz, T.F.</u>; Rojas, M.; Patterson, E.I.; Auguste, D.A.; Fofanov, Y.; Weaver, S.C.; Forrester, N.L. High fidelity TC-83 has reduced growth rate in RNAi competent mosquito cells. 13th International Conference on Molecular Epidemiology and Evolutionary Genetics of Infectious Diseases. May 2016. Antwerp, Belgium.
5. <u>Kautz, T.F.</u>; Guerbois, M; Kong, F.; Patterson, E.I.; Yun R.; Brouwer, D.; Auguste, D.I.; Langsjoen, R.M.; Alcorn, M.D.; Spratt, H.; Luxon, B.; Weaver, S.C.; Forrester, N.L. The reciprocal impact of high fidelity alphaviruses on the host and virus. Microbiology and Immunology Student Research Update Seminar, University of Texas Medical Branch, Galveston, TX. December 2015.
6. **Invited Speaker.** <u>Kautz, T.F.</u> Identificación de CHIKV como agente etiológico de epidemia febril en La Libertad, Chiapas; México. Taller Teorico-Practico Fiebre Chikungunya, Tapachula Chiapas, Mexico. July 2015.
7. **Invited Speaker.** <u>Kautz, T.F</u>. Molecular diagnostics for chikungunya virus using qRT-PCR. Taller Teorico-Practico Fiebre Chikungunya, Tapachula Chiapas, Mexico. July 2015.
8. <u>Kautz, T.F.</u>; Guerbois, M; Kong, F.; Yun R.; Brouwer, D.; Langsjoen, R.M.; Alcorn, M.D.; Spratt, H.; Luxon, B.; Weaver, S.C.; Forrester, N.L. High fidelity mutations in the Venezuelan equine encephalitis vaccine TC-83 increase immunogenicity and attenuation and alter virulence in V3526. 18th Annual Conference on Vaccine Research, Bethesda, MD. April 2015.
9. <u>Kautz, T.F.</u>; Diaz-Gonzalez, E.E.; Erasmus, J.H.; Malo-Garcia, I.R.; Langsjoen, R.M.; Patterson, E.I.; Auguste, D.I.; Forrester, N.L.; Sanchez-Casas, R.M.; Hernandez-Avila, M.; Alpuche-Aranda, C.M.; Weaver, S.C.; Fernandez-Salas, I. First major epidemic of chikungunya fever in North America. Microbiology and Immunology Student Research Update Seminar, University of Texas Medical Branch, Galveston, TX. February 2015.
10. <u>Kautz, T.F.</u>; Guerbois, M.; Kong, F.; Yun R.; Brouwer, D.; Langsjoen, R.M.; Alcorn, M.D.; Spratt, H.; Luxon, B.; Weaver, S.C.; Forrester, N.L. High fidelity mutations in the Venezuelan equine encephalitis vaccine TC-83 increase immunogenicity and attenuation. 63rd Annual Meeting of the American Society of Tropical Medicine and Hygiene, New Orleans, LA. November 2014.
11. <u>Kautz, T.F.</u>; Guerbois, M.; Kong, F.; Yun R.; Brouwer, D.; Langsjoen, R.M.; Alcorn, M.D.; Spratt, H.; Luxon, B.; Weaver, S.C.; Forrester, N.L. High fidelity VEEV: Two ways. Microbiology and Immunology Student Research Update Seminar, University of Texas Medical Branch, Galveston, TX. April 2014.

Publications:

1. <u>Kautz, T.F.</u>; Guerbois, M; Khanipov, K.; Patterson, E.I.; Langsjoen, R.M.; Yun R.; Warmbrod, K.; Fofanov, Y.; Weaver, S.C.; Forrester, N.L. Low-fidelity Venezuelan equine encephalitis virus polymerase mutants to improve live-attenuated vaccine safety and efficacy. Virus Evol. 2018 Mar 6; 4(1):vey001.
2. Patterson, E.I.; Khanipov, K.; Rojas, M.M.; <u>Kautz, T.F.</u>; Brouwer-Rockx, D.; Golovko, G.; Albayrak, L.; Fofanov, Y.; Forrester, N.L. Mosquito bottlenecks alter viral mutant swarm in a tissue and time-dependent manner with contraction and expansion of variant positions and diversity. Virus Evol. 2018 Feb 15; 4(1):vey001. PMID 29479479.

3. Langsjoen, R.M.; Rubinstein, R.J.; <u>Kautz, T.F.</u>; Auguste, A.J.; Erasmus, J.H.; et al. Molecular virologic and clinical characteristics of a chikungunya fever outbreak in La Romana, Dominican Republic, 2014. PLos Negl Trop Dis. 2016 Dec 28;10(12):e0005189. PMID: 28030537.
4. Rodas, J.D.; <u>Kautz, T.F</u>.; Camacho, E.; Paternina, L.; Guzman, H., Diaz, F.J.; Tesh, R.; Weaver, S.C. (2016). Genetic characterization of northwestern Colombian chikungunya virus strains from the 2014-2015 epidemic. Am J Trop Med Hyg. 2016 Jul 18. Pii: 16-0091. PMID: 27430542
5. <u>Kautz, T.F</u>.**;** Diaz-Gonzalez, E.E.***;** Erasmus, J.H.; Malo-Garcia, I.R.; Langsjoen, R.M.; Patterson, E.I.; Auguste, D.I.; Forrester, N.L.; Sanchez-Casas, R.M.; Hernandez-Avila, M.; Alpuche-Aranda, C.M.; Weaver, S.C.; Fernandez-Salas, I. (2015). Chikungunya virus identified as the cause of a febrile illness outbreak, Chiapas, Mexico, 2014. Emerg Infect Dis. 2015 Nov. http://dx.doi.org/10.3201/eid2111.140546
6. Diaz-Gonzalez, E.E.***;** <u>Kautz, T.F.***;**</u> Dorantes-Delgado, A.; Malo-Garcia, I.R.; Langsjoen, R.M.; Auguste, D.I.; Sanchez-Casas, R.M.; Forrester, N.L.; Hernandez-Avila, M.; Alpuche-Aranda, C.M.; Danis-Lozano, R.; Weaver, S.C.; Fernandez-Salas, I. (2015). Incrimination of *Aedes aegypti* as the epidemic vector of chikungunya virus in Chiapas, Mexico. American Journal of Tropical Medicine and Hygiene. 93(6): 1325-9. PMCID: PMC26416113
7. Hanley, K.A.; Guerbois, M.; <u>Kautz, T.F.</u>; Brown, M.; Whitehead, S.S.; Weaver, S.C.; Vasilakis, N.; Marx, P.A. (2014). Infection dynamics of sylvatic dengue virus in a natural primate host, the African green monkey. American Journal of Tropical Medicine and Hygiene. 91(4): 672-676. PMCID: PMC4183386

* Authors contributed equally to this manuscript

Permanent address: 600 19th St. Apt. 19, Galveston, TX 77550

This dissertation was typed by Tiffany Faye Kautz